CHARACTERISATION OF A NOVEL SPINDLE DOMAIN IN MAMMALIAN MEIOSIS

Karmen Bianka Seres

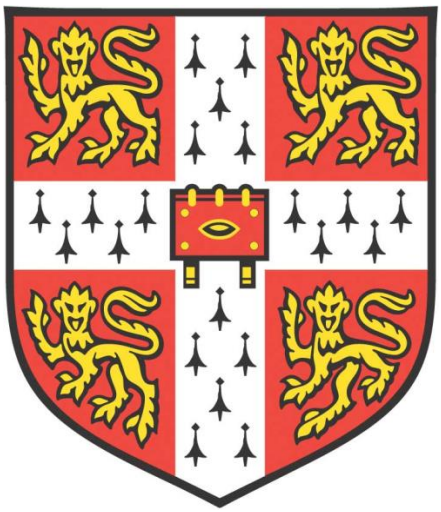

MRC Laboratory of Molecular Biology

University of Cambridge

Wolfson College

This dissertation is submitted for the degree of

Doctor of Philosophy

December 2018

DECLARATION

This dissertation is the result of my own work and includes nothing that is the outcome of work done in collaboration except where specifically indicated in the text. It has not been previously submitted, in part or whole, to the University of Cambridge or to any other university of institution for any degree, diploma, or other qualification. This thesis has been prepared according to the relevant requirements for a thesis of Doctor of Philosophy at the University of Cambridge. It does not exceed the prescribed word limit for the Degree Committee of Biology.

Experiments were performed at the MRC Laboratory of Molecular Biology, the Max Planck Institute (MPI) for Biophysical Chemistry Department of Meiosis), Göttingen and its satellite research lab at Bourn Hall Clinic, Cambridge under the supervision of Dr. Melina Schuh.

Karmen Bianka Seres, M.Sc.

Cambridge, December 2018

Collaborations:

The primary observation of the novel spindle pole meiotic domain in mouse oocytes was done by Dr. Melina Schuh and the initial centrosome protein screen and characterisation of the domain in mouse oocytes was done by Dr. Dean Clift. My work started once PCM1 was identified to localise to this domain. All results shown in Chapters 3 and 5 include my work and any images not taken by me are indicated in the text and in the respective figure legends. The expanded centrosomal protein screen in mouse oocytes and all TACC3 related experiments (Chapter 4) were done in collaboration with Chun So, under the advice and supervision of Dr. Melina Schuh. All images of mouse oocytes in Chapter 4 were taken by Chun So at the MPI-BPC, Göttingen, which is also clearly described in the figure legends. Experiments and methods for data analysis were designed by me and Chun So. All human oocyte work was done by me and for immunofluorescence analysis, I prepared all samples myself. Those samples were then sent to be imaged in Germany by Chun So, due to limitations in microscopy technologies available in the lab at Bourn Hall.

SUMMARY

The organisation of microtubule networks into a bipolar spindle is essential for reliable chromosome segregation during cell division. A pair of centrioles surrounded by pericentriolar material (PCM), define the canonical centrosome that acts as the main microtubule organising centre (MTOC) during mitosis. In mammalian meiosis, centrioles are eliminated early on during oogenesis. Despite the absence of centrosomes, a large number of centrosomal proteins are highly expressed in mouse oocytes. Here, I characterise the localisation and function of centrosomal proteins at a previously undescribed meiotic spindle pole domain (MSPD).

An initial protein screen identified a group of pericentriolar satellite proteins that localised to a previously undescribed spindle pole domain throughout meiotic maturation in mouse oocytes, including Pericentriolar material 1 protein (PCM1). This domain was distinct from spindle microtubules and the acentrosomal microtubule organising centres (aMTOCs). Initial characterisation focused on PCM1, the main centriolar satellite scaffold protein in somatic cells. Depletion of PCM1 revealed interdependence with the essential aMTOC component, Pericentrin. In the absence of PCM1, aMTOCs could no longer assemble or maintain their structural integrity. PCM1 degradation and disassembly of aMTOCs disrupted spindle assembly and reduced the total amount of nucleated microtubules throughout meiosis. In the absence of the main microtubule nucleating aMTOCs, oocytes relied on the Ran GTPase activity to form a small bipolar spindle. A similar mechanism was previously reported in human oocytes that lack prominent MTOCs.

The extended centrosomal protein screen identified additional components of the MSPD. TACC3, under the regulation of Aurora-A at aMTOCs, drive assembly of the MSPD. This domain was absent in MTOC free human oocytes but a second population of TACC3 (identified in mouse oocytes) localised to the meiotic spindle and K-fibres was essential for maintaining spindle pole integrity. Establishing the Lightsheet Z.1 system for live cell imaging of human oocytes enabled us to observe the dynamic distribution of TACC3 in these oocytes. In the absence of prominent MTOCs and the MSPD, human oocytes likely rely on other spindle assembly factors and motor proteins to organise their spindle. Future work to address if the absence of the MSPD could account (in part) for the observed spindle instability in human oocytes is an exciting outlook.

ACKNOWLEDGEMENTS

I would like to thank Dr. Melina Schuh for the opportunity to join her group and the whole Schuhlab for their support throughout my PhD. I am especially grateful to Melina for the opportunity to set up a satellite research lab at Bourn Hall Clinic. A very special thank you to Dr. Dean Clift who started this project.

I would like to thank Dr. Katja Röeper and Dr. Rafael Carazo-Salas, my second supervisors, for all their advice and support. A special thank you to Katja who has taken on the role of first supervisor when the Schuhlab moved to Göettingen.

Importantly, I would like to say thank you to Dr. Sean Munro, the Head of the Cell biology Division at the LMB, for his supportive during my PhD. Thank you to my two examiners, Dr. Julie Welburn and Dr. Simon Bullock for taking the time to read my thesis and for the valuable discussion during my viva.

A special thank you to Dr. Kay Elder, who made it possible to set up such a successful collaboration between our lab and Bourn Hall Clinic. Kay, you have been one of my biggest supporters and I am grateful for everything you have done for me. Thank you for all the advice and encouragement!

I would also like to thank Chun So (Nick), with whom I worked together for the last part of my PhD. Nick, thank you for all the discussions, it was a pleasure working with you. Many thanks to Dr. Lena Wartosch, our lab manager. Lena, thank you for all the encouragements and discussions. Thanks to Julia Uraji for her determination to work on all the troubleshooting experiments. Julia, it was great working with you.

I would also like to say a special thank you to the wonderful Embryology Team at Bourn Hall Clinic for all their help and support. I really felt part of your team and it was a pleasure to get to know every single one of you.

My wonderful parents and siter, I dedicate this thesis to you. Thank you for your endless encouragement and love. Alex, you have been the biggest support I could've ever hoped for.

CONTENTS

LIST OF TABLES

LIST OF FIGURES

LIST OF ABBREVIATIONS AND ACRONYMS

AAA+	ATPases Associated with diverse Activities
ADP	Adenosine diphosphate
AKAP9	A-kinase anchor protein 9 (AKAP450)
APC/C	Anaphase promoting complex/cyclosome
ATP	Adenosine triphosphate
BBS4	Bardet-Biedl syndrome 4 protein
BSA	Bovine serum albumin
C	Carboxyl-terminus
cAMP	Cyclic adenosine monophosphate
CDC20	Cell division cycle protein 20 homolog (p55CDC)
CDK1	Cyclin-dependent kinase 1
CDK5RAP2	CDK5 regulatory subunit-associated protein 2 (CEP215, KIAA1633)
°C	Celsius degree
CENPE	Centromere-associated protein E (Kinesin-7)
CENPs	Centromeric proteins
CEP152	Centrosomal protein of 152 kDa
CEP192	Centrosomal protein of 192 kDa (SPD-2)
CEP290	Centrosomal protein of 290 kDa (BBS14)
CEP72	Centrosomal protein of 72 kDa
CEP90	Centrosomal protein of 90 kDa
CETN2	Centrin-2
cGMP	Cyclic guanosine monophosphate
ch-TOG	Hepatic tumor overexpressed gene protein (CKAP5)
CLASPs	Cytoplasmic linker associated protein 1
C-Nap1	Centrosomal Nek2-associated protein 1 (CEP250)
CO_2	Carbon dioxide
CPC	Chromosomal Passenger Complex
CREST	Calcium-responsive transactivator
CS	Centriolar satellites
Dctn1	Dynactin subunit 1
DHC	Dynein heavy chain
DMSO	Dimethyl sulfoxide
DNA	Deoxyribonucleic acid
EB	End-binding
EGFP, mEGFP	Enhanced green fluorescent protein and its monomeric variant
E-site	Exchangeable-site
F-actin	Filamentous-actin
FBS	Foetal bovine serum

FEP	Fluorinated ethylene propylene
FSH	Follicle stimulating hormone
FVB	Friend leukemia virus B mouse
G phases	Growth phases (G1 and G2)
GCPs	Gamma complex proteins
GDP	Guanosine diphosphate
GTP	Guanosine-5'-triphosphate
GV	Germinal vesicle
h	hour
H2B	Histone H2B
His	Histidine
HOOK3	Protein Hook homolog 3
ICSI	Intracytoplasmic sperm injection
IgG	Immunoglobulin G
INCENP	Inner centromere protein
ITS	Insulin/transferrin/sodium selenite
IVF	In vitro fertilisation
K-fibre	Kinetochore fibre
Kiz	Centrosomal protein kizuna
KLC	Kinesin light chain domain
LH	Luteinizing hormone
Lis1	Lissencephaly-1 protein
LRRC36	Leucine-rich repeat-containing protein 36
LSFM	Light-sheet fluorescent microscopy
M phase	Mitosis phase
MAP4	Microtubule associated protein 4
MAPs	Microtubule associated proteins
MARKs	Microtubule affinity regulating kinases
MCAK	Mitotic centromere-associated kinesin (KIF2C)
mCherry	Monomeric Cherry fluorescent protein
MF	Mobile fractions
MHM	Multipurpose Handling Medium Complete
MI	Meiosis I
µg	microgram
µm	micrometer
µM	micromolar
MII	Meiosis II
min	minute
ml	mililiter
mM	milimolar
MPF	Mitosis promoting factor
mRFP	Monomeric red fluorescent protein

mRNA	messenger RNA
MSPD	Meiotic spindle pole domain
MT	Microtubules
MTBPs	Microtubule binding proteins
MTOCs	Microtubule organising centers
MYO10	Unconventional myosin-10
N	Amino terminus
Nde1	Nuclear distribution protein nudE homolog 1 (NudE)
NE	Nuclear envelope
NEBD	Nuclear envelope breakdown
NEDD1	Neural precursor cell expressed developmentally down-regulated protein 1
NLS	Nuclear localisation signal
N-site	Nonexchangeable-site
NuMA	Nuclear Mitotic Apparatus
OFD1	Oral-facial-digital syndrome 1 protein
PALM	Photo-activated localization microscopy
Par6α	Partitioning defective 6 homolog alpha
PB	Polar body
PBS	Phosphate Buffered Saline
PCM	Pericentriolar material
PCM1	Pericentriolar material-1
PGCs	Primordial germ cells
pH	Power of Hydrogen
PKA	Protein kinase A
pl	picoliter
PLK1	Polo Like Kinase 1
PLK4	Polo-like kinase 4
+TIPs	Plus-end tracking proteins
PN	Pronuclei
PRC1	Protein regulator of cytokinesis 1
RanGTP	GTP-binding nuclear protein Ran
RCC1	Regulator of chromosome condensation
REC8	Meiotic recombination protein
RNA	Ribonucleic acid
RNAi	RNA interference
s	second
S phase	Synthesis phase
s.d.	Standard deviation
SAC	Spindle assembly checkpoint
SAFs	Spindle assembly factors
SGO	Shugoshin
SH	Sample holder

siRNA	Small interfering RNA
spd-5	Spindle-defective protein 5
SSX2IP	Afadin DIL domain-interacting protein (ADIP)
STED	Stimulated emission depletion microscopy
STROM	Stochastic optical reconstruction microscopy
SYCP3	Synaptonemal complex protein 3
$t_{1/2}$	Half-time
TACC3	Transforming acidic coiled-coil-containing protein 3 (ERIC-1)
3D	three-dimensional
3DSIM	3D-structured illumination microscopy
Top2a	DNA topoisomerase 2-alpha
TPX2	Targeting protein for Xklp2
TRIM21	E3 ubiquitin-protein ligase TRIM21
α	alpha
β	beta
γ	gamma
γ-TuRC	γ-tubulin ring complex

1 INTRODUCTION

1.1 Overview

The introduction provides an overview of cell division, with the main focus on female meiosis, describing the whole process of oocyte maturation from folliculogenesis to meiosis II arrest of the mature egg. The main emphasis is to give a detailed overview of the assembly, organisation and key features / components of the microtubule spindle that orchestrates chromosome segregation. The main differences between mitotic and meiotic spindles is highlighted through each of these points. Finally, I will introduce the mechanisms of spindle assembly in mouse and human oocytes.

The subject of this thesis mainly focuses on how meiotic spindle assembly uniquely adopts some of the centrosomal components from mitosis in a centriole-free system (oocytes). Therefore, the overarching focus for the introduction is to give a comprehensive overview of the relevant mitotic components that I investigated in mouse and human meiotic oocytes.

1.2 The cell cycle

The cell cycle is a universal process in all eukaryotes and includes distinct phases that are essential for cell growth and cell division (Figure 1.1). The main stages are the synthesis (S) phase, during which the cell replicates its DNA content, mitosis (M) phase where the cell splits its chromosomal content, followed by cytokinesis during which the cell divides into two daughter cells that are genetically identical (Figure 1.1). The remaining two phases are referred to as growth phases (G1 and G2), important for various checkpoints prior to S phase and M phase, respectively. The period between subsequent mitosis is referred to as interphase (G1, S and G2). The resting (G0) phase represents cells that seized replication and enter a state of quiescence, often triggered by environmental conditions.

Human somatic cells contain 46 chromosomes (22 homologous pairs and two sex chromosomes), referred to as diploid (2n) cells, representing two copies of each chromosome as a result of replication in S phase. The two identical copies (sister chromatids) are joined together at a small region referred to as the centromere (Figure 1.1).

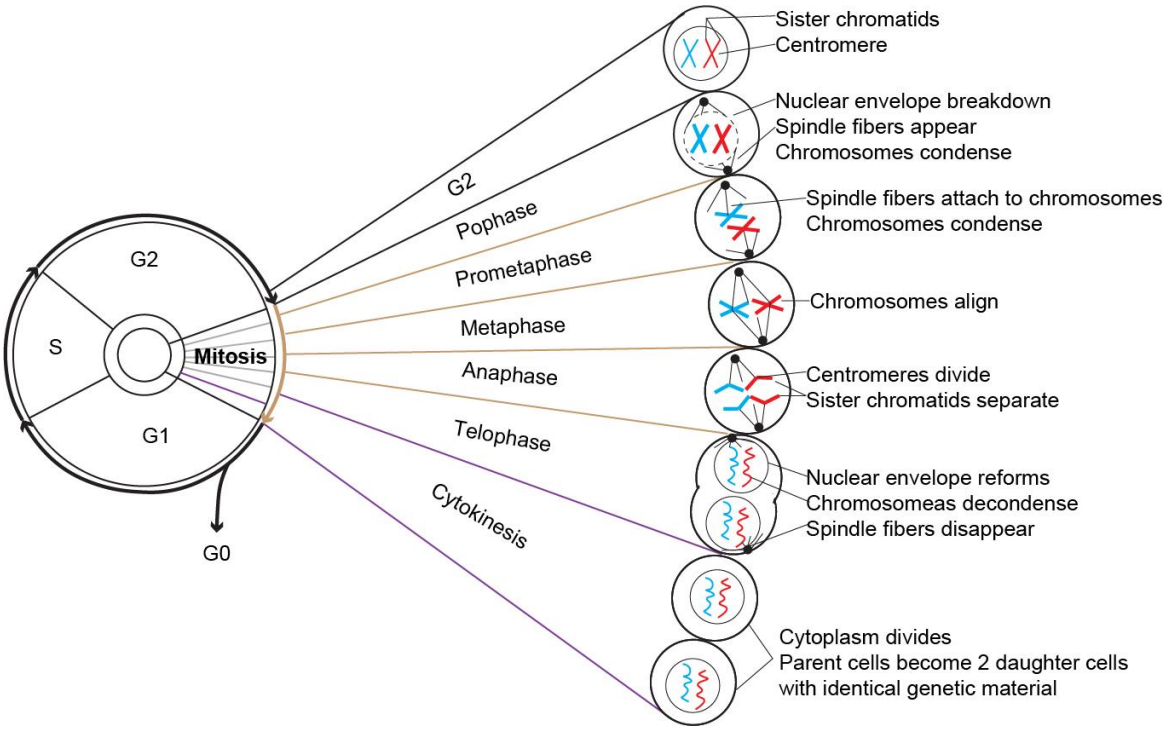

Figure 1.1 Schematic representation of the cell cycle and the phases of mitosis.

Stages of cell cycle, first growth (G1) phase, synthesis (S) phase, second growth (G2) phase and mitosis (M) phase. Resting (G0) represents a phase outside of the replicative cell cycle, when the cell stops proliferation. Specific phases of mitosis are shown on the right. Chromosomes are shown in red (maternal) and blue (paternal). Modified from (Alberts et al., 2002; NatureEducation, 2013).

1.3 From Mitosis to Meiosis

Mitosis governs the replication of all cell types in the body (somatic cells), except reproductive cells, referred to as gametes, which undergo meiosis, a reductive division (Figure 1.2). Two rounds of reductive meiotic divisions (Figure 1.2), first the tetraploid (4n) number of chromosomes are halved between two diploid (2n) cells (Meiosis I) and then halved again to four haploid sets (1n) (Meiosis II), are required for the maturation of sperm and egg cells (Figure 1.5). At the time of fertilisation, the sperm and egg both contribute equally to give rise to a fertilised zygote, with a restored diploid (2n) set of homologous chromosomes (Figure 1.5). While both mitosis and meiosis start with a diploid parental cell and in many aspects share regulatory and mechanistic pathways and components, there are four critical differences that distinguish meiosis from mitosis (Wilkins & Holliday, 2009) (Figure 1.2 and Figure 1.3):

1. Absence of S phase between two successive cell divisions (meiosis I and meiosis II) to achieve haploid gametes (4n after S phase to 1n after MI and MII)
2. Homologous chromosome pairing of maternal and paternal chromosomes (MI)
3. Crossover of the homologous chromosomes and recombination (MI)
4. Homologous chromosome segregation during MI.

In addition, during female meiosis, the segregation of homologous chromosomes is achieved in a highly asymmetrical division that results in the extrusion of two small polar bodies (section 1.4, p20). During mitosis, the cell undergoes the different phases as a continuous process (Figure 1.1), however, in the case of female meiosis, the completion of the first meiotic division can take decades (discussed in section 1.4, p20).

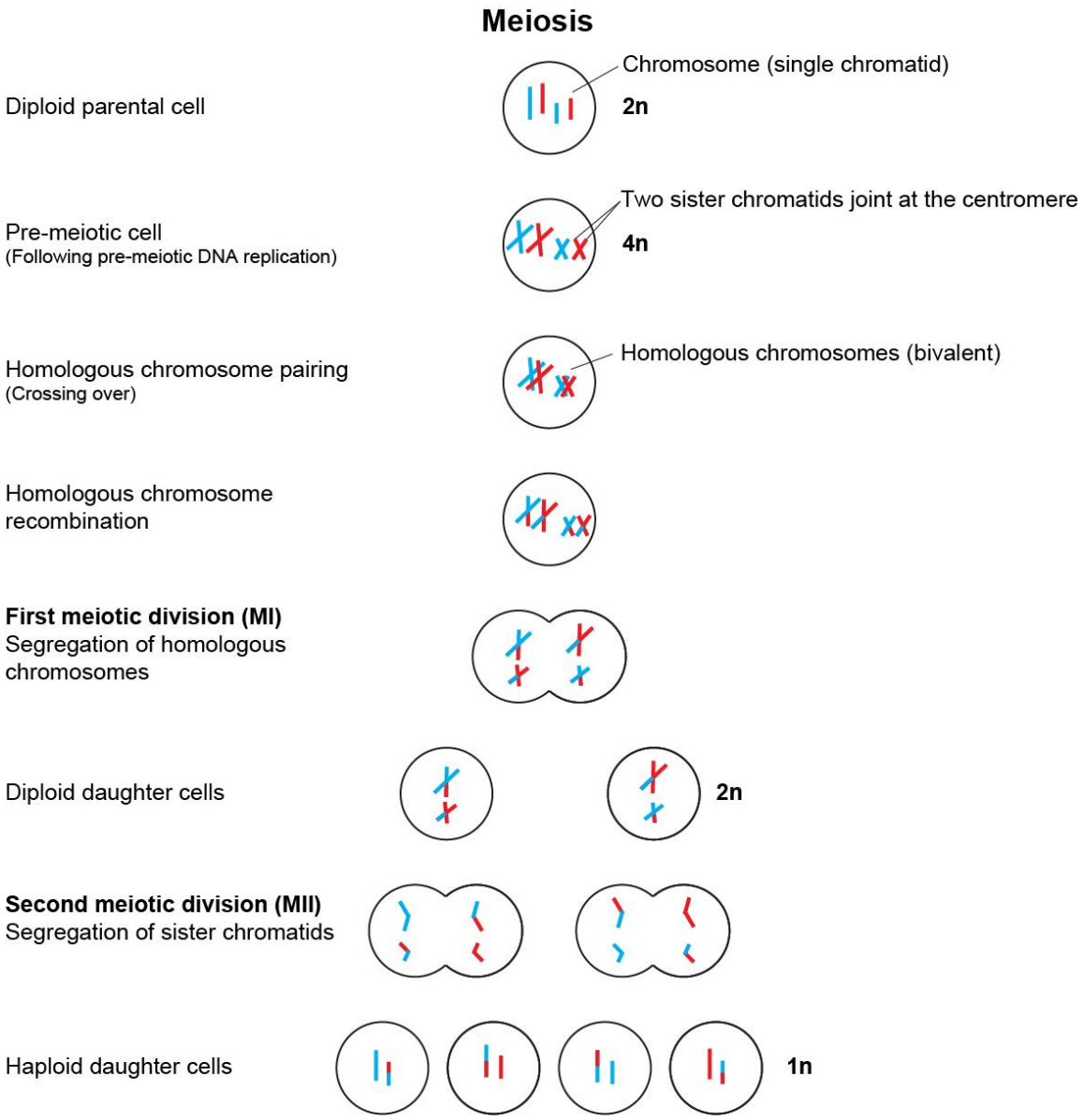

Figure 1.2 Schematic outline of the reductive division during meiosis.

Different colours of chromosomes (red or blue) represent different parental origin. The set of chromosome numbers and the reduction from diploid (2n) to haploid (1n) is shown on the right. Based on (Alberts et al., 2002; NatureEducation, 2013).

1.3.1 The unique segregation event of meiosis I

Meiosis I (MI) adapted a number of unique mechanisms to ensure the correct segregation of homologous chromosome pairs while the sister chromatids are protected against premature separation (Marston & Amon, 2004; Webster & Schuh, 2016). During homologous recombination, the chromosome pairs are linked by chiasmata as a result of crossover and recombination (referred to as bivalents, Figure 1.3.A) (Hunter, 2015). Cohesin is a multi-subunit protein complex that links sister chromatids at the centromeric region (proximal cohesin) and the homologous chromosome arms (distal cohesin) (Figure 1.3.B-C) (Losada et al., 1998; Michaelis et al., 1997; Watanabe & Nurse, 1999). To ensure that bivalents can segregate during MI without the premature separation of the sister chromatids, a stepwise loss of cohesin is required during MI and MII. During anaphase, activation of the protease separase cleaves REC8, the meiotic specific subunit of the cohesin complex to allow chromosome segregation. However, the centromeric proximal cohesin complex holding the two sister chromatids together is protected from cleavage by shugoshin (Sgo) proteins (Figure 1.3.B-D) (Gómez et al., 2007; Lee et al., 2008). In mice, meikin also ensures the coupling of kinetochores of sister chromatids to form a single functional unit for correct microtubule attachment and segregation (Figure 1.3.C-D) (Kim et al., 2015).

1.3.2 Meiosis II

During the second meiotic division, the sister chromatids are aligned on the meiotic spindle. During anaphase II, Sgo proteins relocate and the activated separase can now cleave the Rec8 subunit of the centromeric cohesin and allow sister chromatid segregation (Figure 1.2, similar to that of mitosis, Figure 1.1) (Chambon et al., 2013; Gómez et al., 2007; Lee et al., 2008).

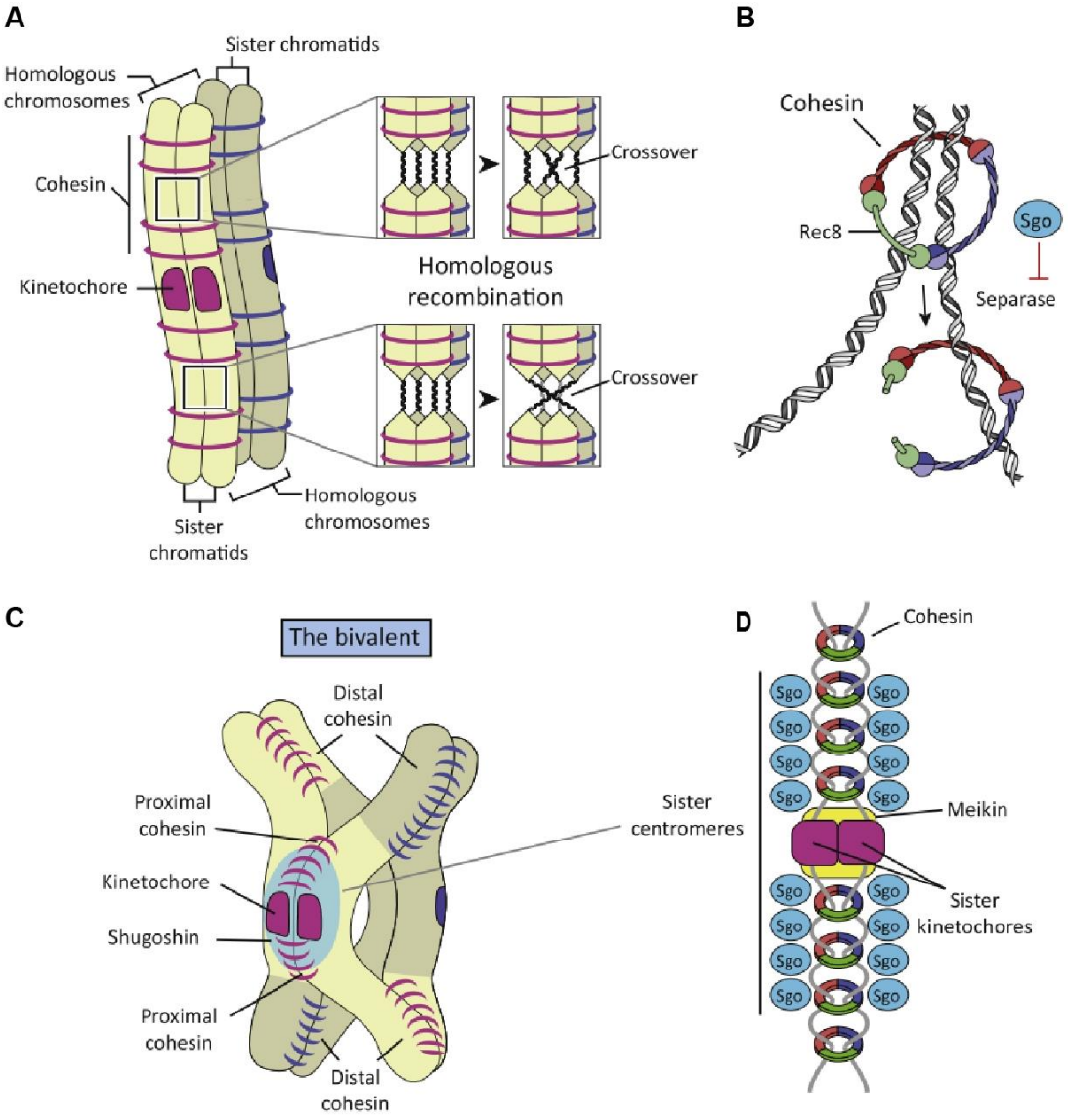

Figure 1.3 Schematic structure of homologous chromosome recombination.

(A) Following pre-meiotic DNA replication, cohesin is connected between the two identical sister chromatids and formation of crossover occurs between the maternal (pink) and paternal (blue) homologous chromosomes during recombination. (B) Multi-subunit cohesin complex holding together two strands of chromosomal DNA. Centromeric region is protected by shugoshin (Sgo) from cleavage of REC8 by separase. (C) Schematic structure of homologous bivalent after recombination. (D) Centromeric region of two sister chromatids showing the protective Sgo localisation and the bioriented sister kinetochores held together by meikin. Taken from (Webster & Schuh, 2016).

1.4 Female meiosis and oocyte maturation

Mammalian female meiosis starts very early during foetal development (Figure 1.4). The diploid primordial germ cells (PGCs) originate from the inner cell mass of the developing embryo. Following migration into the genital ridges, PGCs proliferate via mitosis and differentiate into multipotent germ cells (forms the germ cell cysts). The commitment to either the female (oogenesis) or male (spermatogenesis) reproductive development is based on the timing of meiotic entry (Agrimson & Hogarth, 2016). PGCs in the developing foetal ovary are triggered to enter prophase of MI mediated by retinoic acid signalling during embryonic development (Bowles et al., 2006; Koubova et al., 2006). By activating meiosis specific genes such as meiotic recombination protein (REC8) and synaptonemal complex protein 3 (SYCP3) (Agrimson & Hogarth, 2016), the primordial oocytes undergo condensation of the replicated genetic material to form homologous chromosomes and undergo recombination. Oocyte arrest is maintained in the dictyate (resting) stage of prophase and the oocytes are stored in the ovary surrounded by somatic cells (primordial follicles) to facilitate oocyte growth (Figure 1.4). It is generally thought that the pool of primordial follicles is set at the time of birth (Gosden et al., 1983; Mandl & Zuckerman, 1951). While this dogma has since been challenged suggesting that mitotically active germ cells can replenish the available pool of oocytes (Johnson et al., 2004; White et al., 2012; Wu et al., 2017), there is still considerable debate about their existence (Hernandez et al., 2015; Zhang et al., 2015).

1.4.1 Folliculogenesis

During prophase arrest, oocytes undergo a prolonged growth phase, during which they need to accumulate mRNAs and proteins; crucial for meiotic competence and embryonic development. This growth phase is supported by folliculogenesis (Figure 1.4). Follicles are a densely packed layer of somatic (granulosa) cells surrounding the immature primordial oocyte (Li & Albertini, 2013b). Primordial follicles start to form around the time of prophase arrest. Via a complex series of gene regulation, at the time of puberty the primordial follicles are activated and follicular maturation begins (Figure 1.4) (Sánchez & Smitz, 2012). This process involves the proliferation of granulosa cells that surround the immature oocyte to give rise to primary and secondary (pre-antral) follicles. At this point, follicles express follicle stimulating hormone (FSH) and luteinizing

hormone (LH) receptors and continued proliferation of the granulosa cells triggered by FSH, results in the increase in follicle size and the formation of a fluid filled antrum (early antral and Graafian follicles) (Sánchez & Smitz, 2012). Formation of the antrum divides the granulosa cells, and those cells that remain directly associated with the oocyte are termed cumulus cells (Figure 1.4). Gap junctions with the granulosa and later cumulus cells seem to play an important role in the maturation and growth of oocytes throughout folliculogenesis (Li & Albertini, 2013; Sánchez & Smitz, 2012).

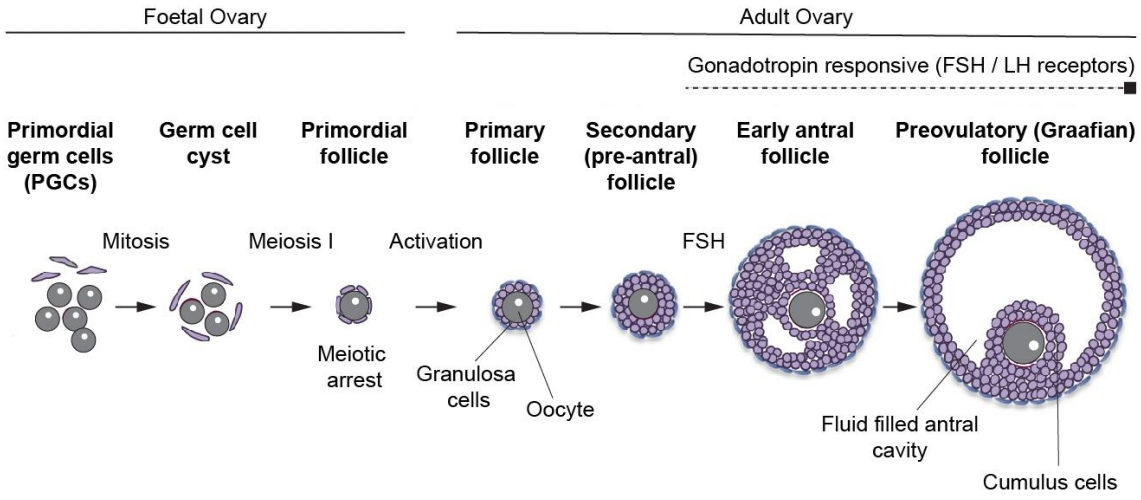

Figure 1.4 Schematic figure showing oogenesis and folliculogenesis from primordial germ cells (PGCs).

Oocytes are shown in grey and somatic cells in purple. Oogenesis begins in the foetal ovary and folliculogenesis continues in the adult ovary, triggered by gonadotropin response of the developing follicles. Modified from (Sánchez & Smitz, 2012).

1.4.2 Meiotic resumption and oocyte maturation

Throughout folliculogenesis, oocytes remain arrested in prophase I. During the late antral stage (Graafian follicle), as the follicles become gonadotropin responsive (Figure 1.4), the surge in LH levels triggers meiotic resumption and ovulation. By the time of meiotic resumption, the oocyte is transcriptionally silent (Pan et al., 2005).

It has long been recognised that oocyte arrest is maintained by cyclic nucleotides (cAMP and cGMP). High intracellular cAMP levels are maintained via both oocyte mediated synthesis and to a major extent via influx of cAMP produced by the surrounding granulosa cells through the connecting gap junctions (Mehlmann et al., 2004; Mehlmann et al., 2002). Following LH-triggered signalling, the degradation of intracellular cAMP results in the de-phosphorylation of protein kinase A (PKA) and the activation of the mitosis promoting factor (MPF), followed by progression to meiotic maturation and nuclear envelope breakdown (NEBD) (Norris et al., 2009; Vaccari et al., 2008).

Meiotic prophase arrested oocytes are morphologically distinct and contain a large, well-defined nucleus (germinal vesicle, GV) that holds decondensed chromatin (Figure 1.5. Stage 1). Meiotic resumption triggers the condensation of chromatin into chromosomes and NEBD. The stages of oocyte maturation have been extensively studied and can be divided into distinct stages, summarised in Figure 1.5. Following NEBD, microtubule nucleation begins around the condensed chromosomes (section 1.6, p52). The microtubule fibres organise into a bipolar spindle structure (Figure 1.5. Stage 2), which captures, aligns, and following spindle relocation to the cortex (Figure 1.5. Stage 3), separates the homologous chromosomes (Figure 1.5. Stage 4). As the homologous chromosome pairs are split during anaphase, the highly asymmetric cell division ensures that the egg retains most of its stored material and only extrudes a small polar body containing half of the homologues. The second meiotic spindle is quickly formed (Figure 1.5. Stage 5), this time aligning the sister chromatid pairs (similar to mitosis), and the egg arrests in MII. At this point, the oocyte reaches its full maturity and it is now referred to as an MII egg, ready for fertilisation (Figure 1.5). Only upon sperm-egg fusion will MII resume, and the separated half of the chromatids are extruded in the second polar body. The haploid male and female pronuclei then form and migrate to the centre of the

fertilised zygote (Figure 1.5), where the first mitotic spindle will form to give rise to a two-cell embryo (Mogessie et al., 2018).

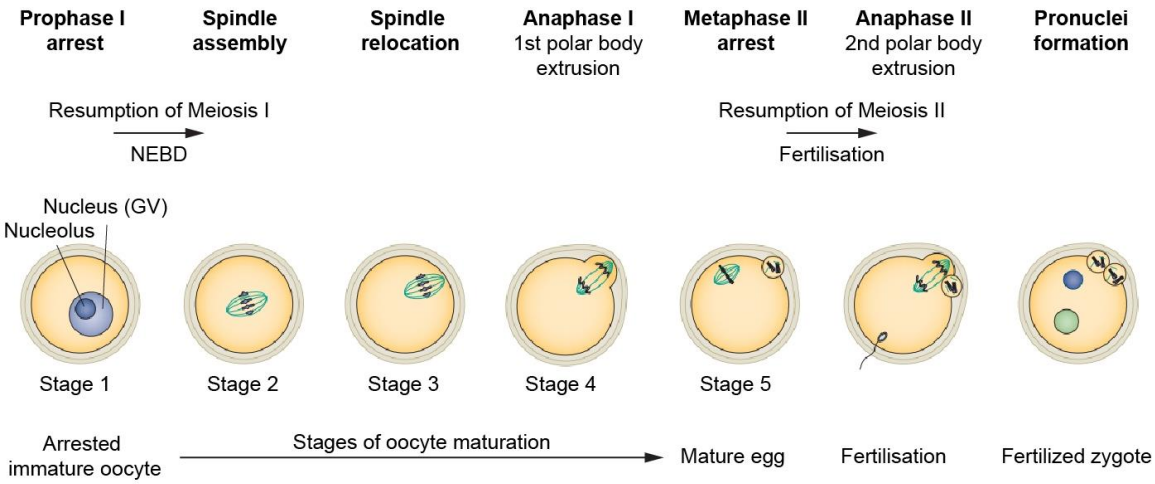

Figure 1.5 Main stages of mouse oocyte maturation and formation of the fertilised zygote.

Stages of oocytes maturation: (Stage 1) Prophase I arrested oocyte with characteristic, large germinal vesicle (GV, purple). (Stage 2) Bipolar spindle in green and aligned homologous chromosomes in blue. (Stage 3) Spindle relocates to the oocyte cortex. (Stage 4) Homologous chromosome separation during anaphase I and extrusion of the 1st polar body. (Stage 5) Second meiotic spindle forms and sister chromatids are aligned while the mature egg awaits fertilisation (metaphase II arrest). Meiosis II resumes upon sperm entry and 2nd polar body is extruded, retaining only half of the sister chromatids. The fertilised zygote forms a maternal (blue) and paternal (green) pronucleus. Modified from (Clift & Schuh, 2013).

1.5 The spindle machinery: structure and dynamics

The spindle machinery is a highly dynamic macromolecular structure, composed of different subsets of microtubules, microtubule-associated proteins and spindle assembly factors. Its function is to orchestrate the capture, alignment and accurate segregation of genetic material in both mitosis and meiosis. Formation of the microtubule cytoskeleton into a bipolar spindle that can exert molecular-scale mechanical forces involves a large number of interacting components. All these components are dynamically organised into specific subunits, and together make up the overall anatomy of the spindle (Figure 1.6.A). While the spindle itself is a universal machinery that drives cell division in eukaryotes, meiotic cells have adapted some key differences at the structural level. In order to fully appreciate these meiosis-specific modifications, one first needs to look at the basic structure of the mitotic spindle.

At the structural level, the spindle can be divided into specific components (Figure 1.6.A). Antiparallel microtubule fibres bundled with their fast-growing plus-ends facing the chromosomes and slow-growing minus-ends are focused at the spindle poles by microtubule organising centres (MTOCs) (Figure 1.6.A). Microtubule bundles that attach directly to the kinetochores, specialised protein complexes at the centromeric region of the chromosomes, are referred to as kinetochore fibres (K-fibres) and are essential for chromosome alignment and segregation (Figure 1.6.A and C). Astral microtubules emanate away from the spindle poles with the plus-tips facing the cytoplasm. Microtubule binding proteins can selectively target specific conformations of tubulin subunits or can be targeted to specific parts of the microtubule spindle to alter microtubule dynamics (section 1.5.2, p28). Chromosomes themselves are not just passive passengers within the spindle, but have a crucial role in organising microtubule assembly and are also the site of the main cell cycle regulatory step (spindle assembly checkpoint, SAC) for progression into anaphase (section 1.5.3, p39). Centrosomes are considered the main MTOCs in animal cells and their absence in meiotic cells represents one of the main differences between mitotic and meiotic spindles, which has a direct impact on their spindle assembly as well as overall morphology (discussed in section 1.5.4, p41).

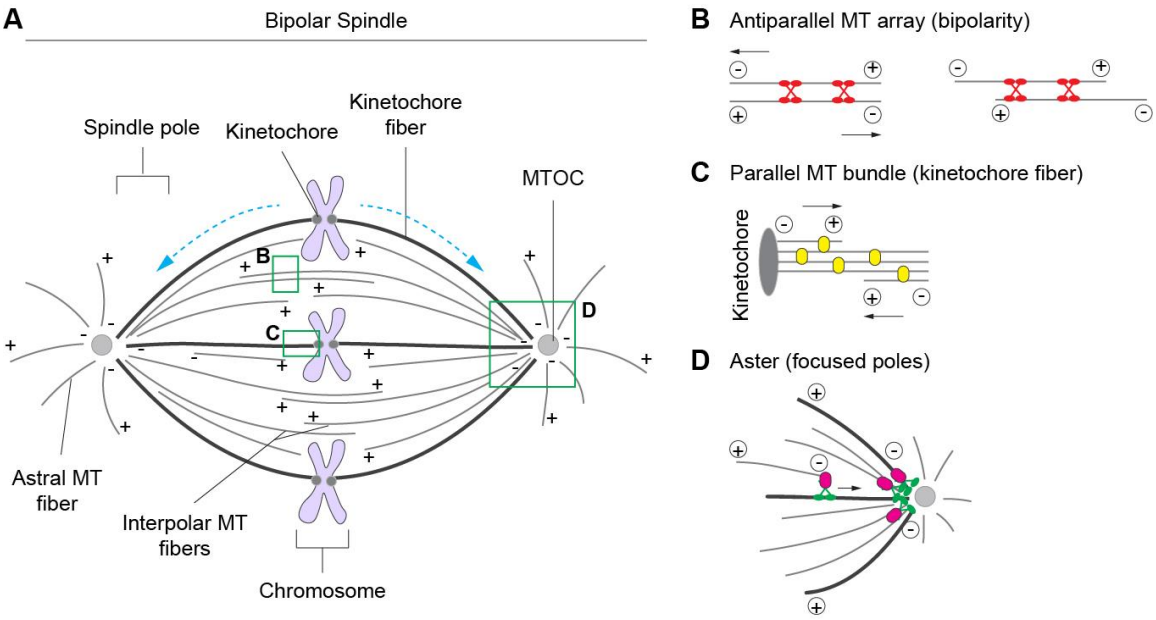

Figure 1.6 Structural features of the bipolar spindle.

(A) Schematic representation of a mitotic bipolar spindle made up of three types of microtubules (MT) (interpolar, kinetochore and astral fibres). Chromosomes are attached to kinetochore fibres (K-fibres) via the centromeric kinetochore. The main MTOCs (centrosomes in mitotic cells) organise the minus-ends of microtubules to form the focused spindle poles. Examples for the organisation of microtubule fibres by different microtubule binding proteins are shown in the boxed regions (B-D). Blue dashed lines indicate the direction of microtubule flux. (B) Antiparallel array of microtubule fibres that drives spindle elongation and bipolarity. Kinesin-5 (Eg5, red), a tetrameric crosslinker, slides the antiparallel microtubules apart. (C) Kinetochores anchor the minus-ends of microtubule fibres that are crosslinked to form the stable K-fibres. (D) Focused array of microtubules anchored by the centrosome. Dynein (green) with its NuMA (Nuclear Mitotic Apparatus, pink) adaptor protein transports minus-ends of the microtubules to the spindle poles and crosslink them. Based on (Elting et al., 2018).

1.5.1 Microtubule structure and dynamics

Microtubules are polymers of αβ-tubulin heterodimers that can grow (microtubule polymerisation) and shrink (microtubule depolymerisation) by the addition or removal of αβ subunits, respectively (Figure 1.7) (Kirschner & Mitchison, 1986; Purich & Kristofferson, 1984). The αβ-tubulin heterodimers are arranged into linear protofilaments in a head-to-tail configuration (Figure 1.7). Typically, microtubules polymerised *in vivo* are formed of thirteen protofilaments, interacting laterally in a hollow cylinder configuration (Akhmanova & Steinmetz, 2015). Two fundamental properties of microtubules are key in the structural integrity and function of the spindle: polarity and dynamic instability.

Due to the asymmetry of the αβ-tubulin heterodimers; the α-subunits of the protofilaments are exposed at the minus-end and the β-subunits are exposed at the plus-end (Figure 1.7). *In vivo,* this structural polarity of the microtubule filament is critical, as the two ends have different capacities for growth. In addition, some of the microtubule-associated proteins that are crucial for the regulation of microtubule dynamics can recognise the polarity of the microtubule lattice (Figure 1.6). This means that they can bind to pole-specific regions of the microtubules, or in the case of most motor proteins, they can move in one direction only, based on microtubule polarity (section 1.5.2, p28).

Both α- and β-tubulin monomers can bind a nucleotide. The N-site- (nonexchangeable) bound GTP in the α-tubulin subunit is trapped within the unpolymerized dimer and cannot be exchanged, whilst the E-site- (exchangeable) bound GTP of the β-subunit is hydrolysed to GDP shortly after incorporation and forms a GTP-tubulin rich cap (GTP cap) at the fast-growing plus-tips (Figure 1.7). Biochemical studies have also demonstrated that efficient microtubule elongation requires the GTP-bound tubulin state, and that following incorporation and hydrolysis to GDP, the tubulin lattice is more prone to depolymerisation (Hyman et al., 1992; Nogales, 2015). It is thought that the loss or reduction of the GTP-cap induces a transition from polymerisation to depolymerisation.

Microtubules are highly dynamic and can stochastically switch between phases of growth and shrinkage, referred to as dynamic instability (Kirschner & Mitchison, 1986). The different states of dynamic instability can be described by the rate of shrinkage, the rate of growth and the transition frequency between catastrophe (growth to shrinkage) and

rescue (shrinkage to growth) (Walker et al., 1988). This steady state of growth and shrinkage is tightly regulated at both ends of the microtubule and it is fundamental to spindle assembly, remodelling and chromosome capture, as well as for microtubule-dependent force generation (Akhmanova & Steinmetz, 2015). While the dynamic nature of microtubules can be observed *in vitro;* microtubules are more dynamic *in vivo*, suggesting that other cellular factors are critical for their regulation.

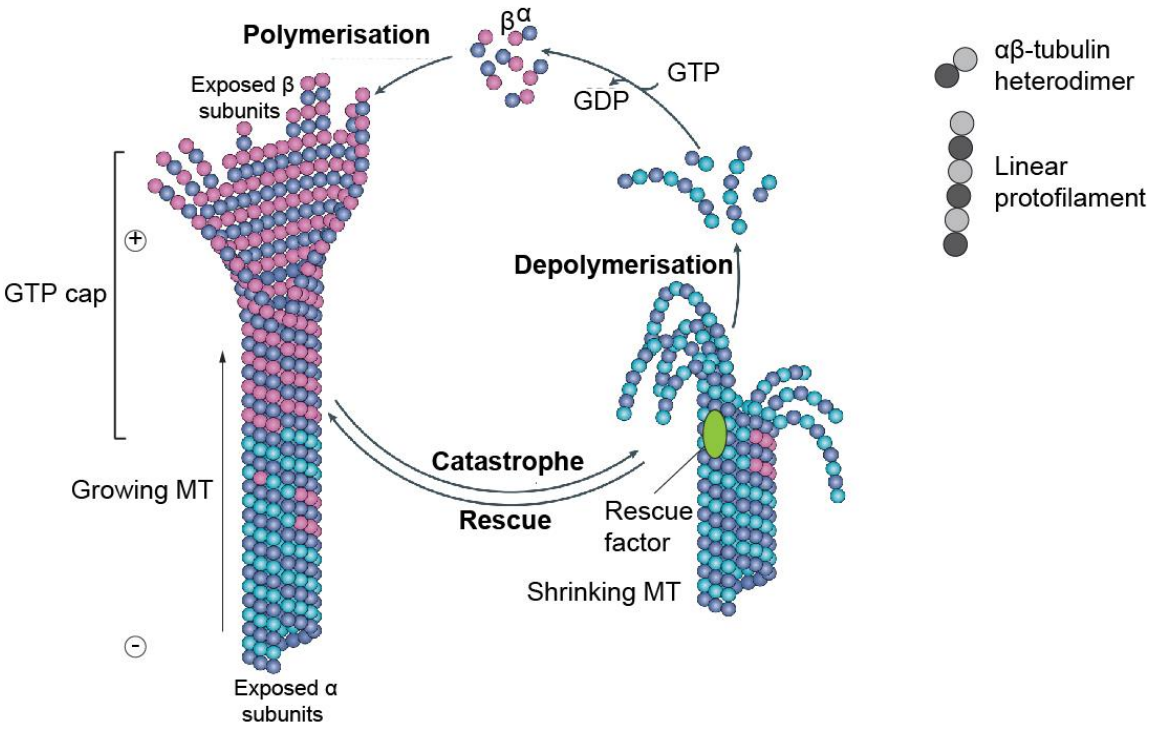

Figure 1.7 Microtubule polymerisation and depolymerisation cycle.

The cycle of tubulin assembly, that is the assembly (polymerisation) and disassembly (depolymerisation) mediated by the hydrolysis of GTP-bound tubulin dimers (pink) to GDP-bound dimers (blue). The GTP-bound dimer incorporation at the growing (plus-ends) forms the GTP cap that provide stability. The switch between assembly and disassembly can be described as catastrophe and rescue events, respectively. Modified from (Akhmanova & Steinmetz, 2015).

1.5.2 Microtubule binding proteins (MTBPs)

A large variety of proteins have been identified that can interact directly with microtubules and regulate microtubule stability (Figure 1.8). Here, the term MTBPs broadly refers to all proteins with experimental evidence showing that they bind microtubules (Goodson & Jonasson, 2018). Another frequently used term, microtubule associated proteins (MAPs) can be considered as a subset of MTBPs that can co-sediment with microtubules and also includes the classical or structural MAPS that bind along the full length of microtubules, such as the MAP1, MAP2 MAP4 family and TAU proteins (not discussed here) (Goodson & Jonasson, 2018).

At the functional level, MTBPs can stabilise and destabilize, bundle and cross-link microtubules and also act as capping proteins. Some can regulate interaction with other components of the cytoskeleton and will be referred to as cytoskeletal integrators. In addition, microtubule-based motor proteins can utilise the energy released from nucleotide hydrolysis and move along the microtubule lattice to mediate short and long-distance cargo transport (Figure 1.8).

A large number of MTBPs modulate their affinity to bind microtubules via phosphorylation by microtubule affinity regulating kinases (MARKs), such as Polo-like kinase 1 (PLK1), Polo-like kinase 4 (PLK4) and Aurora A (Goodson & Jonasson, 2018). A select group of MTBPs that are most relevant for this thesis are introduced below.

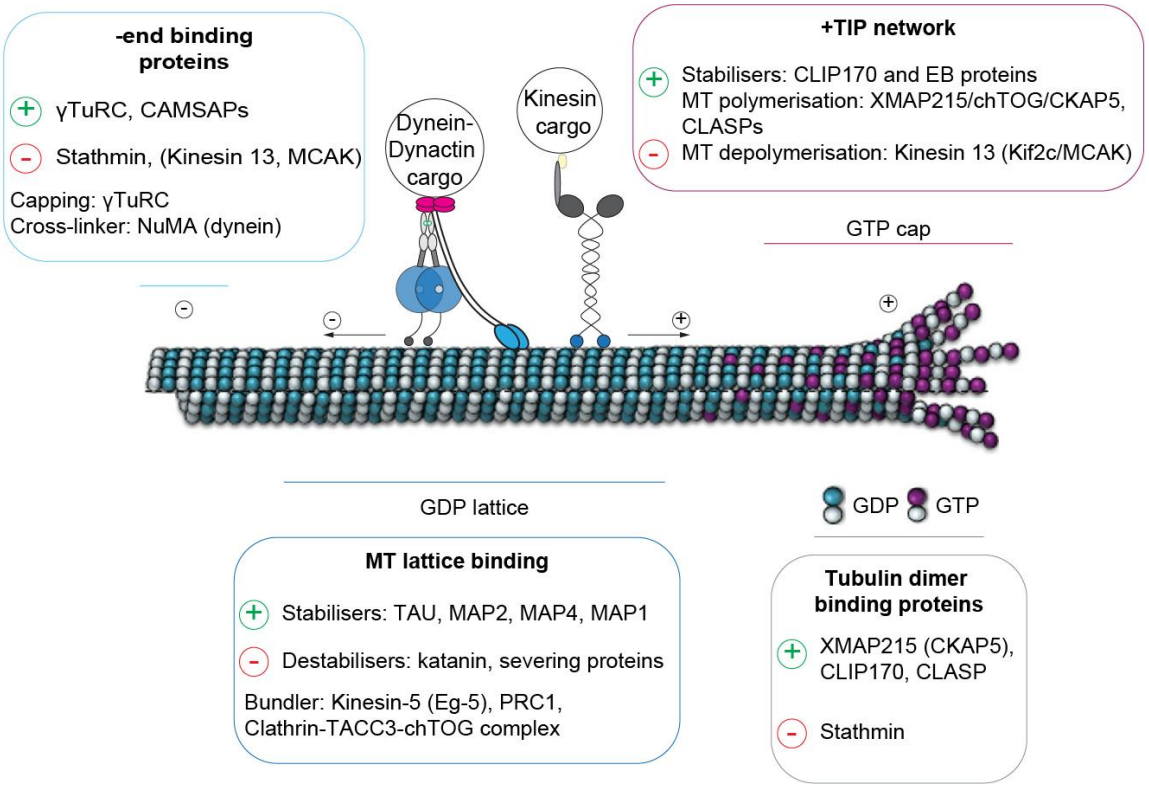

Figure 1.8 Examples of microtubule binding proteins (MTBPs).

Boxed regions represent some of the main categories of MTBPs based on their function and localisation on the microtubule (MT). Green plus signs (+) represent positive regulators of MT growth (promotes polymerisation) and red minus signs (-) mean negative regulation (promotes depolymerisation). Two main examples of motor proteins: minus-end directed cytoplasmic dynein with its adaptor protein dynactin and plus-end directed kinesins. Modified from (Margolin et al., 2012).

1.5.2.1 Microtubule stabilising and polymerising MTBPs

In vivo, microtubule growth rate is accelerated by almost 10-fold compared to *in vitro* polymerised microtubules (Wade, 2009). This is largely achieved by the stabilizing effects of various MTBPs. A group of proteins that belong to the plus-end tracking proteins (+TIPs) are both structurally and functionally diverse, and are distinguished by their ability to selectively associate with the fast growing plus-tips of the microtubules (Figure 1.8) (Akhmanova & Steinmetz, 2015). Once recruited, +TIPs favour polymerisation of microtubules and/or stabilise the growing ends with reduced frequency of catastrophe.

The end-binding (EB) proteins are one of the main families of +TIPs, containing a highly conserved N-terminal domain (calponin homology domain fold) that is responsible for their microtubule binding ability (Hayashi & Ikura, 2003; Korenbaum & Rivero, 2002); the C-terminal contains domains responsible for interaction and recruitment of other proteins. In mammals, three different EBs are found, EB1, EB2 and EB3. Strictly speaking, these proteins are specific to growing microtubule ends and track with the growing tip due to their affinity to bind short-lived, growing tip specific conformations of the protofilaments (Maurer et al., 2014).

Cytoplasmic linker-associated proteins (CLASPs) are another class of +TIP proteins that support microtubule growth rate via stabilising the plus-ends (promoting rescues) and can directly bind tubulin heterodimers. They are found to be important for K-fibre stabilisation at the kinetochores (Pereira et al., 2006).

A highly conserved and prominent microtubule polymerase belongs to the XMAP215 protein family, first identified in frog egg extracts (Gard & Kirschner, 1987). *In vitro* studies demonstrated that XMAP215/ch-TOG/CKAP5[1] accelerated microtubule plus-end growth by almost 10-fold (Gard & Kirschner, 1987). It can directly bind microtubule dimers via its N-terminal TOG domain (Gard & Kirschner, 1987; Widlund et al., 2011), and is considered to be a processive polymerase as it can add multiple tubulin dimers without detaching from the microtubule (Howard & Hyman, 2007). It was shown to antagonise the destabilising effects of XKCM1 (MCAK, section 1.5.2.2, p31) catastrophe factor, and together, the opposing polymerising and depolymerising events determine steady-state microtubule length (Howard & Hyman, 2007; Kinoshita et al., 2002; Tournebize et al., 2000).

[1] CKAP5 (Cytoskeleton-associated protein 5) /ch-TOG: 2,032 amino acids, 225.495 kDa
The five TOG (tumour overexpressed gene) domains arranged in an N-terminal pentameric array with intra-HEAT loops (six HEAT repeats per domain – tandem repeat structural motif composed of two alpha helices linked by a loop) forming an oblong paddle-like structure. Source: UniProtKB.

XMAP215/ch-TOG/CKAP5 was shown to complex with the centrosomal protein TACC3[2] (Maskin in frog/*Xenopus*), and plays an important role in spindle assembly (Gergely et al., 2003; Kinoshita et al., 2005; M. J. Lee et al., 2001). TACC3 is part of the TACC protein family that was suggested to have a role in microtubule nucleation by influencing the assembly at the centrosomes (Singh et al., 2014) and maintains spindle stability via its interaction with ch-TOG (M. J. Lee et al., 2001; Peset et al., 2005). It was proposed that TACC3/ch-TOG, which can form a one-to-one complex at the centrosomes, stabilises the growing plus-tips to promote microtubule polymerisation at the spindle poles (Ding et al., 2017; Gutierrez-Caballero et al., 2015; Kinoshita et al., 2005). TACC3 is a well characterised Aurora A substrate (Kinoshita et al., 2005; LeRoy et al., 2007; Lioutas & Vernos, 2013) and via its microtubule interacting partner, clathrin[3], has been shown to complex with other proteins that enable its participation in different roles during spindle assembly (e.g. section 1.5.2.4) (Hood et al., 2013).

In the context of this thesis, I will present our findings and discuss in more detail the relevance of TACC3 and its known interaction partners (ch-TOG and clathrin) in the formation of a meiotic-specific spindle domain (Chapter 4: Results Part II, p120).

1.5.2.2 Microtubule destabilising MTBPs

Microtubule destabilisers promote dissociation of tubulin dimers and can achieve this by a number of different mechanisms, including the sequestering of free tubulin subunits (e.g. stathmin), destabilisation of microtubule tips (e.g. kinesin-13 and stathmin) and microtubule severing (e.g. katanin, spastin and fidgetin) (Figure 1.8) (Goodson & Jonasson, 2018).

---

[2] TACC3 (Transforming acidic coiled-coil-containing protein 3): 838 amino acids, 90.360 kDa

Transforming acidic coiled-coil containing (TACC) protein domain, C-terminal. Conserved in in TACC1, 2 and 3 proteins.

[3] Clathrin (Clathrin heavy chain 1): 1675 amino acids, 191.615 kDa

WD40-like protein repeats at the N-terminal form the seven-bladed beta-propeller that project inward from the polyhedral outer clathrin coat. Source: UniProtKB

A number of proteins that belong to the kinesin families (motor proteins, section 1.5.2.6, p35) are shown to promote microtubule depolymerisation. In particular, MCAK/Kif2C from the kinesin-13 family is a prominent microtubule depolymerase and one of the best characterised members of this motor family, with a unique ability to rapidly diffuse along microtubules in both directions (Ritter et al., 2016; Claire E. Walczak et al., 2013; Wordeman & Mitchison, 1995). MCAK has a high affinity for microtubule ends and can remove microtubule dimers from the GTP-cap in an ATP-dependent manner, by stabilising the curved protofilament conformation; a structural modification as part of depolymerisation (Figure 1.7) (Howard & Hyman, 2007; Talapatra et al., 2015). It is considered to be one of the most effective catastrophe inducing factors, with a comparable rate of microtubule disassembly at both ends (Newton et al., 2004; Ritter et al., 2016). It has essential functions for spindle length regulation as well as generation of K-fibre chromosome pulling force during anaphase onset (Domnitz et al., 2012; Rogers et al., 2004; C E Walczak et al., 1996).

1.5.2.3 Microtubule capping MTBPs

Capping proteins can stabilise microtubule filaments by associating with either the plus-end or minus-end of the filament (Figure 1.8). One of the best known minus-end cappers, in the context of the spindle, is the γ-tubulin ring complex (γ-TuRC), formed of various gamma complex proteins (GCPs 2-6) and thought to act as a microtubule template (Wiese et al., 2006). While their main role is to nucleate microtubules at MTOCs (section 1.6, p52), they also stabilise minus-ends at the spindle poles (Kollman et al., 2011).

1.5.2.4 Microtubule bundler / crosslinker MTBPs

The linear polymers of microtubule filaments can be cross-linked into bundles of arrays (Figure 1.6.B and D). Kinesin-5 (Eg5/KIF11) is a well characterised, tetrameric plus-end tracking motor protein that can bind two antiparallel microtubule fibres and generate a pushing force that slides the fibres apart from each other (Figure 1.6.B) (Peterman & Scholey, 2009). This sliding activity of Kinesin-5 drives bipolar spindle formation (Waitzman & Rice, 2014). Combined with the depolymerisation / polymerisation at the two ends of the microtubules, Kinesin-5 is thought to drive microtubule flux, the

continuous movement of the microtubule lattice towards the minus-ends (spindle poles) (Figure 1.6, blue arrows) (Peterman & Scholey, 2009).

K-fibres in mammalian spindles are composed of 15-35 parallel microtubule fibres, stabilised at the kinetochores and held together by electron-dense bridges (Figure 1.6.A and C) (Hepler et al., 1970). K-fibres are much more stable compared to the highly dynamic interpolar microtubules (Figure 1.6.A), in part due to the function of a cross-linker complex. TACC3 in complex with ch-TOG and clathrin is important for the cross-linking of the K-fibre bundles (Booth et al., 2011). Clathrin is considered to be a 'moonlighting' membrane trafficking protein (Royle, 2013), with an alternative function in spindle organisation (Foraker et al., 2012; Royle et al., 2005). The interaction between the clathrin heavy chain and TACC3 is dependent on phosphorylation of TACC3 by Aurora A kinase. (Fu et al., 2010; Lin et al., 2010).

Another example is PRC1, a passive crosslinker of antiparallel microtubules. It can bind to microtubule filaments via its C-terminal spectrin domain and bundle the plus-tips of overlapping parallel microtubules in the spindle midzone that forms during anaphase (central spindle), when chromosomes are pulled apart (Bieling et al., 2010; Mollinari et al., 2002; Subramanian et al., 2010). The N-terminal domains mediate protein interactions (kinesin-4 and kinesin-5) and homodimerization so that the microtubule binding domains are at opposite ends and can cross-link microtubule filaments with a defined length of overlapping region (Subramanian et al., 2010). PRC1 is also observed in the midzone of bipolar spindles. Here, it appears to form the bridging microtubule fibres that link the two sister K-fibres together that end at the kinetochores (Kajtez et al., 2016). These bridging fibres are thought to help balance the tension between the two bioriented sister kinetochores and are also hypothesised to enable the curved shape of the spindle (Toli et al., 2016).

In general, most stabilisers have some bundling activity - however whether their role is physiologically relevant remains unclear. Motor proteins do have a wide range of functions in the bundling and cross-linking of microtubule fibres. For instance, dynein with the minus-end focusing NuMA adapter is essential for spindle pole focusing (Figure 1.6.D, section 1.5.2.6, p35) (Merdes et al., 2000; Quintyne & Schroer, 2002).

1.5.2.5 Cytoskeletal integrators

Although spindles are considered to be microtubule-based structures, actin microfilaments (F-actin) have also been described in meiotic spindles (Mogessie & Schuh, 2017; Weber et al., 2004). Recently, it was reported that prominent actin microfilaments infiltrate the entire meiotic spindle in various mammalian oocytes examined (mouse, pig, cow, sheep and human) and resembles a spindle-like structure (Mogessie & Schuh, 2017). This work also described an actin-dependent mechanism in mouse oocytes that is important for K-fibre assembly and correct chromosome attachments. In this context, proteins that have the ability to bind both microtubules and F-actin (a type of cytoskeletal integrator) are of high interest. One example for such a potential integrator is myosin-10 (Myo10)[4], an unconventional myosin that was shown to have an important function during spindle assembly in frog oocytes (Weber et al., 2004). Myo10 is an F actin-based motor protein, which interacts with F actin via its PH motor domain but also contains a C-terminal MyTH4-FERM domain for the binding of microtubules (Hine & Sandquist, 2014; Weber et al., 2004; Woolner et al., 2008).

My PhD work looked at Myo10 localisation as I found that among other prominent MTBPs and PCM components, it also localises to a unique spindle domain that I began to characterise (Chapter 3: Results: Part I: section 3.2, p86).

[4] Myosin-10 (Myo10) / Unconventional myosin-X: 2069 amino acids, 238.517 kDa
Contains an N-terminal motor domain and two Pleckstrin homology (PH) domains. C-terminal Myosin Tail Homology 4 (MyTH4) domain is a conserved tail domain of several unconventional myosins. Also at the C-terminus, a FERM domain (F for 4.1 protein, E for ezrin, R for radixin and M for moesin) found in cytoskeletal associated proteins. Source: UniProtKB

1.5.2.6 Microtubule motor proteins

Motor proteins have the ability to use energy from ATP hydrolysis via their catalytic domain to power directed movement along the cytoskeleton. Microtubule based motor proteins can be grouped into two main families of proteins, dyneins and kinesins (Figure 1.8) (Sweeney & Holzbaur, 2018). Both can bind to a wide range of organelles and proteins and move them along the microtubules as cargo. Depending on the location of the motor domain, the direction of movement can be either towards the plus-end or the minus-end.

Dyneins

Dyneins are minus-end directed motor proteins that belong to the AAA+ superfamily (ATPases Associated with diverse Activities), formed of a large, multi-subunit complex that contains two heavy chains (DHC) with ATPase activity (Neuwald et al., 1999). The DHC is composed of six AAA+ modules arranged in a ring that catalysis its processive movement along microtubules, with the ability to interact with a large variety of cargoes. While there is a diverse group of axonemal dyneins, according to our current knowledge, there is only one cytoplasmic dynein that functions as the main minus-end directed microtubule motor in eukaryotic cells (Reck-Peterson et al., 2018). Cytoplasmic dynein function, besides various organelle and cargo transport within the cell, is also essential for spindle assembly, positioning and function. It is activated via its essential cofactor, dynactin subunit that binds to the dynein intermediate chains via its $p150^{Glued}$ subunit (Figure 1.8) (McKenney et al., 2014; Schlager et al., 2014; Waterman-Storer et al., 1995). Apart from dynactin, Lis1 is another essential dynein activator that binds to the DHC ring to promote a strongly bound state for an extended period of microtubule attachment (Huang et al., 2012). For a single motor protein to show such a variety of interacting partners and roles, it must be tightly regulated and able to adapt specificity, which is achieved via different activating adaptors (Table1.1) (Kardon & Vale, 2009; Raaijmakers et al., 2013; Reck-Peterson et al., 2018). These proteins are thought to both activate the motility and link the dynein-dynactin complex to specific cargoes (Reck-Peterson et al., 2018). A few examples of such activating adaptor proteins are shown in Table1.1.

Table 1.1 Examples of activators and candidate activators of cytoplasmic dynein.

Modified from (Reck-Peterson et al., 2018).

Activator or Candidate activator	Cargo
Confirmed activating adaptors (active in in vitro motility assays)	
BICD2	COP1-independent Golgi-to-ER vesicles, Golgi vesicles, Nuclear pore complexes
SPDL1	Kinetochore
HOOK1	RAB5 early endosomes, Clathrin-independent cargoes
HOOK3	RAB5 early endosomes, Golgi
NIN	Unknown
Candidate activating adaptors	
BICD1	COP1-independent Golgi-to-ER vesicles, Microtubule arrays
HOOK2	Centrosomal proteins, Spermatid intramanchette trafficking
NUMA	Minus ends of microtubules in the spindle
HAP1	Many membrane cargoes

Kinesins

Kinesins are a superfamily of motor proteins that have been classified into 14 kinesin families (Lawrence et al., 2004). Their structure contains a conserved, catalytic kinesin light chain domain (KLC) and their specificity is adapted for cargo binding, regulation and localisation via a diverse range of non-motor domains (Table 1.2). The majority of kinesins have an N-terminal motor domain and direct movement towards the plus-ends. However, the motor domain resides at the C-terminal in the minus-end directed kinesin-14 family motor proteins. In addition, some of the kinesin-13 family proteins have a central motor domain: these have microtubule depolymerising activity, and can diffuse along microtubules in both direction (e.g. MCAK, see section 1.5.2.2, p31) (Helenius et al., 2006). Kinesins have essential roles during cell division and are regulated spatially and temporally (Verhey & Hammond, 2009). In general, this can be done by controlling protein levels (e.g. cell cycle-dependent ubiquitylation and degradation of Kinesin-7, Kinesin-10 and Kinesin-13 during anaphase), nuclear or cytoplasmic sequestration (e.g. cytoplasmic sequestration of kinesin-7, CENPE, can only interact with its chromosomal cargo at kinetochores, after nuclear envelope breakdown), activation and deactivation by GTPases and kinases (e.g. RanGTP activation of Kinesin-10 and 14 at nuclear envelope breakdown, around chromosomes) and recruitment to specific spindle components (Verhey & Hammond, 2009).

Table 1.2 Examples of kinesin families related to spindle function.

Modified from (Verhey & Hammond, 2009).

Family	Functions	Commonly studied family members
Kinesin-4	Chromosome positioning	KIF4 (chromokinesin) and KLP1
Kinesin-5	Spindle pole separation and spindle bipolarity	KIF11 (Eg5)
Kinesin-6	Central spindle assembly and cytokinesis	Subfamily: MKLP2 (KIF20A), KIF20A (Rab6 kinesin) Subfamily: MKLP1 (KIF23)
Kinesin-7	Kinetochore–microtubule attachment and chromosome congression	KIF10 (CENPE)
Kinesin-8	Chromosome congression	Subfamily: KIF18 Subfamily: KIF19
Kinesin-10	Chromosome positioning	KIF22 (KID)
Kinesin-12	Spindle pole organization	KIF12 , KIF15 and KLP2
Kinesin-13	Kinetochore–microtubule error correction and chromosome segregation	Subfamily: KIF2A, KIF2B, MCAK (KIF2C) Subfamily: KIF24
Kinesin-14	Spindle pole organization and cargo transport	Subfamily: KIFC1 (HSET) Subfamily: KIFC2

1.5.3 Chromosomes

Chromosomes undergo major structural and organisational changes during the cell cycle and are active components of the spindle machinery (Müller & Almouzni, 2017). During mitosis and meiosis, the chromatin is condensed into chromosomes. In this tightly packed configuration, chromosomes no longer act as accessible genetic material for transcription, but instead are active passengers of the spindle apparatus (Figure 1.6), with an essential role for microtubule nucleation (section 1.6, p52) as well as stabilisation of specialised microtubule fibres (K-fibres) and regulation of spindle dynamics.

An important part of each sister chromatid is the centromeric kinetochore, a large macromolecular complex made up of centromeric proteins (CENPs) that link the spindle microtubules to the centromeric region of the chromosomes (Figure 1.6.A) (Welburn & Cheeseman, 2008). The inner plate of the kinetochore assembles on the centromeric heterochromatin, while the outer plate contains microtubule plus-end (K-fibre) anchoring sites that can stabilise up to 15-35 microtubule fibres (K-fibres). Sister chromatids are correctly attached when each kinetochore established an end-on microtubule attachment, originating from opposite spindle poles (Figure 1.9.A, amphitelic attachment), in order to ensure equal tension for the alignment on the metaphase plate and correct segregation of chromosomes (Figure 1.9.B). Mistakes in the attachment, or no attachment (Figure 1.9.A, monotelic, syntelic and merotelic) can lead to segregation errors, such as misaligned and lagging chromosomes (Figure 1.9.C).

Kinetochores also act as the regulatory sites for cell cycle progression. Anaphase onset is triggered only when the kinetochore attachment signal, the spindle assembly checkpoint (SAC), is satisfied (Musacchio & Hardwick, 2002). SAC is a signalling network that detects both tension and unattached K-fibres at kinetochores. The active SAC signal is maintained at kinetochores by high SAC protein concentrations (Mps1, Bub1, Bub3, BubR1, Mad1 and Mad2) that maintain CDC20, the APC/C co-activator, in an inactive state; this blocks cohesin disassembly during anaphase onset mediated by Cyclin B and Securin (Sanders & Jones, 2018). This property of the SAC can be experimentally used to check for K-fibre attachment, by measuring SAC protein signal at kinetochores. Once all K-fibres are correctly attached to the bioriented chromatids (Figure 1.9.B), SAC

proteins disassemble, the kinetochore attachment signal is satisfied and anaphase is triggered (Sanders & Jones, 2018).

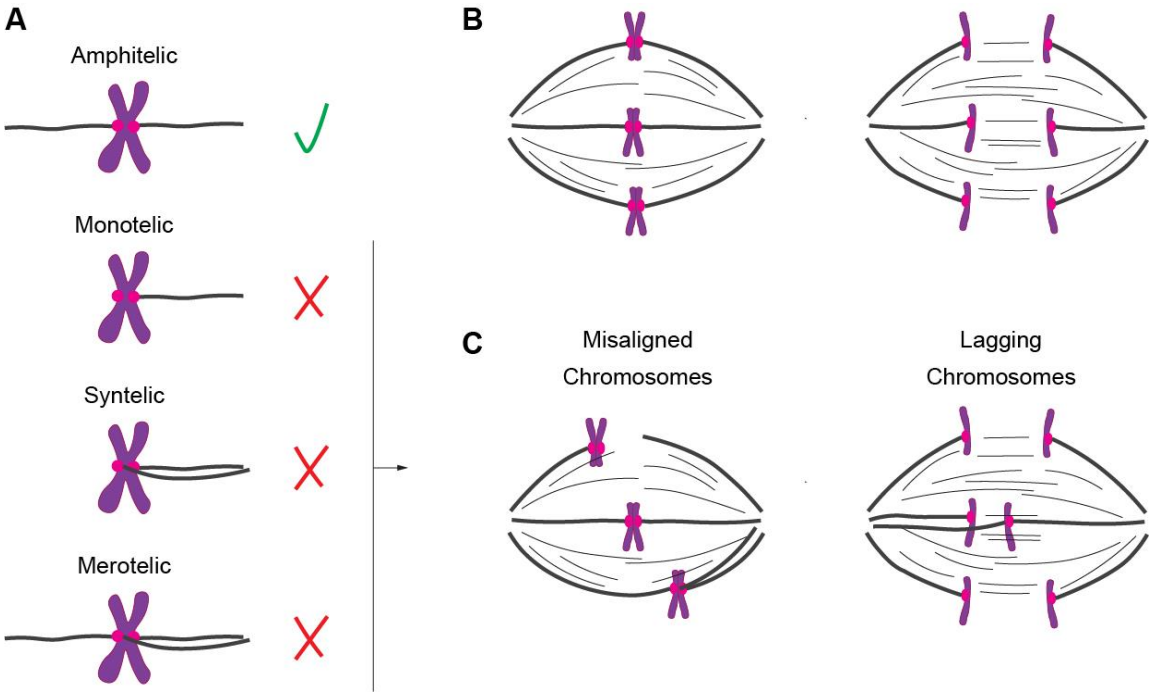

Figure 1.9 Kinetochore microtubule fibre attachments.

(A) Correct attachment (green tick, amphitelic). Incorrect attachments (red cross) when one kinetochore is unattached (monotelic), both sister kinetochores attached to K-fibres from the same pole (syntelic) or one of the kinetochores attached to K-fibres from opposite poles (merotelic). (B) With a balanced, amphitelic attachment, chromosomes are aligned and sister chromatid separation is synchronised. (C) Incorrect attachments can lead to unbalanced tension and chromosome alignment defects (misaligned chromosomes) or lagging chromosomes during anaphase. Modified from (Mogessie & Schuh, 2017).

1.5.4 Microtubule organising centres (MTOCs)

Microtubule dynamics and morphology changes throughout the cell cycle. In order to assemble and remodel microtubules into an ordered bipolar structure (Figure 1.6), cells need to be able to spatiotemporally regulate the formation and assembly of microtubules via organisers (Sanchez & Feldman, 2017). These spindle organisers, also referred to as microtubule organising centres (MTOCs), recruit nucleators (section 1.6, p52) and a wide range of microtubule associated proteins to mediate such control over microtubules. Throughout the different cell types and organisms, MTOCs appear in different size, organisation and distribution, which in turn also determines the overall spindle morphology (Figure 1.10).

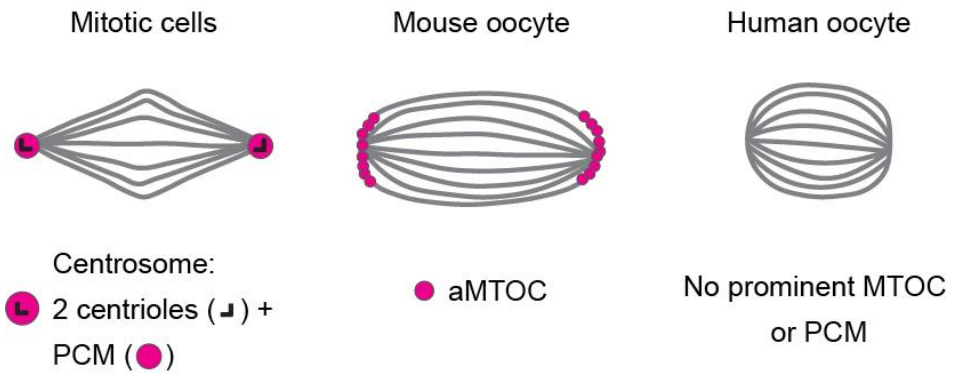

Figure 1.10 Examples of different spindle morphology and spindle pole organisation.

Microtubules shown in grey. Bipolar spindle morphology in mitotic cells shows sharp, pointy spindle poles organised by centrosomes (two centrioles in orthogonal arrangement surrounded by the pericentriolar material PCM). The barrel-shaped meiotic spindle in mouse oocytes is organised by the coalescence of multiple acentrosomal microtubule organising centres made up of PCM components (aMTOCs). The small, barrel-shaped spindle in human oocytes does not contain prominent MTOCs or foci of PCM. Modified from (Bennabi et al., 2016).

In mitotic cells, centrosomes are considered to be the main site of microtubule nucleation, organising the minus-ends of microtubule fibres to form focused arrays of well-defined spindle poles (Figure 1.10). Centrosomes are the earliest recognised

MTOCs for spindle function in animal cells (section 1.5.4.1, p42). However, other, non-centrosomal forms of microtubule organisers can also be found in higher plants, multiciliated epithelial cells, myoblasts and neuronal cells (Bartolini & Gundersen, 2006). In addition, centriole elimination was documented in the oocytes of mouse, rabbit, pig, cow, sea urchin, frog, worm, flies and humans (Hertig & Adams, 1967; Manandhar et al., 2005; Mikeladze-Dvali et al., 2012; Pimenta-Marques et al., 2016; Szollosi et al., 1972). Female meiosis, therefore has also adopted specialised, non-centrosomal MTOC organisers during meiosis (Figure 1.10, section 1.5.4.2, p50).

The structural composition and function of centrosomes has been extensively studied since their discovery. However, the organisation and role of centrosomal proteins in acentrosomal MTOC spindles is still poorly understood: this represents the main focus of the present thesis. An overview of centrosome composition and function is essential in order to appreciate the special adaptations, as well as the conserved functions of centrosomal proteins in acentrosomal meiotic oocytes.

1.5.4.1 The centrosome

The centrosome is a structurally complex, non-membrane bound organelle that can be divided into distinct structural and functional units (Figure 1.11). It is composed of a large number of proteins and protein complexes that make up the two centrioles (mother and daughter centrioles) and the surrounding pericentriolar material (PCM). A single centriole holds nine microtubule triplets that form a cylinder 200 nm wide and 400 nm long (Fujita et al., 2016). The older, mother centriole can be distinguished by the presence of two appendages, while the younger, daughter centriole contains an intermediate cartwheel (Fujita et al., 2016). In dividing cells, the centrosomes are also replicated following centriole disengagement (G1 phase) only once per S phase. This involves procentriole nucleation, followed by centriole elongation. At the end of G2 phase, once centriole replication is complete, the PCM increases in size (centrosome maturation) and in preparation for M phase, the centrosomes separate to form the two poles of the spindle (Fujita et al., 2016). Overall, this process is referred to as the centrosome cycle (not further discussed here).

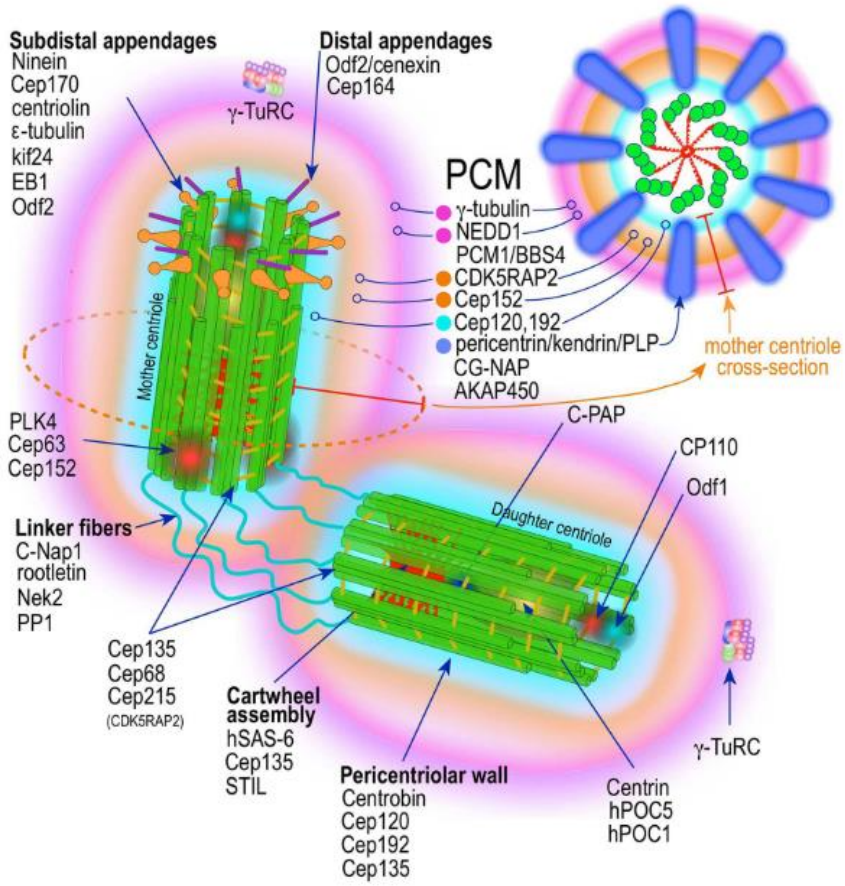

Figure 1.11 Schematic structure of the mature centrosome.

Architecture of the post-mitotic centrosome (after centriole disengagement but before procentriole nucleation), contains the fully mature mother centriole marked by the distal and subdistal appendages and the daughter centriole containing the intermediate cartwheels. Structured pericentriolar material (PCM) appear as toroidal around the centrioles, shown in the cross section of the mother centriole. Taken from (Pihan, 2013).

Pericentriolar material (PCM)

The mature centrioles (two centrioles in orthogonal configuration) are thought to act as the recruiting scaffold for a large number of PCM proteins, most of which are coiled-coil proteins. The coiled-coil motif is composed of intertwined α-helices that facilitate a wide range of protein-protein interactions (Lupas et al., 1991). During the cell cycle, the PCM is highly dynamic and serves as the recruiting platform for the γTuRC complexes, the origin of microtubule nucleation (section 1.6, p52) and the site where microtubule minus-ends are anchored (Figure 1.12) (Zheng et al., 1995).

Early electron microscopy images revealed no detailed structural insights of the PCM, which appeared highly dense and amorphous around the well-defined centrioles. The traditional view of an unstructured cloud of PCM has since been shown to be an inaccurate description (Lawo et al., 2012). Images from super resolution immunofluorescence microscopy methods (3DSIM, STROM, PALM and STED) mapped specific components of the PCM, revealing a well-structured, higher order organisation with PCM components localised to specific domains, forming a toroidal distribution around the interphase centrioles (Figure 1.12) (Fu & Glover, 2012; Lawo et al., 2012; Mennella et al., 2012; Sonnen et al., 2012). During interphase, distinct concentric rings with increasing diameter around the mother centriole include Pericentrin [5], CEP152, CEP192 [6] and CDK5RAP2 (Figure 1.12). Together, these components form the PCM proximal layer in the immediate vicinity of the centriole wall (Fry et al., 2017). Using domain specific immunofluorescence imaging, Pericentrin and CEP152 were shown to assemble into elongated, rod-like filaments, extending away from the centriole wall where the C-termini are anchored (Lawo et al., 2012; Mennella et al., 2012; Sonnen et al., 2012) and it is thought that they may also provide a molecular

[5] Pericentrin/Kendrin/Pericentrin-B: 3336 amino acids, 378.037 kDa

Contains six coiled-coil central regions flanked by non-helical N- and C-terminals. A pericentrin-AKAP-450 centrosomal targeting (PACT) domain is present at the C-terminus, responsible for centrosomal recruitment.

[6] Centrosomal protein of 192 kDa (CEP192): 2537 amino acids, 279.111 kDa

Source: UniProtKB

ruler for the diameter of the PCM (Figure 1.12) (Fry et al., 2017). While the interaction of CEP152 with centrioles is not well understood, Pericentrin C-terminal interaction is in line with previous structural studies showing that the C-terminal PACT domain is essential for centrosome targeting of Pericentrin (Gillingham & Munro, 2000).

In between the Pericentrin and CEP152 molecular filaments, other PCM proximal layer components form a branched matrix that includes CDK5RAP2 and CEP192, as well as anchored γTuRCs via other adaptor proteins, such as NEDD1 (Figure 1.11 and 1.12) (Cota et al., 2017; Fry et al., 2017; T.-C. Lin et al., 2016). The localisation of the proximal matrix proteins CEP192 and CDK5RAP2 are dependent on Pericentrin, suggesting that these components form a functional complex (Dix & Raff, 2007; Gomez-Ferreria et al., 2007; Lawo et al., 2012; O'Connell et al., 2000; Zhu et al., 2008).

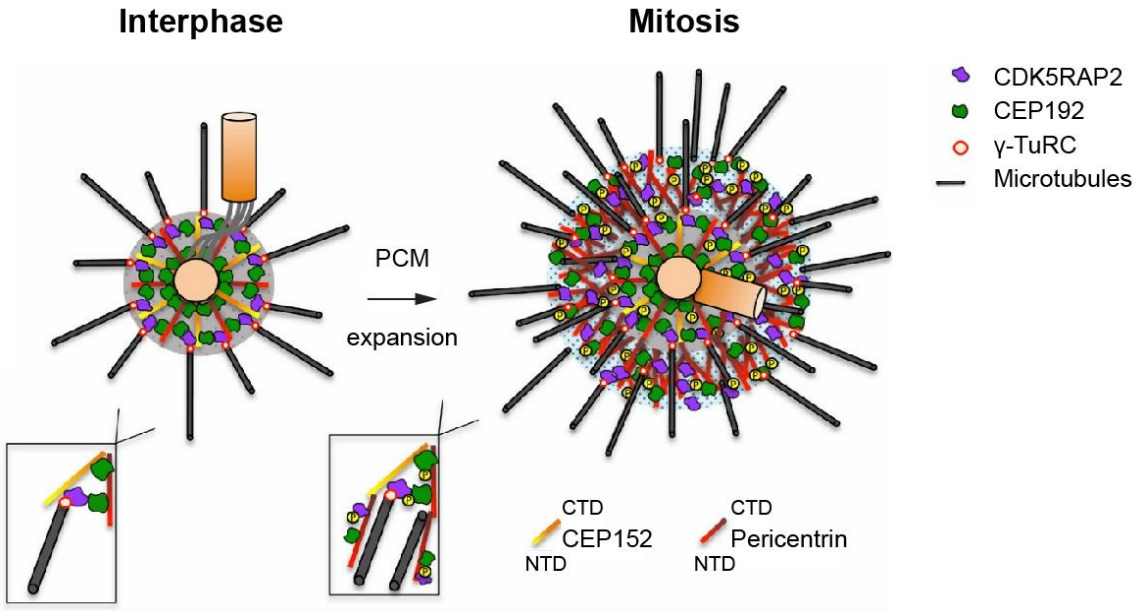

Figure 1.12 Schematic structure of the centrosomal PCM.

Figure shows a simplified overview of the centrosome structure. The well-structured interphase centrosome shown on the left. The expanded PCM during mitosis shown on the right, as a result of phosphorylation by PLK1 of multiple PCM components, such as Pericentrin, CDK5RAP2 and CEP192. Taken from (Fry et al., 2017).

During centrosome maturation, PCM expansion is driven by PLK1 and Aurora A kinase activity (Barr & Gergely, 2007; Blagden & Glover, 2003; Mahen & Venkitaraman, 2012). Both kinases phosphorylate multiple PCM components and significantly increase recruitment of PCM proteins to the centrosome. Pericentrin is considered to be a main PCM scaffold protein. Its phosphorylation by PLK1 is thought to drive PCM expansion and recruitment of centrosomal proteins, such as CEP192, NEDD1, γ-tubulin, Aurora A, and PLK1 (K. Lee & Rhee, 2011). This is in line with work done in roundworm (*C.elegans*), where the PCM is described as a two component system, with a main scaffold recruiting other PCM components referred to as "PCM clients" (Woodruff et al., 2017).

Compared to the interphase PCM, mitotic PCM expands in both volume and microtubule nucleation capacity (Fry et al., 2017). While it stays spherical around the centrioles, it becomes less ordered at the level of molecular structure (Figure 1.12). How an organelle that undergoes significant expansion can determine its size and shape without a well-defined boundary such as a lipid-membrane remained unclear until recently. *In vitro* studies of *C. elegans* PCM component SPD-5 (CDK5RAP2 analogue), suggested that recombinant SPD-5 has the ability to phase separate and form PLK1-dependent micron-scale droplets (Wueseke et al., 2016). This work led to the theory that the expanded mitotic PCM could be considered a macromolecular condensate that forms a compartmentalised unit during mitosis (Woodruff et al., 2017). While this seems to be an attractive model to explain PCM expansion and dynamics, further assessments *in vivo* and *in vitro* reconstitution systems are required to investigate whether phase-separation could explain PCM formation in different species.

Centriolar satellites (CS)

So-called centriolar satellites (CS) that form cytoplasmic granules (membraneless, 70-100 nm in size) (Figure 1.13.B) are relevant to the organisation and integrity of the centrosome (Hori & Toda, 2017). These dynamic structures, predominantly localised around the centrosome, were first identified in the 1960s (Bärenz et al., 2011) and have also been observed around basal bodies during ciliogenesis (Anderson & Brenner, 1971; Dirksen, 1991; Sorokin, 1968; Steinman, 1968). The first main component in human interphase cells, pericentriolar material-1 (PCM1)[7] was identified in 1994 (Figure 1.13) (R Balczon et al., 1994; R Balczon & West, 1991). PCM1 is considered to be the fundamental scaffold protein of CS. In line with this, PCM1 depletion results in disassembly of CS granules (Tollenaere et al., 2015). PCM1 is a large, coiled coil protein containing 8 predicted coiled-coil motifs that are thought to mediate most of its interactions with other proteins (Tollenaere et al., 2015). While the mechanism of CS assembly is not known, PCM1 also contains an oligomerisation motif, suggesting that it may serve as the main assembly factor and carrier protein.

CS localisation and transport is microtubule-dependent (Figure 1.13.A). Using live cell imaging techniques, PCM1 labelled CS granules showed dynamic movement along microtubule fibres originating from the centrosome and PCM1 *in vitro,* and also co-purified with microtubules (Ron Balczon et al., 1999; Kubo et al., 1999a). In line with this, microtubule depolymerisation leads to dispersion of CS granules in the cytoplasm (Dammermann & Merdes, 2002; Kubo et al., 1999a; Kubo & Tsukita, 2003). It has since been established that, at least in part, centrosome-directed CS movement is mediated by dynein-dynactin motor proteins. A number of CS components, such as BBS4, Par6α, CEP72 and CEP290 have been shown to facilitate the direct interaction between CS and the dynein complex (Hori & Toda, 2017; Kim et al., 2004; Kim et al., 2008; Kodani et al., 2010b; Stowe et al., 2012).

---

[7] Pericentriolar material-1 (PCM1): 2024 amino acids, 228.544 kDa
Contains eight central coiled-coil repeats essential for its molecular activity as a scaffold protein.
Source: UniProtKB

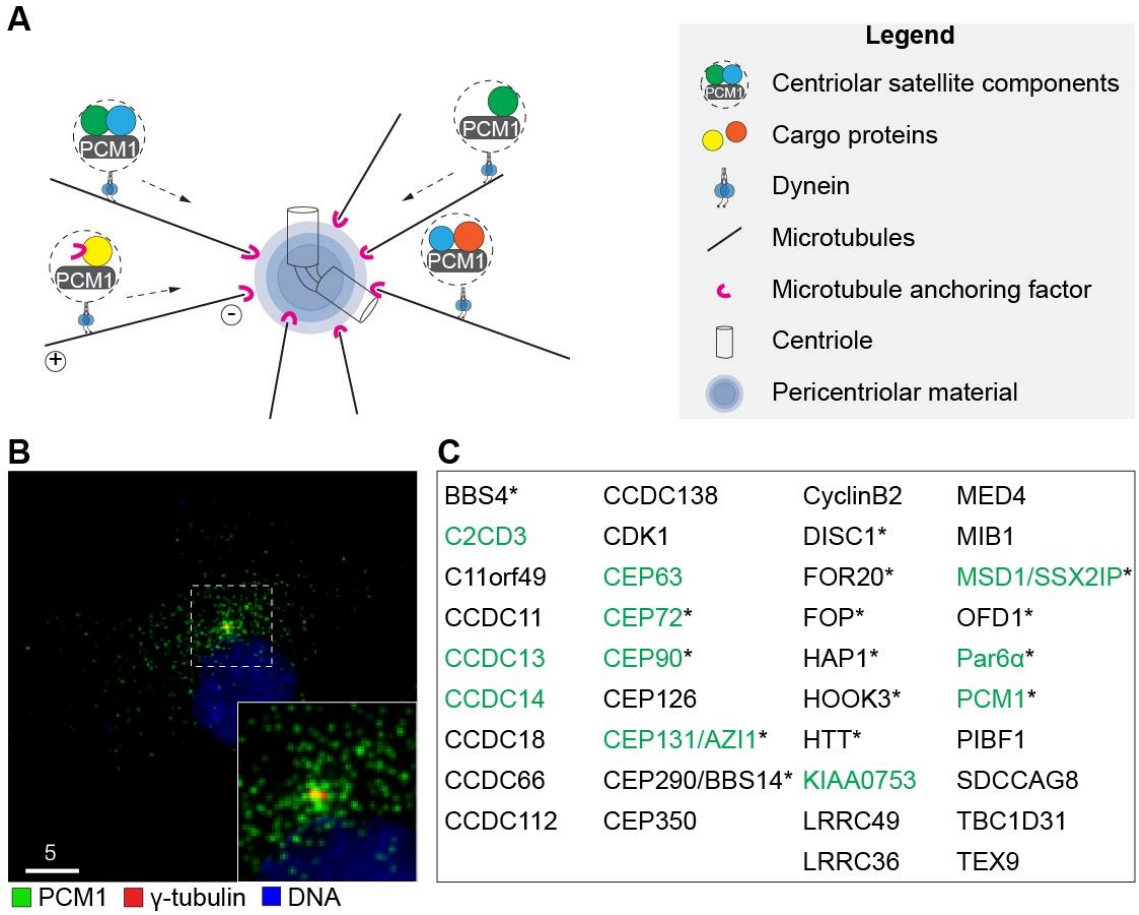

Figure 1.13. Centriolar satellite components.

(A) Schematic representation of centriolar satellite (CS) movement along the microtubules via dynein motor protein. (B) Immunofluorescence image of human interphase cell (h-TERT-RPEI), labelled for centriolar satellites (green, PCM1) around the centrosome (red, γ-tubulin) (Hori & Toda, 2017). (C) Selected examples of centriolar satellite proteins. Those highlighted in green have known functions for centrosome maintenance and maturation. Those highlighted with an asterix (*) are important for either the structural integrity or the localisation of CS granules (Tollenaere et al., 2015). Modified from (Hori & Toda, 2017).

Over a hundred different proteins have been identified to localise to the CS since its first discovery (examples shown in Figure 1.13.C). While its main cellular function as a cargo transport between the cytoplasmic and centrosomal pool of proteins is still valid, a number of novel functions have also been identified that are relevant not only for centriole replication and centrosome maturation, but also for maintaining centrosome proteostasis, microtubule organisation and spindle pole integrity (Hori & Toda, 2017). Indeed, with the exception of PCM1, CS proteins are also found to localise to centrosomal sites. The first components shown to be transported via the CS to the centrosome were Centrin, Pericentrin and Ninein (Bärenz et al., 2011; Dammermann & Merdes, 2002). This initial study also revealed an important functional role of CS for microtubule organisation at the centrosomes, as mislocalisation of Ninein after PCM1 knockdown leads to microtubule anchoring defects (Dammermann & Merdes, 2002). Other CS components, such as FOP and MSD1/SSX2IP have also been shown to be involved in microtubule tethering (Hori & Toda, 2017). More recent studies revealed that some centrosomal protein concentrations (OFD1 and CEP290) are not affected by the absence of the CS pool, suggesting that these proteins may be required for the integrity of the CS but use different centrosome targeting mechanisms (Kim et al., 2008; Lopes et al., 2011). Other examples demonstrated that CS may also act as a storage site, and in its absence, an increase in centrosomal concentration of CEP72 and CEP90 was detected (K. Kim & Rhee, 2011; Oshimori et al., 2009; Tollenaere et al., 2015). Other components of the CS have been found to have a potential function for spindle pole integrity (CEP72, Par6α and CEP90) (Tollenaere et al., 2015).

At the protein level, PCM1 remains unchanged, however, the number of granular structures labelled by PCM1 and their association with the centrosome shows variability throughout the cell cycle (Hori & Toda, 2017). The highest levels of CS granules are observed during interphase and these significantly decrease during M phase, thus suggesting that CS organisation is regulated by the cell cycle. While the mechanisms of CS assembly and disassembly are not known, PCM1 was found to have a number of phosphorylation sites (Hori et al., 2016). One such site was shown to be phosphorylated by PLK4 (S372), regulating self-dimerisation of PCM1 as well as interaction with other CS components (BBS4 and CEP290). In addition to PLK4, PCM1 is also a CDK1 and PLK1 substrate (Hori et al., 2016; Hori & Toda, 2017). Based on these findings, one may

speculate that CDK1 and PLK1 driven phosphorylation at early M-phase may mediate CS disassembly, while PLK4 phosphorylation during G1 phase promotes CS assembly. This is also in line with previous findings that PLK4 is the master regulator of centrosome duplication during interphase, while CDK1 peaks in early mitosis (Hori & Toda, 2017).

Centriolar satellites are considered to be an essential accessory domain of the centrosome, but their role in centrosome-free meiotic cells is not characterised. Part of this thesis aims to describe the localisation of some of these CS components in mouse and human oocytes and investigate the role of the main CS scaffold protein, PCM1 (Chapter 3: Results Part I).

1.5.4.2 Acentriolar MTOCs during meiosis

The centrosome is considered to be the main MTOC in animal cells, but oocytes of many animal species eliminate their centrioles and form MTOCs in their absence; these are referred to as acentriolar MTOCs (aMTOCs) (Figure 1.10). In mouse oocytes, centrioles are lost early during oogenesis and centrioles are no longer detectable after pachytene stage (Manandhar et al., 2005; Szollosi et al., 1972).

Centriole elimination is a poorly understood process and our current knowledge of the different steps is based on fly (*Drosophila*) oocytes (Mogessie et al., 2018; Pimenta-Marques et al., 2016). During the initial stages, the centriolar aggregates lose their pericentriolar material and their ability to nucleate microtubules. Prior to meiotic resumption, the centriolar proteins disperse into the cytoplasm and can no longer be detected. It appears that the timing of centriole elimination differs between different species. While centrioles can only be detected in mammalian and insect oocytes until the pachytene stage, starfish and crayfish oocytes degrade them only during meiosis I (Longo & Anderson, 1969; Ruthmann, 1959; Sluder et al., 1989).

Although why centriole elimination is evolutionarily favoured in female gametes is not fully understood, a number of theories have been proposed for its significance (Manandhar et al., 2005; Mogessie et al., 2018). In species where the sperm brings a pair of centrioles during fertilization (sheep (Crozet, 1990), bull (Sutovsky et al., 1996), rhesus monkey and human (Sathananthan et al., 1996; Zamboni & Stefanini, 1971)), it is

thought that the male centrioles organise the maternal centrosomal proteins into a functional centrosome, which ensures balanced centrosome numbers (Manandhar et al., 2005). In the special case of rodents however, the sperm does not contribute a pair of centrioles upon fertilisation and the embryos rely on *de novo* centrosome formation from the maternal pool of centrosomal proteins, which happens gradually as the embryos reach the blastocyst stage (Clift & Schuh, 2013; Courtois et al., 2012). It has also been suggested that the absence of centrosome nucleated astral microtubules is important for the asymmetric positioning of spindles to facilitate extrusion of a small polar body in the oocyte, as well as to avoid problems with centriole numbers due to lack of S phase between the two subsequent meiotic division during oocyte maturation (Figure 1.2) (Manandhar et al., 2005; Mogessie et al., 2018). In fact, in the absence of centrosomes, microtubule fibres emanating from the spindle poles into the cytoplasm can be observed in mouse oocytes. However, the plus-ends are mostly incorporated into the barrel-shaped spindle and elongate to form astral-like microtubules towards the oocyte cortex to aid in spindle positioning (Schuh & Ellenberg, 2007).

As a direct consequence of centriole elimination, oocytes adopted a unique, centriole free organisation of microtubules in the form of aMTOCs that have the ability to nucleate microtubules and organise the spindle microtubules into a bipolar structure (Figure 1.10). The mechanism by which aMTOCs can form bipolar spindles in the absence of the main PCM organisers, the centrioles, is an intriguing question. Transcriptomic, proteomic and immunofluorescence studies have established that oocytes contain a large number of centrosomal proteins (Evsikov & Evsikova, 2009; Łuksza et al., 2013; Schuh & Ellenberg, 2007; Su et al., 2004; S. Wang et al., 2010; Yan et al., 2013; Zhang et al., 2009). In mouse oocytes, PCM core components, Pericentrin, γ-tubulin, CEP192 and CDK5RAP2 form small aMTOC foci that join during spindle formation to organise the two spindle poles (section 1.7, p56) (Dziugiel, 2015; Schuh & Ellenberg, 2007). On the other hand, no microtubule organisers have been detected in human oocytes to date (section 1.8, p60) (Holubcová et al., 2015; Mogessie et al., 2018). A number of studies have investigated the assembly, fragmentation and reorganisation of these aMTOCs to form the meiotic spindle; however, a large number of centrosomal proteins, including those forming the centriolar satellites and pericentriolar material have not been investigated in detail during meiosis. Therefore, my aim was to understand how some of

these centrosomal proteins that are found to be highly expressed in both mouse and human oocytes are organised and to investigate their roles in meiotic spindle assembly and maintenance (Chapter 3: Results Part I and Chapter 4: Results Part II).

1.6 Spindle assembly pathways

The microtubule cytoskeleton undergoes dramatic reorganisation during the cell cycle. Notably, as oocytes resume meiosis, the nuclear envelope disassembles and microtubule fibres are quickly assembled to form the dense spindle structure.

In vitro, microtubule assembly can occur spontaneously above a critical threshold of αβ-tubulin dimers (Wiese et al., 2006). However, under physiological conditions, microtubule nucleation is kinetically not favoured, and cells modulate microtubule assembly by recruiting nucleation factors to specific intracellular sites. Three main nucleation pathways are known to contribute to spindle assembly (Figure 1.14). These pathways associate with specific spindle components, namely MTOCs, chromosomes and pre-existing microtubules (Figure 1.14).

Across all species studied, γ-tubulin is considered an essential microtubule nucleation factor that forms a multi-subunit γ-TuRC thought to act as a microtubule template (Wiese et al., 2006). γ-TuRC is formed of various gamma complex proteins (GCPs 2-6). γ-tubulin can also associate with GCP2 and GCP3 alone, to form a smaller complex, γTuSC (γ-tubulin small complex) (Raynaud-Messina & Merdes, 2007; Wiese et al., 2006). Studies showed that the microtubule nucleation activity of γ-tubulin complexes has an essential role in spindle formation and structure across different species (Job et al., 2003; Raynaud-Messina & Merdes, 2007). Apart from the main microtubule nucleation pathways, other spindle assembly factors (SAFs, e.g. TPX2 and HURP) and microtubule associated proteins (MAPs, e.g. TACC3-ch-TOG) all contribute to spindle assembly and regulation of microtubule dynamics (section 1.5.2, p28) (Prosser & Pelletier, 2017).

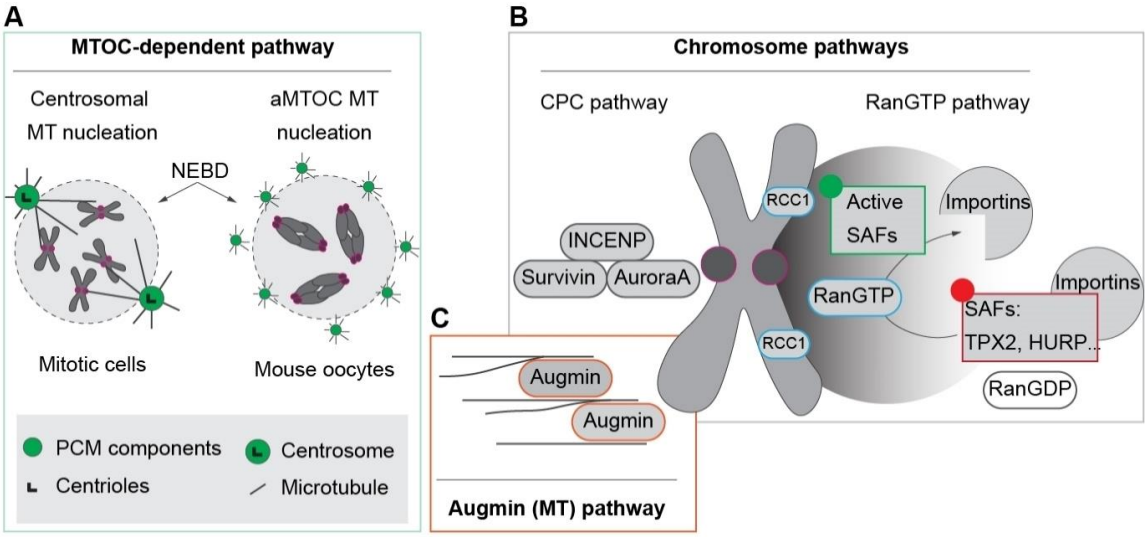

Figure 1.14 Main microtubule nucleation pathways.

(A) MTOC-dependent microtubule (MT) nucleation pathway in the centrosomal mitotic cells and acentrosomal mouse oocytes. (B) Chromosome pathways activated at kinetochores (CPC pathway) and chromatin (RanGTP pathway). (C) Augmin pathway, mediate low-angle, branched microtubule nucleation on the sides of pre-existing microtubules. Modified from (Bennabi et al., 2016)

1.6.1 MTOC-dependent microtubule nucleation pathway

MTOCs are considered to be the dominant pathway for microtubule nucleation. Recruitment of γ-TuRCs to PCM of MTOCs is well characterised and a number of adaptor proteins that are thought to anchor γ-TuRCs at these sites have been identified (e.g. AKAP9, Pericentrin, NEDD1 and CDK5RAP2) (Petry & Vale, 2015).

The ‘search and capture’ model has been proposed for spindle assembly and attachment of chromosomes (Heald & Khodjakov, 2015). According to this model, the plus-end microtubule fibres emanating from the MTOCs probe (‘search’) the cytoplasm until it finds a kinetochore (‘capture’) on the chromosome (Figure 1.14.A). The kinetochore-microtubule attachment is then stabilised and forms the K-fibre. Once the kinetochores are captured from the opposite poles, the pulling forces are balanced, and the chromosomes are aligned on the metaphase plate at spindle equator (Figure 1.9).

1.6.2 Chromosome nucleation pathways

Several studies have demonstrated that following removal of MTOCs, microtubules can still nucleate and form a bipolar spindle, suggesting that other, centrosome-independent nucleation pathways are active (Khodjakov et al., 2000; Mahoney et al., 2006). Assembly of spindle-like structures around DNA coated beads in centrosome-free frog egg extracts demonstrated the presence of a chromatin mediated nucleation pathway for the first time (Heald et al., 1996). Since its discovery, two distinct chromosome nucleation pathways have been described, namely RanGTP-dependent and chromosomal passenger complex (CPC)-dependent pathways (Figure 1.14.B).

RanGTP-dependent pathway

The small GTPase Ran is activated by a guanine nucleotide exchange factor, RCC1 that is localised on chromatin (Ohtsubo et al., 1989). Activated RanGTP diffuses away from the chromosomes, creating a gradient that locally activates various spindle assembly factors (SAFs) that mediate microtubule assembly (Figure 1.14.B). A number of SAFs that contain nuclear localisation signal (NLS) are blocked by importins. Activated RanGTP dissociates the importin bound complex that in turn releases the SAF to promote spindle assembly (Kalab & Heald, 2008; Kaláb et al., 2006). One important SAF regulated by RanGTP is TPX2 (Gruss & Vernos, 2004). TPX2 plays an important role in promoting early microtubule assembly around chromosomes.

The role of Ran-mediated microtubule nucleation is conserved from yeast to mammalian oocytes (Askjaer et al., 2002; Cesario & McKim, 2011; Dumont et al., 2007; Fleig et al., 2000). In particular, RanGTP was shown to have an essential role in spindle assembly in human oocytes where no prominent MTOCs are detected (section 1.8, p60) (Holubcová et al., 2015; Mogessie et al., 2018). On the other hand, experiments in mouse oocytes, where aMTOCs are present indicate that RanGTP inhibition does not block spindle assembly completely (Bury et al., 2017; Dumont et al., 2007; Schuh & Ellenberg, 2007). This suggests that the RanGTP pathway only partially contributes to spindle assembly in the presence of MTOCs.

CPC-dependent pathway

The CPC-dependent microtubule nucleation pathway is often referred to as the kinetochore pathway, due to its localisation at the inner centromeres. The CPC complex is composed of INCENP, Survivin, Borealin and Aurora B kinase (Figure 1.14.B) (Sampath et al., 2004). *In vitro* experiments using frog egg extracts demonstrated that in the absence of MTOCs and RanGTP, CPC coated beads can promote microtubule assembly and form spindle-like structures (Kelly et al., 2007; Maresca et al., 2009). It has an essential role in activating the spindle assembly checkpoint and amendment of incorrect kinetochore-microtubule attachments (Trivedi & Stukenberg, 2016).

1.6.3 Microtubule-dependent microtubule nucleation pathway

Microtubule-dependent microtubule nucleation is essential to form and maintain the highly dynamic spindle microtubules (Goshima & Kimura, 2010). This autocatalytic mechanism leads to microtubule amplification and is responsible for producing a dense array of spindle microtubules with varying length between interpolar microtubule fibers. This mechanism supplements the other microtubule nucleation pathways and contributes to spindle assembly, chromosome alignment and spindle stability.

The Augmin-complex identified in the fly S2 cell line via large-scale RNA interference screens and quantitative image analysis, was the first pathway to demonstrate an autocatalytic model dependent on pre-existing microtubules (Goshima et al., 2008, 2007; Kamasaki et al., 2013). However, more recently a novel form of oocyte specific microtubule-dependent microtubule nucleation pathway was reported in fly oocytes that is uniquely driven by a kinesin motor protein, kinesin-6, Subito/MKlp2 (Das et al., 2018, 2016; Radford et al., 2017; Romé & Ohkura, 2018). It is proposed that these two microtubule-dependent microtubule nucleation pathways (Augmin- and Subito/MKlp2-dependent pathways) act complementary by recruiting γ-TuRCs to spindle microtubules (Romé & Ohkura, 2018).

Augmin-dependent pathway

The Augmin protein complex, made up of eight subunits (HAUS 1-8) mediates nucleation of branched microtubules (Goshima et al., 2008; Kamasaki et al., 2013). Via direct interaction with the γ-TuRC component NEDD1, Augmin complexes recruit γ-

TuRCs to the lateral aspect of spindle microtubules and supplement the other nucleation pathways (Figure 1.14.C) (Hayward et al., 2014). Apart from its important role in bipolar spindle assembly (Colombié et al., 2013; Wainman et al., 2009), Augmin was also shown to have an essential role in central spindle assembly during anaphase (Uehara & Goshima, 2010; Uehara et al., 2009).

Subito/MKlp2 -dependent pathway

Subito/MKlp2 belongs to the plus-end directed kinesin-6 family of motor proteins with microtubule bundling activity that localises to the central spindle (Neef et al., 2003). It is known to have an essential role in forming the central spindle and required to maintain a robust bipolar structure during meiosis (Giunta et al., 2002; Jang et al., 2005). In a recent study carried out in out in fly oocytes, Subito was shown to mediate a novel microtubule nucleation pathway specific to oocytes, via its interaction with Grip71/NEDD1 to recruit γ-TuRC to the central spindle (Romé & Ohkura, 2018). This nucleation capacity of Subito was also shown *in vitro*, where the Subito/Grip71 complex could nucleate microtubules from αβ-tubulin subunits (Romé & Ohkura, 2018). Microtubule nucleation activity was shown to be regulated via the N-terminal domain, by reducing its efficiency to bind γ-TuRC and restrict its activity to the vicinity of the chromosomes (Das et al., 2018; Romé & Ohkura, 2018).

The authors propose a model that is unique to oocytes, where the Augmin-pathway at the spindle poles and the Subito-pathway at the central spindle recruit γ-TuRCs to microtubules and complement each other to form a highly dense and stable bipolar spindle. All components identified in fly oocytes are widely conserved (Laurence; Haren et al., 2006; Jang et al., 2005; Kollman et al., 2011) and suggest that this Subito-driven novel nucleation pathway may function in oocytes of other species to assemble a robust acentrosomal spindle.

1.7 Acentrosomal spindle assembly in mouse oocytes

Mouse oocytes are one of the best studied models for the assembly and function of aMTOCs as well as meiotic spindle assembly. Since the first study that paved the way for high resolution live imaging in oocytes over a decade ago (Schuh & Ellenberg, 2007), we now have a more detailed understanding of the mechanistic of aMTOC formation and its

role in spindle assembly as well as the processes that govern mouse oocyte maturation (Figure 1.15).

Pericentriolar material components, such as γ-tubulin, Pericentrin, CEP192, and the γ-TuRC adaptor protein NEDD1 are known to associate with the aMTOC foci (Clift & Schuh, 2015; Łuksza et al., 2013; Ma et al., 2010; Ma & Viveiros, 2014; Schuh & Ellenberg, 2007). Both immunofluorescence and live cell imaging studies of mouse oocytes suggest that aMTOCs contribute to meiotic spindle assembly (Maro et al., 1985; Schuh & Ellenberg, 2007; Van Blerkom, 1991). Unlike mitotic cells, where the duplicated centrosomes (during S phase) are the two dominant sites of microtubule nucleation forming and stabilising the bipolar spindle structure, mouse oocytes form multiple aMTOCs *de novo* via remodelling the interphase-like microtubule network (Schuh & Ellenberg, 2007). These aMTOCs start microtubule nucleation following exit from prophase arrest both at cytoplasmic sites and around the nuclear envelope (Figure 1.15) (Schuh & Ellenberg, 2007). Their capacity to nucleate microtubules was shown to be comparable to that of centrosomes (Schuh & Ellenberg, 2007), supporting the idea that centrioles are structural pillars of the centrosome and the PCM is responsible for nucleation capacity.

A stable bipolar spindle is formed within three-to-four hours after NEBD, while chromosome biorientation and formation of a stable metaphase plate is only established towards the end of meiosis I (Brunet et al., 1999; Kitajima et al., 2011).

In mouse oocytes, bipolar spindle formation is driven by two rounds of aMTOC fragmentation, which allows the redistribution of smaller aMTOC foci, followed by clustering of multiple aMTOCs to form the two main spindle poles (Figure 1.15) (Clift & Schuh, 2015; Łuksza et al., 2013; Schuh & Ellenberg, 2007). Prior to NEBD, PLK1 decondenses aMTOCs (increase in volume and decrease in density) and the dissociation of C-Nap1 from aMTOCs marks the onset of the first round of aMTOC fragmentation (Clift & Schuh, 2015). In fact, this mechanism is remarkably similar to that adapted by mitotic cells, where C-Nap1 was found to act as the main centrosomal linker protein (Figure 1.11) and as the cell enters mitosis , PLK1 activity dissociates C-Nap1 and the centrosomes begin to separate and form opposite spindle poles (Mardin et al., 2011; Mardin & Schiebel, 2012). The first phase of aMTOC fragmentation is driven by the

minus-end motor protein dynein (section 1.5.2.6, p35). Dynein is recruited to the nuclear envelope via its adaptor protein, BicD2 (section 1.5.2.6, Table 1.1), where it is responsible for stretching and fragmenting aMTOCs (Clift & Schuh, 2015; Łuksza et al., 2013). Following NEBD, the motor protein KIF11 (Eg5) further fragments aMTOCs (Figure 1.15) (Clift & Schuh, 2015). While the first phase of aMTOC fragmentation does not seem to be essential for bipolarisation, inhibition of the second phase results in severe bipolar spindle defects, with assembly of transient monopolar spindles (Clift & Schuh, 2015).

The sudden increase in microtubule number following NEBD was found to be dependent on RanGTP activity (Schuh & Ellenberg, 2007). As a result, a multipolar microtubule ball is formed, on the surface of which the chromosomes are individualised (Schuh & Ellenberg, 2007). Driven by the motor activity of KIF11 that slides antiparallel microtubules apart (section 1.5.2.4, p32), the spindle elongates into a bipolar structure and the aMTOCs are redistributed to the two poles. This aMTOC sorting involves HURP activities (Balboula et al., 2016; Breuer et al., 2010). HURP is a microtubule associated protein that is responsible for K-fibre stabilisation (Koffa et al., 2006; Silljé et al., 2006). During meiosis, the Ran-effector HURP is not only essential for aMTOC sorting but also for the formation of central microtubules around the chromosomes (Breuer et al., 2010). Once at the spindle poles, aMTOCs merge to form a characteristic ring-like or flattened cluster of aMTOCs (Clift & Schuh, 2015; Mogessie et al., 2018; Schuh & Ellenberg, 2007). The merging of aMTOC foci along with the activity of the minus-end anchor protein NuMA and dynein (section 1.5.2, p28) stabilises the two spindle poles to form the characteristic barrel shape (Figure 1.15) (Merdes et al., 1996).

The cytoskeleton component actin (F-actin) has been implicated in a number of oocyte related functions, including cytoplasmic vesicle transport, positioning of the spindle and cytokinesis (Azoury et al., 2008, 2009; Sybille Pfender et al., 2011; Schuh & Ellenberg, 2008). In a recent study, prominent actin filaments were shown to infiltrate the entire meiotic spindle (spindle actin) in mammalian oocytes (mouse, pig, sheep and human) (Mogessie & Schuh, 2017). In terms of morphology, these actin filaments look very similar to the microtubule spindle and becomes prominent at late MI. Functional studies combined with live cell imaging revealed that the actin spindle is important for K-fibre

integrity, and when depolymerised, causes chromosome segregation defects in both MI and MII divisions.

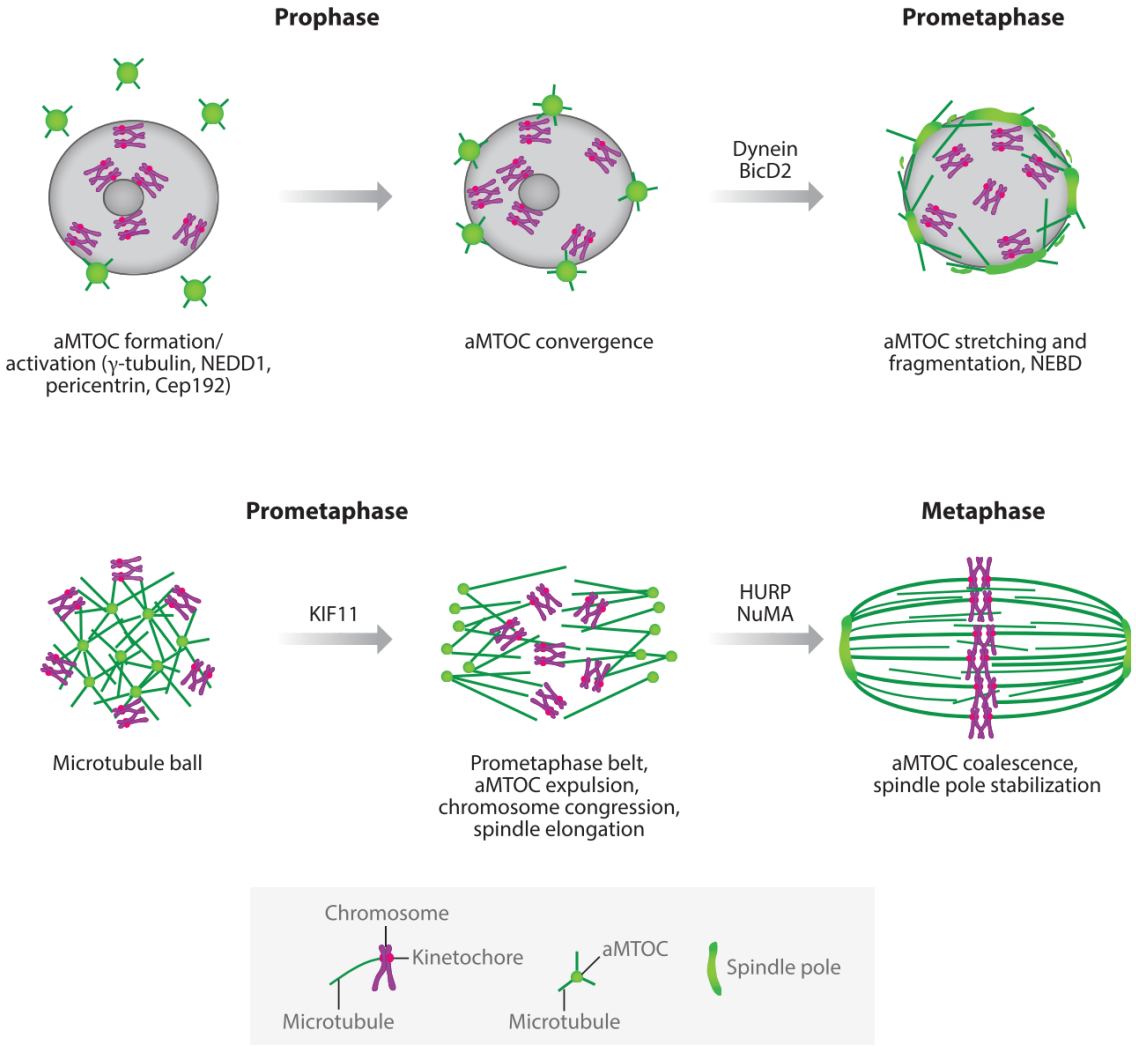

Figure 1.15 Schematic representation of acentriolar spindle assembly and bipolarisation in mouse oocytes.

At prophase, following resumption of meiosis, acentriolar microtubule organising centres (aMTOCs) converge around the nuclear envelope and start nucleating microtubule asters. aMTOCs associated with the nuclear envelope are stretched and fragmented via the BicD2-dynein complex. Following nuclear envelope breakdown (NEBD), a microtubule ball forms, the surface of which is decorated with the chromosomes. The aMTOCs are further fragmented and redistributed to the two poles by KIF11 motor activity, during spindle bipolarisation, while the chromosomes for the prometaphase belt. As the aMTOCs at the two poles coalesce, the bipolar spindle is stabilised and chromosomes are aligned on the metaphase plate, mediated by the microtubule-associated proteins nuclear mitotic apparatus (NuMA) and hepatoma-upregulated protein (HURP) (Mogessie et al., 2018).

1.8 MTOC free spindle assembly in human oocytes

The study of meiosis in human oocytes has lagged behind compared to all other animal models due to the low availability of human samples and the lack of microscopy assays (Mogessie et al., 2018). While animal models have proven to be powerful tools to understand the principles and mechanisms that govern meiosis, it is known that meiotic errors are more frequently observed in human oocytes than in any other cell types studied (e.g. mitotic and sperm cells) (Kolano et al., 2012; Nagaoka et al., 2012; Webster & Schuh, 2016). Aneuploidy in human eggs as a result of meiotic defects is one of the leading causes of pregnancy loss and congenital defects such as Down Syndrome (Nagaoka et al., 2012; Webster & Schuh, 2016). Therefore, the detailed investigation of meiosis in human oocytes directly is of immense benefit to human fertility.

Until recently, our understanding of human oocyte maturation mostly came from snapshot immunofluorescence observations. Advances in live-cell imaging enabled the detailed study of spindle assembly and chromosome segregation in live human oocytes (Holubcová et al., 2015). Overall, human oocyte maturation takes much longer (bipolar MII spindle formation from NEBD: 23.0 ± 3.2 h) (Holubcová et al., 2015) compared to mouse oocytes (bipolar MII spindle formation from NEBD: ~11 h) for instance. Following NEBD, microtubule nucleation is delayed for several hours (onset of microtubule nucleation from NEBD: 4.7 ± 1.4 h) (Holubcová et al., 2015). Microtubules begin to assemble within chromosomal aggregates and at distinct sites around kinetochores. Human oocytes also express a large number of centrosomal proteins (Yan et al., 2013; Zhang et al., 2009), but no prominent MTOC or PCM foci have been observed. This finding suggested that human oocytes rely completely on microtubule nucleation mechanisms that are independent of MTOCs. Indeed, functional studies revealed that inhibiting the RanGTP pathway prevented oocytes from assembling meiotic spindles (Holubcová et al., 2015). One striking observation from live cell imaging was that these small, MTOC free spindles that showed broad spindle poles and small overall volume (Figure 1.10) are highly unstable and frequently form multipolar intermediates. This spindle instability was directly linked to error-prone kinetochore-microtubule attachments, leading to lagging chromosomes during anaphase (Holubcová et al., 2015). Considering the importance of oocyte maturation for human fertility, more information is

required to understand the error-prone nature of the human spindle apparatus. It is also evident that the mouse model is not directly comparable both in spindle morphology and spindle assembly mechanism, and therefore direct studies in human oocytes is essential to further dissect this rather fragile mechanism.

1.9 Objectives

The mechanism of spindle microtubule assembly and its function is of fundamental importance for the inheritance of genetic material. In the context of oocytes, the correct segregation of chromosomes represents an essential point for reproduction.

Microtubule organising centres (MTOCs) are key co-ordinators and regulators of spindle microtubules. Animal cells contain centrosomes, the main microtubule organising centres (MTOCs) that define the focused spindle poles during mitosis. Though centrosomes are highly efficient microtubule nucleation platforms and have a key role in the organisation of the mitotic spindle poles, they are dispensable for bipolar spindle assembly (Chavali et al., 2015; Hinchcliffe et al., 2001; Khodjakov et al., 2000). Mouse oocytes eliminate their centrioles early on during oogenesis (Manandhar et al., 2005) and form acentriolar MTOCs (aMTOCs) *de novo* that contain main pericentriolar proteins (Calarco, 2000; Carabatsos et al., 2000; Schuh & Ellenberg, 2007). Mouse oocyte spindles are barrel-shaped, with a distinctly different spindle pole morphology compared to the focused mitotic spindles, suggesting that these cells adopted different mechanism(s) for spindle assembly and pole focusing (Bennabi et al., 2016). Interestingly, a large number of centrosomal proteins are highly expressed throughout oocyte maturation (Pfeiffer et al., 2011; Virant-Klun et al., 2013; S. Wang et al., 2010; Yan et al., 2013; Zeng et al., 2004). We already have a good understanding of how some of the core PCM proteins self-organise into acentriolar MTOC (aMTOC) foci in mouse oocytes (Clift & Schuh, 2015; Łuksza et al., 2013; Schuh & Ellenberg, 2007). However, we still do not have a full understanding of how such centrosome free spindles are organised and function.

Another interesting question comes from spindle assembly mechanisms where all prominent MTOCs are absent, such as in human oocytes (Holubcová et al., 2015). We only recently gained a detailed insight into the assembly and dynamics of these spindles that are known to be highly prone to meiotic errors (Webster & Schuh, 2016). Notably, human oocyte spindles have a prolonged assembly period with a high frequency of spindle instability (Holubcová et al., 2015). These highly unstable spindles were found to correlate with an increased frequency of lagging chromosomes. This was a rather interesting finding as both mitotic spindles and aMTOC organised meiotic spindles do not show such intrinsic instability and can form robust, bipolar spindle structures. These

cells also show a much lower incidence of segregation errors, compared to human oocytes (Nagaoka et al., 2012; Pacchierotti et al., 2007; Templado et al., 2011). However, mitotic cells devoid of centrosomes could form bipolar spindles, although their assembly period was delayed and resulted in a high rate of chromosomal instability (Chavali et al., 2015; Sir et al., 2013).

Based on the above points, we hypothesised that centrosomal proteins could also have important roles during meiosis. Considering the vast number of proteins required for centrosome assembly and function, there is very little knowledge about how the different centrosomal components and appendages may contribute to spindle assembly and function during meiosis. It is possible that in the absence of centrioles that define the centrosome structure, these proteins adopted additional mechanism(s) and arrangements that are unique to meiotic cells. Perhaps some specialised mechanism(s) exist uniquely in mouse oocytes that can achieve a much more stable bipolar structure, compared to the unstable spindle structure of human oocytes.

The overarching goal of my PhD was to characterise centrosomal proteins in the acentrosomal mouse spindle. Following the discovery of a unique, spindle domain in mouse oocytes, initially thought to form by centriolar satellite proteins, my main focus was to characterise the localisation, function and dynamics of this domain during meiosis. This work was initially narrowed down to the main centriolar satellite scaffold protein, PCM1 (Chapter 3: Results Part I) and later extended via a collaboration to other centrosomal proteins that we later on found to localise to this domain (Chapter 4: Results Part II). My second aim was to characterise centrosomal protein localisation in human oocytes directly and address our previous findings that showed the high instability of these spindles (Chapter 4: Results Part II). As human oocytes are highly sensitive to laser light and require much longer imaging intervals to capture their long maturation period, I also had a side project that focused on establishing light-sheet microscopy for the imaging of live human oocytes at our satellite lab at Bourn Hall Clinic (Chapter 5: Results Part III).

2 MATERIALS AND METHODS

2.1 Oocyte preparation and culturing

2.1.1 Mouse oocytes and follicles

According to the guidelines of the UK Home Office regulations and the animal facility of Max Planck Institute for Biophysical Chemistry, mice were bred and maintained in a pathogen-free environment. During this study the mouse strains used were either hybrid (C57BL x CBA) F1 for follicle culture or inbred FVB for fully grown oocytes.

2.1.1.1 Isolation of oocytes from FVB mice

Isolation of ovaries was performed from 8-12-week-old FVB mice. Ovaries were collected and punctured in 250 µM dibutyryl cyclic AMP (dbcAMP) (Sigma-Aldrich) containing (phenol red-free) M2 medium (homemade). This medium was also used to maintain fully-grown oocytes (~75 µm in diameter) in prophase arrest under paraffin oil (ACROS Organics) at 37^{o}C.

2.1.1.2 Isolation of follicle-enclosed oocytes from F1 mice

Follicles were isolated as previously described (S Pfender et al., 2015) from 10- to 12-day-old female (C57BL x CBA) F1 mice. GlutaMax (Gibco) supplemented MEM-alpha medium with 5% foetal bovine serum (FBS; Gibco), 1× insulin/transferrin/sodium selenite (ITS; Sigma-Aldrich), 0.01 µg/ml ovine follicle stimulating hormone (FSH; National Hormone and Peptide Program) and 0.1× penicillin G/streptomycin (Gibco) was used to culture follicles (~100 µm in diameter) on inserts coated with collagen (Corning) at 37^{o}C and 5% CO_2 in a humidified incubator. *In vitro* grown oocytes were matured in M2 medium with 10% FBS instead of 4 mg/ml BSA for 10-12 hours. 1 ml of medium was replenished after 4-5 days of culture.

2.1.2 Human oocytes

The use of unfertilised human oocytes has been approved by the UK National Research Ethics Service under the REC reference 11/EE/0346 (IRAS Project ID 84952). Oocytes were donated for research by patients who were undergoing assisted reproduction treatment in Bourn Hall Clinic, Cambridge, United Kingdom between January 2017 and May 2018. 66 oocytes from 38 women between the ages of 23 and 45 years old, who were undergoing ovarian stimulation for intracytoplasmic sperm injection (ICSI), took part in this study. The cause of infertility for these patients were due to male factor infertility, endometriosis, polycystic ovaries or polycystic ovarian syndrome, absence of a male partner, fallopian tube damage, idiopathic infertility or the combination of the above factors. All patients gave informed consent for the use of their oocytes and this study used only oocytes that did not mature fast enough and were thus not suitable for ICSI and *in-vitro* fertilization. Oocyte collection and culture was done as previously described (Holubcová et al., 2015). After retrieval of oocytes, samples were collected within 3-5 hours in G-MOPS medium (Vitrolife) supplemented with 10 % FBS (Gibco) and incubated under paraffin oil at 37^{o} C. The development of the oocytes was monitored using a Primo Vision EVO+ time-lapse camera (Vitrolife), which was installed inside the incubator. Oocytes at the MI stage were fixed at 15 hours post NEBD. This study used only oocytes that matured normally and had NEBD within 24 hours after retrieval and that displayed no morphological abnormalities. Frozen-thawed oocytes were only used for the initial Light-sheet optimisation.

2.1.3 Microinjections

Oocytes were microinjected as previously described (Jaffe & Terasaki, 2004; Schuh & Ellenberg, 2007) with 7pl of mRNA in mouse oocytes and 10-11pl mRNA in human oocytes (1-2 µg/µl mRNA). Follicle-enclosed mouse oocytes were microinjected with 6 pl of 2 µM siRNA in culture medium supplemented with HEPES (Sigma), as previously described (S Pfender et al., 2015). The fully-grown mouse oocytes were loaded into the injection chamber via a glass capillary, between two pieces of cover slips spaced by a single layer of double-sided tape. Both human oocytes and follicle-enclosed mouse oocytes were loaded in microinjection chamber prepared with two double stick tapes as spacer.

Mouse oocytes microinjected with mRNA were cultured at 37°C for 3–4 hours in M2 medium or M2 supplemented with 10% FBS (instead of BSA; *in vitro* grown oocytes from follicles) containing dbcAMP to allow efficient translation of the injected mRNA before resumption of meiosis. Prior to live cell imaging, mouse oocytes were washed in 6 x 20 µl of dbcAMP-free M2 medium. RanGTP inhibition in mouse oocytes were done by microinjection of reporter mRNAs first and following 3 hours of expression, second microinjection with 12 pl of 2 mg/ml His-RanT24N mutant protein (Cytoskeleton) with 1 mM DTT before oocytes were released into dbcAMP-free medium for imaging.

Human oocyte microinjections were performed in GMOPS supplemented with 10% FBS at 37°C in a custom designed environmental chamber (Digital Pixel, Biomedical Imaging & Microscopy) for Zeiss A1 inverted microscope, fitted with a microprocessor temperature controller (DP_MTC_2000), two vibration free heater modules (DP_150_VF) and P100 temperature sensor (DP_P100_TS).

2.1.4 Immunofluorescence

Mouse and human MI spindles were imaged after the respective oocytes have been incubated at 37ºC for approximately 6-7 and 15 hours after NEBD, respectively. Prior to imaging, oocytes were fixed in 100 mM HEPES (pH 7.0, titrated with KOH), 50 mM EGTA (pH 7.0, titrated with KOH), 10 mM MgSO4, 2% methanol-free formaldehyde and 0.5% triton X-100 at 37ºC for 30 min (mouse oocytes) or 60 min (human oocytes). Phosphate-buffered saline (PBS) supplemented with 0.5% triton X-100 (PBST) was used to extract fixed oocytes overnight at 4ºC. The samples were incubated in PBST supplemented with 3% BSA as a blocking agent overnight at 4ºC. Primary antibodies were added and the samples were incubated overnight at 4ºC (Table 2.1). Secondary antibodies were added after several washing steps with PBST at a final concentration of 20 µg/ml (1:400) and the samples incubated overnight for 2 hours at room temperature. Secondary antibodies were purchased from Molecular Probes and were Alexa Flour 405-, 488-, 568- or 647-conjugated anti-human IgG, goat IgG, mouse IgG, mouse IgM, rabbit IgG, rat IgG or sheep IgG. DNA staining was performed with Hoechst 33342 (Molecular Probes, 1:1000).

Table 2.1 Primary antibodies used.

Antibody name	Identifier	Reference/Origin/Supplier
rabbit anti-AKAP450	NBP1-89167	Novus Biological
rat anti-α-tubulin	MCA78G	Bio-Rad
mouse anti-γ-tubulin	T6557	Sigma-Aldrich
mouse anti-AURA	NBP2-50041	Novus Biological
rabbit anti-CDK5RAP2	ABE236	Merck Millipore
rabbit anti-CEP120	PA5-55985	Thermo Fisher Scientific
rabbit anti-CEP135	ab75005	Abcam
rabbit anti-CEP152	ab183911	Abcam
rabbit anti-CEP192	18832-1-AP	Proteintech
mouse anti-CLTC (clathrin)	610500	BD Biosciences
rabbit anti-CLTC (clathrin)	ab21679	Abcam
rabbit anti-CHTOG	PA5-59150/PA5-58763	Thermo Fisher Scientific
rabbit anti-HOOK3	NBP2-44279	Novus Biological
rabbit anti-KIZ	21177-1-AP	Proteintech
mouse anti-LIS1	H00005048-M03	Abnova
goat anti-MYO10	sc-23137	Santa Cruz Biotechnology
rabbit anti-NDE1	10233-1-AP	Proteintech
rabbit anti-NDEL1	H00081565-D01P	Abnova
mouse anti-NEDD1	H00121441-M05	Abnova
goat anti-DCTN1	AF5720-SP	R&D Systems
mouse anti-p150	612708	BD Bioscience

rabbit anti-PCM1	HPA023374	Sigma-Aldrich
rabbit anti-PCM1	(Dammermann & Merdes, 2002)	
mouse anti-pericentrin	611814	BD Biosciences
mouse anti-PLK1	ab17056	Abcam
goat anti-PLK4	NB100-894	Novus Biological
mouse anti-TACC3	H00010460-M02	Abnoa
rabbit anti-TACC3	ab134154	Abcam
mouse anti-TOP2A	MAB4197	Merck Millipore
rabbit anti-TPX2	NB500-170	Novus Biological

2.1.4.1 Phalloidin staining

Oocytes were fixed as described above (section 2.1.4). Following overnight extraction, F-actin was stained via Alexa Fluor 488 phalloidin (Molecular Probes; 0.33 mM /10 units/ml) in PBS, 0.1% Triton X-100, and 3% BSA for 2 hours at room temperature. Phalloidin staining was done as a separate step and was not mixed with other primary or secondary antibodies.

2.1.5 Drug treatment and washout

Drugs were purchased from Sigma-Aldrich as 1000x stocks in DMSO. Microtubule depolimerization experiments in mouse oocytes were performed with 1 or 10 µM Nocodazole in M2 medium or 10 µM colchemid in G-MOPS medium supplemented with 10% FBS. For Nocodazole regrowth experiments, oocytes were matured to the MI stage and washed with 10 µM Nocodazole containing M2 medium for 45-60 minutes, microtubule regrowth was initiated through the washout in Nocodazole-free M2 medium. Oocytes were fixed at specific time points following washout to assess microtubule regrowth in the different experimental groups. For F-actin depolymerisation, oocytes were treated with cytochalasin D (Calbiochem) at a final concentration of 5 mg/ml.

(Aurora A, PLK1 and PLK4 were inhibited with 500 nM MLN8237 (Selleckchem), 100 nM BI2536 (Selleckchem) and 5 µM centrinone (Tocris Bioscience), respectively. (Only relevant to additional experiments done by Chun So, as mentioned in the discussion).

2.1.6 Trim-Away in mouse and human oocytes

The antibodies used for Trim-Away were all tested for specificity using immunofluorescence imaging first (Table 2.2). Antibodies for microinjections were washed and concentrated as described previously (Clift et al., 2017). In brief, antibody is diluted in PBS to 450 µl final volume and loaded into the Amicon Ultra-0.5 100 KDa centrifugal filter devices (Millipore). Antibody is washed three more times in PBS in the Amicon Ultra-0.5 device and the final concentrated antibody is aliquoted in 2µl and snap frozen (stored at -80°C).

Trim-Away was performed in mouse GV oocytes by microinjecting 7 pl of mRNA (mouse Trim21 and other fluorescent reporters, Table 2.3) and 5-6 pl of antibody (Table 2.2) according to previously published protocols (Clift et al., 2017). Following mRNA injection, oocytes were incubated for 3-4 hours to allow sufficient expression. Antibodies were injected at a needle concentration of 1 mg/ml containing 0.03% NP-40 (492016, Merck Millipore). After the antibody microinjection, samples were incubated for 1 hours to aid recovery and oocytes were then released into dbcAMP-free medium for subsequent imaging. Acute Trim-Away based depletion was performed by microinjection of 7 pl of mRNA (mouse Trim21 and other fluorescent reporters, Table 2.3) and oocytes were incubated for 3-4 hours to allow sufficient expression mRNA prior to release of oocytes in dbcAMP-free medium. After an incubation period of 6 hours to allow maturation of oocytes to the bipolar MI stage, oocytes were microinjected with 5-6 pl of antibody (Table 2.2) and imaged immediately.

Trim-Away was performed in human GV oocytes by injecting 10-12 pl of recombinant His-Lipoyl-TRIM21 protein (Clift et al., 2017) at a needle concentration of 4.4 mg/ml. 12 pl of antibody (Table 2.2) was subsequently injected at a needle concentration of 1.3 – 1.8 mg/ml supplemented with 0.03% NP-40. The treated oocytes were incubated in GMOPS (supplemented with 10% FBP) medium for 3-4 hours and subsequently imaged live or allowed to mature to the MI stage (15h post NEBD) and fixed.

Table 2.2 Antibodies used for Trim-Away.

Antibody name	Identifier	Reference/Origin/Supplier
Polyclonal anti-PCM1	HPA023374	Sigma-Aldrich
Monoclonal anti-Pericentrin	611815	BD Biosciences
Monoclonal anti-TACC3	ab134154	Abcam
Polyclonal Normal Rabbit IgG	12-370	Millipore
Polyclonal Normal Mouse IgG	12-371	Millipore

2.1.7 Cold-mediated microtubule depolymerization assay

MI human (15h post NEBD) and mouse (7h post NEBD) oocytes were incubated for 6.5 and 15 minutes on ice, respectively to induce the depolymerisation of cold sensitive non-kinetochore microtubules. The samples were subsequently fixed and imaged by immunofluorescence.

2.2 Molecular biology

2.2.1 Expression constructs and mRNA synthesis

Constructs used in this thesis are listed in Table 2.3. For expression in mouse oocytes the previously published coding sequences were first fused at either the C- or N- terminal with the desired fluorescence reporters mEGFP (pmEGFP-C1, pmEGFP-C3, pmEGFP-N1, pmEGFP-N3, Clonetech), mClover3 (Bajar et al., 2016), mCherry (pmCherry-C1, pmCherry-N1, Clonetech (Shaner et al., 2004)), mScarlet (Bindels et al., 2017), or mPA-GFP (Patterson & Lippincott-Schwartz, 2002) and were sub-cloned into pGEMHE (Liman et al., 1992). *In vitro* mRNA transcription was performed from linearized (AscI) pGEMHE plasmids or (NotI) (pCR3.1, Cep192) and the capped mRNA was synthesised using T7 polymerase (Ambion mMessage mMachine T7 kit) according to manufacturer's

instructions. Concentration of the mRNA was measured using agarose gels by comparison with an RNA standard (Ambion).

2.2.2 Short-interfering RNAs (siRNAs)

The following mix of siRNAs (purchased from Quiagen) were used for the knockdown of Pericentrin:

5’-TGGGATGTAATTGATATTATT-3’, 5’-CCGCCAGATTCTACTCAGAAA-3’ and 5’-AAGGAGATCCATGCAAAGCAA-3’.

Pcm1:

5’-TTGATGTTCGCTACTACCATA-3’, 5’-AAGTAATAGTGTGAAGGACTA-3’ and 5’- CAGTGGTCTTAGAACATGTTA -3.

AllStars Negative Control (Qiagen) was used as a control. siRNA stocks were stored at -80°C (6.6 μM) in 96-well plates closed with PCR adhesive foil or as working dilutions (2 μM) in nuclease-free tubes (Axygen).

Table 2.3 List of expression constructs

Construct	Reference/Origin
mEGFP-AKAP450 (human)	(Gillingham & Munro, 2000)
Bbs4-mEGFP (mouse)	(Berbari et al., 2008)
CEP72-mEGFP (human)	(Stowe et al., 2012)
mEGFP-Cep290 (mouse)	Addgene 27379 (Valente et al., 2006)
mCherry-CEP192 (human)	(Gomez-Ferreria et al., 2007)
CETN2-mEGFP (human)	(Wang et al., 2010)
mEGFP-centrobin (rat)	(Liska et al., 2009)
mClover3-CHC17 (human)	(Booth et al., 2011)
CHTOG-mScarlet (human)	(Nixon et al., 2015)
mEGFP-CPAP (human)	(Kohlmaier et al., 2009)
H2B-miRFP (human)	(Schuh & Ellenberg, 2007)
H2B-mCherry (human)	(Schuh & Ellenberg, 2007)
mEGFP-Hook3 (mouse)	(Ge et al., 2010)
LRRC36-mEGFP (human)	(Stowe et al., 2012)
LRRC45-mEGFP (human)	(He et al., 2013)
mEGFP-MAP4-MTBD (mouse)	(Mogessie & Schuh, 2017)
mCherry-MAP4-MTBD (mouse)	(Mogessie & Schuh, 2017)
NEDD1-mCherry (human)	(Laurence Haren et al., 2009)
mEGFP-NEK2 (human)	(Hames & Fry, 2002)
mEGFP-PAR6α (human)	Addgene 15472 (Kodani et al., 2010a)
PCM1-mEGFP (chicken)	(Dammermann & Merdes, 2002)

mEGFP-Pericentrin (human)	(Lee & Rhee, 2011)
mEGFP-PLK1 (human)	(Clift & Schuh, 2015)
mEGFP-rootletin (human)	(Bahe et al., 2005)
mEGFP-SAS6 (human)	(van Breugel et al., 2011)
TACC3-mClover3 (human)	(Nixon et al., 2015)
TACC3-mPA-GFP (human)	(Nixon et al., 2015)
mEGFP-TPX2 (human)	(Ma et al., 2010)
mouse Trim21	(Clift et al., 2017)
TUBG-mEGFP (human)	(Gerlich et al., 2001)
EB3-3×mEGFP (human)	J. Ellenberg, unpublished
mPA-GFP-α-tubulin (mouse)	J. Ellenberg, unpublished
pCR3.1-mCherry-CEP192 (human)	(Gomez-Ferreria et al., 2007)
mEGFP-MAP4 (mouse)	(Clift et al., 2017)
mCherry-MAP4 (mouse)	(Clift & Schuh, 2015)
CEP250-mEGFP (human)	(Clift & Schuh, 2015)

2.2.3 Immunoblotting

For immunoblotting, 30 mouse oocytes were used per gel lane. The oocytes were washed with and resuspended in BSA-free M2 medium. Oocytes were transferred into 0.65 ml centrifuge tubes (with attached caps; non-sterile) and pelleted by short pulses at 3000 rpm. Medium volume was reduced to 1-2 µl. Added 1 × sample buffer (NuPage LDS Sample Buffer, Invitrogen) with NuPage antioxidant (Invitrogen) to samples and heated at 95 °C for 5 min with. The samples were resolved on 4 - 12% bis-tris NuPAGE gels (Thermo Fisher Scientific). Electrophoresis was conducted according to manufacturer's instructions using NuPAGE MOPS SDS Running Buffer (Thermo Fisher Scientific). The proteins were transferred to 0.45 µm PVDF membranes using SDS-free Towbin buffer at 200 mA for 2 hours on ice. The membranes were incubated with the respective

antibodies in tris-buffered saline (TBS) supplemented with 5% skim milk and 0.1% tween-20. Membranes were incubated with primary antibody at 4 °C overnight. The primary antibodies that were used for immunoblotting are listed in Table 2.4. After washing the membranes several times with PBST, secondary antibodies (1:10,000) were added and the membranes were incubated in for 2 hours at room temperature. The secondary HRP-tagged antibodies are listed in Table 2.5. Membranes were washed five times in PBST and developed using ECL Prime or ECL Advanced (Amersham) and Kodak X-Ray films.

Table 2.4 Primary antibodies used for immunoblotting

Antibody name	**Identifier**	**Reference/Origin/Supplier**
Mouse anti-Pericentrin	611815	BD Biosciences
Rabbit anti-PCM1	HPA023374	Sigma-Aldrich
Rat-α-tubulin	MCA78G	Bio-Rad

Table 2.5 Secondary HRP-tagged antibodies used for immunoblotting

Antibody name	**Identifier**	**Reference/Origin/Supplier**
Anti-mouse	P0447	Dako
Anti-rabbit	31462	Invitrogen
Anti-rat	sc-2032	Santa Cruz Biotechnology

2.3 Human oocyte vitrification and thawing

2.3.1 Vitrification

Human oocytes were vitrified at the MI or GV stage by the Embryology team at Bourn Hall Clinic, using the Kitazato® Vitrification Cryotop method.

2.3.2 Thawing of Vitrified Oocytes

Thawing of vitrified oocytes were done using the Kitazato® vitrification warming media (VT802-0, Hunter Scientific) with the Cryotop method (Figure 2.1). The protocol was provided by Bourn Hall Clinic (Revision 5.00, issued 30.06.2016). All Kitazato media was stored between 2ºC and 8ºC, out of sunlight. Preparation steps for thawing on vitrified oocyte(s) involves pre-warming of thawing solution (TS) at 37°C and dilution solution (DS) and washing solution (WS) at room temperature. Thawing dish was warmed up on 37°C heated insert. Vitrified oocyte(s) were moved into a small liquid nitrogen container. TS vial was expelled into the first well of the thawing dish and Cryotec top with the oocyte(s) were immediately plunged horizontally from the liquid nitrogen into the TS well and incubated for 1 min on heated stage (37°C). Oocyte(s) were aspirated into the stripper tip (RI EZ-Tip, 290 µm) and expelled into the DS. Incubated for 3 min at RT. Oocyte(s) were next aspirated from the DS and released into the first WS (WS1) and incubated for 5 min at RT. In the last step, oocyte(s) were washed in the second WS (WS2) by placing them on the top of the medium and allowing it to sink twice (1 min at heated stage, 37°C). In between manipulations the lid was put back on the dish. Oocytes were moved into GMOPS, supplemented with 10% FBS under paraffin oil and allowed to recover for 2 hours prior to mRNA injection and imaging.

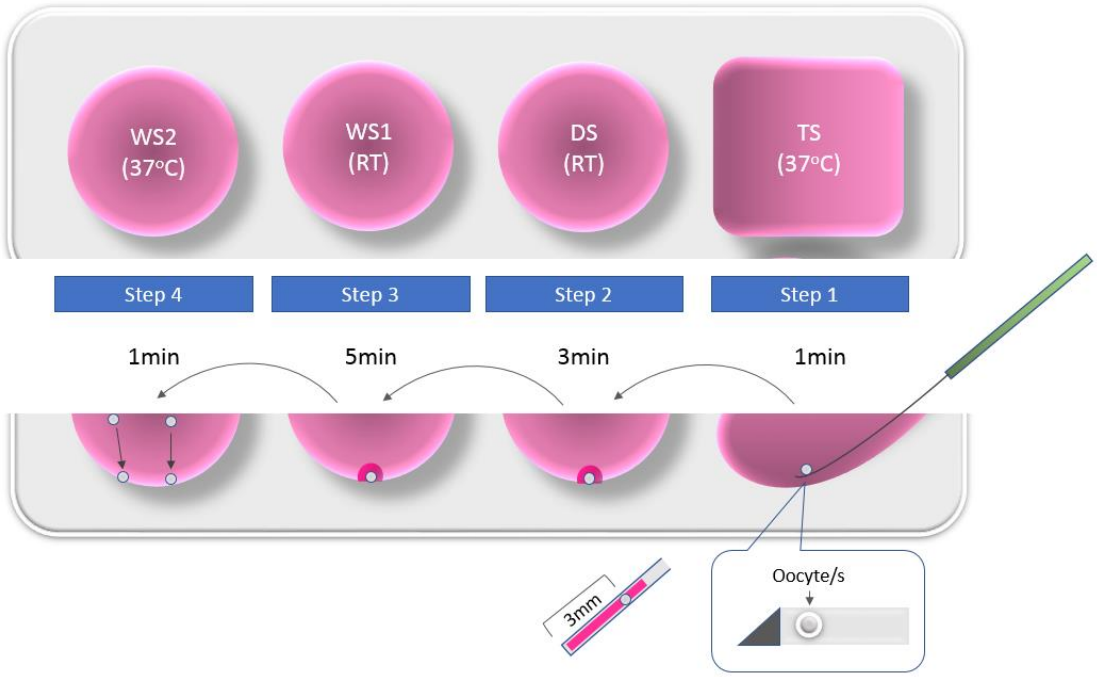

Figure 2.1. Schematic showing warming of vitrified oocyte.

Image shows the main steps of the warming protocol of vitrified human oocytes using the Kitazato® vitrification warming kit (based on protocol from Bourn Hall (Revision 5.00, issued 30.06.2016)). Step 1: oocyte is quickly plunged into the pre-warmed (37°C) thawing solution (TS) for 1 minute (min). Step2: oocyte is moved to the dilution solution (DS) for 3 min at room temperature (RT). Step 3: oocyte is moved to the 1st washing solution (WS1) for 5 min at RT. Step4: oocyte is moved to the 2nd washing solution (WS2) for 1 min at 37°C. Oocyte is then moved into the pre-warmed (37°C) culture medium under paraffin oil.

2.4 Microscopy

2.4.1 Confocal and super-resolution microscopy

1 - 2 µl of M2 medium or PBS was used for confocal imaging of live or fixed mouse oocytes, respectively. Samples were covered with paraffin oil in a 35 mm glass-bottom dish (MatTek). Live cell images were acquired with Zeiss LSM710 microscope equipped with BiG (Binary GaASP) detectors and Zeiss LSM880 or Zeiss LSM800 microscopes using a 40x C-Apochromat 1.2 NA water-immersion objective and a Zeiss environmental incubator box. Immunofluorescence image acquisition was done with a 63x C-Apochromat 1.2 NA oil immersion objective. Automatic 3D tracking was used for time-

lapse imaging with a 5 - 15 min resolution using AutofocusScreen (Rabut & Ellenberg, 2004) or MyPiC (Politi et al., 2018). The excitation wavelengths and the detection spectra used for each fluorophore are listed in Table 2.6. Control oocytes within the same experiment were always imaged under the same conditions and the same microscope as the experimental group. In most of the images, shot noise was reduced using a Gaussian filter. Super-resolution Airyscans were performed with the Airyscan module on LSM800 and LSM880 confocal laser scanning microscopes (Zeiss) and subsequently processed in ZEN (Zeiss).

Table 2.6 Imaging settings for fluorophores used in confocal and super-resolution microscopy.

Fluorophore	**Excitation λ (nm)**	**Detection λ (nm)**
mClover3	488	493 - 571
mEGFP	488	493 – 571
mScarlet	561	571 - 638
mCherry	561	571 – 638
miRFP	633	638 – 700

2.4.2 Light-sheet microscopy

A customized sample holder (section 5.2) constructed from Tantalum (Ta, TaW2.5, TaW10, whs sondermetalle, ThyssenKrupp Materials Schweiz) with various window sizes were prepared by the fine mechanical workshop at Max Planck Institute for Biophysical Chemistry for Biophysical Chemistry, Göttingen for the imaging of human oocytes in 5-25 µl G-MOPS medium supplemented with 10% FBS. The customized sample holder was sealed with silicone grease (85402-1EA from Sigma-Aldrich or 11989387 from Fisher Scientific) and two 12.5 µm thick FEP films (DuPont Teflon FEP fluoroplastic film, FEP 50A, 12.5 um thickness, ordered from Lohmann Technologies UK Limited). Image acquisition was performed using the Lightsheet Z.1 microscope (Zeiss) equipped a 40× or 63× Plan-Apochromat NA 1.0 water-dipping objective and

temperature module. The excitation wavelengths and the detection spectra used for each fluorophore are listed in Table 2.7. Samples used for control experiments were imaged under the same conditions with the same microscope. Images were processed in ZEN black (Zeiss). The GMOPs medium within the main Lighsheet (LS) chamber (30 ml) was supplemented with 60ul, final concentration of 100 µg/ml of Normocin (Invivogen, ant-nr-1, aliquots in -20ºC). All media for live-cell imaging were incubated overnight at 37°C incubator.

Table 2.7 Imaging settings for fluorophores used in light-sheet microscopy.

Fluorophore	**Excitation λ (nm)**	**Detection λ (nm)**
mClover3 and mEGFP	488	505 – 545
mCherry	561	575 – 615

2.4.2.1 Preparation of sample holder

FEP foil was cut to size using a puncturing hammer (designed by the fine mechanical workshop at Max Planck Institute for Biophysical Chemistry for Biophysical Chemistry, Göttingen). Cut FEP foils were dipped into 70% EtOH and then rinsed in embryo tested H2O (W1503, Sigma-Aldrich) and dried with tissue paper. Tantal sample holder was stored in 70% EtOH and prior to use rinsed with embryo tested H_2O. Both surface of the Tantal sample holder was dabbed with silicone grease. Excess grease was removed using gloved figures and lens paper. Using fine tweezers, sample holder chamber was sealed with the cut and washed FEP foil. Culture medium (GMOPS + 10% FBS) was loaded into the sample chamber (5-20 µl) using a clean glass capillary via a mouth pipette. Sealed sample holder was incubated overnight at 37°C incubator. For the loading of oocytes, using the fine tweezer, one side of the sample holder foil is lifted and oocyte(s) placed onto the imaging surface and resealed. Fixed oocytes were also imaged in GMOPS + 10% FBS within the sample holder.

2.4.3 Fluorescence recovery after photobleaching (FRAP)

Oocytes that were co-expressing fluorescent reporter(s) of interest and H2B-mCherry, were allowed to reach the bipolar MI stage (6-7 hours post NEBD) and oocytes were rotated on the microscope stage to align the meiotic spindles in a parallel orientation to the imaging plane. Circular (aMTOCs) or rectangular (spindle region between poles and metaphase plate) regions of interest (ROIs) were marked and subsequently photobleached using the respective excitation laser setting (488 or 561 nm) at the maximum power after the third time point. Time-lapse images were taken to analyse the mobility of the proteins in the ROIs every second for the total duration of 2 minutes.

2.4.4 Photoactivation

Assessment of poleward flux rate and the rate of protein mobility was measured in oocytes co-expressing mPA-GFP-α-tubulin and H2B-mCherry or TACC3-mPA-GFP and H2B-mCherry. MI oocytes were rotated on the microscope stage to align the meiotic spindles in a parallel orientation to the imaging plane (based on H2B-mCherry signal). Rectangular (spindle region between poles and metaphase plate) ROIs were marked and photoactivation was triggered via the 405 nm laser line at high excitation laser setting. Photoactivation was triggered after the third time point. Time-lapse images were taken to analyse the mobility of the proteins in the ROIs every second for the total duration of 2 minutes.

2.5 Quantifications

2.5.1 General quantifications

Analysis of phenotypes were carried out manually using Zen image software (Zeiss) or ImarisXT (Bitplane). Scored time points and specific phenotypes were recorded in Microsoft Excel and statistics were calculated as described in section 2.5.6. Oocytes that failed to mature and undergo NEBD or died, were not analysed. Meiotic progression was quantified relative to the time of NEBD, which was defined as the disappearance of the sharp boundary between the cytoplasm and the nucleus. The last time point of metaphase (usually 5-6 minutes), before chromosome separation could be observed, was defined as anaphase. Chromosome misalignment was scored at the last time-frame before anaphase

onset and only those were considered as misaligned that have clearly separated from the metaphase plate and maintained and did not join the main chromosome mass prior to anaphase onset. Lagging chromosomes were defined as chromosomes that trailed behind and could not clear the central spindle region within 10-12 minutes after the start of anaphase. Misaligned and lagging chromosomes were further confirmed by chromosomes reconstruction using Imaris.

Images that are shown in this thesis as examples from both live cell imaging and immunofluorescence were prepared in ImageJ (win64) and all figure panels were created in Adobe Illustrator CC 2018.

2.5.2 Quantification of volume and fluorescence intensities

Using Isosurface function of ImarisXT (Bitplane), the microtubule spindle or aMTOC surfaces were reconstituted in 3D using the automated threshold function within the corresponding channel. Microtubule signal was identified by fluorescently tagged MAP4 expression or labelled via anti-α-tubulin in fixed samples and aMTOC signal was labelled with CEP192 (live) or anti-Pericentrin (fixed). Cytoplasmic signal was excluded from the analysis by specifying a region of interest around the spindle. All analysed images were checked for saturation to ensure that intensity measurements are not skewed. In the case of K-fibre 3D surface reconstitution, individual fibre surfaces sometimes did not connect. To ensure that the total volume and intensity measurements reflect the total K-fibre signal, separate surfaces were unified to give a single measurement value. Measurements of calculated total surface volumes, mean fluorescence and total fluorescence intensities were exported into Microsoft Excel where statistical analysis was performed as described in section 2.5.6. The time points of measurements from live-cell images were aligned from NEBD. Normalisation of datasets were carried out by dividing each datapoint by the average steady state value of all data within the control group. In some datasets, to ensure that time-lapse measurements are aligned at the same time point, datasets were interpolated using the Linear Interpolate/Extrapolate Y from X function of OriginPro (OriginLab, 2017). Normalisation of immunofluorescence datasets were done by dividing each value by the average value of all control datapoints within the same channel.

2.5.3 Quantification of FRAP experiments

Mean intensity datapoints from live cell imaging of photobleached regions of interest (ROIs) were exported from Zen (Zeiss) to Microsoft Excel for analysis. In order to correct for background signal, datapoints were subtracted by the measured intensity in the unbleached area in the cytoplasm of the same oocyte. Normalisation of the background subtracted datasets was carried out by dividing all datapoints with the average intensity of the pre-bleach time points, F_0 (three time points recorded prior to photobleaching). Due to variable photobleaching efficiency, post-bleach intensity could not be normalized between individual plots. Plots of intensity (F) against time were fitted to single exponential functions in OriginPro (OriginLab, 2017). Half-times of maximum recovery ($t_{1/2}$) and mobile fractions were determined by $\tau \times \ln(2)$ and $F_\infty/(F_0\text{-}F')$ (where F' is the minimum intensity measured immediately after photobleaching), respectively.

2.5.4 Quantification of photoactivation experiments

To analyse flux rates, recorded images were aligned in ImageJ (win64). A perpendicular line was drawn in the centre of the spindle from the metaphase plate (marked by chromosomes) to the spindle pole. The line intensities from ImageJ were exported using the Stack profile data plugin to Microsoft Excel. Flux rates were calculated by following the position of the local maxima over time (amplitude version of Gaussian peak function in OriginPro) within the photoactivated region.

To calculate dissipation rates, in ImageJ the mean intensities within the rectangle drawn around the photoactivated areas were exported into Microsoft Excel via the Plot X-axis profile list plugin. Datapoints were background subtracted by the measured intensity of the ROI before photoactivation. Normalisation was done by dividing each datapoint with the intensity measured at the first time point of the photoactivated ROI. Normalised mean intensities over time were fitted to a one- or two-component exponential function in OriginPro and half-times of fluorescence decay ($t_{1/2}$) were determined. For α-tubulin, single-component exponential fitting was used as described in (Mogessie & Schuh, 2017). For TACC3, double-component exponential fitting gave a better goodness of fit as described by the coefficient of determination (R^2 closest to 1, Figure 4.6, p135).

2.5.5 Quantification of EB3 plus-end growth velocities

Oocytes overexpressing EB3-3×mEGFP were imaged at 6-7 hours post NEBD. Oocytes were rotated on the microscope stage to align the meiotic spindles in a parallel orientation to the imaging plane. Images were taken every 1.5 seconds to record the EB3 plus-end microtubule growth as shown by the movement of the EB3 plus-tip comet movements. For the analysis, the ImageJ MultiKymograph plugin (EMBL) was used. First, images were opened in ImageJ and using the Walking Average plugin, maximum intensity projections of 3 consecutive time points were generated to follow the growing EB3 comets more easily. Using the segmented line tool, the EB3 comet was marked on the projected image, which was then overlayed onto the original image. When running the MultipleKymograph plugin on the selected region, the distance travelled (x) over time (y) was plotted on the kymograph. The determined datapoints (x and y) were recorded in Microsoft Excel. Based on the calculated micron/pixel size, the growth velocity was calculated by displacement / time (μm/min).

2.5.6 Statistical analysis

Average (mean) and standard deviation (S.D.) were calculated in Microsoft Excel. Statistical significance (p values) were calculated in Microsoft Excel with two tailed Student's t test for absolute values or Fisher's exact test for categorical data. P values show significance as: *P $\leq$ 0.05, **P $\leq$ 0.01, ***P $\leq$ 0.001 and ****P $\leq$ 0.0001. Nonsignificant values are indicated as N.S.

3 RESULTS: PART I

Characterisation of a new spindle domain in mouse meiosis

3.1 Overview

The organisation of microtubule networks into a bipolar spindle is essential for reliable chromosome separation during cell division. A pair of centrioles surrounded by pericentriolar material (PCM), define the canonical centrosome that acts as the main microtubule organising centre (MTOC) during mitosis (Bornens, 2012; Sanchez & Feldman, 2017). In mammalian meiosis, centrioles are eliminated during pachytene arrest of oogenesis (Manandhar et al., 2005). In mouse oocytes, spindle microtubules are predominantly nucleated by acentriolar MTOCs (aMTOCs) that self-organise and form a barrel-shaped bipolar spindle (Schuh & Ellenberg, 2007).

Despite the absence of centrosomes, a large number of centrosomal proteins are highly expressed in mouse oocytes (Pfeiffer et al., 2011; Virant-Klun et al., 2013; Wang et al., 2010; Yan et al., 2013; Zeng et al., 2004). In somatic cells, the function and composition of the centrosome and its accessory domains have been extensively studied; however, the conservation of their function or perhaps previously undescribed mechanism(s) in the acentrosomal spindle is still poorly understood. During his time in the Schuh lab, Dean Clift initially showed that centrosomal proteins localise to two distinct sites at the acentrosomal mouse spindle (Figure 3.1). Pericentriolar material proteins (Pericentrin, CEP192, CDK5RAP2 and γ-tubulin) localised to the aMTOCs that form a pole ring domain at the spindle poles. Unexpectedly, a group of pericentriolar satellite proteins (PCM1, CEP72, LRRC36 and BBS4) and AKAP9 that contains the centrosome targeting PACT domain localised to a previously undescribed domain throughout meiotic maturation of mouse oocytes (Figure 3.1). This domain, which I will refer to as the meiotic spindle pole domain (MSPD), is distinct from spindle microtubules and the acentrosomal microtubule organising centres (aMTOCs). Our hypothesis was that this

domain might be important for spindle assembly and organisation in mouse oocyte meiosis.

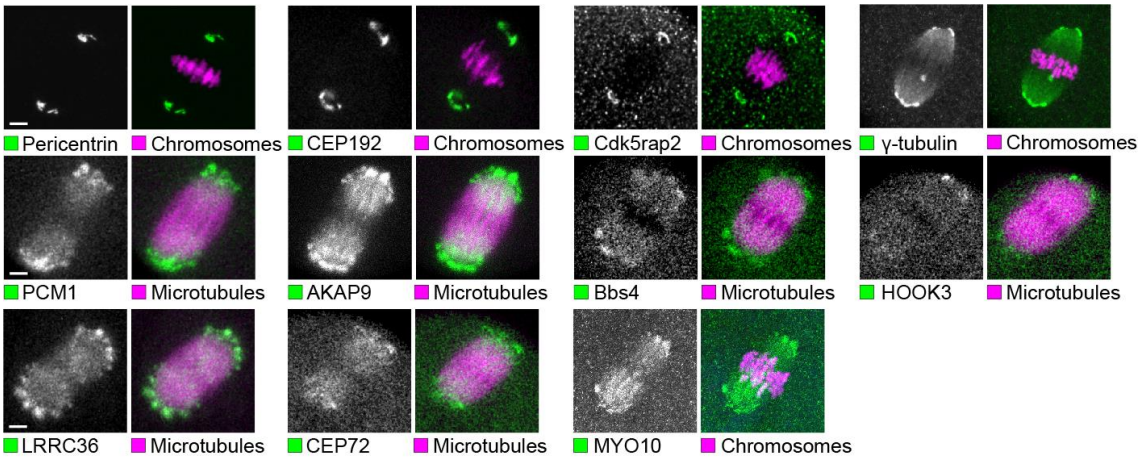

Figure 3.1. Localisation of centrosomal proteins in mouse meiosis I spindles.

Selected examples showing anti-Pericentrin, CEP192-mCherry, anti-CDK5RAP2, anti-γ-tubulin localising to aMTOCs. Selected examples showing PCM1-mEGFP, mEGFP-AKAP9 (image taken by Dean Clift), Bbs4-mEGFP (image taken by Dean Clift), mEGFP-HOOK3 (image taken by Dean Clift), LRRC36-mEGFP, CEP72-mEGFP (image taken by Dean Clift) and anti-MYO10 localising to the meiotic spindle pole domain. Scale bar shows 5 µm.

To characterise the MSPD domain further, I investigated the localisation and function of PCM1, because it is known to act as a scaffold protein to recruit other centriolar satellites and pericentriolar material proteins in mitotic cells (Hori & Toda, 2017) and therefore is likely to play an important role in MSPD function.

Trim-Away, an antibody-based protein depletion method, was used to study the function of PCM1 (Clift et al., 2017). Analysis of PCM1-depleted oocytes revealed that PCM1 is critical for the assembly and maintenance of the aMTOCs. I also observed that PCM1 and the main MTOC component Pericentrin are interdependent during mouse meiosis, and depletion of both proteins show similar phenotypes. Importantly, in the absence of PCM1 and aMTOCs, the onset of microtubule nucleation is significantly delayed and the total amount of nucleated microtubules throughout meiosis is reduced. PCM1 and aMTOC function was also important at the later stages of meiosis. Acute depletion at 7 hours post nuclear envelope breakdown (NEBD) revealed that aMTOCs maintained a 20-40% contribution to the total nucleated microtubule mass. In the absence of functional

aMTOCs, spindle formation was fully dependent on the RanGTP pathway, which is activated at the chromosome surface. A similar mechanism of spindle assembly was previously reported in human oocytes that lack any detectable MTOCs (Holubcová et al., 2015).

3.2 PCM1 localises to a unique domain within mouse meiotic spindles

In order to describe the recruitment and localisation of MSPD in detail, I initially focused on PCM1, the main centriolar satellite scaffold protein that had not been previously characterised in mouse meiosis.

Immunofluorescence revealed that PCM1 initially localised to the inner part of both cytoplasmic and nuclear envelope-associated aMTOCs in prophase I arrested oocytes (Figure 3.2A). Following resumption of meiosis, those aMTOCs associated with the nuclear envelope (NE), show a different localisation pattern, with small PCM1 foci localised along the length of stretched out aMTOCs (Figure 3.2A). Interestingly, these foci did not completely co-localise but were closely associated with the aMTOCs (Figure 3.2A). Following NEBD and the onset of microtubule nucleation, PCM1 started to accumulate within the microtubule spindle ball. During spindle bipolarisation, PCM1 was gradually distributed to the poles (Figure 3.2B and C). Closer examination of the spindle and spindle poles showed that PCM1 formed foci of various sizes predominantly concentrated at the poles and extended beyond the aMTOC ring domain (Figure 3.2D). To a lesser extent, PCM1 also infiltrated the whole of the meiotic spindle. The filamentous signal ending at the chromosomes may also indicate co-localisation/enrichment on kinetochore fibres (Figure 3.2B and E). Live cell imaging of fluorescently tagged full-length PCM1 (Gallus gallus, chicken PCM1 construct) gave the same localisation pattern as seen with immunofluorescence, confirming that no staining artefacts were present (Figure 3.2C).

Early studies in mitotic cells showed that both the amount and localisation of PCM1 can vary between different cell types; and it cannot be excluded that these results also varied due to the different antibodies used (Balczon et al., 1994; Dammermann & Merdes, 2002; Kubo & Tsukita, 2002). To ensure the specificity of the PCM1 antibody and

confirm that the results are not specific to only certain mouse strains, I tested another PCM1 antibody from the Merdes lab (Figure 3.3A) (Dammermann & Merdes, 2002) and imaged oocytes from a hybrid mouse strain; F1 (C57BL x CBA) (Figure 3.3B). This confirmed that the localisation of PCM1 is specific and is conserved between mouse strains.

Together, this shows that PCM1 localises to a unique spindle domain throughout meiosis and forms a distinctive network of foci/spherical protrusions at the spindle poles (MSPD) that is closely associated with the aMTOC ring domain and spindle microtubules.

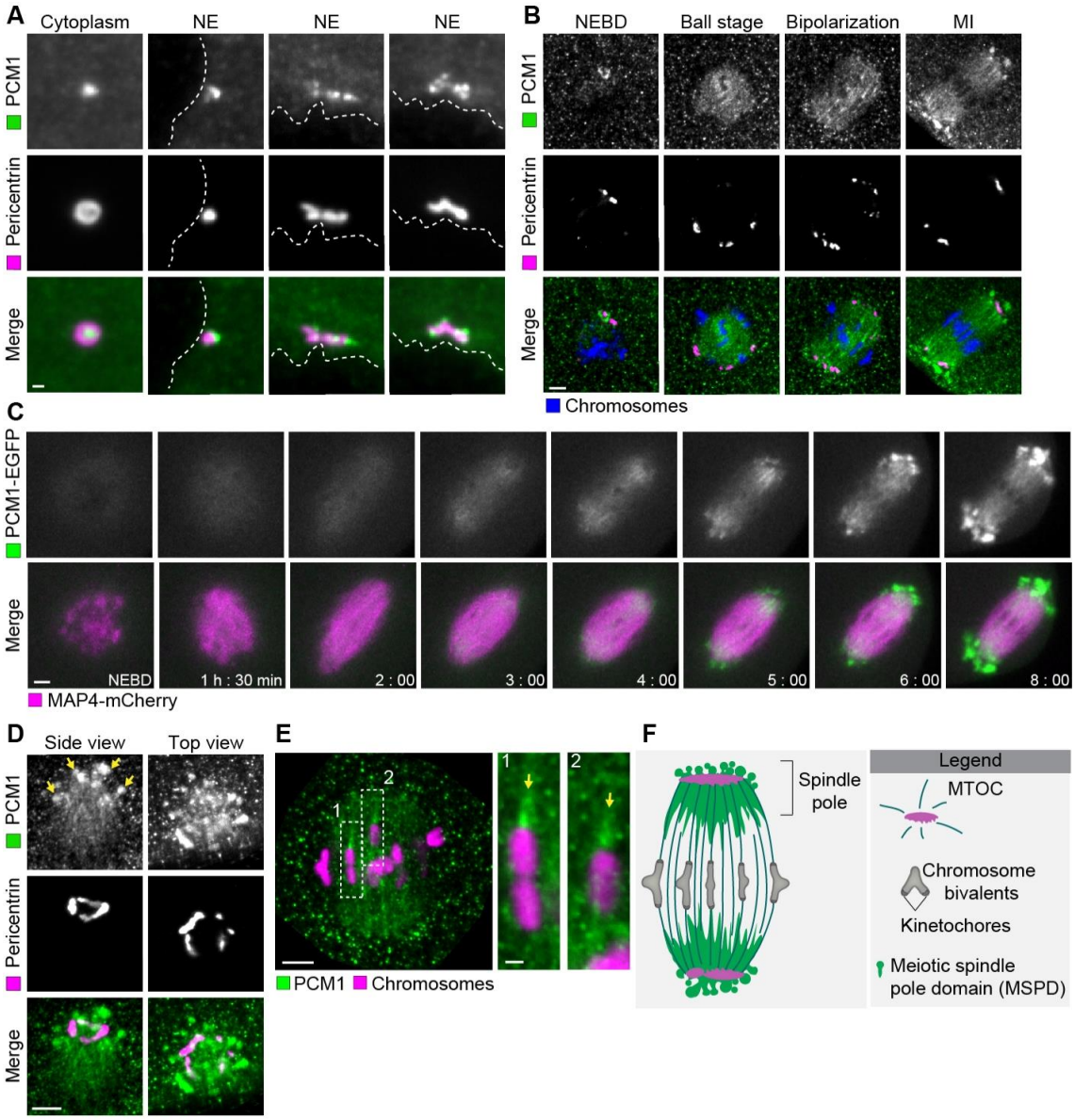

Figure 3.2 PCM1 localises to a unique domain in meiosis I mouse spindles.

(A) Immunofluorescence of PCM1 in prophase mouse oocytes. Antibody from (Dammermann & Merdes, 2002). Examples showing aMTOCs labelled with anti-Pericentrin in cytoplasm or on the nuclear envelop (NE) prior to NEBD. Dashed lines show borders of the nuclear envelope. Images were taken with the Lightsheet Z.1 microscope. Scale bar shows 1 µm.

(B) Immunofluorescence of PCM1 localisation at different time points during meiosis I. Antibody from Sigma (HPA023374) was used. Oocytes were fixed at NEBD, ball stage (2h post NEBD), spindle bipolarisation (4h post NEBD) and MI spindle (7h post NEBD). aMTOCs are labelled with anti- Pericentrin. Scale bar shows 5 µm.

(C) Live cell imaging of PCM1 localisation in mouse oocytes undergoing meiosis I. Oocytes overexpressed PCM1-mEGFP (green) and MAP4-mCherry (magenta) to label microtubules. Time shows hours (h) and minutes (min) from NEBD. Scale bar shows 5 µm.

(D) Immunofluorescence of PCM1 localisation at spindle poles. Antibody from Sigma (HPA023374) was used. Oocytes were fixed at late MI (7h post NEBD). aMTOCs labelled with Pericentrin (showing the ring domain). Pcm1 foci are highlighted with arrows at the poles. Images show examples from side and top view of the spindle pole. Scale bar shows 5 µm.

(E) Immunofluorescence of PCM1 localisation in early bipolar MI spindle (4h post NEBD). Antibody from Sigma (HPA023374) was used. Boxed regions are magnified on the right and the filamentous localisation within the spindle, ending at chromosomes are highlighted with arrows. Scale bar shows 5 µm and 1 µm for magnified images.

(F) Schematic drawing of MI spindle showing peri-aMTOC domain (PAD) in green at spindle poles. The different objects are specified in the legend.

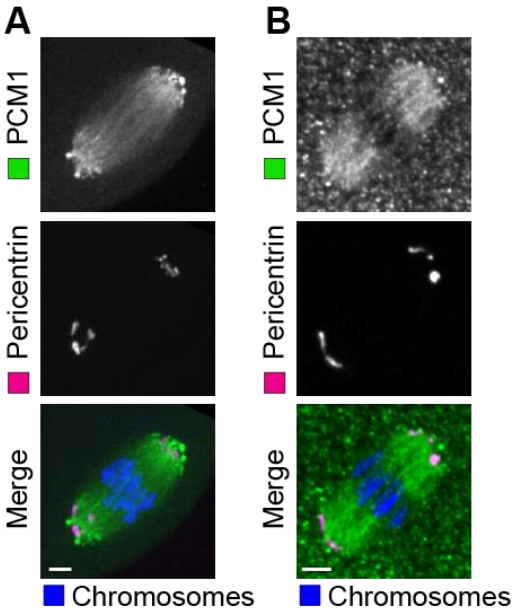

Figure 3.3 PCM1 localisation in fixed MI oocytes (7h post NEBD).

(A) Immunofluorescence staining of endogenous PCM1 (green) labelled with antibody from (Dammermann & Merdes, 2002).

(B) Immunofluorescence staining of endogenous PCM1 (green) using the commercially available Sigma antibody (HPA023374) in F1 (C57BL x CBA) hybrid mouse strain.

aMTOCs labelled with Pericentrin (magenta) and chromosomes with Hoechst (blue). Scale bar shows 5 µm.

3.3 PCM1/MSPD localisation is microtubule-dependent

To investigate if PCM1/MSPD is microtubule-dependent, I looked at immunofluorescence localisation of PCM1 following Nocodazole treatment of MI mouse spindles (Figure 3.4). It is evident that the domain organisation is no longer maintained with minimal PCM1 signal only visible around the aMTOCs in the absence of microtubules. It would be interesting to also image Nocodazole depolymerisation and microtubule regrowth following washout in live mouse oocytes, to see in more detail how the MSPD is recruited and sorted around the spindle poles. More details on this is provided in section 4.3, p130 (Figure 4.5).

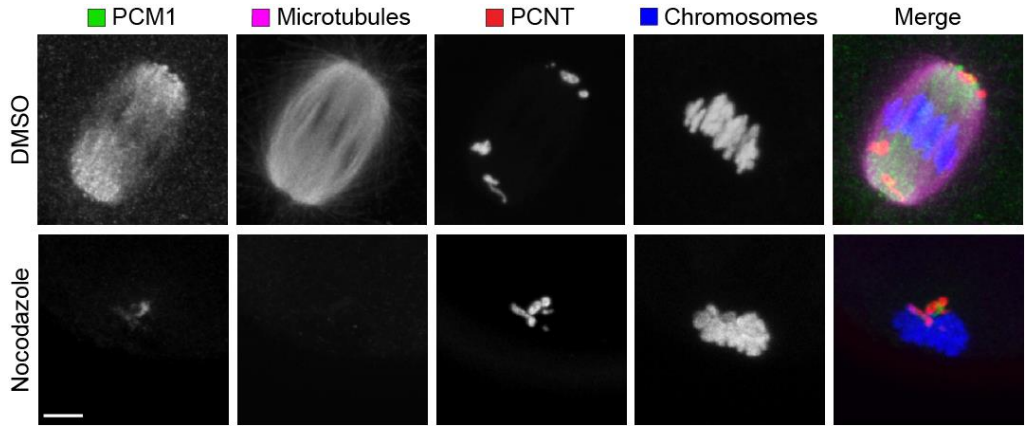

Figure 3.4 PCM1/MSPD localisation is microtubule-dependent.

Immunofluorescence of anti-PCM1 (green), anti-α-tubulin (magenta), anti-Pericentrin (PCNT, red) and Hoechst (blue). Oocytes were allowed to mature (7 hours post NEBD) and treated with either DMSO (control) or Nocodazole (10 µM for 20 minutes) prior to fixing. Scale bar shows 5 µm.

3.4 Depletion efficiency of PCM1 in oocytes

To investigate the function of PCM1 during meiosis, it was necessary to deplete the protein from oocytes. My first approach was to prevent the expression of PCM1 by RNAi (Figure 3.5A and B). Immunofluorescence showed that PCM1 could not be depleted using this approach, and that the endogenous protein still localised to the spindle (Figure 3.5A). Western blot analysis also confirmed that endogenous PCM1 was still present after RNAi treatment (Figure 3.5B, lane 3). Oocytes accumulate maternal mRNA and proteins in their large cytoplasm during their follicular development (Clift & Schuh, 2013). Depending on the time a particular protein is translated, depletion of stable maternal proteins is not always possible with RNAi depletion methods. In this case, PCM1 is an example of a stable maternal protein that is likely translated early on during oogenesis, with the protein being stored in the large cytoplasm of the oocyte.

One way to overcome this problem is to deplete PCM1 at the protein level. While there are limited means available for this, I made use of the Trim-Away method, an antibody-based protein degradation technique developed in our lab (Clift et al., 2017). The principle of the Trim-Away method is summarised in Figure 3.5E. Because Trim-Away utilises antibodies that are concentrated and microinjected into oocytes (Figure 3.5E), as part of the optimisation, I tested that the specificity and activity of the antibody is maintained following microinjection. Concentrated and microinjected anti-PCM1 antibody sustained its activity and specificity as confirmed by immunofluorescence (Figure 3.5D).

Using the specific anti-PCM1 antibody, I was able to successfully deplete PCM1 at the protein level (Figure 3.5B, C and F). Efficient depletion was confirmed by immunofluorescence (Figure 3.5C), Western blotting (Figure 3.5B) and live cell imaging of fluorescently tagged PCM1 protein (Figure 3.5F).

Since the Trim-Away method can acutely degrade endogenous proteins, the target protein could be depleted at different time points during meiosis (Figure 3.5G). PCM1 at late MI stage (7h post NEBD) was rapidly depleted (within 25-30 min, Figure 3.5H and I), and with this modified experimental design the role of PCM1 could be further investigated, not only for spindle assembly (Figure 3.6) but also for its function in the later stages of meiosis (Figure 3.7).

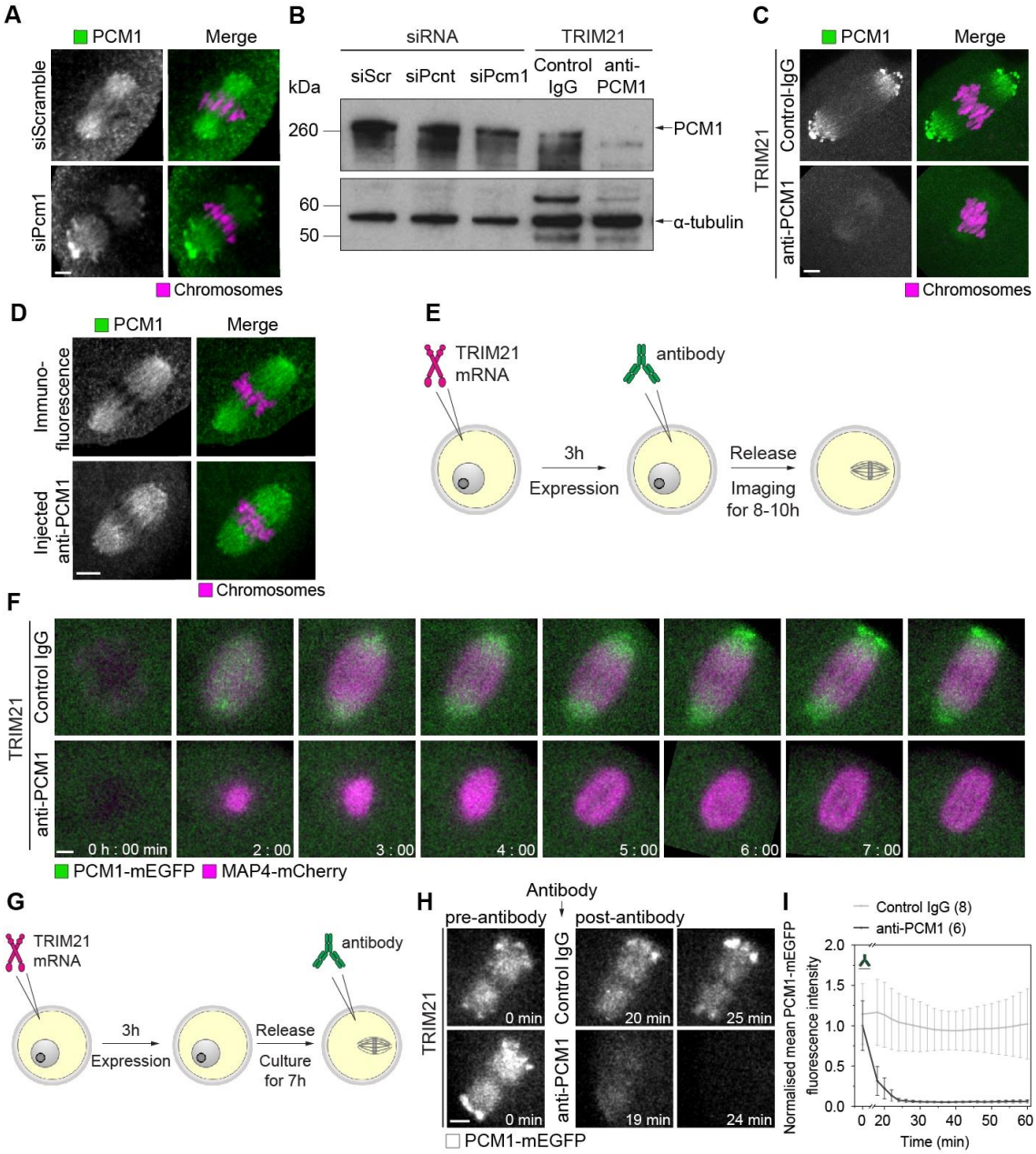

Figure 3.5 Degradation of PCM1 in mouse oocytes by RNAi and Trim-Away.

(A) Immunofluorescence of PCM1 in mouse oocytes. Oocytes were microinjected with siScramble (siScr) control or siPcm1 and fixed at the MI stage (7h post NEBD). Scale bar shows 5 µm.

(B) Western blot showing endogenous PCM1 in MI mouse oocytes. Whole oocyte lysates were pooled from two separate experiments and blotted once. PCM1 was detected with a specific antibody (HPA023374, Sigma-Aldrich), detection of α-tubulin served as loading control.

(C) Oocytes overexpressing TRIM21 mRNA and microinjected with anti-PCM1 antibody were allowed to mature to the MI stage and fixed. Scale bar shows 5 µm.

(D) Top row showing oocyte fixed at the bipolar MI stage (7h post NEBD) and conventional immunofluorescence staining with primary rabbit anti-PCM1 and secondary anti-rabbit 488 antibodies. Bottom row showing oocyte microinjected with rabbit anti-Pcm1 and then fixed at the bipolar MI stage (7h post NEBD) and stained with anti-rabbit 488 secondary antibody only. Scale bar shows 5 µm.

(E) Schematic of Trim-Away approach. Modified from (Clift et al., 2017).

(F) Oocytes overexpressing PCM1-mEGFP and MAP4-mCherry were microinjected with either non-specific control IgG antibody or anti-PCM1 antibody. Time shows hours (h) and minutes (min) from NEBD. Scale bar shows 5 µm.

(G) Schematics of acute PCM1 Trim-Away at the MI stage. Modified from (Clift et al., 2017).

(H-I) Oocytes overexpressing PCM1-mEGFP were microinjected with either non-specific control IgG antibody or anti-PCM antibody. Time shows minutes (min) from antibody microinjection, 0 min is immediately before antibody microinjection. Scale bar shows 5 µm.

(I) Data from one experiment. Error bars show SD. Number of oocytes is specified in brackets.

3.5 PCM1-depleted oocytes show delayed microtubule nucleation and overall reduction in spindle microtubule nucleation efficiency

After validating the Trim-Away method with anti-PCM1 antibody, I investigated the phenotype in PCM1-depleted oocytes via live cell imaging of microtubules and chromosomes (Figure 3.6). Notably, PCM1 depletion influenced the timing of the early stages of meiotic events (Figure 3.6A). Firstly, the onset of microtubule nucleation following NEBD was significantly delayed (Figure 3.6A and E). Compared to control oocytes, where microtubule nucleation began immediately after NEBD (time lapse interval 10 min, onset of microtubule nucleation 10.7 ± 2.7 min post NEBD), PCM1-depleted oocytes had on average a three-fold delay before MAP4 signal could be detected (32.9 ± 14.0 min post NEBD, Figure 3.6E and J). Although there was also a significant delay in the formation of bipolar spindle and chromosome alignment, oocytes were able to enter anaphase and complete meiosis I with the extrusion of the first polar body at a comparable rate to the control group (Figure 3.6A). No significant chromosome segregation defects were observed in PCM1-depleted oocytes (Figure 3.6C and D). This is also consistent with the data showing efficient progression into anaphase (73% control vs. 69% PCM1-depleted), suggesting that the spindle assembly checkpoint (SAC) was silenced in these oocytes, despite the delay in microtubule nucleation, (Figure 3.6B).

The most striking phenotype was seen in the morphology of the spindle (Figure 3.6J), with PCM1-depleted oocytes forming smaller spindles (Figure 3.6F-J). The total amount of microtubules nucleated, as indicated by the sum intensity of microtubules (MAP4), as well as the overall spindle volume, were significantly lower throughout meiosis (Figure 3.6F-I).

I then investigated whether PCM1 is required not only for spindle assembly, but also for maintaining spindle morphology when the bipolar spindle is fully formed. Oocytes were allowed to assemble a mature bipolar MI spindle and PCM1 was then acutely-depleted using Trim-Away (Figure 3.7G). Two hours after anti-PCM1 antibody injection, spindles had dramatically shrunk/decreased in size, suggesting that PCM1 has an essential role in maintaining spindle morphology (Figure 3.7). These spindles were of a similar morphology to those where PCM1 had been depleted prior to spindle assembly in

prophase I, with significantly reduced total amount of spindle microtubules as well as reduced overall spindle volume (Figure 3.7A-E).

In summary, depletion of PCM1 disrupted the dynamics of spindle assembly with a significant delay in the onset of microtubule nucleation and reduction in the total amount of nucleated microtubules throughout meiosis. Acute depletion confirmed that PCM1 is not only important for initial spindle assembly, but it is also essential for maintaining spindle morphology during meiosis.

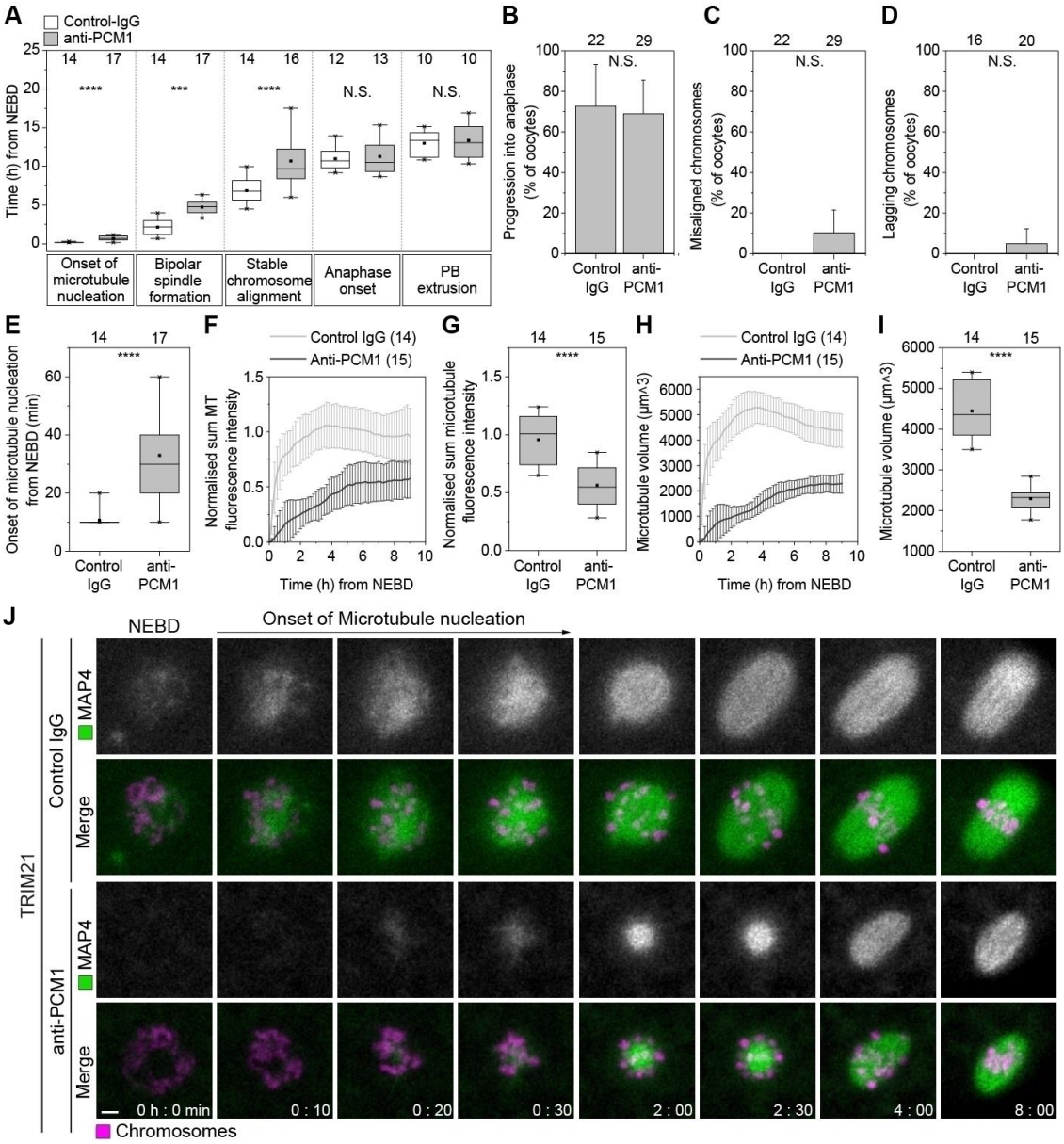

Figure 3.6 Loss of PCM1 delays microtubule nucleation and disrupts spindle morphology.

(A) Oocytes overexpressing TRIM21, H2B-mCherry and MAP4-mEGFP and microinjected with either control antibody or anti-PCM1 antibody were scored for the percentage of oocytes progressing through meiotic events and the timing of events.

(B-D) Oocytes overexpressing TRIM21, H2B and MAP4 and microinjected with either control antibody or anti-PCM1 antibody were scored for the frequency of oocytes progressing into anaphase (B), misaligned chromosomes (C) and lagging chromosomes (D).

(E) Timing of the onset of microtubule nucleation is shown in minutes (min).

(F-G) Quantification of normalised sum microtubule fluorescence intensity (MAP4-mEGFP) over time (hours). Time 0 is the onset of microtubule nucleation (F).

Normalised sum fluorescence intensity (MAP4-mEGFP) at 8 hours from microtubule nucleation (G).

(H-I) Quantification of spindle volume (MAP4-mEGFP) over time (hours). Time 0 is the onset of microtubule nucleation (F). Spindle volume (MAP4-mEGFP) at 8 hours from microtubule nucleation (I).

(J) Examples from time-lapse imaging of oocytes overexpressing TRIM21, H2B-mCherry and MAP4-mEGFP and microinjected with either control antibody or anti-PCM1 antibody. Time shows hours (h) and minutes (min) from NEBD (time 0). Scale bar shows 5 µm.

Data from two independent experiments (A-I). Number of oocytes shown above the dataset or in brackets. P values were calculated with Student's t test (A, E, G, I) or Fisher's exact test (B-D).

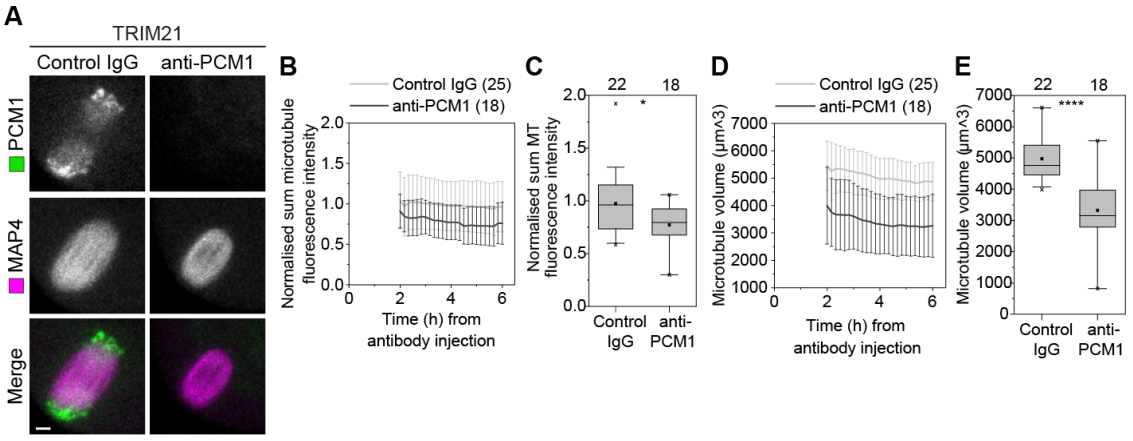

Figure 3.7 Acute PCM1 depletion at the MI stage.

(A) Examples from time-lapse imaging of oocytes overexpressing TRIM21, MAP4-mCherry and PCM1-mEGFP. Oocytes were left to mature *in vitro* and microinjected at 7 hours post NEBD with either control antibody or anti-PCM1 antibody. Scale bar shows 5 µm.

(B-C) Quantification of normalised sum microtubule fluorescence intensity (MAP4-mEGFP) over time (hours). Oocytes overexpressing TRIM21, MAP4-mCherry were left to mature *in vitro* and microinjected at 7 hours post NEBD with either control antibody or anti-PCM1 antibody. Time 0 is the time of antibody injection (B). Normalised sum fluorescence intensity (MAP4-mEGFP) at 2 hours from antibody injection (C).

(D-E) Quantification of spindle volume (MAP4-mEGFP) over time (hours). Oocytes overexpressing TRIM21, MAP4-mCherry were left to mature *in vitro* and microinjected at 7 hours post NEBD with either control antibody or anti-PCM1 antibody. Time 0 is the time of antibody injection (D). Spindle volume (MAP4-mEGFP) at 2 hours from antibody injection (E).

Data from two independent experiments (B-E). Number of oocytes shown above the dataset or in brackets. P values were calculated with Student's t test (C and E).

3.6 PCM1 is required for efficient chromosome congression

Live cell imaging of microtubules and chromosomes in PCM1-depleted oocytes also revealed disruption to the alignment of chromosomes on the metaphase plate of the MI spindle. Stable chromosome congression was delayed (Figure 3.6A), and oocytes could not achieve a tightly organised metaphase plate compared to control oocytes (Figure 3.8A-D). Chromosomes appeared unstretched even after stable alignment (Figure 3.8A) and only about 10% of PCM1-depleted oocytes showed tight chromosome congression (Figure 3.8B). This was also marked by the significantly wider metaphase plate width compared to control oocytes (8.0 ± 0.8 μm control vs. 12.0 ± 1.5 μm PCM1-depleted, Figure 3.8C-D).

It was previously shown that chromosome congression in mouse oocytes precedes biorientation during which kinetochore fibres (K-fibres) attach to kinetochores from opposite poles (amphitelic) (Kitajima et al., 2011). The balance of force generated, stretches the chromosomes, leading to stable biorientation on the metaphase plate. PCM1-depleted oocytes could not achieve chromosome congression within the same time-frame as controls (Figure 3.6A), and bivalents appeared to be unstretched on the metaphase plate (Figure 3.8A), which could indicate compromised K-fibre formation or attachment.

During the initial immunofluorescence imaging, the fibre-like localisation of PCM1 within the spindle that ends at the chromosomes indicated co-localisation of PCM1 with K-fibres (Figure 3.2F). Cold-mediated microtubule depolymerisation assay (methods section 2.1.7, p70) was used to selectively visualise the more stable K-fibres. Indeed, PCM1 co-localised with α-tubulin on K-fibres (Figure 3.8E). When PCM1 is depleted, there is a reduction in the total K-fibre volume (Figure 3.8I), which could be an indirect consequence of reduced microtubule nucleation (Figure 3.6E-J), although it is possible that PCM1 plays a direct role in K-fibre function. Nonetheless, the reduction in K-fibres as indicated by their reduced overall volume (Figure 3.8I) may explain the chromosome alignment defects in PCM1-depleted oocytes.

Unstretched bivalents and loose chromosome alignment might also be due to incorrect attachment of K-fibres to kinetochores (section 1.5.3, p39). Correct attachment of bivalents is referred to as amphitelic, where K-fibres emanating from the two opposite

poles attach to the kinetochores (Figure 1.9). Unbalanced attachments such as those where both kinetochores originate from K-fibres from the same poles (syntelic) or when one kinetochore has no attachment to K-fibres (monotelic) can lead to chromosome alignment problems. Considering the reduction in microtubule nucleation and spindle assembly, it would be interesting to test whether oocytes depleted of PCM1 may have a higher frequency of incorrect K-fibre attachments or altered microtubule dynamics. The frequency of the different types of attachments can be quantified by labelling the kinetochores with CREST antibody, and the K-fibres with α-tubulin of oocytes treated with cold stable assay. In addition, measurement of interkinetochore distance within the bivalents reflects spindle tension, which can be affected by altered microtubule dynamics.

Altogether, live cell imaging revealed that the efficiency of chromosome congression in PCM1-depleted oocytes is disrupted. As stated above, K-fibres are reduced in PCM1-depleted oocytes, but this might simply be a consequence of fewer microtubules. Nonetheless, it may explain the observed chromosome defects. Future experiments investigating K-fibre dynamics and the frequency of different K-fibre and kinetochore attachment types would be of interest in order to test this hypothesis.

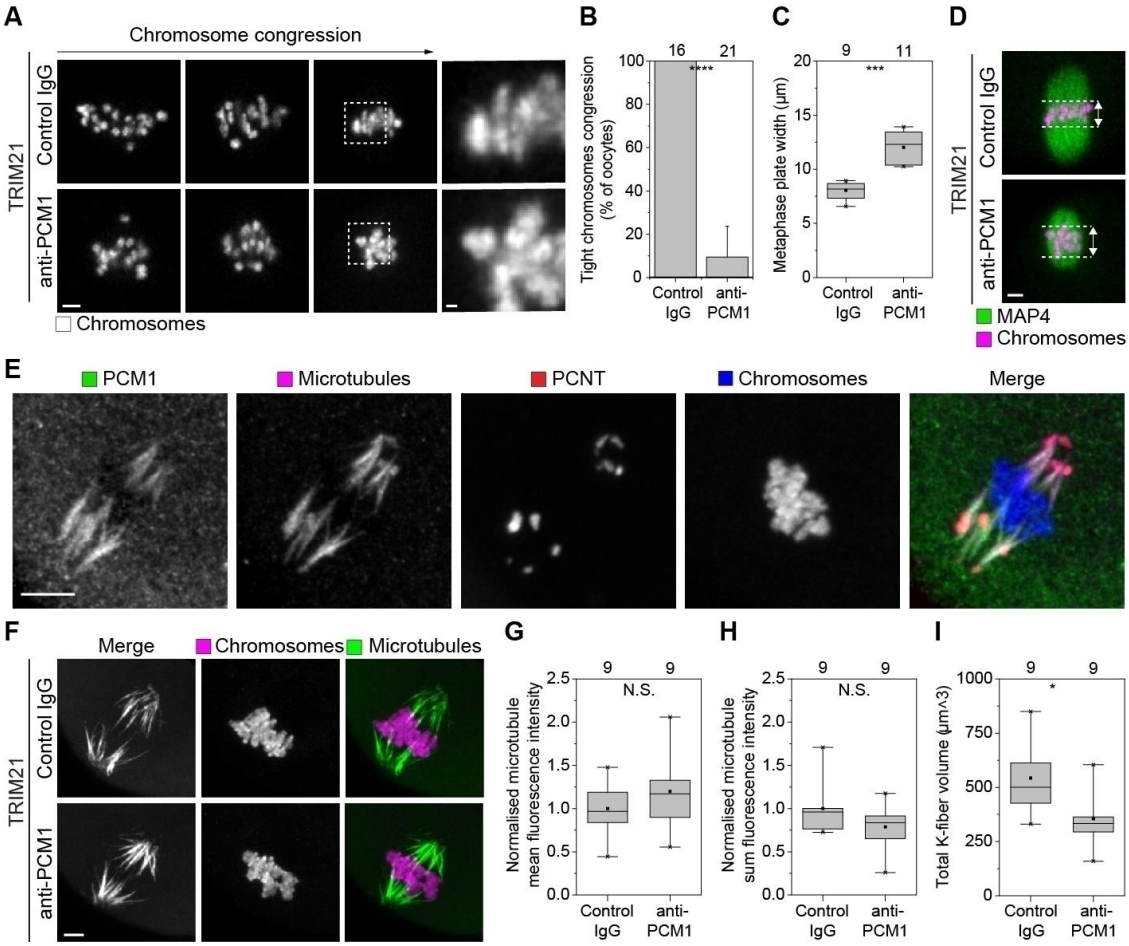

Figure 3.8 Reduced chromosome congression in PCM1-depleted oocytes is not linked to K-fibre formation.

(A) Examples from time-lapse imaging of chromosomes (H2B-mCherry) congression of oocytes microinjected with either control antibody or anti-PCM1 antibody. Boxed regions are magnified on the right and individual chromosomes are highlighted with an arrow. Scale bar shows 5 µm and 1 µm for magnified images.

(B) Frequency of tight chromosome congression in oocytes microinjected with either control antibody or anti-PCM1 antibody.

(C) Metaphase plate width measured in oocytes microinjected with either control antibody or anti-PCM1 antibody.

(D) Examples from time-lapse imaging of oocytes overexpressing TRIM21, H2B-mCherry and MAP4-mEGFP and microinjected with either control antibody or anti-PCM1 antibody. Dashed lines highlight the boundaries of chromosomes on the metaphase plate and arrows show the width of the metaphase plate.

(E) Immunofluorescence of anti-PCM1 (green), anti-α-tubulin (magenta), anti-Pericentrin (PCNT, red) and Hoechst (blue). Oocytes were allowed to mature (7 hours post NEBD) and treated with cold prior to fixing. Scale bar shows 5 µm.

(F) Immunofluorescence of anti-α-tubulin (green) and Hoechst (magenta). Oocytes overexpressing TRIM21 and microinjected with either control antibody or anti-PCM1 antibody were allowed to mature and treated with cold prior to fixing. Scale bar shows 5 μm.

(G-I) Quantification of normalised mean (G), normalised sum microtubule fluorescence intensity (α-tubulin) (H) and spindle volume (α-tubulin). All oocytes were fixed at 7 hours post NEBD.

Data from two independent experiments (B-C, G-I). Number of oocytes shown above the dataset or in brackets. P values were calculated with Student's t test (C, G-I) or Fisher's exact test (B).

3.7 Spindle actin is prominent in the absence of the meiotic spindle pole domain.

Among the screened proteins, the unconventional Myosin-10 (Myo10) protein also co-localised with PCM1 at the meiotic spindle pole domain in mouse oocytes (Figure 3.2A). Myo10 contains a motor domain that binds actin as well as a MyTH4 domain that binds microtubules (section 1.5.2.5, p34) (Weber et al., 2004). It was previously shown that actin infiltrates the spindle microtubules and is important for chromosome alignment and segregation (Mogessie & Schuh, 2017). To test whether the formation/maintenance of PCM1/MSPD depends on an intact actin network in meiosis I, the actin cytoskeleton was depolymerised using cytochalasin D. Immunofluorescence images revealed that PCM1 could still localise and assemble the spindle pole domain in the absence of F-actin (Figure 3.9A).

Depletion of PCM1 resulted in disappearance of the Myo10 signal, suggesting that PCM1 is required for Myo10 localisation (Figure 3.9B). Considering that this unconventional myosin localises to the meiotic spindle and has the ability to bind actin directly, one intriguing possibility might be that spindle actin network is altered by PCM1 depletion and loss of Myo10 localisation. In order to investigate this possibility, I stained mouse oocytes expressing TRIM21 and microinjected them with either Control IgG or anti-PCM1 antibody and stained MI oocytes with Phalloidin, a selective F-actin label. However, spindle actin was still prominent in PCM1-depleted oocytes although the organisation and internal density would require further investigation (Figure 3.9C).

Overall, these results did not show a clear link between spindle actin and the described PCM1 spindle pole domain, but indicate that localisation of Myo10 is PCM1-dependent. This is in line with the described phenotype of PCM-depleted oocytes, where no significant increase in chromosome defects, such as misalignment or lagging chromosomes could be seen, a reported phenotype of disrupted spindle actin (Mogessie & Schuh, 2017).

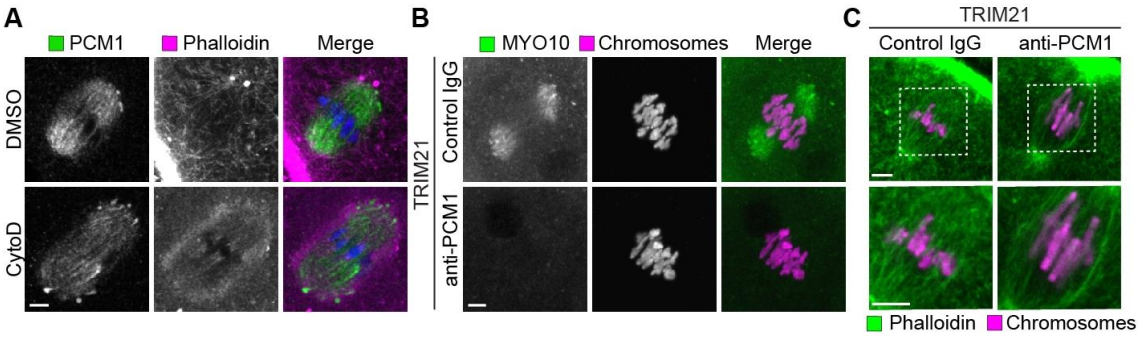

Figure 3.9 Meiotic pole domain is not dependent on the actin cytoskeleton

(A) Immunofluorescence of anti-PCM1 (green), Phalloidin (magenta) and Hoechst (blue). Oocytes were treated with either DMSO (control) or cytochalasin D (CytoD). Scale bar shows 5 µm.

(B) Immunofluorescence of MYO10 (green) and Hoechst (magenta). Oocytes overexpressing TRIM21 and microinjected with either control IgG or anti-PCM1 antibody were allowed to mature and fixed at 7 hours post NEBD. Scale bar shows 5 µm.

(C) Immunofluorescence of Phalloidin (green) and Hoechst (magenta). Oocytes overexpressing TRIM21 and microinjected with either control antibody or anti-PCM1 antibody were allowed to mature and fixed at 7 hours post NEBD. Boxed regions are magnified below. Scale bar shows 5 µm.

3.8 PCM1 is required for aMTOC formation and maintenance

Since PCM1 is a critical scaffold protein for centriolar satellites and plays an essential role in centrosome assembly (Hori & Toda, 2017), I decided to look at the expression and subcellular distribution of key components of the aMTOC components in PCM1-depleted oocytes. In particular, Pericentrin was previously reported to directly interact with PCM1 in somatic cells (Li et al., 2000) and Pericentrin levels were reduced at the centrosome after PCM1 depletion (Dammermann & Merdes, 2002; Li et al., 2000).

I first tested the subcellular localisation of the main aMTOC associated proteins in PCM1-depleted oocytes (Figure 3.10A-C). Depleting Pericentrin at this point provided a negative control. Depletion of Pericentrin was previously described in mouse oocytes, with data showing disruption of aMTOCs and loss of key Pericentrin interacting proteins, including γ-tubulin, which is essential for microtubule nucleation (Baumann et al., 2017). Surprisingly, the aMTOCs were absent when the localisation of various aMTOC components, including CEP192 (Figure 3.10A) and Pericentrin (Figure 3.10B) was tested, and γ-tubulin (Figure 3.10C) no longer localised to aMTOCs in PCM1-depleted oocytes. Pericentrin-depleted oocytes displayed the same phenotype. In the case of γ-tubulin, there was no recruitment to the aMTOCs and only weak labelling was seen on the meiotic spindle (Figure 3.10C). The fact that γ-tubulin was still visible within the spindle suggests that these components are not degraded/depleted, but simply cannot localise due to the absence of aMTOCs. The absence of aMTOCs at the spindle poles in PCM1-depleted oocytes suggests that PCM1 is essential for aMTOC function and could also explain the delay in microtubule nucleation, as aMTOCs are considered to be the main site of microtubule nucleation in mouse oocytes (Baumann et al., 2017; W. Ma & Viveiros, 2014; Schuh & Ellenberg, 2007).

Live cell imaging of CEP192, another major regulator of pericentriolar recruitment, showed that aMTOCs were present throughout meiosis at both spindle poles and cytoplasm in control oocytes, and all populations of CEP192 labelled aMTOCs were absent in PCM1 and Pericentrin-depleted oocytes (Figure 3.10D).

Since PCM1 was reported to directly bind Pericentrin, I wanted to confirm that the absence of Pericentrin following PCM1 depletion is not due to a non-specific degradation of the protein complex by the Trim-Away method. Western blot experiments showed that

endogenous Pericentrin was still present after PCM1-depletion (Figure 3.10E) and that the anti-Pericentrin antibody indeed specifically recognises endogenous Pericentrin. (siPcnt, Figure 3.10E, lane 2). Oocytes overexpressing TRIM21 and microinjected with either control antibody or anti-PCM1 antibody showed comparable Pericentrin signal on the Western Blot (Figure 3.10E, lanes 4 and 5). This result confirmed that Trim-Away was specifically depleting PCM1 and did not have an off-target effect due the proximity of Pericentrin to PCM1. These data provide support for the initial hypothesis that Pericentrin interacts with PCM1 and that this interaction is required for aMTOC function and maintenance.

I then further investigated if PCM1 is required for maintaining the structural integrity of aMTOCs once Pericentrin is recruited and has formed the aMTOC pole ring domain in MI oocytes. Acute depletion of PCM1 was performed as shown in Figure 3.7G. CEP192 signal was used as the marker for aMTOCs in live oocytes, and sum fluorescence intensity showed complete loss of signal from aMTOCs within 20-25 minutes following anti-PCM1 antibody injection (Figure 3.10F and J). The timing of complete loss of CEP192 signal was consistent with the time required for PCM1 degradation, previously shown in MI oocytes (Figure 3.5H-I). Total CEP192 intensity remained at a constant level in control oocytes, indicating that loss of CEP192 signal in PCM1-depleted oocytes was not due to bleaching.

High resolution 3D imaging also suggested that loss of aMTOCs from the spindle poles was not due to dissociation or fragmentation, but to a continuous disassembly and loss of aMTOCs themselves (Figure 3.10F-G and J). Importantly, loss of aMTOCs from the spindle pole also coincided with a gradual reduction in spindle volume (Figure 3.10H-J). A significant reduction in spindle volume occurred once all aMTOCs had disassembled, at around 20-25 min following anti-PCM1 microinjection (Figure 3.10F-J).

It was previously shown that aMTOC localisation to the nuclear envelope as well as its association with microtubule asters is important for oocyte competence to resume meiosis (Łuksza et al., 2013). As oocytes undergo different growth phases, aMTOCs reorganise and large aMTOCs associate with the nuclear envelope to become the main sites of microtubule nucleation following NEBD. The nucleation ability of aMTOCs, as measured by the number of microtubule foci nucleated aMTOC areas, increases during

oocyte growth phase (Łuksza et al., 2013). One of the most striking phenotypes of PCM1-depleted oocytes was the significant delay in the onset of microtubule nucleation following NEBD (Figure 3.6A and E). Therefore, I further investigated aMTOC numbers (labelled with CEP192) associated with the nuclear envelope (NE) via high resolution 3D imaging of prophase I arrested oocytes (Figure 3.10K). Images taken just before and after anti-PCM1 antibody microinjection clearly show the complete disassembly of NE-associated aMTOCs. This experiment suggested two things: firstly, PCM1 depletion in prophase I disrupted all aMTOCs on the NE and therefore resulted in the loss of the main microtubule nucleation site as oocytes resumed meiosis (Figure 3.10K). This is also indicated by the delay of nucleation onset in these oocytes (Figure 3.6A and E). Secondly, PCM1 is required for the integrity of all pools of aMTOCs throughout meiosis as seen by the disassembly of CEP192 labelled aMTOCs in the cytoplasm, associated with the NE in prophase I and at spindle poles following entry to meiosis I (Figure 3.10D, J and K).

Overall, these results confirm that PCM1 not only has a central role in the recruitment of aMTOC core components, a conserved function when compared to mitosis, but also in maintaining their integrity throughout meiosis once Pericentrin has formed the aMTOC ring.

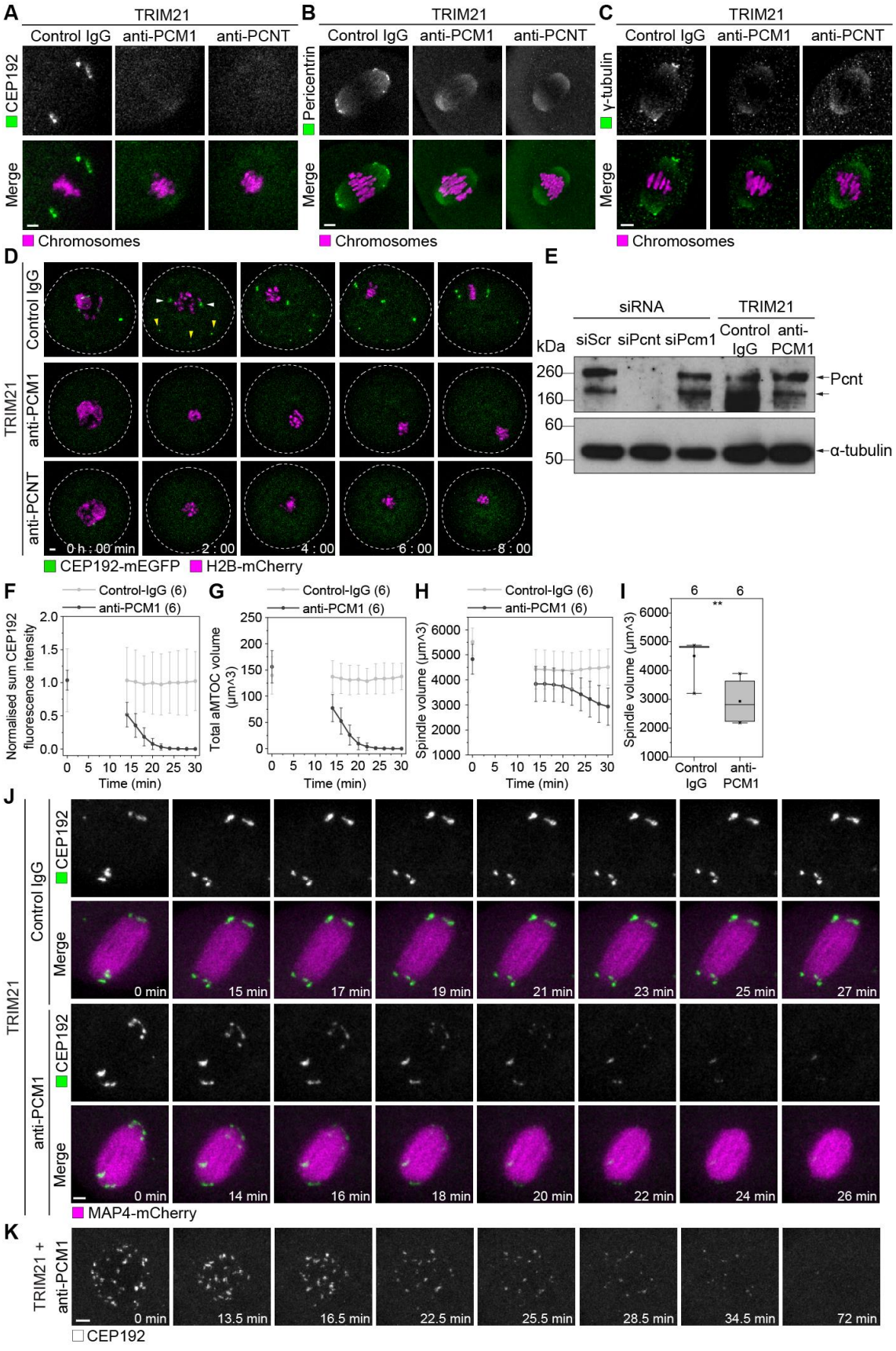
A
TRIM21
Control IgG
anti-PCM1
anti-PCNT
CEP192
Merge
Chromosomes
B
TRIM21
Control IgG
anti-PCM1
anti-PCNT
Pericentrin
Merge
Chromosomes
C
TRIM21
Control IgG
anti-PCM1
anti-PCNT
γ-tubulin
Merge
Chromosomes
D
TRIM21
Control IgG
anti-PCM1
anti-PCNT
0 h : 00 min
2 : 00
4 : 00
6 : 00
8 : 00
CEP192-mEGFP
H2B-mCherry
E
siRNA
TRIM21
siScr
siPcnt
siPcm1
Control IgG
anti-PCM1
kDa
260
160
60
50
Pcnt
α-tubulin
F
Control-IgG (6)
anti-PCM1 (6)
Normalised sum CEP192 fluorescence intensity
Time (min)
G
Control-IgG (6)
anti-PCM1 (6)
Total aMTOC volume (µm^3)
Time (min)
H
Control-IgG (6)
anti-PCM1 (6)
Spindle volume (µm^3)
Time (min)
I
6
6
**
Spindle volume (µm^3)
Control IgG
anti-PCM1
J
TRIM21
Control IgG
anti-PCM1
CEP192
Merge
0 min
15 min
17 min
19 min
21 min
23 min
25 min
27 min
0 min
14 min
16 min
18 min
20 min
22 min
24 min
26 min
MAP4-mCherry
K
TRIM21 + anti-PCM1
0 min
13.5 min
16.5 min
22.5 min
25.5 min
28.5 min
34.5 min
72 min
CEP192

Figure 3.10 PCM1 is required for recruitment of aMTOC components and maintenance of MTOC integrity throughout meiosis.

(A) Localisation of CEP192-mCherry (green) in oocytes overexpressing TRIM21 and microinjected with control, anti-PCM1 or anti-Pericentrin antibody. Scale bar shows 5 μm.

(B) Immunofluorescence of Pericentrin localisation (green) in oocytes overexpressing TRIM21 and microinjected with control, anti-PCM1 or anti-Pericentrin antibody. Scale bar shows 5 μm.

(C) Immunofluorescence of γ-tubulin localisation (green) in oocytes overexpressing TRIM21 and microinjected with control, anti-PCM1 or anti-Pericentrin antibody. Scale bar shows 5 μm.

(D) Examples from time-lapse imaging of oocytes overexpressing TRIM21, H2B-mCherry and CEP192-mEGFP and microinjected with control, anti-PCM1 or anti-Pericentrin antibody. Time shows hours (h) and minutes (min) from NEBD (time 0). White arrows show spindle pole aMTOCs, yellow arrows show cytoplasmic aMTOCs. Scale bar shows 5 μm.

(E) Western blot showing endogenous Pericentrin in MI mouse oocytes. Lanes 1-3 show oocytes injected with siRNA. Lanes 4-5 show oocytes overexpressing TRIM21 and microinjected with either control or anti-PCM1 antibody. Whole oocyte lysates were pooled from two separate experiments and blotted once. Detection of α-tubulin served as control.

(F) Quantification of normalised sum aMTOC fluorescence intensity (CEP192-mEGFP) over time (minutes). Oocytes overexpressing TRIM21, MAP4-mCherry and CEP192-mEGFP were left to mature *in vitro* and microinjected at 7 hours post NEBD with either control antibody or anti-PCM1 antibody. Time 0 is just before antibody injection.

(G) Quantification of total aMTOC volume (CEP192-mEGFP) over time (minutes). Oocytes overexpressing TRIM21, MAP4-mCherry and CEP192-mEGFP were left to mature *in vitro* and microinjected at 7 hours post NEBD with either control antibody or anti-PCM1 antibody. Time 0 is just before antibody injection.

(H-I) Quantification of spindle volume (MAP4-mCherry) over time (minutes). Oocytes overexpressing TRIM21, MAP4-mCherry and CEP192-mEGFP were left to mature *in vitro* and microinjected at 7 hours post NEBD with either control antibody or anti-PCM1 antibody. Time 0 is just before antibody injection (H). Spindle volume (MAP4-mEGFP) at 30 minutes (min) from antibody injection (I).

(J) Examples from time-lapse imaging of oocytes overexpressing TRIM21, MAP4-mCherry and CEP192-mEGFP. Oocytes were left to mature *in vitro* and microinjected at 7 hours post NEBD with either control antibody or anti-PCM1 antibody. Time shows minutes (min) just before antibody injection (time 0). Scale bar shows 5 μm.

(K) Examples from time-lapse imaging of oocytes overexpressing TRIM21 and CEP192-mEGFP. Oocytes were left to mature *in vitro* and microinjected at 7 hours post NEBD with either control antibody or anti-PCM1 antibody. Time shows minutes (min) just before antibody injection (time 0). Scale bar shows 5 μm.

3.9 Microtubule nucleation is reduced throughout meiosis in the absence of functional aMTOCs

In order to investigate whether the loss of aMTOCs in PCM1 or Pericentrin-depleted oocytes results in a comparable loss of microtubules, I compared the total nucleating capacity of both PCM1 and Pericentrin-depleted oocytes. An assumption was made that the total amount of microtubules nucleated by control oocytes represent 100% of nucleation capacity at every measured time point, as all microtubule nucleation pathways are active. I then compared the sum microtubule intensity of PCM1 and Pericentrin-depleted oocytes as a percentage of the total amount of microtubules in control oocytes over time (Figure 3.11). This data could indirectly show the average contribution of aMTOCs to overall microtubule nucleation at different stages of meiosis. This analysis suggested that aMTOCs are essential for the initial microtubule nucleation immediately after NEBD, as previously reported (Baumann et al., 2017; Schuh & Ellenberg, 2007), with a gradual recovery of nucleation 1-3 hours post NEBD, accounting for about 20-40% of nucleation activity (Figure 3.11B). Another increase in nucleation activity is observed at around 4 hours post NEBD, following bipolar spindle formation, reaching 60-80% of the nucleation capacity of controls, which then remains at this level until anaphase (Figure 3.11B).

While PCM1-depleted oocytes are unable to assemble aMTOCs, similar to Pericentrin depletion, their overall microtubule nucleation activity seems to be further reduced compared to Pericentrin depletion alone (Figure 3.11B). This may suggest that, owing to its role as a scaffold protein, other components that could be important for microtubule nucleation are affected by depletion of PCM1, further reducing their nucleation capacity by about 20% throughout meiosis. When comparing the significance of this difference at specific timepoints, the sum microtubule intensity was significantly lower in the absence of PCM1 only at 8 hours post NEBD compared to Pericentrin-depleted oocytes ($p=0.05$). Further experiments are required to confirm that this is a consistent trend between the two depletion groups.

Thus, interpretation of the sum microtubule fluorescence intensity as a percentage of the total microtubule nucleation in control oocytes suggests that aMTOCs contribute to the overall nucleating activity of the oocyte during meiosis to a different extent; this

indicates that the most critical contribution of aMTOCs lies within the first 30 minutes of NEBD, and then with decreasing extent as meiosis progresses. Of course, one needs to consider the potential adjustment the cell may use to compensate for the absence of MTOCs, and perhaps also upregulates other pathways (Hayward et al., 2014). However, it is evident that aMTOCs are essential for microtubule nucleation during initial spindle assembly with a gradual decrease in the contribution at later stages of meiosis.

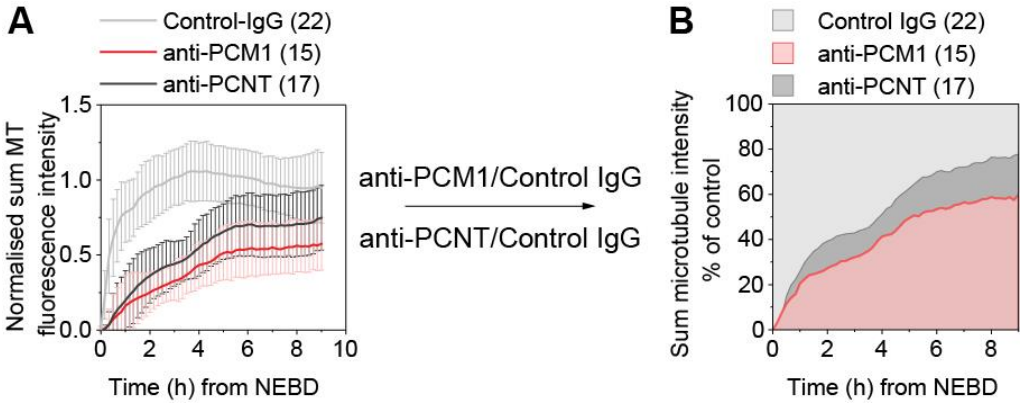

Figure 3.11 Overall spindle microtubule nucleation in the absence of aMTOCs.

(A) Quantification of normalised sum microtubule fluorescence intensity (MAP4-mEGFP) over time (hours). Time (0) from NEBD.

(B) Percentage conversion of sum microtubule fluorescence intensity (MAP4-mEGFP) compared to control oocyte values. Average sum microtubule fluorescence intensity of PCM1 or Pericentrin-depleted oocytes was divided by the average sum microtubule fluorescence intensity of oocytes microinjected with Control IgG and displayed as a percentage value over time (hours). Time 0 is the onset of microtubule nucleation.

3.10 Localisation of PCM1 and Pericentrin at the spindle poles is interdependent during meiosis

Since Pericentrin and PCM1 have been shown to directly interact in mitotic cells (Dammermann & Merdes, 2002; Li et al., 2000), I also wanted to check PCM1 localisation in Pericentrin-depleted oocytes.

Pericentrin depletion by either RNAi or Trim-Away, showed that Pericentrin is required for correct PCM1 localisation (Figure 3.12A-B), suggesting an interdependence as previously shown: Pericentrin localisation is dependent on PCM1 (Figure 3.10). This was also confirmed with live cell imaging where fluorescently tagged PCM1 no longer formed the meiotic spindle pole domain in the absence of Pericentrin (Figure 3.12C). Pericentrin depletion by both siRNA and Trim-Away had no apparent effect on endogenous PCM1 protein levels (Figure 3.12D), confirming that depletion is specific to the target protein as shown for PCM1-depletion (Figure 3.5B). Analysis of Pericentrin-depleted oocytes showed the same phenotype as for PCM1 depletion (section 3.5, p93). Notably, the onset of microtubule nucleation following NEBD was delayed (Figure 3.12E) with significant reduction in the total microtubules nucleated (Figure 3.12F-G) as well as the overall spindle volume (Figure 3.12H-I).

Acute depletion of Pericentrin once the spindle has fully formed at 7 hours post NEBD, also confirmed that Pericentrin is indeed a main scaffold protein required for maintaining the integrity of the aMTOCs at spindle poles. Complete depletion of Pericentrin after about 30 minutes of antibody microinjection showed disassembly of CEP192 labelled aMTOCs in live mouse oocytes (Figure 3.12N). Once aMTOCs disassembled, total spindle microtubules (measured by MAP4 sum fluorescence intensity) were reduced significantly, as was the spindle volume (Figure 3.12J-M).

Together, these results show that Pericentrin is an essential scaffold protein in assembling and maintaining aMTOCs organisation. Due to the interdependence in the localisation of PCM1 and Pericentrin, the observed spindle phenotype following PCM1 depletion cannot be fully dissected in mouse oocytes. Further experiments, such as rescuing the spindle phenotype by reintroducing either PCM1 and/or Pericentrin would be important to show specificity of the reported phenotypes.

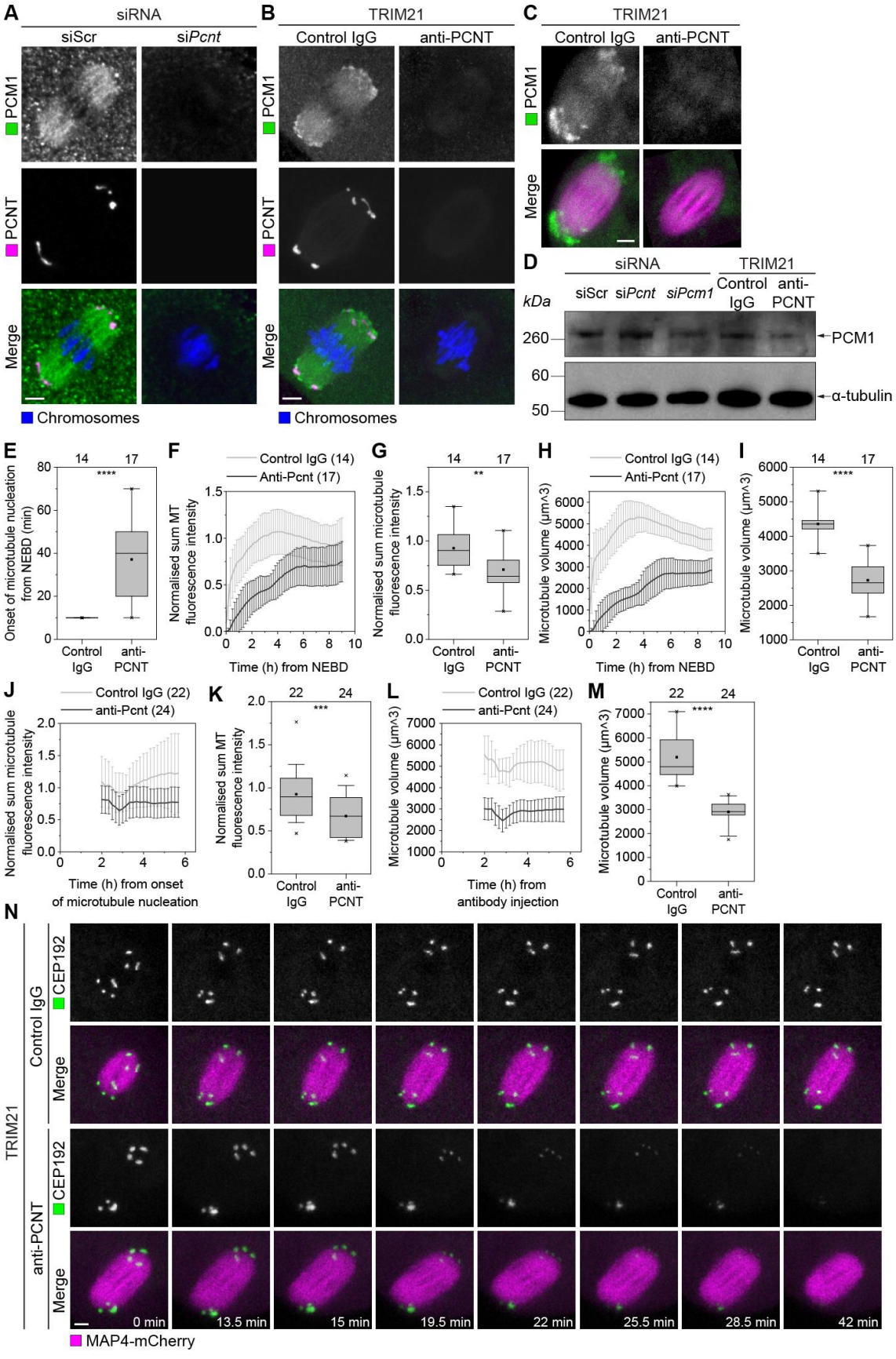
A
siRNA
siScr
siPcnt
PCM1
PCNT
Merge
Chromosomes
B
TRIM21
Control IgG
anti-PCNT
C
D
siRNA
TRIM21
siScr
siPcnt
siPcm1
Control IgG
anti-PCNT
kDa
260
60
50
PCM1
α-tubulin
E
Onset of microtubule nucleation from NEBD (min)
F
Control IgG (14)
Anti-Pcnt (17)
Normalised sum MT fluorescence intensity
Time (h) from NEBD
G
Normalised sum microtubule fluorescence intensity
H
Microtubule volume (µm^3)
I
J
Control IgG (22)
anti-Pcnt (24)
Time (h) from onset of microtubule nucleation
K
L
Time (h) from antibody injection
M
N
TRIM21
Control IgG
anti-PCNT
CEP192
Merge
0 min
13.5 min
15 min
19.5 min
22 min
25.5 min
28.5 min
42 min
MAP4-mCherry

Figure 3.12 PCM1 and Pericentrin are interdependent in mouse oocytes.

(A) Immunofluorescence of PCM1 (green), Pericentrin (magenta) and Hoechst (blue). Oocytes were microinjected with negative control siRNA (Scr-control) or Pcnt-siRNA and fixed at the MI stage (7h post NEBD). Scale bar shows 5 µm.

(B) Immunofluorescence of PCM1 (green), Pericentrin (magenta) and Hoechst (blue) in oocytes overexpressing TRIM21 and microinjected with control or anti-Pericentrin antibody. Scale bar shows 5 µm.

(C) Live cell imaging of PCM1 localisation in mouse oocytes undergoing meiosis I. Oocytes overexpressing PCM1-mEGFP (green) and MAP4-mCherry (magenta) to label microtubules. Examples are shown after formation of the bipolar spindle. Scale bar shows 5 µm.

(D) Western blot showing endogenous PCM1 in MI mouse oocytes. Whole oocyte lysates were pooled from two separate experiments and blotted once. Detection of α-tubulin served as loading control.

(E) Timing of the onset of microtubule nucleation is shown in minutes (min).

(F-G) Quantification of normalised sum microtubule fluorescence intensity (MAP4-mEGFP) over time (hours). Time 0 is the onset of microtubule nucleation (F). Normalised sum fluorescence intensity (MAP4-mEGFP) at 8 hours from microtubule nucleation (G).

(H-I) Quantification of spindle volume (MAP4-mEGFP) over time (hours). Time 0 is the onset of microtubule nucleation (F). Spindle volume (MAP4-mEGFP) at 8 hours from microtubule nucleation (I).

(J-K) Quantification of normalised sum microtubule fluorescence intensity (MAP4-mEGFP) over time (hours). Oocytes overexpressing TRIM21, MAP4-mCherry were left to mature *in vitro* and microinjected at 7 hours post NEBD with either control antibody or anti-Pericentrin antibody. Time 0 is the time of antibody injection (J). Normalised sum fluorescence intensity (MAP4-mEGFP) at 2 hours from antibody injection (K).

(L-M) Quantification of spindle volume (MAP4-mEGFP) over time (hours). Oocytes overexpressing TRIM21, MAP4-mCherry were left to mature *in vitro* and microinjected at 7 hours post NEBD with either control antibody or anti-Pericentrin antibody. Time 0 is the time of antibody injection (L). Spindle volume (MAP4-mEGFP) at 2 hours from antibody injection (M).

(N) Examples from time-lapse imaging of oocytes overexpressing TRIM21, MAP4-mCherry and CEP192-mEGFP. Oocytes were left to mature *in vitro* and microinjected at 7 hours post NEBD with either control antibody or anti-Pericentrin antibody. Time shows minutes (min) from antibody microinjection, 0 min is just before antibody microinjection. Scale bar shows 5 µm.

Data from two independent experiments (E-M). Number of oocytes shown above the dataset or in brackets. P values were calculated with Student's t test (E, G, I, K and M).

3.11 Absence of PCM1 and aMTOCs affects microtubule dynamics.

Nucleation of microtubules is a well characterised function of aMTOCs. I therefore investigated the origin of microtubule nucleation in the absence of aMTOCs and PCM1. In addition, I sought to discover whether the absence of PCM1 and aMTOCs has a direct effect on microtubule dynamics.

Firstly, the growing microtubule plus-tips in oocytes that had just undergone NEBD were imaged by expressing EB3-EGFP, one of the main plus-end binding (EB) proteins (Figure 3.13A). As previously described (section 3.8, 3.10), CEP192 labelled aMTOCs no longer assembled in PCM1 and Pericentrin-depleted oocytes (Figure 3.10 and Figure 3.12). Once NEBD commenced, control oocytes rapidly nucleated microtubules with EB3 plus-tips predominantly emanating from aMTOC foci and between the individualised chromosomes (Figure 3.13A). In the absence of PCM1 or Pericentrin, EB3 comets were reduced and originated from the chromosome mass (Figure 3.13A). Projections of EB3 over a period of 5 minutes clearly show that the pattern of microtubule growth is different between control and depleted groups (Figure 3.13A). Although, it is visually clear that the total EB3 labelled microtubule coments are significantly reduced compared to controls, accurate quantification of the signal was difficult, as it was not possible to align live cell imaging at exactly the same time following NEBD between experimental groups. Therefore, I decided to use a Nocodazole regrowth assay and fix oocytes at specific time points in order to have a more accurate analysis of the site of microtubule nucleation and the total oocyte microtubule regrowth capacity.

It was important to optimise the microtubule regrowth assay prior to setting up the experiment, by testing the duration of Nocodazole treatment required to fully depolymerise all spindle microtubules (Figure 3.13B). Complete depolymerisation of spindle microtubules was achieved after 1 hour of Nocodazole treatment, while 30 minutes' incubation still showed spindle microtubules around chromosomes (Figure 3.13B). To ensure that oocytes could fully recover and form bipolar spindles following prolonged Nocodazole treatment and washout, I also fixed oocytes after washout and further incubation for an hour. This showed that oocytes could recover and form a well

organised bipolar spindle following complete microtubule depolymerisation (one hour, 1 µM Nocodazole treatment), comparable to control oocytes treated with DMSO (Figure 3.13B).

Having optimised the Nocodazole regrowth assay, I looked at the microtubule regrowth capacity of oocytes depleted of PCM1 or Pericentrin (Figure 3.13C). Oocytes were fixed at 2.5 and 5 minutes following Nocodazole washout. Quantification of the total sum intensity of microtubules nucleated at each time point clearly showed that both PCM1 and Pericentrin-depleted oocytes had reduced nucleating capacity, with significantly lower total microtubule intensities (Figure 3.13D). Analysis of the total microtubule volume also showed the same trend (Figure 3.13E).

The site of nucleation was scored based on 3D image recording of the full microtubule mass and chromosomes. Images were analysed by tracking the microtubule filaments through the imaged Z stacks to the site of origin. The site of microtubule nucleation was primarily from aMTOCs in control oocytes, but nucleation was also visible around chromosomes in oocytes labelled with Pericentrin. In the case of control oocytes, this qualitative scoring may not accurately demonstrate the contribution of microtubule regrowth from the aMTOCs and the chromosome surface; however, it was clear that in the presence of aMTOCs, the majority of microtubules were emanating from the Pericentrin labelled aMTOC foci. In the absence of PCM1 and aMTOCs, microtubules were seen only around and radiating outward from chromosomes (Figure 3.13C and F).

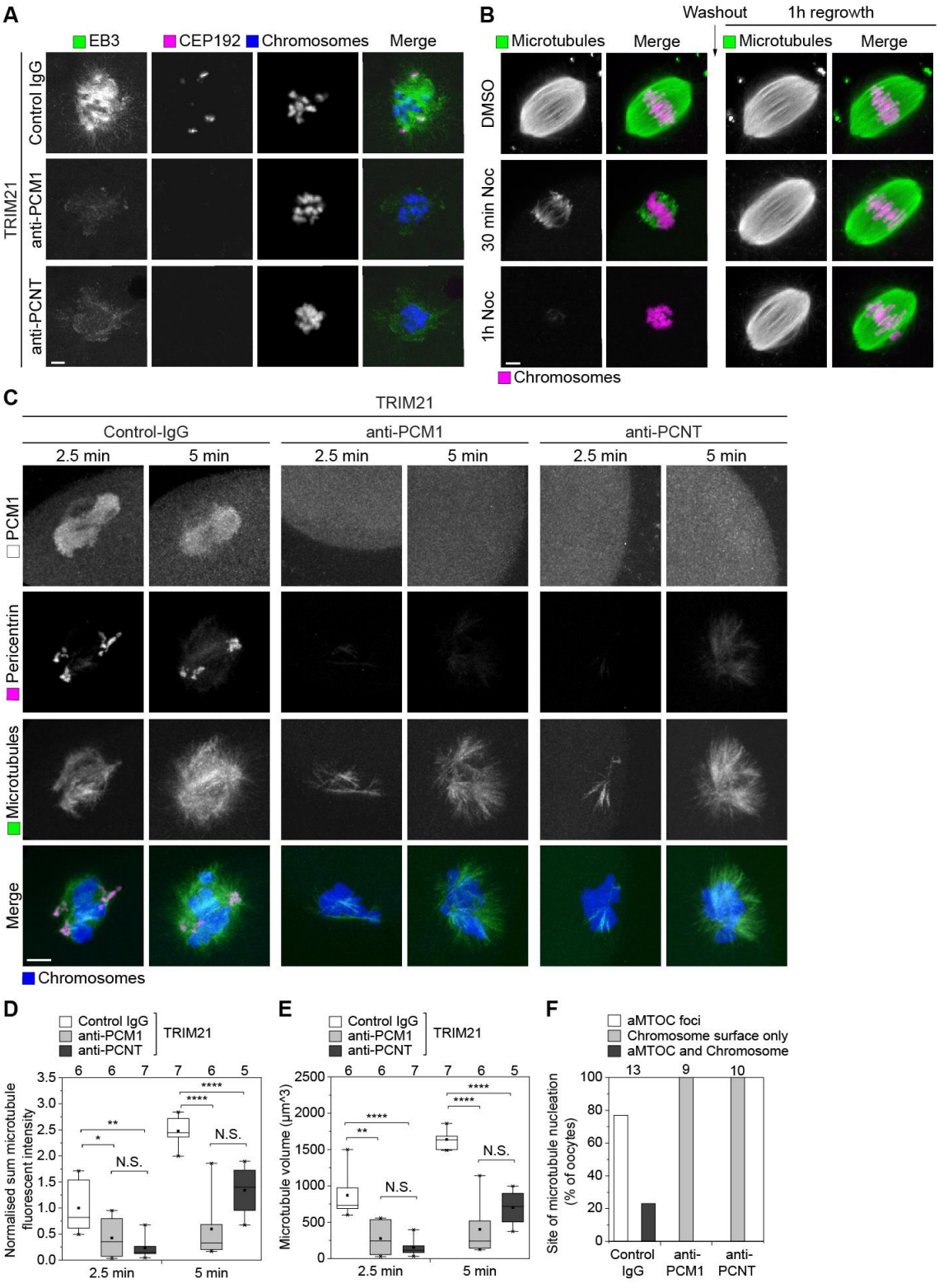

Figure 3.13 In the absence of PCM1 and aMTOCs, microtubule regrowth is significantly compromised and originates from the chromosome surface.

(A) Live cell imaging of EB3-EGFP (green), CEP192-mCherry (magenta) and H2B-iRFP (blue). Images show projections over a period of 5 minutes, immediately after NEBD. Scale bar shows 5 µm.

(B) Immunofluorescence of α-tubulin (green) and Hoechst (magenta) in oocytes treated with DMSO or Nocodazole. Left side panels show oocytes following DMSO or Nocodazole treatment. Right side panel shows oocytes following Nocodazole washout and after regrowth for 1 hour (h). Scale bar shows 5 µm.

(C) Immunofluorescence of microtubule regrowth following 1-hour Nocodazole treatment. Time shows minutes (min) from Nocodazole washout. Oocytes overexpressing TRIM21 and microinjected with control, anti-PCM1 or anti-Pericentrin antibody. Scale bar shows 5 µm.

(D) Quantification of normalised sum microtubule fluorescence intensity (α-tubulin) at 2.5 and 5 minutes (min) from Nocodazole washout.

(E) Quantification of total microtubule volume (α-tubulin) at 2.5 and 5 minutes (min) from Nocodazole washout.

(F) Quantification of site of microtubule regrowth following Nocodazole treatment for 1 hour and washout.

Data from one experiment (D-F). Number of oocytes shown above the dataset. P values were calculated with Student's t test (D-E) or Fisher's exact test (F).

Fluorescent photoactivation of α-tubulin is a useful method to assess poleward flux rate and the rate of microtubule turnover in order to investigate if microtubule dynamics are affected in the absence of PCM1 and aMTOCs. Microtubule flux can be described as the continuous movement of the microtubule lattice towards the minus-ends (spindle poles) (Figure 1.6, blue arrows), a mechanism that requires a steady state depolymerisation / polymerisation at the two ends of the microtubules. Photoactivation of low or no fluorescence of a labelled protein is achieved by the irradiation of a specific wavelength that converts the photoactivable molecules into a higher fluorescence state (Lukyanov et al., 2005).

Microtubule dynamics based on the measured flux rate between the different experimental groups, i.e. the displacement of the photoactivated α-tubulin molecules within the spindle microtubule lattice over time, showed comparable results (Figure 3.14A-B). This could indirectly suggest that microtubule associated proteins that are known to contribute to microtubule flux, such as Kinesin-5, still function at a comparable rate (Peterman & Scholey, 2009). This is also in line with the fact that in the absence of PCM1 and aMTOCs, mouse oocyte are still able to form a bipolar spindle structure, a known function of Kinesin-5 (Waitzman & Rice, 2014). Measurement of the half-life of fluorescence α-tubulin signal dissipation were also comparable in the absence of PCM1 and aMTOCs (Figure 3.14C-E).

While microtubule flux rate was not affected by the depletion of PCM1, EB3 plus-tip tracking revealed a significant increase in microtubule growth rate when PCM1 or Pericentrin was depleted (Figure 3.14H). All oocytes analysed for microtubule growth rate were also injected with CEP192 to ensure depletion efficiency and confirmed the loss of aMTOC fluorescence signal in both PCM1 and Pericentrin-depleted oocytes (Figure 3.14F). It is important to mention however, that microtubule growth velocities were only measured in one experiment and should be repeated to confirm the observed trend.

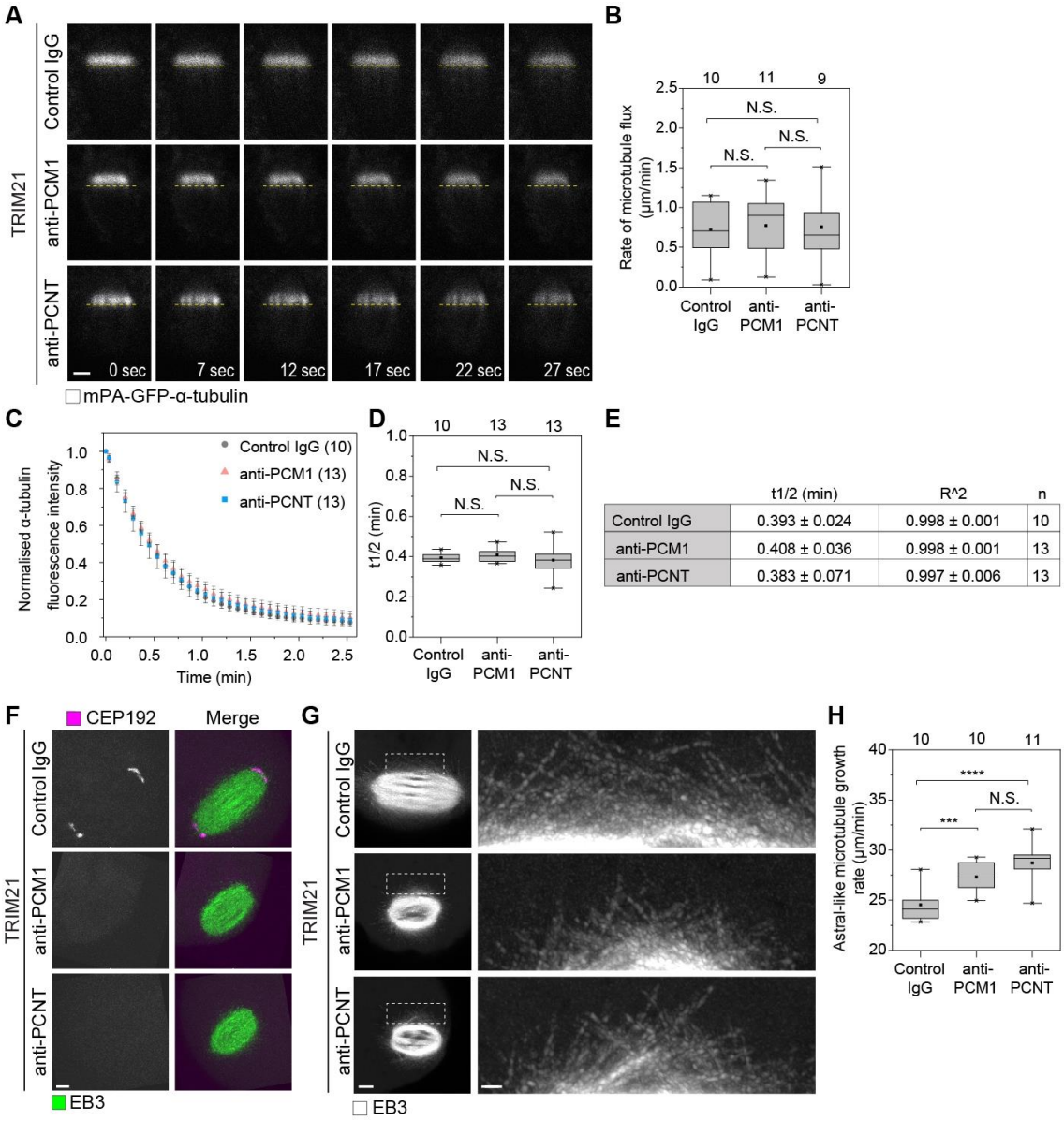

Figure 3.14 Microtubule growth rate is increased in the absence of PCM1 and aMTOCs

(A) Examples of single-section, time-lapse imaging of mPA-GFP-α-tubulin photoactivation in oocytes overexpressing TRIM21 and microinjected with either control, anti-PCM1 or anti-PCNT antibody. Time shows seconds (s) from photoactivation. Scale bar shows 5 μm.

(B) Quantification of microtubule flux rate in oocytes overexpressing TRIM21 and microinjected with either control, anti-PCM1 or anti-PCNT antibody.

(C) Quantification of photoactivated tubulin fluorescence signal dissipation half-life in oocytes overexpressing TRIM21 and microinjected with either control, anti-PCM1 or anti-PCNT antibody.

(D-E) Distribution of photoactivated tubulin fluorescence signal dissipation half-life in oocytes overexpressing TRIM21 and microinjected with either control, anti-PCM1 or anti-PCNT antibody. Half-life values and coefficient of determination (R^2) of the single exponential curves fitted are shown in table (E).

(F) Live cell imaging of EB3-EGFP (green) and CEP192-mCherry (magenta) in oocytes overexpressing TRIM21 and microinjected with either control, anti-PCM1 or anti-PCNT antibody. Images show projections over a period of 2 minutes. Scale bar shows 5 µm.

(G) Live cell imaging of EB3-EGFP (green) in oocytes overexpressing TRIM21 and microinjected with either control, anti-PCM1 or anti-PCNT antibody. Boxed regions are magnified on the right. Scale bar shows 5 µm and 1 µm for magnified images.

(H) Distribution of astral-like microtubule growth rate in oocytes overexpressing TRIM21 and microinjected with either control, anti-PCM1 or anti-PCNT antibody.

Data from one experiment. Number of oocytes shown above the dataset. P values were calculated with Student's t test (B-D, H).

3.12 Microtubule nucleation is dependent on RanGTPase activity in the absence of aMTOCs.

Evidence from previous studies revealed that RanGTPase microtubule nucleation plays an important role in spindle microtubule assembly during meiosis, in combination with aMTOCs (Dumont et al., 2007; Schuh & Ellenberg, 2007), serving as the main nucleating pathway around chromosomes in the absence of centrosomes or other MTOCs (Carazo-Salas et al., 1999; Holubcová et al., 2015). Following the observation that PCM1 is essential for the structural integrity of aMTOCs throughout meiosis, an obvious question is to elucidate the mechanism that allows microtubules to nucleate in their absence, and whether these oocytes can switch to RanGTPase activity, as shown in somatic cells (Carazo-Salas et al., 1999).

Ran(T24N) is a dominant-negative mutant with a low affinity for GTP/GDP binding, and as a result inhibits RCC1, Ran guanine nucleotide exchange factor activity and the formation of active RanGTP (Carazo-Salas et al., 2001; Klebe et al., 1995). Microinjecting the mutant Ran(T24N) recombinant protein into control and aMTOC depleted oocytes revealed that nucleation of the meiotic spindle in mouse oocytes is dependent on both pathways (Figure 3.15A). While all aMTOC-free (Pericentrin-depleted) oocytes with BSA microinjection could nucleate spindle microtubules at a reduced rate, only one oocyte in the Ran(T24N) microinjected group showed any

microtubule nucleation, with a delay of over 8 hours following NEBD (Figure 3.15A-C). This observation is also in agreement with the microtubule regrowth assay showing microtubule growth originating only from the chromosome surface in the absence of PCM1 and aMTOCs (section 3.11).

Overall, this data suggest that the RanGTP-dependent microtubule nucleation pathway has an essential role in mouse oocytes, as shown previously (Schuh & Ellenberg, 2007). The results show that in the absence of aMTOCs, oocytes fully rely on GTP-bound Ran-induced microtubule nucleation from the chromosome surface.

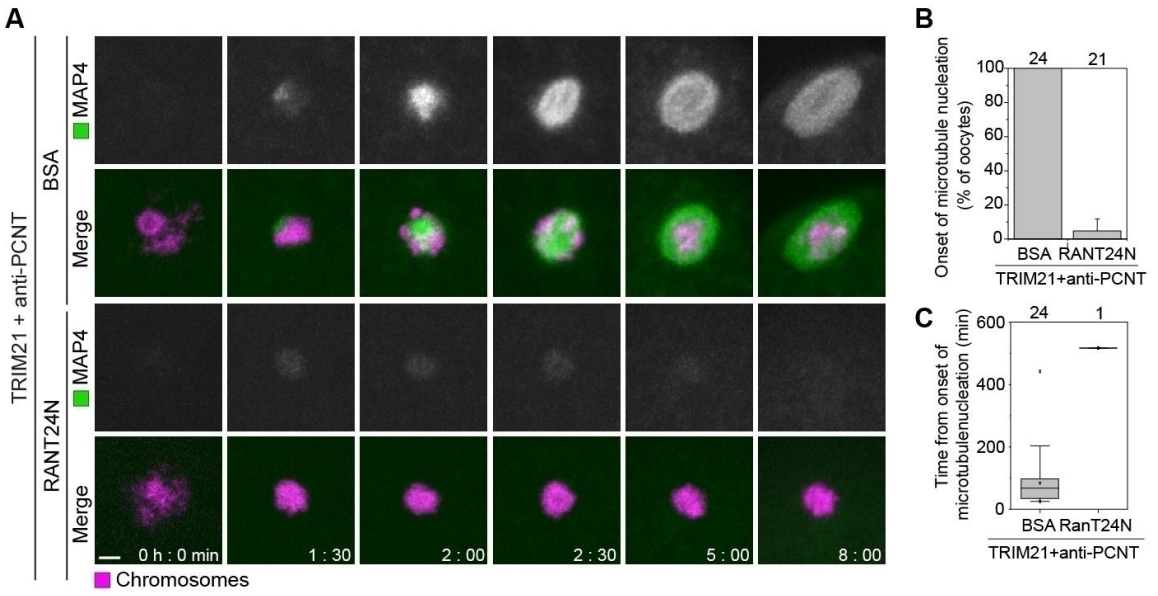

Figure 3.15 RanGTPase mediated microtubule nucleation plays a primary role in the absence of aMTOCs in mouse oocytes.

(A) Examples from time-lapse imaging of oocytes overexpressing TRIM21, H2B-mCherry and MAP4-mEGFP and microinjected with anti-Pericentrin antibody and BSA or RAN(T24N). Time shows hours (h) and minutes (min) from NEBD (time 0). Scale bar shows 5 µm.

(B) Oocytes overexpressing TRIM21 and microinjected with anti-Pericentrin antibody in combination with BSA or RAN(T24N) were scored for the frequency of oocytes that nucleated microtubules following NEBD.

(C) Timing of the onset of microtubule nucleation is shown in minutes (min).

Data from two independent experiments (B-C). Number of oocytes shown above the dataset or in brackets. P values were calculated with Student's t test (C) or Fisher's exact test (B). Images were taken by Chun So, Schuh lab.

4 RESULTS: PART II

TACC3: important assembly factor for MSPD formation in acentrosomal mouse oocytes.

4.1 Overview

One of the main limitations of the mouse model was that the functions of PCM1 and aMTOCs could not be separated, due to its interdependence with Pericentrin. Centrioles and pericentriolar material inheritance differ between mammalian species, and one possibility was to look at oocytes that lack MTOCs. Although mouse oocytes lack centrioles, they do form foci of PCM and γ-tubulin that act as aMTOCs and these are considered to be the main sites of microtubule nucleation (Schuh & Ellenberg, 2007). However, pig (porcine), cow (bovine), sheep and human oocytes have different distributions of γ-tubulin, with no cytoplasmic or spindle pole foci detected (Holubcová et al., 2015; Guen & Crozet, 1989; Lee et al., 2000; Long et al., 1993). In the absence of any detectable MTOCs, microtubules start accumulating around the chromatin clusters following NEBD, and γ-tubulin localises along microtubules in the meiotic spindle (Holubcová et al., 2015; Lee et al., 2000). In the absence of MTOC foci, one can further investigate a specific function of the centrosomal proteins previously identified as forming the unique meiotic spindle pole domain in mouse oocytes. Most importantly, one can also investigate if this is a conserved domain among mammalian species, as meiotic spindle assembly of mouse oocytes is considered to be more of an exception in many aspects.

Porcine oocytes were a promising starting point; however, the main limitation of this system is that the oocytes are highly opaque, filled with lipid droplets. This resulted in variable immunofluorescence staining. The Trim-Away method also had to be first optimised to confirm efficient depletion. The other possibility was to work with human oocytes. As I was setting up the research satellite lab at Bourn Hall Clinic, I started optimisation of the Trim-Away method as well as screening all the centrosome

associated antibodies tested in mouse oocytes. Immunofluorescence of γ-tubulin and other aMTOC markers (Pericentrin, CDK5RAP2) (Figure 4.8) all supported the previously described absence of MTOC foci in human oocytes (Holubcová et al., 2015). Dean Clift from our lab had previously shown that PCM1 does localise to the meiotic spindle in human oocytes and therefore could have a meiosis-specific role, which is conserved between mouse and aMTOC free oocytes.

The initial centrosomal localisation screen by Dean Clift, which included the unique spindle domain formed by the tested pericentriolar satellite proteins (Figure 3.1), was expanded in a collaboration with Chun So (Table 4.1, Figure 4.1 and Figure 4.2). 38 targets representing 9 different groups of proteins related to the centrosome or spindle pole in mitotic cells were systematically selected and investigated (Table 4.1). The localisation of these proteins was analysed and confirmed by immunofluorescence, live-cell imaging, or both, wherever possible. Proteins within the same group mostly showed a similar pattern of localisation (Figure 4.1 and Figure 4.2). Most of the centriolar and linker fibre proteins showed either no localisation or only localised to aMTOCs in prophase, and were absent from aMTOCs following NEBD, consistent with previous evidence that MTOCs in mouse oocytes are acentriolar (Figure 4.1). Pericentriolar wall and pericentriolar material proteins, regulatory kinases and dynactin mostly localised to aMTOCs (Figure 4.2). In addition to the pericentriolar satellite proteins, several other centrosomal proteins (clathrin, ch-TOG, KIZ and TACC3) and dynein cargo adaptors (Hook3, Nde1 and Ndel1) were also found in the meiotic spindle pole domain (MSPD) (Figure 4.2). Overall, the localisation of canonical centrosomal and spindle pole proteins were found either at aMTOCs or the MSPD.

Table 4.1 List of centrosomal and spindle pole associated proteins tested in mouse oocytes.

No.	Group	Protein	Localization in mouse MI oocytes	Confirmed by
1	Centriolar proteins	Cenpj/Cpap	No localization (lost from aMTOCs after NEBD)	Live imaging
2		Sas6	No localization (lost from aMTOCs after NEBD)	Live imaging
3		Cep135	No localization	IF
4		Cetn2	No localization	Live imaging
5	Linker fiber proteins	Cep250/Cnap1	aMTOCs (first lost from aMTOCs after NEBD)	Live imaging
6		Crocc/Rootletin	No localization (lost from aMTOCs after NEBD)	Live imaging
7		Nek2a	No localization (lost from aMTOCs after NEBD)	Live imaging
8		Lrrc45	No localization (lost from aMTOCs after NEBD)	Live imaging
9	Pericentriolar wall protein	Cntrob	aMTOCs	Live imaging
10	Pericentriolar material proteins	Cep215/Cdk5rap2	aMTOCs	IF, live imaging
11		Cep120	aMTOCs, microtubules	IF
12		Cep192	aMTOCs	IF, live imaging
13		Nedd1	aMTOCs	IF, live imaging
14		Pcnt2/Pericentrin	aMTOCs	IF, live imaging
15		Tubg1/Tubg/γ-tubulin	aMTOCs, microtubules	IF, live imaging
16		Akap9/Akap450	MSPD	IF, live imaging
17		Cep152	MTs (non-specific)	IF
18	Pericentriolar satellite proteins	Cep72	MSPD	Live imaging
19		Lrrc36	MSPD	Live imaging
20		Pcm1	MSPD	IF, live imaging
21		Cep290/Bbs14	No localization (lost from aMTOCs after NEBD)	Live imaging
22		Bbs4	MSPD	Live imaging
23		Pard6α/Par6α	No localization	Live imaging
24	Regulatory kinases	Aurka/AurA	aMTOCs, MTs	IF, live imaging
25		Plk1	aMTOCs, kinetochores	IF, live imaging
26		Plk4/Sak	aMTOCs	IF
27	Other centrosomal/ centrosome-related proteins	Top2a	aMTOCs, kinetochores	IF
28		Cltc/Chc17	MSPD	IF, live imaging
29		Ckap5/Chtog	MSPD	IF, live imaging
30		Kiz	MSPD	IF
31		Tacc3	MSPD	IF, live imaging
32	Dynein-related proteins	Dctn1/p150	aMTOCs, kinetochores	IF
33		Hook3	MSPD	IF, live imaging
34		Lis1	Kinetochores	IF
35		Nde1/Nude	MSPD	IF
36		Ndel1/Nudel	MSPD	IF
37	Other spindle pole-related proteins	Myo10	MSPD	IF
38		Tpx2	MTs	IF, live imaging

Meiosis spindle pole domain (MSPD)
Acentrosomal microtubule organising centre (aMTOC)
Nuclear envelope breakdown (NEBD)
Microtubules (MTs)

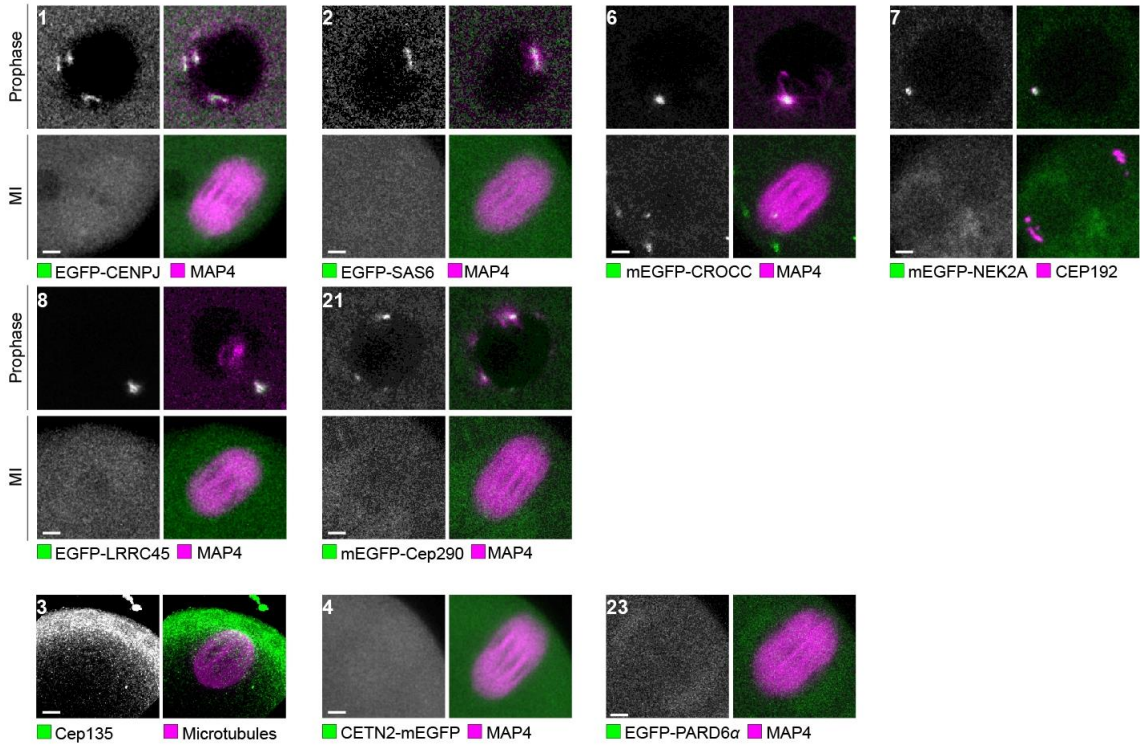

Figure 4.1 Localisation of centrosomal proteins in mouse meiosis I spindles.

Examples showing EGFP-CENPJ, EGFP-SAS6, mEGFP-CROCC, EGFP-LRRC45 (images taken by Dean Clift), mEGFP-Cep290, Cep135 (images taken by Chun So), CETN2-mEGFP and EGFP-PARD6α (images taken by Dean Clift). Numbers at top left corner correspond to Table 4.1. Scale bar shows 5 µm.

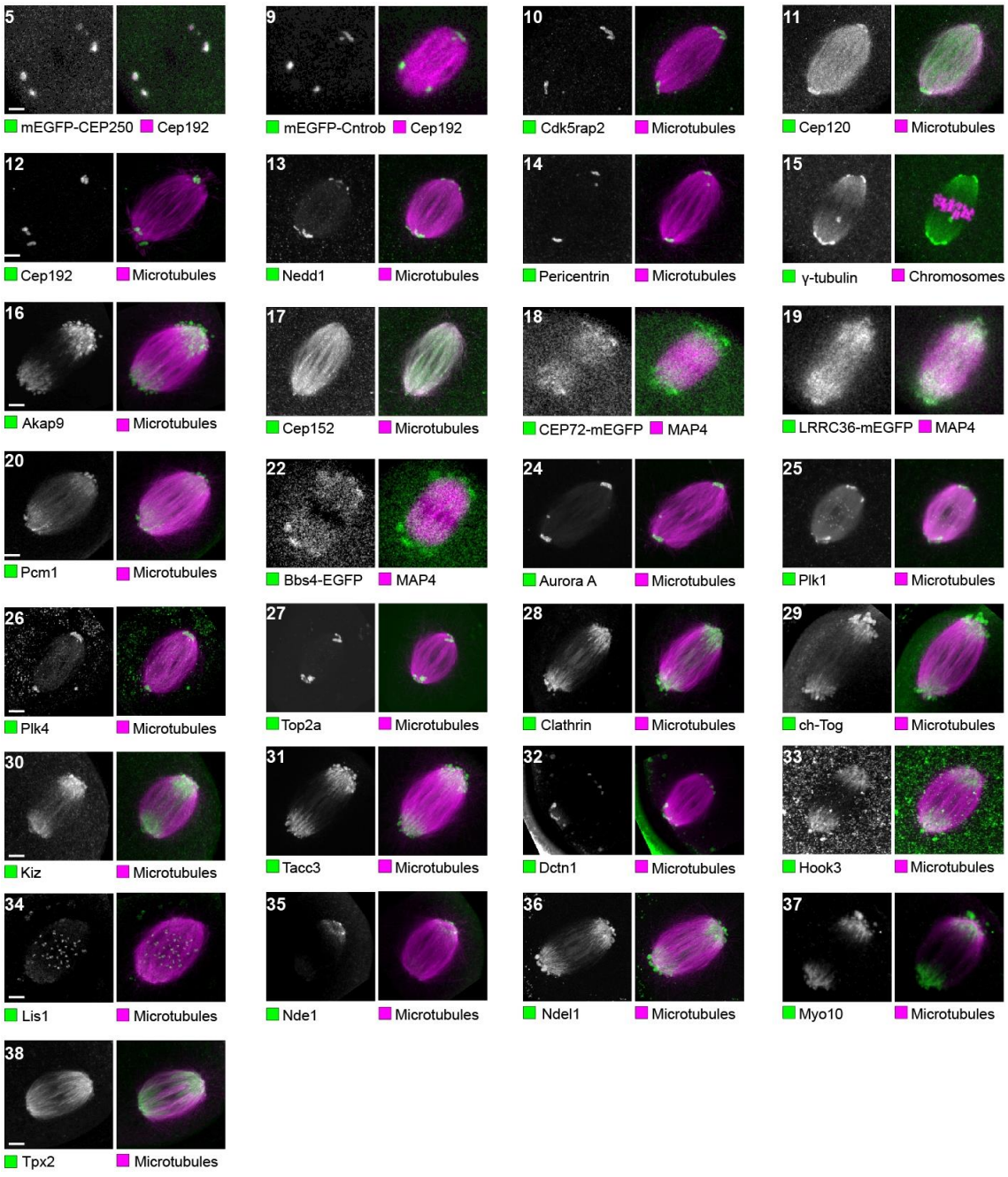

Figure 4.2 Centrosomal and spindle pole protein localisation in mouse oocytes.

Examples showing centrosomal or spindle pole proteins in green and microtubules or chromosomes in magenta (n≥3 oocytes). Images taken by Chun So, Dean Clift and Bianka Seres. Numbers at top left corner correspond to Table 4.1. Scale bar shows 5 µm.

Based on the initial results, we planned experiments to further dissect the role of this domain in mouse meiosis and investigate whether this is a conserved domain in human oocytes, a naturally MTOC-free system. All antibodies were first tested and optimised in mouse oocytes by Chun So. While this does not guarantee that the tested antibody will work in human oocytes, it increases the chances that it will recognize the native protein and work for Trim-Away depletion.

We were particularly interested in TACC3, as it is known to have an important function in regulating microtubule growth rate and also known to stabilise K-fibres via interactions with other components also found in the MSPD, such as clathrin and ch-TOG (Figure 4.2) (Booth et al., 2011; Cheeseman et al., 2013; Hood et al., 2013). Following Trim-Away depletion, it became clear that TACC3 is essential for the localisation of all tested components of the MSPD and we therefore decided to characterise it further. At this point I had already moved to Bourn Hall to set up the research lab and to optimise live cell imaging of human oocytes as well as the Trim-Away method for endogenous protein depletion. The TACC3 part of the project was a team effort with Chun So, who was working on mouse oocytes in Germany. All experiments were designed and analysed jointly. As I had only the Light-sheet system available at this location, I carried out all experiments on human oocytes myself and for immunofluorescence samples, these were prepared by myself at Bourn Hall and subsequently sent to Germany for imaging by Chun So. For the data involving mouse oocytes, I participated in the planning of experiments and data analysis and interpretation. Data presented here is relevant to the previously described MSPD and aMTOC properties (Chapter 3: Results: Part I) and the MTOC free human oocyte system, although our investigations were more extensive. Some of the extended data is included in the discussion (Chapter 6) in order to give a more comprehensive conclusion.

4.2 TACC3 is essential for the MSPD in mouse oocytes

It is now well established that centrosomes in mitotic cells include a large number of proteins and protein complexes that are highly organised, as opposed to being amorphous as previously described (section 1.5.4.142) (Lawo et al., 2012). Organisation of the PCM and pericentriolar satellites is highly dynamic throughout mitosis and follows a hierarchical recruitment with continuous remodelling (Dammermann & Merdes, 2002; Lawo et al., 2012). In *C.elegans,* the PCM was described as a two component system, with a main scaffold recruiting other PCM components referred to as "PCM clients" (Woodruff et al., 2017).

In order to investigate if the aMTOCs and the MSPD components show a similar 'scaffold-client' relationship in the meiotic spindles of mouse oocytes, we first looked at the dynamics of four MSPD and four aMTOC components (Figure 4.3). *In vivo,* proteins form dynamic macromolecular complexes and their turnover is determined by the stability of their interactions as well as by diffusion within the cytoplasm. Using fluorescence recovery after photobleaching (FRAP), a method used to examine protein turnover *in vivo*, a small region of interest is bleached and fluorescent recovery is measured (Fritzsche & Charras, 2015). Quantification of the half time of fluorescence recovery ($t_{1/2}$) and the fraction of protein that appears mobile within the measured time scale, i.e. able to recover compared to the total initial protein pool (mobile fraction, MB) indicates if a protein is mobile or not. This information about protein dynamics can be extracted from the FRAP curve as shown in Figure 4.3.

Using FRAP, we were able to show that the previously described scaffold complex of Pericentrin, CEP192 and CDK5RAP2 which had been shown to recruit other PCM components (Barr et al., 2010; Choi et al., 2010; Gomez-Ferreria et al., 2007; Kim & Rhee, 2014; Zhu et al., 2008) did not recover after photobleaching (Figure 4.3). The recovery kinetics of Aurora A however was different, with over 50% of the Aurora A population free moving (Figure 4.3). On the other hand, components of the MSPD (TACC3, ch-TOG, clathrin and PCM1) showed a similar rate of recovery, TACC3 representing the smallest mobile fraction.

These results suggest that aMTOC core components (Pericentrin, CEP192 and CDK5RAP2) in mouse oocytes adopt a hierarchical relationship that is similar to that described in mitotic cells.

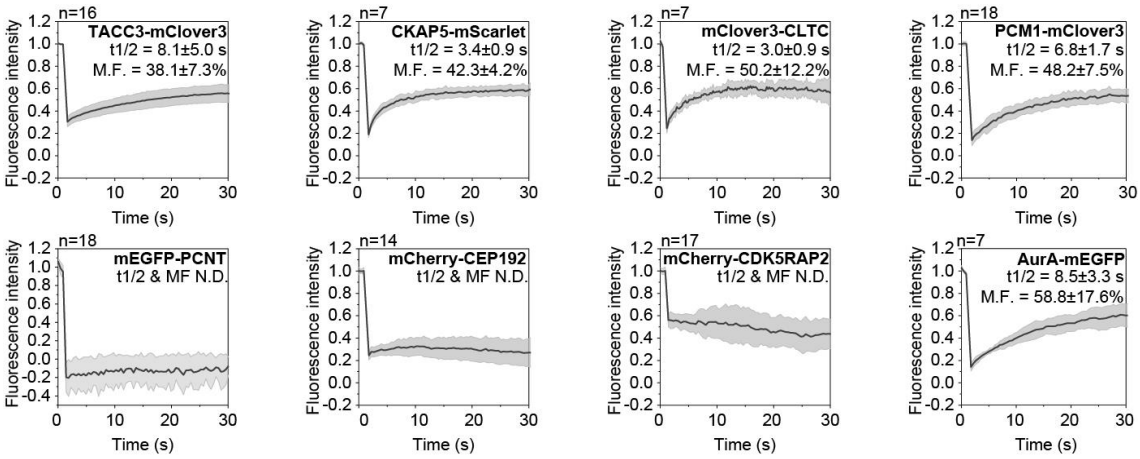

Figure 4.3 Quantification of FRAP of selected PCM and MSPD proteins in live mouse oocytes.

Fluorescence recovery after photobleaching (FRAP) of selected PCM and MSPD proteins in live mouse oocytes, co-expressing fluorescent reporter(s) of interest and H2B-miRFP. Half-times of maximum recovery ($t_{1/2}$) and mobile fractions (MF) are shown ± standard deviation (SD). Data from two independent experiments. Number of oocytes shown above the dataset.

TACC3 has been previously reported to play a role in K-fibre stability (Booth et al., 2011; Cheeseman et al., 2013; Hood et al., 2013) and we therefore decided to characterise this protein further. Considering that its other interacting partners ch-TOG and clathrin were both found in the same domain (Figure 4.2), we hypothesised that TACC3 may have an important function in the MSPD. Live cell imaging and immunofluorescence confirmed that TACC3 is recruited and localises in a similar manner to the previously described PCM1 (compare Figure 3.2, p87 and Figure 4.4A-D). While it initially localises to the inner part of the aMTOCs in prophase (Figure 4.4B-C), TACC3 is released from the aMTOCs associated with the nuclear envelope (NE) after NEBD (Figure 4.4D) and infiltrates the spindle microtubules during bipolar spindle formation (Figure 4.4A-D). At this point, TACC3 is no longer localised within the aMTOCs at the spindle poles (Figure 4.4B, merge panel, boxed region).

Importantly, TACC3-depletion via the Trim-Away method showed no spindle pole localisation of the other tested components of the MSPD (Figure 4.4E), which suggested that TACC3 acts as a central MSPD platform. Its role as a potential scaffold or main recruiter of the MSPD component is also suggested by the FRAP curve results, showing that TACC3 has the lowest mobile fraction from the other tested MSPD components (Figure 4.3).

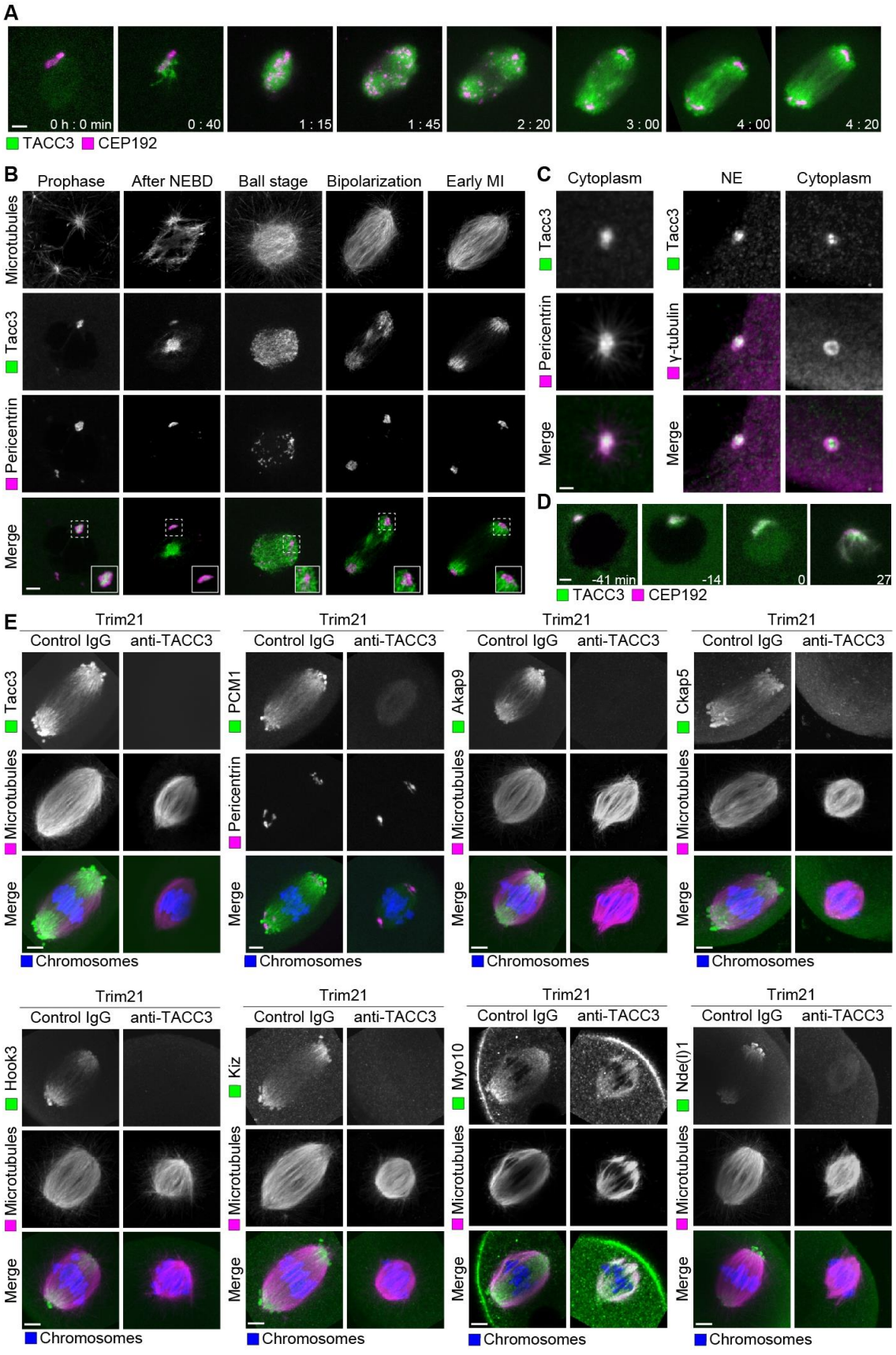
A
0 h : 0 min
0 : 40
1 : 15
1 : 45
2 : 20
3 : 00
4 : 00
4 : 20
TACC3 CEP192
B
Prophase
After NEBD
Ball stage
Bipolarization
Early MI
Microtubules
Tacc3
Pericentrin
Merge
C
Cytoplasm
NE
Cytoplasm
Tacc3
Pericentrin
γ-tubulin
Merge
D
-41 min
-14
0
27
TACC3 CEP192
E
Trim21
Control IgG
anti-TACC3
Tacc3
PCM1
Akap9
Ckap5
Hook3
Kiz
Myo10
Nde(l)1
Microtubules
Merge
Chromosomes

Figure 4.4 TACC3 localisation in mouse oocytes and Trim-Away depletion.

(A) Live cell imaging of TACC3 localisation in mouse oocytes undergoing meiosis I. Oocytes overexpressed TACC3-mEGFP (green) and CEP192-mCherry (magenta) to label aMTOCs. Time shows hours (h) and minutes (min) from NEBD. Scale bar shows 5 µm.

(B) Immunofluorescence of TACC3 localisation at different time points during meiosis I. aMTOCs are labelled with anti- Pericentrin. Boxed regions are magnified in the right corner. Scale bar shows 5 µm.

(C) Immunofluorescence of TACC3 in prophase mouse oocytes. Examples showing aMTOCs labelled with anti-Pericentrin in cytoplasm or on the nuclear envelop (NE) prior to NEBD. Scale bar shows 5 µm.

(D) Live cell imaging of TACC3 localisation in mouse oocytes undergoing nuclear envelope breakdown. Oocytes overexpressed TACC3-mEGFP (green) and CEP192-mCherry (magenta) to label aMTOCs. Time shows hours minutes (min) from NEBD. Scale bar shows 5 µm.

(E) Oocytes overexpressing TRIM21 mRNA and microinjected with either control IgG or anti-TACC3 antibody were allowed to mature to the MI stage and fixed. Immunofluorescence of selected MSPD components (green), α-tubulin (magenta) and chromosomes (blue) are shown. Scale bar shows 5 µm.

(Images taken by Chun So).

4.3 MSPD localisation is dependent on aMTOCs

High resolution three-dimensional live cell imaging of TACC3 and CEP192 suggested that full spindle pole localisation was completed only after aMTOCs sorted to the two spindle poles (Figure 4.4A). In order to test if aMTOCs are indeed required for the formation of the MSPD, which was also suggested from the PCM1 results (Figure 3.12), we planned three different experiments. We first looked at RanGTP inhibition alone (Figure 4.5A-B), as inhibition of the RanGTP pathway resulted in the monopolar distribution of aMTOCs (Figure 4.5C). The asymmetric distribution of aMTOCs provided a good experimental design to test if the MSPD can form at the aMTOC free spindle pole. Indeed, TACC3 in oocytes microinjected with Ran(T24N) mirrored the asymmetric distribution of aMTOCs (Figure 4.5A and C), with the characteristic spindle pole protrusions forming only at the spindle pole that contained the over clustered aMTOC (Figure 4.5A).

In a separate experiment, we looked at microtubule regrowth following Nocodazole washout at the late MI stage (once the bipolar spindle was fully formed) and imaged oocytes overexpressing CEP192/MAP4 and TACC3 live (Figure 4.5D). As the spindle collapsed and all microtubules depolymerised, aMTOCs clustered together (Figure 4.5D, time 0). Following Nocodazole washout, spindle microtubules started to nucleate and the bipolar spindle formed quickly. In some cases, the aMTOCs had to be redistributed to the two poles as it initially formed an asymmetric, monopolar localisation (Figure 4.5D, time 0:12 and 1:00). Capturing this reorganisation live, showed that TACC3/MSPD trafficked together with aMTOCs and was redistributed to the second pole resulting in a bipolar distribution (Figure 4.5D).

In order to show that the MSPD is indeed aMTOC-dependent, we repeated Pericentrin-depletion, this time imaging fluorescently labelled TACC3 live (Figure 4.5E). High resolution live cell imaging revealed that TACC3 could no longer assemble the spindle pole domain (Figure 4.5E-F), although on closer observation a small population of TACC3 could be seen to localise along the spindle microtubules. Quantification of TACC3 mean fluorescent intensity in live oocytes depleted of Pericentrin also showed that the majority of TACC3 is no longer associated with the spindle (Figure 4.5G). However, there was a slight increase of mean TACC3 intensity over time, suggesting that a second population is independent of aMTOC recruitment (Figure 4.5G). We hypothesized that this population might be linked to K-fibres as previously described (Booth et al., 2011; Cheeseman et al., 2013; Hood et al., 2013). Indeed, immunofluorescence of cold treated oocytes confirmed that TACC3 co-localised with α-tubulin in cold-stable K-fibres (Figure 4.5H).

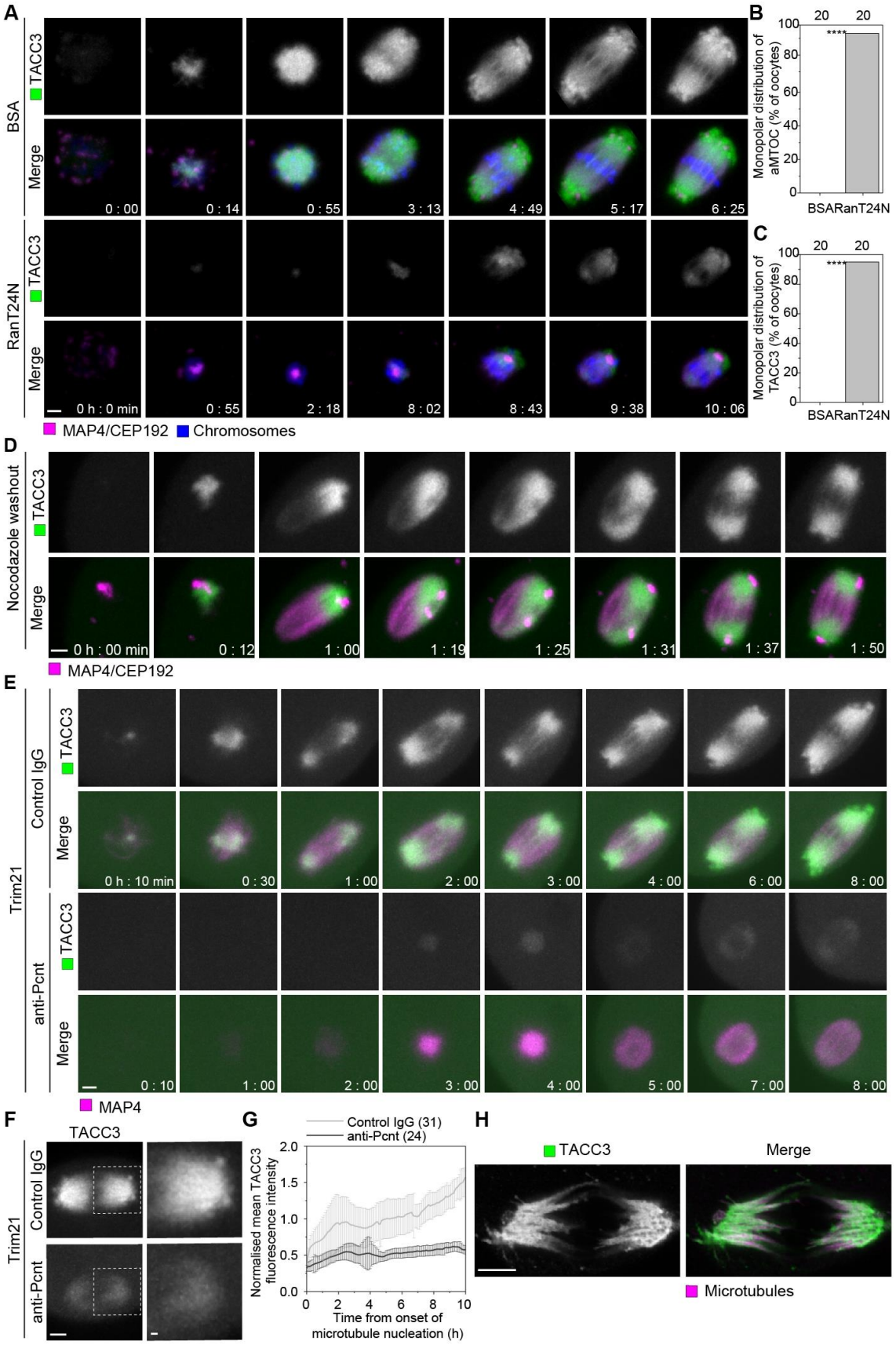
A
BSA
TACC3
Merge
0 : 00
0 : 14
0 : 55
3 : 13
4 : 49
5 : 17
6 : 25
RanT24N
TACC3
Merge
0 h : 0 min
0 : 55
2 : 18
8 : 02
8 : 43
9 : 38
10 : 06
MAP4/CEP192
Chromosomes
B
Monopolar distribution of aMTOC (% of oocytes)
20
20
****
BSA
RanT24N
C
Monopolar distribution of TACC3 (% of oocytes)
20
20
****
BSA
RanT24N
D
Nocodazole washout
TACC3
Merge
0 h : 00 min
0 : 12
1 : 00
1 : 19
1 : 25
1 : 31
1 : 37
1 : 50
MAP4/CEP192
E
Trim21
Control IgG
TACC3
Merge
0 h : 10 min
0 : 30
1 : 00
2 : 00
3 : 00
4 : 00
6 : 00
8 : 00
anti-Pcnt
TACC3
Merge
0 : 10
1 : 00
2 : 00
3 : 00
4 : 00
5 : 00
7 : 00
8 : 00
MAP4
F
TACC3
Trim21
Control IgG
anti-Pcnt
G
Control IgG (31)
anti-Pcnt (24)
Normalised mean TACC3 fluorescence intensity
Time from onset of microtubule nucleation (h)
H
TACC3
Merge
Microtubules

Figure 4.5 MSPD is dependent on aMTOCs.

(A) Examples from time-lapse imaging of oocytes overexpressing H2B-iRFP and MAP4/CEP192-mCherry and TACC3-mEGFP, microinjected with BSA or RAN(T24N). Time shows hours (h) and minutes (min) from NEBD (time 0). Scale bar shows 5 µm.

(B-C) Oocytes microinjected with BSA or RAN(T24N) were scored for the frequency of monopolar distribution of aMTOCs (B) and TACC3 (C). Data from two independent experiments. Same data used to analyse both parameters. Number of oocytes shown above the dataset. P values were calculated with Fisher's exact test.

(D) Live cell imaging of TACC3 and CEP192 localisation of microtubule regrowth following 1-hour Nocodazole treatment at MI. Time shows hours (h) and minutes (min) from Nocodazole washout. Scale bar shows 5 µm.

(E) Live cell imaging of oocytes overexpressing TRIM21, MAP4-mCherry and TACC3-mEGFP and microinjected with either control IgG or anti-Pericentrin (Pcnt) antibody. Time shows hours (h) and minutes (min) from NEBD (time 0). Scale bar shows 5 µm.

(F) Examples from time-lapse imaging of oocytes overexpressing TRIM21 and TACC3-mEGFP and microinjected with either control IgG or anti-Pericentrin (Pcnt) antibody. Boxed regions are magnified on the right. Scale bar shows 5 µm and 1 µm for magnified images.

(G) Quantification of normalised mean TACC3 fluorescence intensity (TACC3-mEGFP) over time (hours). Time 0 is the onset of microtubule nucleation. Oocytes overexpressing TRIM21 and TACC3-mEGFP were microinjected with either control IgG or anti-Pericentrin (Pcnt) antibody. Data from two independent experiments.

(H) Immunofluorescence of anti-TACC3 (green) and anti-α-tubulin (magenta). Oocytes were allowed to mature (7 hours post NEBD) and treated with cold prior to fixing. Scale bar shows 5 µm.

(Images taken by Chun So)

In order to further investigate the dynamics of the TACC3/MSPD, we looked at fluorescent photoactivation of TACC3 to assess its rate of decay and stability. We carried out live cell imaging of photoactivated TACC3-mPA-GFP in a small region of interest, between the metaphase plate and spindle pole (Figure 4.6A, time point 0). This showed that TACC3 dissipated bidirectionally and that the photoactivated TACC3-mPA-GFP quickly infiltrated the whole spindle (Figure 4.6A). We found that a two-component exponential curve gave the best fit for the decay rate ($R^2 = 0.986 \pm 0.012$, Figure 4.6B-C), with two distinct $t_{1/2}$ values for a slow- (1.60 ± 1.54 min) and a fast-moving (0.24 ± 0.28 min) population (Figure 4.6C). The difference between the $t_{1/2}$ was around six-fold (Figure 4.6C). Previously it was shown that microtubules in mitotic spindles comprise two distinct populations, a short half-life of non-K fibre microtubules and a longer half-life of K-fibre microtubules (Q.-H. Zhang et al., 2017). Considering that TACC3 is also associated with K-fibres in meiotic mouse spindles (Figure 4.5H), the two distinct $t_{1/2}$ measured could mean that TACC3 may have a more dynamic population forming the aMTOC-dependent MSPD and a slower, K-fibre associated population that is aMTOC independent. Consistent with this, the $t_{1/2}$ value for the 'slow' component was similar to that of K-fibres measured in meiotic spindles at the MII stage (2.5 ± 0.5 min) (Q.-H. Zhang et al., 2017).

Overall, we show that the TACC3/MSPD, is dependent on aMTOCs at the spindle poles and aMTOC-free mouse oocytes (Pericentrin-depleted) could no longer form the pole domain protrusions (Figure 4.5 and Figure 4.7). This is consistent with our previous data looking at PCM1 previously (Figure 3.12). Our results also suggest that there are two distinct TACC3 spindle populations, aMTOC-dependent MSPD and aMTOC-independent K-fibre / spindle associated population (Figure 4.7).

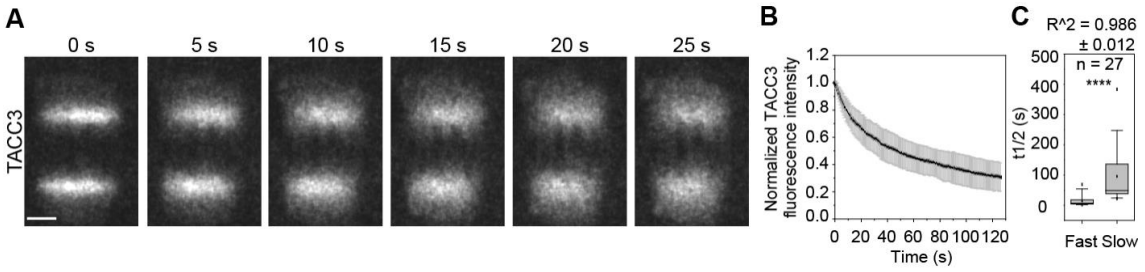

Figure 4.6 TACC3 dynamics show two distinct protein populations in the mouse meiotic spindle.

(A) Examples of single-section, time-lapse imaging of TACC3 photoactivation of oocytes overexpressing TACC3-mPA-GFP (images taken by Chun So). Time shows seconds (s) from photoactivation. Scale bar shows 5 µm.

(B) Quantification of photoactivated TACC3 fluorescence signal dissipation in oocytes overexpressing TACC3-mPA-GFP. Time shows seconds (s) from photoactivation.

(C) Distribution of photoactivated TACC3 fluorescence signal dissipation half-life in oocytes overexpressing TACC3-mPA-GFP. Coefficient of determination (R^2) are shown ± standard deviation. Data from two independent experiments. Number of oocytes shown above the dataset. P values were calculated with Student's t test.

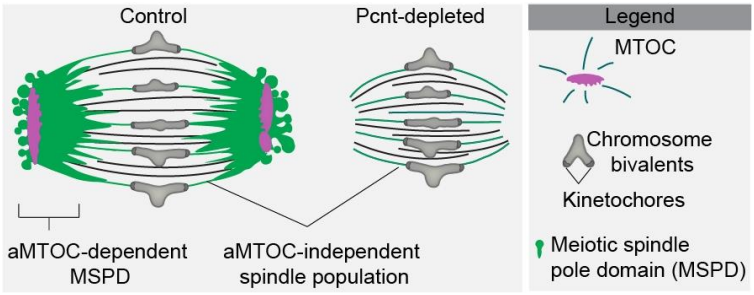

Figure 4.7 Schematic representation of the different populations of TACC3.

Bipolar spindle structure on the left, showing the native structure of a mouse meiotic spindle, with the microtubule organising centres (MTOCs, pink) and the meiotic spindle pole domain (MSPD, green) protrusions marking the spindle poles. MTOC free (Pericentrin-depleted) mouse meiotic spindle is shown on the right, where both MTOCs and MSPD protrusions at the spindle poles are absent. The highlighted lines point to the proposed second population of TACC3/MSPD, that localise to the K-fibres in an MTOC-independent manner.

4.4 MSPD protrusions are absent in human oocytes

It was previously shown that similar to other mammalian species, such as cow, pigs and sheep, human oocytes not only lacked canonical centrioles but also any PCM foci that could act as the main microtubule organising centres during meiosis (Holubcová et al., 2015). Consistent with this, in the absence of prominent MTOCs, human oocytes rely on the RanGTP mediated microtubule nucleation pathway (Holubcová et al., 2015).

We showed that the newly described spindle pole domain (MSPD) in mouse oocytes is dependent on the aMTOCs (Figure 4.5). Therefore, we wanted to further investigate whether this domain is present in human oocytes, which according to our currently knowledge, are naturally MTOC free.

We first tested the available antibodies that showed specificity in mouse oocytes in order to map their localisation pattern in human oocytes (Figure 4.8). Unlike the mouse, all tested PCM, pericentriolar satellite and regulatory kinases localised to the meiotic spindle, apart from PLK1, which in addition to spindle also showed kinetochore localisation (Figure 4.8). As previously reported, no PCM foci were detected at the spindle poles, with only the microtubule-associated γ-tubulin population distinguished (Figure 4.8).

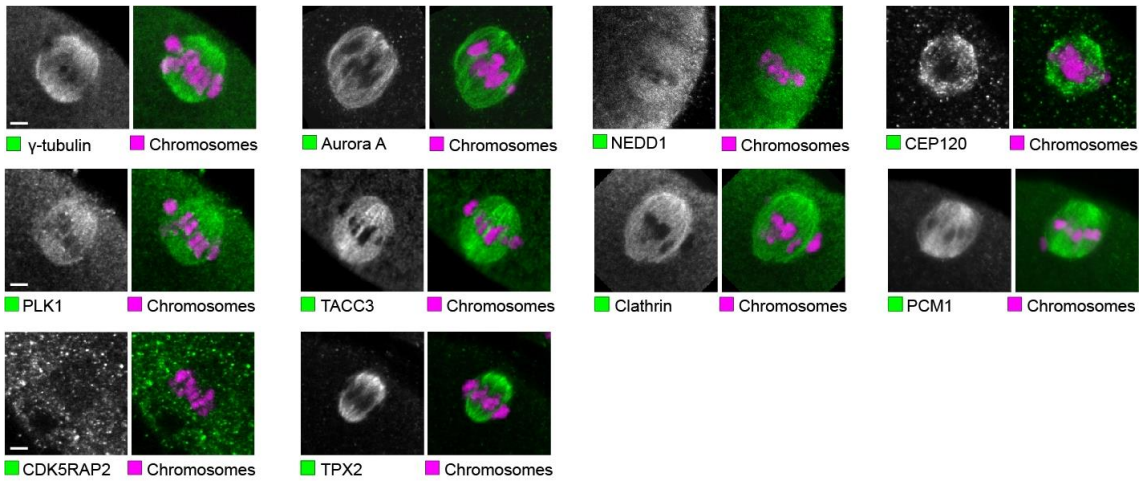

Figure 4.8 Immunofluorescence of centrosomal and spindle pole protein localisation in human MI oocytes.

Human oocytes were fixed 15h post NEBD and stained for different spindle proteins (green) (n= 1 or 2 oocytes). Hoechst staining is shown in magenta. Scale bar shows 5 μm. (Images taken by Bianka Seres and Chun So).

Components of the MSPD, previously identified in mouse oocytes, all showed a more homogeneous spindle localisation, with no micron-sized spindle pole protrusions present (Figure 4.8 and Figure 4.9). High resolution three-dimensional live cell imaging of fluorescently labelled TACC3 (Figure 4.9A) and immunofluorescence of endogenous TACC3 (Figure 4.9B) in human oocytes showed initial recruitment of TACC3 to microtubules. Consistent with this observation, the time of TACC3 recruitment (4.4 ± 1.5 h post NEBD) was comparable to the time of microtubule nucleation previously reported by Holubcová *et al.* (2015) (4.7 ± 1.4 h post NEBD). During bipolar spindle formation, TACC3 showed stronger localisation at the spindle poles. Just before anaphase, as chromosome alignment was achieved, TACC3 distributed homogeneously within the meiotic spindle. Consistent with mouse oocyte data, TACC3 also localised to K-fibres in human oocytes (Figure 4.9F).

Together, it is evident from both live cell imaging and immunofluorescence that TACC3 did not form the spindle pole protrusions characteristically seen in the presence of aMTOCs in mouse oocytes, in both aMTOC-free mouse spindles (depleted of Pericentrin) and MTOC-free human oocytes (Figure 4.9E). Together with the immunfluorescence images showing K-fibre localisation of TACC3 (Figure 4.5H and Figure 4.9F), this suggests that while the TACC3-mediated MSPD protrusions do not appear to be conserved in the absence of aMTOCs (also shown by PCM1 and clathrin, Figure 4.8 and Figure 4.9E), the aMTOC-independent population of TACC3 that is associated with K-fibre / spindle is detected in human oocytes (Figure 4.9E-F).

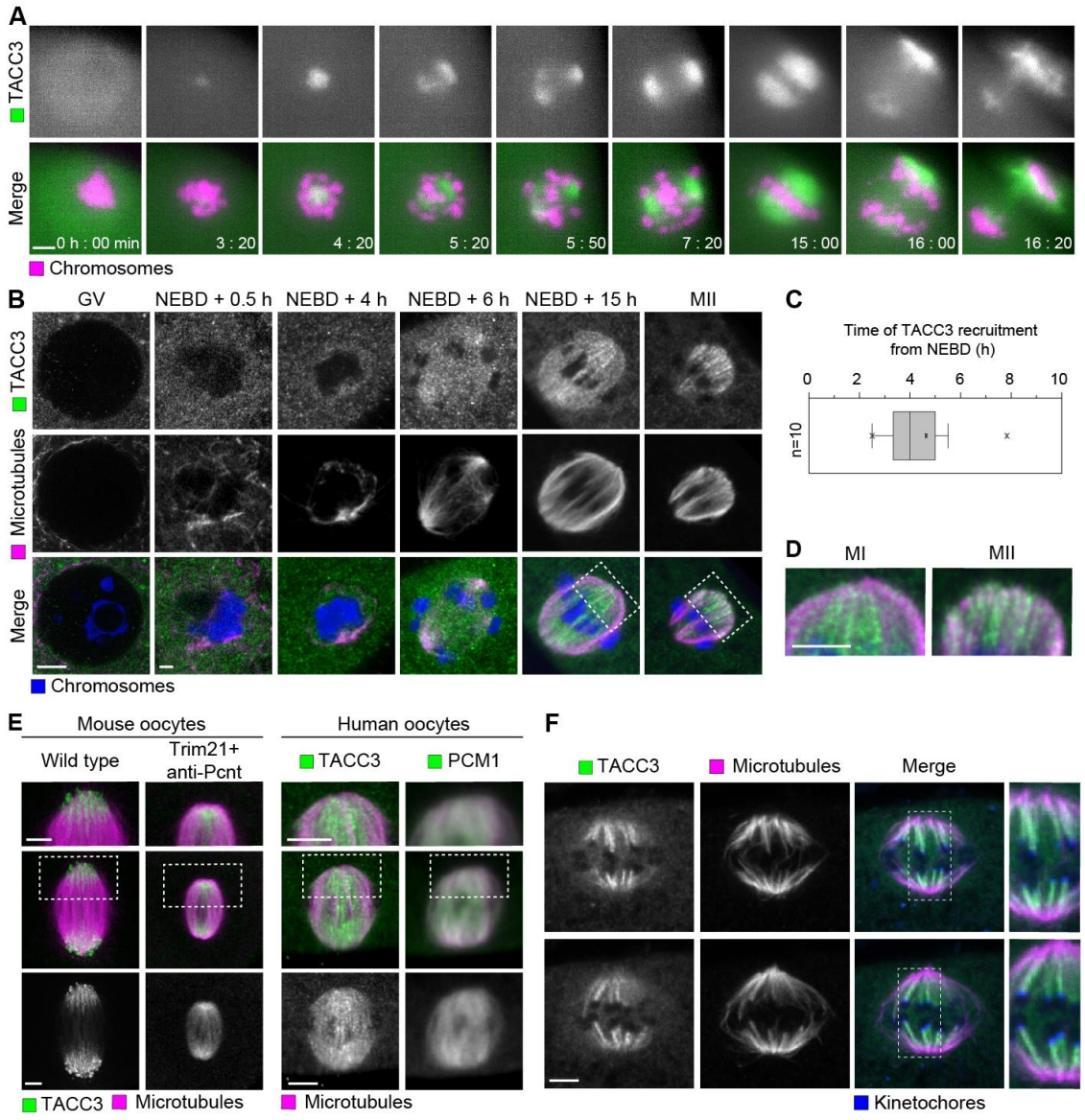

Figure 4.9 The MSPD pole protrusions are absent in aMTOC free human oocytes.

(A) Live cell imaging of TACC3 localisation in human oocyte undergoing meiosis I. Oocytes overexpressed TACC3-mClover (green) and H2B-mCherry (magenta). Time shows hours (h) and minutes (min) from NEBD. Images were taken via the Lightsheet Z.1 microscope. Scale bar shows 5 µm.

(B) Immunofluorescence of TACC3 (green) localisation at different time points during meiosis I of human oocytes (images taken by Chun So). Microtubules, labelled with α-tubulin are shown in magenta and Hoechst in blue. Boxed regions are magnified on the right, showing spindle poles in MI and MII oocytes (D). Scale bar shows 5 µm. (images taken by Chun So)

(C) Quantification of time of TACC3 recruitment from live oocytes overexpressing TACC3-mClover as shown in (A). Time is shown in hours (h) from NEBD.

(E) Immunofluorescence of TACC3 (green) and α-tubulin (magenta) of mouse and human oocytes (apart from the PCM1, images taken by Chun So). Mouse oocyte examples showing wild type MI spindle on the left and Pericentrin-depleted MI oocytes on the right. Human oocyte examples showing anti-TACC3 and anti-PCM1 (images taken via the Lightsheet Z.1) localisation in MI spindles (15h post NEBD). Boxed regions are magnified above, showing spindle poles. Scale bars show 5 µm.

(F) Immunofluorescence of anti-TACC3 (green), anti-α-tubulin (magenta) and kinetochores (blue) (images taken by Chun So). Oocytes were allowed to mature (15 hours post NEBD) and treated with cold prior to fixing. Scale bar shows 5 µm. Boxed regions are magnified on the right. Scale bars show 5 µm.

4.5 TACC3 localisation is microtubule-dependent in human oocytes

In order to investigate if TACC3 localisation is dependent on microtubules, depolymerisation assays using Nocodazole and Colcemid were tested. My initial choice was to test Nocodazole, a synthetic tubulin-binding agent that depolymerises microtubules, as this worked reliable in mouse oocytes Figure 3.13B). Suprisingly, I was not able to disrupt microtubules with 10 µM Nocodazole treatment, even with prolonged incubation time (Figure 4.10A). In contrast, 1 µM Nocodazole gave good depolymerisation efficiency in mouse oocytes (Figure 3.13B). While microtubule dynamics may have been affected by the prolonged Nocodazole treatment, it was evident that human spindle microtubules were resistent to this tubulin-binding agent.

As an alternative method, I decided to test Colcemid, another known drug with microtubule depolymerising effects (Figure 4.10B). Human oocytes treated with Colcemid quickly depolymerised all microtubules, within minutes (Figure 4.10B). To ensure that following Colcemid washout microtubules can reassemble, I imaged the treated oocyte live, in Colcemid-free medium (Figure 4.10B). While the oocyte could form a bipolar spindle, this took over one hour. Microtubules started to nucleate within the chromosome mass, around 45 minutes following Colcemid washout. Spindle microtubules quickly ejected two poles.

Having tested the conditions that achieved efficient depolymerisation of microtubules, I wanted to assess if TACC3 localisation is dependent on microtubules (Figure 4.10C). Live cell imaging showed that TACC3 localistion was lost within 5-7 minutes of Colcemid treatment, which coinside with the time it took to depolymerise all microtubules (Figure 4.10B). To ensure that TACC3 was not sequestered away from the spindle once microtubules were gone and perhaps could form cytoplasmic aggregates or foci, I scanned through the entire oocyte, which showed only homogenious cytoplasmic localisation of TACC3 (Figure 4.10D).

Overall, these experiemnts revealed an unusual characteristic of human oocyte microtubules, showing resistance to Nocodazole treatment but highly prone to Colcemid mediated depolymerisation. It is also evident that TACC3 localisation to the meiotic spindle is indeed microtubule-dependent in human oocytes.

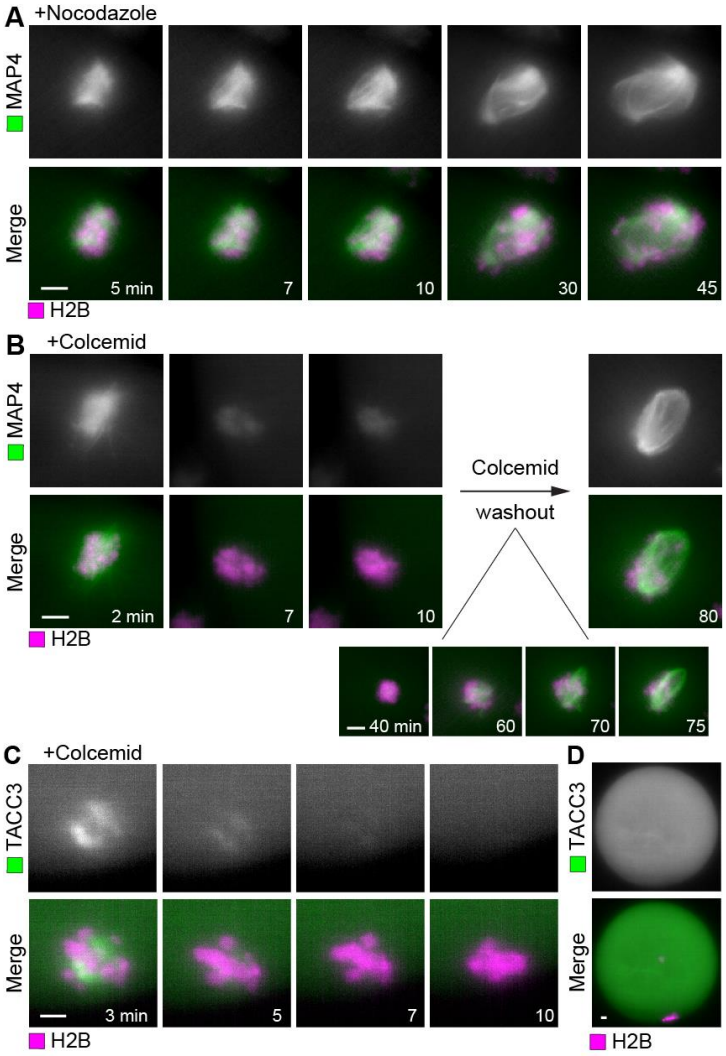

Figure 4.10. Microtubule dependence of TACC3 localisation

(A) Live cell imaging of human oocyte overexpressing MAP4-EGFP (green) and H2B-mCherry at meiosis II. Oocyte was treated with 10 µM of Nocodazole. Time shows minutes (min) from Nocodazole treatment.

(B) Live cell imaging of human oocyte overexpressing MAP4-EGFP (green) and H2B-mCherry at meiosis II. Oocyte was treated with 10 µM of Colcemid. Time shows minutes (min) from Nocodazole treatment. Small image series show microtubule regrowth following Colcemid washout. Time indicates minutes (min) from washout.

(C) Live cell imaging of TACC3 localisation in human oocyte at meiosis I (15h post NEBD). Oocyte overexpressed TACC3-mClover (green) and H2B-mCherry (magenta), treated with 10 µM of Colcemid. Time shows minutes (min) from Colcemid treatment.

(D) Live cell example of full oocyte (maximum projection of 185 Z stacks, 90 µm) treated with 10 µM of Colcemid.

Images were taken via the Lightsheet Z.1 microscope. Scale bars show 5 µm.

4.6 TACC3 is essential for spindle pole integrity in human oocytes

We used the Trim-Away method in order to investigate the role of aMTOC-independent TACC3 in human oocytes that localised to the meiotic spindle microtubules and K-fibres. Translation is highest during prophase arrest; therefore, oocytes are microinjected with mRNA reporters at this stage. For mouse oocytes, dbcAMP can be used to synchronise NEBD (section 1.4.2, p22) and ensure comparable expression levels. However, resumption of human oocyte meiosis from samples collected as part of the clinical IVF cycle cannot be synchronised. Therefore, overexpression of microinjected mRNA in human oocytes is achieved at various levels, depending on the time of exit from prophase arrest. A more reliable approach to ensure comparable protein levels, is to microinject recombinant proteins directly into oocytes. In the case of the Trim-Away method, this was an important optimisation to ensure that TRIM21 protein levels and depletion of endogenous proteins are reproducible and comparable between experiments. Microinjection of human, His-Lipoyl-TRIM21 protein (Clift et al., 2017) into oocytes, successfully depleted endogenous TACC3 using the specific anti-TACC3 antibody (Figure 4.11A). This method allowed depletion of an endogenous protein in human oocytes for the first time.

TACC3-depleted oocytes were examined via immunofluorescence, which facilitates a more detailed, high-resolution imaging (Figure 4.11). Oocytes were depleted in prophase arrest and fixed at late MI stage (15h post NEBD as previously shown by Holubcová *et al.* 2015). While all oocytes microinjected with control IgG antibody formed bipolar spindles, suprisingly around 60% of TACC3-depleted oocytes assembled either multipolar spindles or showed spindle pole fragmentation (Figure 4.11A-B). The total amount of nucleated microtubules and spindle volume was comparable to control oocytes (Figure 4.11C-D). However, spindle microtubule morphology appeared to be unorganised, with microtubule bundles radiating abnormally from spindle poles in TACC3-depleted oocytes compared to the ordered, paralell organisation seen in control oocytes (Figure 4.11E). By measuring the total surface area of microtubules per unit of volume (SA:V ratio), this phenotype could be quantitatively described, showing that the

unorganised TACC3-depleted spindles had a significantly higher SA:V ratio compared to the control group (Figure 4.11F).

Similar to mouse oocytes (Figure 4.5H), TACC3 also localises to K-fibres in human oocytes (Figure 4.9F and Figure 4.11G). Consistent with the total spindle microtubule amount and volume, K-fibre total intensity and volume was not affected in TACC3-depleted oocytes (Figure 4.11H-I), although its morphology was again visibly different and radiated outwards compared to control spindles (Figure 4.11G).

Overall, we could for the first time carry out a functional study in human oocytes using the antibody-based Trim-Away method. Our findings show that TACC3 has an essential role in spindle pole integrity in human oocytes and in its absence the organisation of the microtubule filaments within the full spindle volume is disrupted.

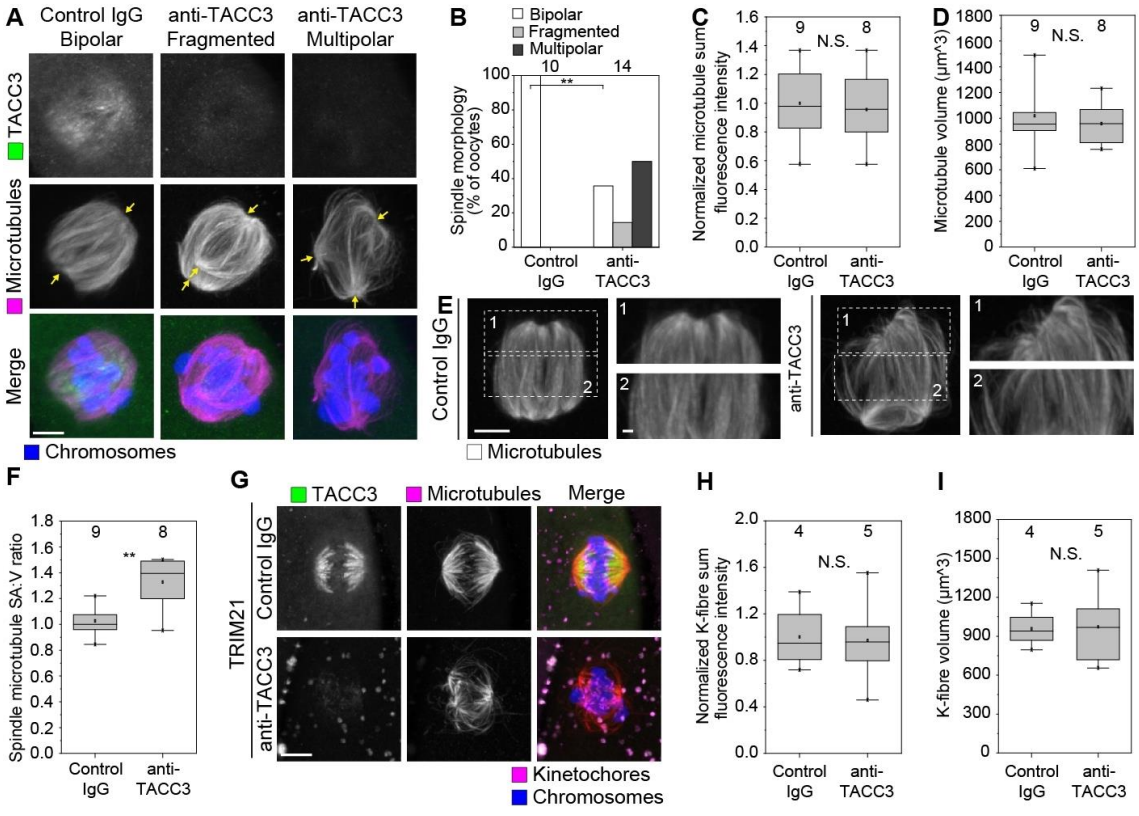

Figure 4.11. TACC3 is essential for spindle pole integrity in human oocytes.

(A) Immunofluorescence of oocytes microinjected with His-Lipoyl-TRIM21 and either Control IgG or anti-TACC3 at the MI stage (15h post NEBD). Examples showing

bipolar, fragmented or multipolar spindle pole morphology, number of poles are highlighted with yellow arrows. Scale bar shows 5 µm.

(B) Quantification of fixed oocytes microinjected with His-Lipoyl-TRIM21 and either Control IgG or anti-TACC3 at the MI stage (15h post NEBD) were scored for the frequency of spindle pole morphology.

(C-D) Quantification of normalised sum (C) and spindle volume (α-tubulin) (D). All oocytes were fixed at 15 hours post NEBD.

(E) Immunofluorescence examples of microtubule organisation (α-tubulin) in MI oocytes microinjected with His-Lipoyl-TRIM21 and either Control IgG or anti-TACC3. Boxed regions are magnified on the right, showing microtubule bundles at the spindle poles (1) and within the spindle (2). Scale bar shows 5 µm.

(F) Quantification of microtubule (α-tubulin) surface area to volume ratio in MI oocytes microinjected with His-Lipoyl-TRIM21 and either Control IgG or anti-TACC3.

(G) Immunofluorescence of anti-TACC3 (green), α-tubulin (magenta) and Hoechst (blue). Oocytes microinjected with His-Lipoyl-TRIM21 and either Control IgG or anti-TACC3 were allowed to mature (15h post NEBD) and treated with cold prior to fixing. Scale bar shows 5 µm.

(H-I) Quantification of normalised sum (C) and spindle volume (α-tubulin). All oocytes were cold treated at 15 hours post NEBD and fixed.

Data from five (B-D and F) and two (H-I) independent experiments. Number of oocytes shown above the dataset. P values were calculated with Student's t test (C-D, F and H-I) or Fisher's exact test (B).

.

5 RESULTS PART III

Light-sheet microscopy: Establishing a novel tool for live visualisation of meiosis in human oocytes

5.1 Overview

Powerful microscopy techniques and the advent of fluorescent proteins for targeted labelling of intracellular molecules have revolutionised live-cell imaging (Chalfie et al., 1994; Shaner et al., 2004). While it is possible to look at endogenous proteins and structures within cells via immunofluorescence and electron microscopy, these methods only give snapshot information and the specimens cannot be examined live. Biological processes are highly dynamic and therefore it is essential to look at interactions and molecular mechanisms in real time, *in vivo*. When studying the dynamic maturation of oocytes, high-resolution, 3D live-cell imaging has proven to be a powerful tool. However, one of the major limitations of live-cell imaging is phototoxicity (Icha et al., 2017).

Human oocytes in particular are a challenging system to work with for a number of reasons. First of all, meiosis in human oocytes takes a long period of time (23-26 hours) and the length of time-lapse imaging required to capture the temporal dynamics of this process is therefore much longer, compared to mouse oocytes (10-12 hours) (Holubcová et al., 2015; Schuh & Ellenberg, 2007). Secondly, fluorescent probes are required to label the specific components of the spindle apparatus. Human oocytes are extremely sensitive to light exposure and in the case of high-resolution live-cell imaging, the prolonged illumination of fluorophores generates free radicals upon photobleaching, leading to cell damage (Icha et al., 2017). In addition, oocytes are the largest cells in the human body, with a diameter of around 100-120 micron. This in itself, the imaging of a large, cytoplasm-filled sphere, represents some unique challenges.

Laser scanning confocal microscopy offers an important improvement for live-cell imaging, as it enables optical sectioning of thick specimens (Whitehead et al., 2017).

Coupled with time-lapse imaging software, the 3D reconstruction of the digitalised images has proved to be an excellent tool for live-cell imaging of oocytes (Schuh & Ellenberg, 2007). In the case of human oocytes however, the frequency and length of time-lapse imaging has a detrimental effect on cell viability. Therefore, new tools are required to maintain the viability of the samples being imaged, while pushing the boundaries of spatiotemporal resolution of the acquired images.

Light-sheet fluorescent microscopy (LSFM) has provided breakthroughs in a wide range of disciplines, including cell and developmental biology (Elisa et al., 2018). The concept of LSFM is very simple: it is essentially a wide-field microscope that illuminates the sample from the side, with the signal detected only from regions that are in focus. Therefore, total light exposure to the sample is reduced. The illumination and detection paths are separate, and the signal is collected by a camera. This provides a parallelized imaging process.

The attraction of LSFM as an imaging tool for oocytes, lies in the exceptional speed of high-resolution image acquisition, with minimal exposure time and low phototoxicity (Elisa et al., 2018; Heddleston & Chew, 2016; Lim et al., 2014; Power & Huisken, 2017). Although good LSFM systems can be built and customised, we decided to start with the commercially available LSFM from Zeiss (Lightsheet Z.1). This system comes with a number of built-in advantages: multi-view imaging gives flexibility for sample positioning, optimised optics allow homogeneously illuminated optical sections, and laser intensities can be set extremely low. This is all in a chamber that can maintain stable temperatures and humidity for optimal long-term imaging of live samples.

This system was ideally designed for sample loading and imaging larger specimens, such as tissues, organs and even whole organisms with limited phototoxicity; however, this system was not ideally suited to image the small human oocytes live. Our first challenge was to design a custom-made sample loading method, which had to satisfy three main points:

1. Oocytes must be reliably loaded into a culture medium, capable of maintaining development for 2-3 days.
2. The spherical shape of the sample had to be considered, with movement avoided during acquisition.

3. Recovery of the oocyte/s following live-cell imaging in order to carry out further assays and immunofluorescence.

The LSFM Z.1 is designed to hold the sample vertically, embedded in a cylindrical agarose mold. However, embedding the oocytes did not support oocyte development in our hands, and instead we designed a thin, vertical sample holder made of tantalum, a biocompatible, corrosion-resistant metal. A medical grade, thin tantalum sample holder has an imaging window cut out in the middle, and this is prepared in a sandwich layer of FEP film (13 µm thickness), which has the same refractive index as water (Figure 5.1) (Strnad et al., 2016). The original sample holder design was invented by Dr. Melina Schuh and Dr. Zuzana Holubcová in our lab. In this sample holder, the oocytes are cultured in pH stable medium, between the FEP – tantalum – FEP sandwich, and this is sealed with biocompatible silicone grease.

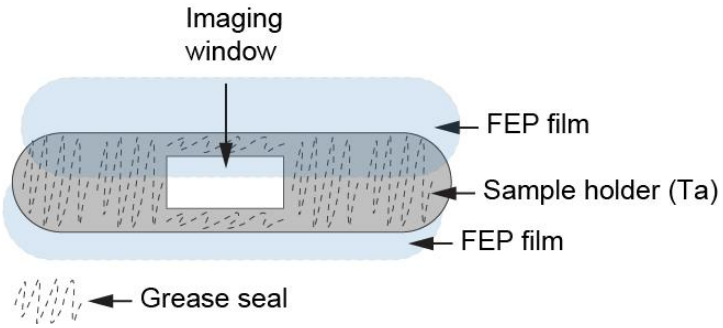

Figure 5.1 LSFM sample holder design.

While I had the prototype of the original sample holder to start with, this could not maintain oocyte viability, even during an overnight culture of mouse oocytes and at this point it was not clear why oocytes could not develop in this set up. Thus, in order to achieve reliable imaging of human oocytes, I decided to systematically test all essential components of oocyte culture, starting with optimisation of culture conditions. This included cytotoxicity analysis of all materials used, and validation of optimal temperature, medium, pH and osmolality conditions. Culture volumes, culture media osmolality and supplementation with additional antimicrobial reagent were the most crucial steps, as shown by the results. Once culture conditions in the LSFM chamber were suitable for reproducible mouse oocyte development, the acquisition parameters

were optimised, initially using mouse oocytes and frozen-thawed human oocytes. Overall, oocyte development was best supported by low exposure time and higher laser settings. After optimising sample loading, culture conditions and imaging settings, both mouse and human oocytes were successfully imaged to their full maturation stage (Meiosis II) in the Lighstheet Z.1 microscope system using a new sample holder design.

5.2 Design of new LSFM sample holder for oocytes

The commercially available agarose embedded sample loading method designed by Zeiss was initially tested for oocytes. This method was not suitable to support long-term culture of these cells (preliminary optimisation did not yield viable oocytes). I initially tested the agarose embedded sample imaging with larger tissues and zebrafish embryos (Figure 5.2A), which gave homogeneously illuminated, high-resolution images. Using the thinnest capillary available to embed mouse oocytes did not result in clear and even images (images were not saved). Oocytes also moved around within the solidified agarose gel and due to their small size, there was a large excess of gel around the oocytes that probably created the blurring of the images. Recovery of oocytes following embedding was also not possible.

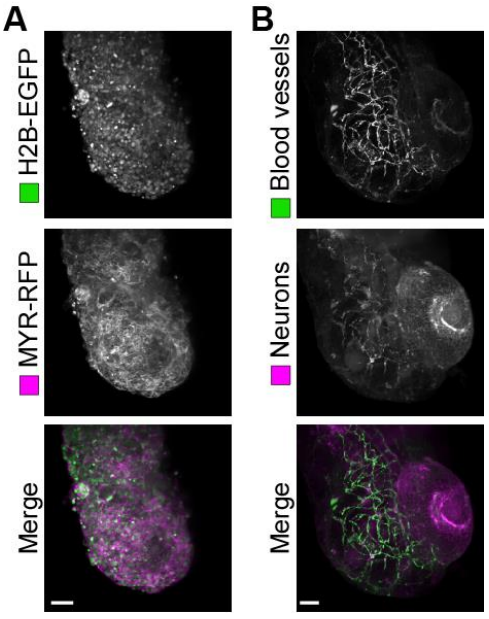

Figure 5.2 Example images taken with the Lightsheet Z.1 using the agarose embedded sample holder setup.

(A) Live imaging of part of a gonad from 12.5 E CAGTAG/B6129 embryo (sample provided by Chloe Charalambous, Schuh lab). Projection of 126 Z stacks (1 µm thickness).

(B) Immunofluorescence of zebrafish embryo head (sample provided by Carl Zeiss). Projection of 265 Z stacks of 0.5 µm thickness.

Scale bars shows 50 µm.

In order to reliably load and recover oocytes from the imaging holder, we designed a vertical sample holder made out of Tantalum (Ta), a biocompatible and corrosion resistant metal. In order to achieve sharp and high-resolution images, it was important to find a very thin material that does not scatter or band light, i.e. has the same refractive index as the surrounding solution that the light sheet has to path through. The light-sheet chamber was filled with aqueous culture medium. We used a commercially available FEP film (13 µm thickness) that was previously suggested to have the same refractive

index as water and had been successfully used in an inverted LSFM set up (Strnad et al., 2016).

The sample holder is prepared in a sandwich with two FEP foils cut to size, sealed with biocompatible silicone grease (Figure 5.3).

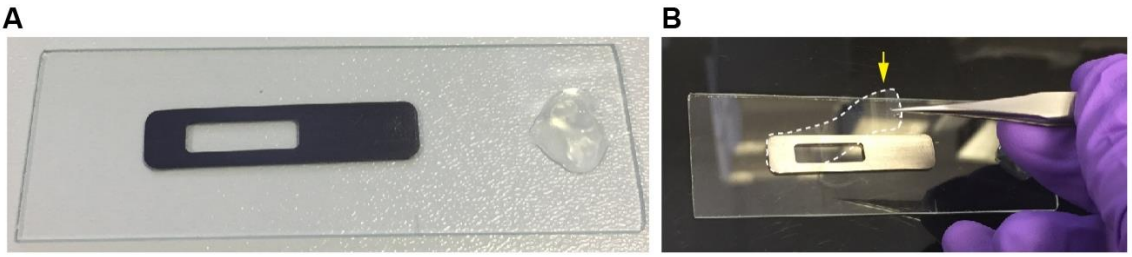

Figure 5.3 LSFM Sample holder preparation.

(A) Tantalum sample holder on a glass slide. On the right, silicone grease is used to coat a thin layer on both surfaces.

(B) FEP film cut out to size is placed on both sides of the sample holder, sealed with the grease. Yellow arrow indicates FEP foil and dashed white line highlights the borders of the transparent FEP film.

The original design of the sample holder is illustrated in Figure 5.4A. The imaging window is filled with culture medium and sealed again with the FEP film. When oocytes are loaded, the FEP foil is lifted and resealed carefully after loading. The imaging window is essentially also the culture chamber where the oocytes sink down vertically, onto the oocyte culture surface (Figure 5.4A, red line, 3). The loading of oocytes into the imaging window is carried out in a manner so that the oocytes sink down in one line onto the culture surface, in order to avoid any overlap between oocytes that would hinder imaging. The sealed sample holder that contains the oocyte/s is loaded via the sample holder attachment into the light-sheet imaging chamber (filled with 35 ml of culture medium) (Figure 5.4C-D). The sample holder disk was not modified from the original manufacturer's design, only the sample holder stem. This was necessary in order to allow the attachment of the oocyte sample holder, which is secured with a screw at the tip of the stem (Figure 5.4C).

Using the Specimen Navigator tool (built in Zen black software, Z.1 special edition), the sample holder can be lowered into the chamber, positioned accurately and rotated at around 45° so that the light sheet can illuminate the oocytes that have now sunk down to the oocyte culture surface (Figure 5.4A).

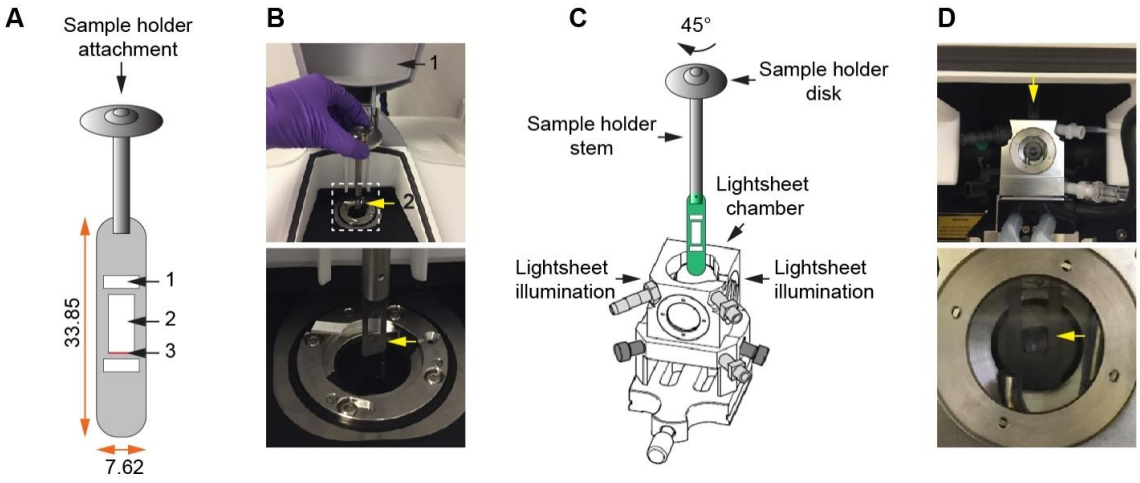

Figure 5.4 Sample loading for Lightsheet Z.1.

(A) Schematics of sample holder design. Dimensions shown with orange arrows, numbers are in millimetres (mm). Arrows indicate excess grease reservoir (1), oocyte culture chamber and imaging window (2), oocyte culture surface (3). Numbers associated with orange arrows are shown in millimetre (mm).

(B) Sample holder with attachment loaded into the Lightsheet Z.1 via the upper system cavity (1). Boxed region is magnified to highlight sample holder (2) below, marked with yellow arrow.

(C) Components of the sample holder (highlighted in green) with attachment, showing the position of loading into the imaging chamber. Arrows show the light sheet illumination direction from the sides. Sample holder is rotated to achieve a 45° angle. Schematics of light-sheet chamber taken from Carl Zeiss (Lightsheet Z.1 Operating Manual).

(D) Photo of the sample chamber filled with culture medium. Yellow arrow indicates the sample holder. Zoomed in photo shown below.

Initial troubleshooting steps involved modifications to the original sample holder design (Figure 5.5). At this point, loading was not reproducible and oocytes were frequently lost, as the sealing of the FEP film was not holding properly. This was overcome by removing the excess grease reservoir from the original design (Figure 5.5, Design 1) and increasing the overall surface area to ensure proper sealing (Figure 5.5B, Design 2).

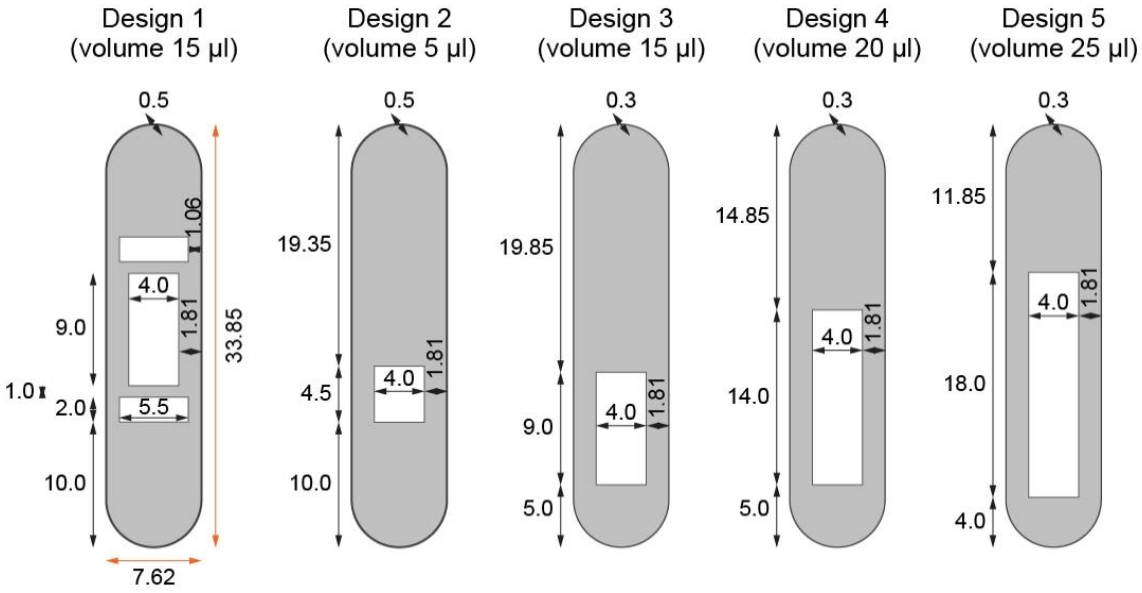

Figure 5.5 Oocyte sample holder design parameters.

Volumes refer to the amount of medium the imaging window can hold. Numbers are shown in millimetre (mm).

5.3 Optimisation of culture conditions

In order to support long -term viability and achieve maturation of both mouse and human oocytes, culture conditions within the oocyte sample holder were optimised. The sample holder is essentially a micro-culture system that supports group-culture of

oocytes, as it has a single compartment. The initial optimisation was done with mouse oocytes due to the limited availability of human samples.

During the first attempts of oocyte culture in the Lightsheet Z.1, frequent contamination of the large imaging chamber was a major problem. The chamber is open on the top to allow sample loading (Figure 5.4C), which can be covered but not completely sealed. For live cell imaging, the whole volume of the chamber medium (30-35 ml) is heated to 37ºC for over 24h. Although the medium is supplemented with antibiotics, following overnight culture bacterial growth was frequently observed, and oocytes all degenerated within the sample holder. In order to overcome this, the medium in the light-sheet chamber was supplemented with Normocin^{TM} antimicrobial reagent (protects against mycoplasma, bacterial and fungal contamination), which eliminated this problem.

While contamination was no longer an issue, oocytes cultured in the oocyte sample holder (SH) all arrested in MI (Figure 5.6A). This was a clear indication that the culture environment was not optimal. It was not possible to accurately determine the exchange of culture medium between the sealed SH chamber and the large light-sheet chamber. The light-sheet chamber could not be overlaid with oil as this would coat the sample holder during loading and distort the light passing through the FEP film. Therefore, the large volume of medium, heated to 37ºC for days, is highly prone to evaporation, even when covered. In order to exclude negative effects of the SH environment on the medium in the light-sheet chamber, I tested to see whether evaporation could be a cause of the poor oocyte development. Oocyte development was compared between those cultured in the conventional culture dish, those cultured in the SH in a loose capped 50 ml falcon tube (35 ml medium) in order to mimic the open light-sheet chamber and those where the medium (35 ml in 50 ml falcon tube) was overlaid with oil and tightly capped to eliminate evaporation completely. Results shown in Figure 5.6B demonstrate that none of the oocytes cultured in the SH reached the full stage of maturation. This result narrowed the issue down to the SH itself.

I decided to systematically test the main aspects of culture conditions in order to narrow down the problem (Elder et al., 2015). This included testing different culture media, cytotoxicity test of all components used for oocyte culture, and monitoring pH,

temperature and osmolality (Figure 5.6). Any one of these parameters, if not within the homeostatic range can be detrimental to oocyte development (Elder et al., 2015).

Culture media is one of the most essential starting points for troubleshooting culture systems. Ideally, oocytes should be cultured in high CO_2 (6%) and low O_2 (5%). The Lightsheet Z.1 is equipped with a CO_2 module to supply the sample environment; when tested, this resulted in major evaporation of the culture medium in the light-sheet chamber. In addition, as the large chamber cannot be fully sealed, maintaining critical gas concentrations within specific values is not possible. Therefore, media supplemented with CO_2-independent buffer were tested, to ensure physiological pH levels (pH 7.2-7.4) throughout oocyte culture. All tested media were supplemented with 10% FBS (Foetal Bovine Serum). M2 is a commonly used medium for oocyte and early stage embryo culture. G-MOPS™ is a commercially available (Vitrolife), IVF grade medium, developed for manipulation of gametes outside of the incubator. MHM® (Multipurpose Handling Medium Complete®) is also an IVF grade medium from Irvine Scientific. From the three tested media, all showed comparable MII oocyte formation rates (72.2% M2, 88.9% G-MOPS™ and 77.8% MHM®) (Figure 5.6C). As we had previously successfully used G-MOPS™ for human oocyte maturation, we decided to continue with this commercial medium. As expected, pH levels were maintained within physiological range across different temperatures at ambient CO_2 levels (Figure 5.6D).

Plasticware and consumables can represent a major source of toxic compounds if not tested carefully. In order to exclude toxicity or detrimental effects on oocyte development of any of the SH components, I tested oocyte development cultured with each component in isolation (Figure 5.6E). The results show that oocyte development was comparable with all tested consumables.

The Lightsheet Z.1 is equipped with a highly sensitive temperature probe that can be secured within the light-sheet chamber to monitor temperature throughout culture. Temperature can vary between different parts of a compartment, and therefore I wanted to make sure that there are no major temperature fluctuations within the chamber that could impact oocyte development. A calibrated IVF grade thermometer was used with three different probes (Figure 5.6F), each positioned at different locations within the chamber. The sample holder probe was secured within the holder itself, giving the closest

possible reading of temperatures that the oocytes would be directly exposed to the light-sheet (LS) chamber probe was positioned where the internal LS temperature probe is located, and the LS chamber probe (top) was positioned at the top surface of the medium within the chamber. Temperature was monitored continuously, every minute for over 20 hours. The results of this clearly showed that temperature equilibrated after 3-4 hours. This indicates the time that must be allowed for the system to reach a stable temperature, before starting oocyte culture. The sample holder and main LS chamber probes showed stable temperatures during the monitoring period. LS chamber (top) probe however showed a gradual decrease in temperature, measured at the top part of the chamber. This indicates the importance of positioning the oocytes well within the middle of the chamber to ensure optimal temperature. Most importantly, these measurements also provided evidence that the built-in LS temperature probe readouts were reliable for temperature monitoring.

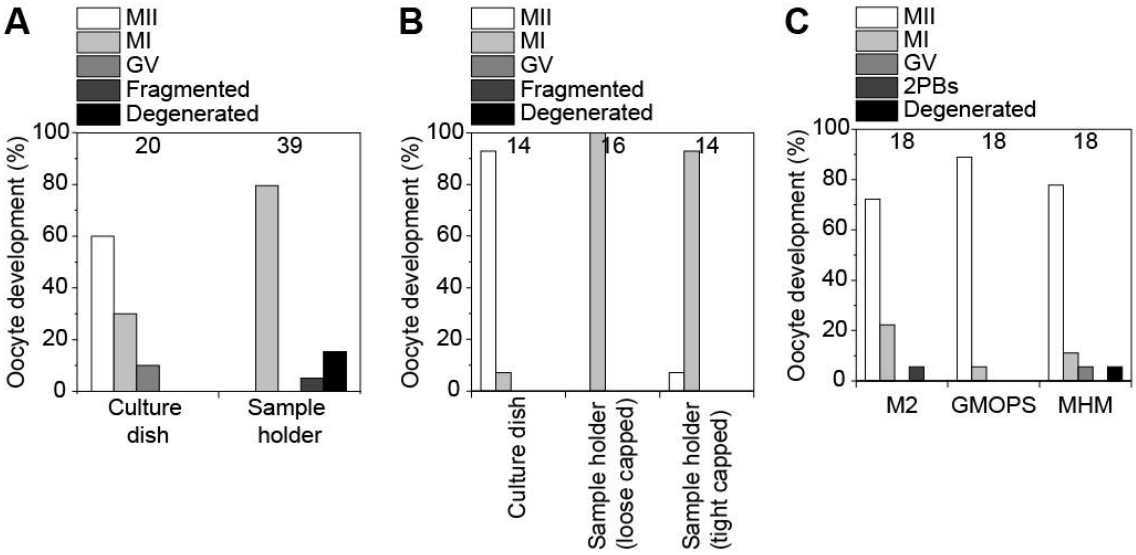

D

	GMOPS		GMOPS+10% FBS		
Temperature	4 °C	37°C (2h)	4 °C	37°C (2h)	37°C (ON)
pH	7.40	7.26	7.43	7.27	7.29

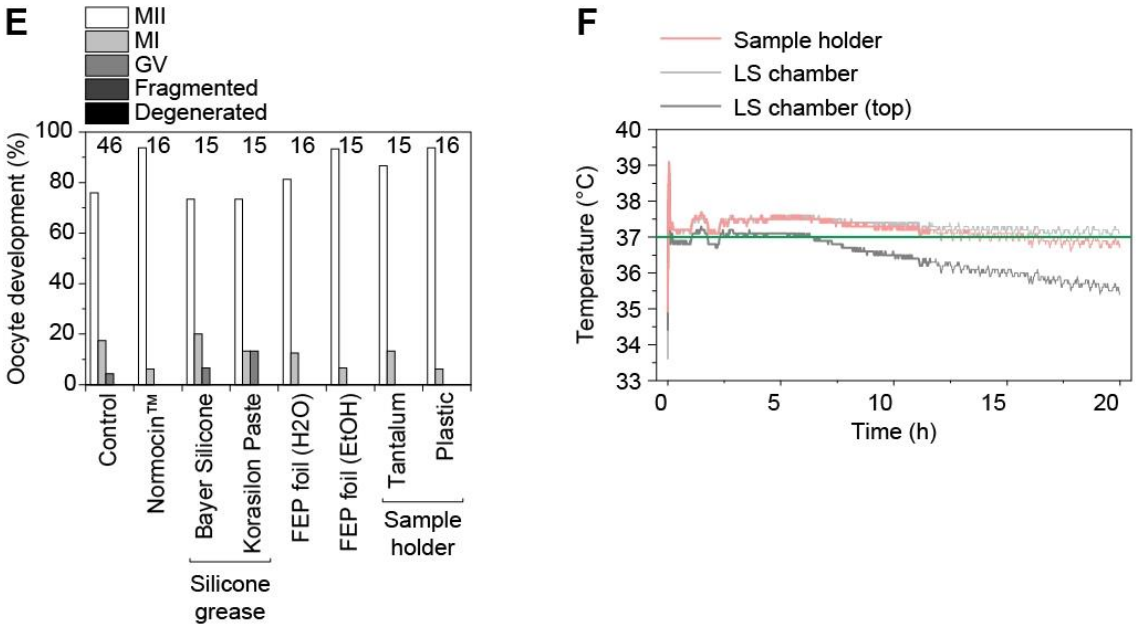

Figure 5.6 Optimisation of culture conditions in oocyte sample holder

(A) Mouse oocytes cultured overnight in a conventional 35mm culture dish versus the oocyte sample holder for the light-sheet. Oocyte development was scored for progression through meiosis.

(B) Mouse oocytes cultured overnight in a conventional 35mm culture dish versus the oocyte sample holder for the light-sheet containing 35 ml of loosely capped culture medium in a 50 ml falcon tube, or tightly capped and overlaid with oil. Oocyte development was scored for progression through meiosis.

(C) Oocyte maturation rate in different culture media. M2 Millipore - EmbryoMax M-2 powder, G-MOPS^{TM} from Vitrolife and MHM® (Multipurpose Handling Medium Complete®) from Irvine Scientific. All media supplemented with 10% FBS (Foetal Bovine Serum).

(D) pH measurement at different temperatures at ambient CO_2 concentration. Time in hours (h) or ON (overnight), shown in brackets.

(E) Cytotoxicity test of all culture components. Control oocytes were cultured overnight in a conventional 35mm culture dish. Silicone grease from two different suppliers (used for sealing the sample chamber with the FEP film). FEP was washed either in embryo tested water (H_2O) or 70% ethanol (EtOH). Two different materials for the sample holder were tested, Tantalum (Ta) and plastic.

(F) Temperature monitoring in light-sheet (LS) sample holder or chamber. Measurements were obtained with Squirrel Data logger from Grant (2010 Series), with calibrated temperature probes. Time is shown from start culture in hours (h).

Number of oocytes shown above the dataset.

5.4 Change in osmolality is the main factor affecting culture conditions in light-sheet sample holder

Osmolality is a measure of the osmolar concentration of solutes in a solution. *In vitro* culture of cells are highly sensitive to even small levels of changes in osmolality (Elder et al., 2015). Osmotic pressure within the cells regulates cell volume and under suboptimal culture conditions, it can lead to swelling or shrinkage of the cells. Oocytes in particular, due to their large cytoplasmic volume are highly prone to changes in the surrounding osmolality of the culture medium. Prolonged or high osmotic stress can lead to developmental arrest and cell death (Elder et al., 2015). Observations from *in vitro* culture of human embryos revealed that osmolalities higher than 300 mOsm/kg resulted in developmental arrest. Developments in medium formulation suggested that the optimal range for embryo development is between 255-295 mOsm/kg (Elder et al., 2015).

IVF grade osmometers are available for the accurate measurement of osmolality in aqueous solutions, but these require a minimum of 200 µl of testing volume, which is much higher than the microculture in the SH. One of the key observations from culturing mouse oocytes in the light-sheet SH for long periods of time was cell shrinkage prior to cell death (Figure 5.7A). Cells regulate their intracellular volume in response to osmotic

pressure, therefore looking at the changes in cell volume over time would be an indirect measure of osmotic environmental changes. Estimated oocyte volume over time (calculated by measuring the cell diameter at specific time points) clearly indicated that oocytes lost almost half their volume during 25-30-hour culture in the SH (Figure 5.7B). This was a clear indication that the cells were trying to compensate for an increased osmolality within the culture medium. When the sample holder was removed following overnight culture, large air bubbles filled the imaging window, which also interfered with imaging of oocytes (Figure 5.7C-D). Within the large air bubbles, condensation on the FEP film suggested that there could be some evaporation within the holder that may lead to osmotic changes of the culture medium, especially at such small volumes.

Aqueous solvents contain dissolved gases that can vary at different temperatures. In general, liquids dissolve less gas at higher temperatures. Therefore, when heated, degasification of the dissolved gases creates bubbles in the culture medium. This can be overcome by ensuring that prior to *in vitro* culture, the medium is pre-warmed overnight and degassed of soluble gases, such as water. This step has significantly improved oocyte developmental rate (Figure 5.7E).

Another way to ensure stable osmolality is to avoid evaporation when setting up culture dishes (Elder et al., 2015). One of the crucial steps is to ensure this is done quickly, at room temperature and overlaid with oil to minimise evaporation. When setting up the culture system for the light-sheet, the medium volume is very small (5-20 µl) and oil cannot be used to cover the culture drops, therefore it is extremely prone to evaporation. I measured the rate of evaporation during set-up of the SH on a heated microscope stage versus cold stage and at different volumes (Figure 5.7F-G). By modifying the Tantalum sample holder design to increase the culture volume up to 25 µl (Figure 5.5) and setting up dishes on a cold microscope stage with cold medium, evaporation could be reduced to below 5% (Figure 5.7G).

Prior to optimisation, oocyte maturation rate was severely reduced in the light-sheet sample holder compared to the control oocytes cultured in a conventional culture overlaid with oil (Figure 5.7H). Following optimisation, most importantly by minimising evaporation rate during culture preparation, increased culture volume and degassing of

culture medium, maturation rate of oocytes were now comparable to controls (Figure 5.7I).

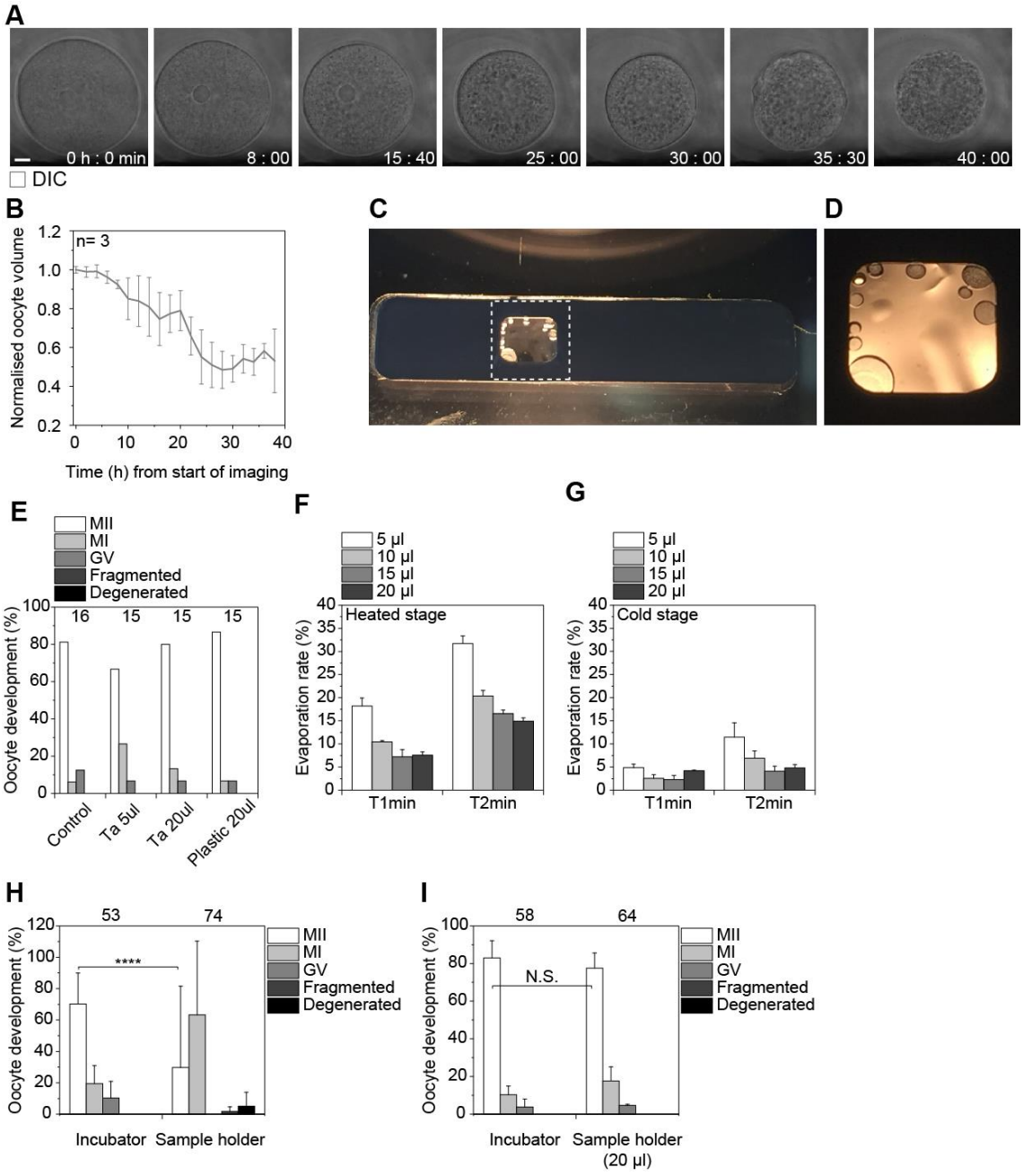

Figure 5.7 Optimisation of culture volume and osmolality.

(A) Examples of mouse oocytes cultured in the light-sheet sample holder. Time shows hours (h) and minutes (min) from start of imaging. Scale bar shows 5 µm.

(B) Quantification of oocyte volume over time. Relative volume is calculated by measurement of oocyte oolemma diameter.

(C-D) Photograph of light-sheet sample holder with culture medium in the imaging window, following overnight incubation at 37^{o}C. Boxed region is magnified on the right (D). Air bubbles in the imaging window are shown in the magnified image.

(E) Mouse oocytes cultured overnight in a conventional 35mm culture dish (control) or different volumes of sample holder made of Tantalum (Ta) or plastic. Oocyte development was scored for progression through meiosis.

(F-G) Quantification of culture media evaporation rate at different volumes and time points. Sample holder culture was either set up on a heated (F) or cold microscope stage (G).

(H-I) Mouse oocytes cultured overnight in a conventional 35mm culture dish (control) or in the light-sheet sample holder. Oocyte development was scored for progression through meiosis prior to optimisation (H) and following optimised conditions (I).

Number of oocytes shown above the dataset. P values were calculated with Fisher's exact test (H-I).

5.5 Optimisation of imaging conditions in the LSFM

Following the optimisation of culture conditions in the new sample holder, designed for long-term oocyte culture in the Lightsheet Z.1, the next step was to adjust the live cell imaging settings. The aim was to expose the oocytes to as little light as possible, while still being able to acquire high-resolution, detailed live cell images.

I started with imaging mouse oocytes, microinjected with fluorescently tagged mRNA reporters. Oocytes were imaged overnight for 16 hours and with low laser light and exposure times. Under these conditions, oocytes developed to the MII stage at a comparable rate to control oocytes that were matured in the incubator in conventional culture dishes with no laser light exposure (Figure 5.8A). Image quality was excellent with high resolution, detailed images taken at 10-minute intervals (Figure 5.8B-C). The main difference compared to the confocal image set-up was that the whole oocyte could be imaged, with a z range of 80 µm, over 30 z stacks. In comparison, mouse oocytes imaged with confocal microscope were imaged within a range of 20-40 µm z range, over 6-10 z sections. Images were taken only of the region of interest, rather than the whole oocyte.

While mouse oocyte development was optimised at this stage, human oocyte imaging takes much longer and therefore it was important to test the optimised conditions directly on human oocytes. As samples are very limited, we decided to use vitrified and thawed oocytes donated for research for the initial optimisation steps. To ensure that these samples will give comparable results to fresh oocytes, I compared frozen-thawed oocyte maturation rate to that of fresh oocytes (Figure 5.8D). This suggested that polar body (PB) extrusion rate was comparable to oocytes that were collected fresh.

I next designed experiments to test three different imaging parameters and assess oocyte health by scoring for the stage of development the oocytes reached over a period of 40-45 hours' time-lapse imaging (Figure 5.8E-G). The first experiment used the imaging settings that were optimised for mouse oocytes (Figure 5.8E). A total of four oocytes were thawed and imaged over a 42-hour period. Three out of the four oocytes entered meiosis, however all of them stopped development before anaphase onset and formed pronuclei (PN) (PN pre-anaphase, Figure 5.8E). The second experiment was carried out with three frozen-thawed human oocytes. Laser intensity and exposure time were

reduced, and oocytes were imaged over a 40-hour period (Figure 5.8F). The reduced light exposure resulted in better oocyte development, with two out of the three oocytes entering anaphase. Developmental arrest occurred at a later point compared to the first experiment as both oocytes formed pronuclei immediately after anaphase (Figure 5.8F). The third experimental design further reduced the laser intensities by 30% (laser 0.7 vs 1) and the exposure time by 40% (exposure time 30 vs 50) compared to the starting point in experiment one. Oocyte development with these imaging parameters further improved: two out of the three oocytes imaged underwent anaphase and formed MII spindles.

Overall, it is clear from these results that human oocytes are extremely sensitive. While mouse oocytes were a useful tool for the initial optimisation of the culture and imaging parameters, due to their faster rate of maturation, it was not possible to fully adjust imaging settings that are suitable for human oocyte development. Frozen-thawed human oocytes were used to further optimise imaging parameters in a three-step experiment design. At the end of the third adjustment, over 60% of human oocytes reached full maturity. A nice example of the quality of live cell imaging of human oocytes using the optimised light-sheet system is shown in Figure 4.9A.

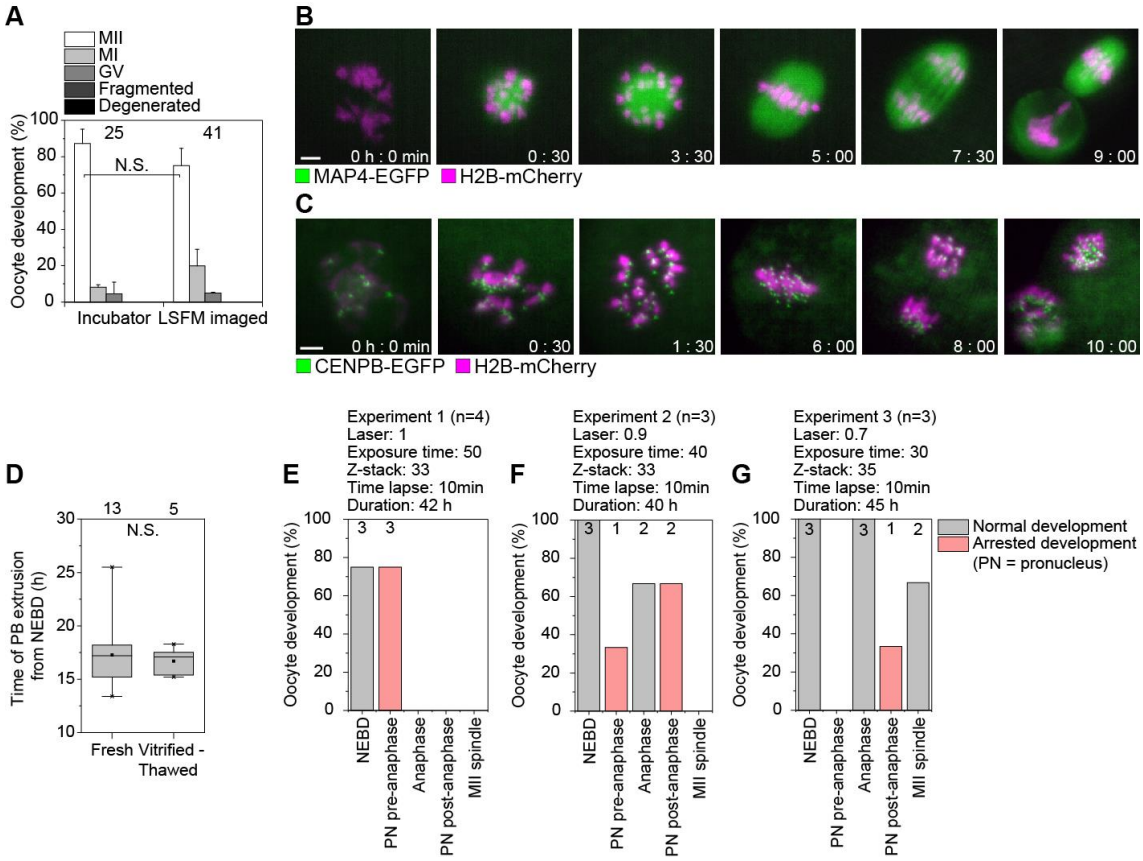

Figure 5.8 Optimisation of imaging settings for LSFM.

(A) Mouse oocytes microinjected with fluorescently labelled mRNA were cultured overnight in a conventional 35mm culture dish (incubator – not imaged) or in the Lightsheet Z.1, imaged overnight (LSFM imaged). Oocyte development was scored for progression through meiosis.

(B-C) Examples from time-lapse imaging of mouse oocytes overexpressing H2B-mCherry and MAP4-mEGFP (B) or CENPB-mEGFP (C) using the Lightsheet Z.1 and the tantalum sample holder, design 4 (20 µl culture volume). Time shows hours (h) and minutes (min) from NEBD (time 0). Scale bar shows 5 µm.

(D) Comparison of the distribution of polar body (PB) extrusion rate from NEBD between human oocytes collected fresh or frozen-thawed. Oocytes were incubated and imaged in the PrimoVision time-lapse monitoring system in a conventional culture dish.

(E-G) Quantification of human oocyte development at different imaging conditions in the Lightsheet Z.1, in the tantalum sample holder, design 4 (20 µl culture volume). Acquisition parameters are shown above for three independent experiments.

Data from two independent experiments (A). Number of oocytes shown above the dataset. P values were calculated with Fisher's exact test (A) or Student's t test (D).

6 DISCUSSION

MTOCs play a key role in the assembly and morphology of the bipolar spindle. While centrosomes are well characterised, very little is known about the organisation and function of centrosomal proteins in oocytes. Immunofluorescence and live cell imaging studies have revealed that core pericentriolar proteins surrounding the centrioles of the mitotic spindle also have important functional relevance in mouse oocytes, where centrioles are eliminated early on (Schuh and Ellenberg, 2007; Łuksza *et al.*, 2013; Clift and Schuh, 2015a). However, considering the vast number of proteins required for centrosome function and organisation, there is very little knowledge about how the different centrosomal components and appendages may contribute to spindle assembly and function during meiosis. In addition, the high frequency of spindle instability in human oocytes, which contain no prominent MTOCs (Holubcová et al., 2015), supports the hypothesis that mouse oocytes might have specific mechanism(s) to ensure spindle stability, likely related to the presence of aMTOCs.

In order to address this question, we looked at centrosomal proteins that proteomic and transcriptomic data indicated their expression in mouse oocytes (Zeng, Baldwin & Schultz, 2004; Wang *et al.*, 2010; Pfeiffer *et al.*, 2011; Virant-Klun *et al.*, 2013; Yan *et al.*, 2013). We initially screened for localisation of proteins for which specific antibody and live cell markers were easily available. Based on the initial screen, a previously undescribed meiotic spindle pole domain (MSPD) is presented here. For the primary characterisation for this domain I focused on a large coiled coil scaffold protein, Pericentriolar material 1 (PCM1), which has been shown to interact with a large number of centrosomal proteins via the centriolar satellite trafficking mechanism (Tollenaere, Mailand & Bekker-Jensen, 2015; Hori & Toda, 2017). This work was later extended to a broader screening of centrosomal and spindle pole associated proteins, which identified TACC3 as a key organiser of this domain. The conserved role of this domain was an important focus of my work and I also present here some of the preliminary results that may suggest a mechanism for spindle pole organisation in MTOC-free human oocytes.

The aim of the discussion is to summarise my findings and present them in the context of current literature. The outlook of this work will also be discussed and included some extended data that is relevant to our current understanding of the assembly, regulation and function of the MSPD during meiosis.

6.1 Characterisation of centrosomal proteins in acentrosomal mouse oocytes

PCM1 was an interesting candidate to initially focus on, as it is the main scaffold protein of the centrosomal satellites and has been shown to interact directly with a large number of PCM proteins (Hori & Toda, 2017). My initial work involved detailed characterisation of PCM1 localisation in mouse oocytes (Chapter 3: Results: PartI), which revealed a number of interesting points.

Firstly, the aMTOCs in interphase cells are organised in two distinct compartments (Figure 3.2B). Core PCM components, such as Pericentrin and γ-tubulin, form the outer layer of the spherical aMTOC and PCM1 is localised to the internal compartment. This was consistently the case for both the cytoplasmic population of aMTOCs as well as those surrounding the nuclear envelope (NE), prior to aMTOC fragmentation. Interestingly, as meiosis resumed, PCM1 remained enclosed within the spherical aMTOCs in the cytoplasmic pool, while those associated with the NE could be seen as small foci on the outer surface of the now stretched MTOCs. It is possible that the MSPD domain content within the aMTOCs are released upon stretching of aMTOCs by dynein along the NE, or as PLK1 decondenses the aMTOCs (Clift & Schuh, 2015), which could explain the change in the localisation pattern. As aMTOCs are stretched and fragmented, PCM1 can no longer be seen within the internal compartment of aMTOCs associated with the spindle, but it does remain enclosed within the spherical cytoplasmic population throughout meiosis. This suggests that aMTOCs undergo a compositional change as meiosis resumes. In line with the proposed two component aMTOC structure, previous studies have shown that the structural organisation of the aMTOCs is not homogeneously dense, but instead contains small, lower density compartments that appear alveolar-like under high resolution imaging (Clift & Schuh, 2015; Łuksza et al., 2013). Closer examination of my images also shows that the interior of spherical aMTOCs is not fully dense. While this organisation does not resemble the complex structure of the centrosomal PCM (Fry et al., 2017), it does suggest a partially conserved organisation of distinct but closely associated populations of centrosomal proteins.

Secondly, following nuclear envelope breakdown, marked by a burst in microtubule nucleation, PCM1 starts to accumulate within the microtubule ball (Figure 3.2B-C).

During bipolarisation, aMTOCs are sorted to the two poles and PCM1 also progressively accumulate at the poles. As the MTOCs coalesce to form the pole ring domain, PCM1 gradually forms the characteristic spindle pole protrusions (Figure 3.2D). Overall, the subcellular localisation of PCM1 is surprisingly different in oocytes compared to mitotic cells, where the satellite foci stained with PCM1 are concentrated around centrosome markers (e.g. γ-tubulin) predominantly during interphase and mostly disperse within the cytoplasm following mitotic entry (Balczon et al., 1994; Dammermann & Merdes, 2002; Hoang-Minh et al., 2016; Kimura et al., 2013; Kubo, 2003). Association of the PCM1/MSPD with the meiotic spindle is microtubule dependent, as shown by the loss of MSPD organisation when microtubules are depolymerised with Nocodazole (Figure 3.4). This is in line with previous reports that PCM1 localisation along the centrosomes is microtubule dependent, perhaps linked to dynein transport towards the minus-ends of the microtubules, which could in part also explain the accumulation of the PCM1/MSPD at the poles (Dammermann & Merdes, 2002; Hori & Toda, 2017; Li et al., 2000).

The above described localisation of PCM1/MSPD was later also confirmed for TACC3 and its known interacting partners clathrin and ch-TOG (Figure 4.2), and the other identified components found to localise to this domain (Table 4.1, Figure 4.2), confirming that the described localisation pattern is conserved for proteins within the MSPD. In addition, detailed high-resolution live cell imaging of TACC3 captured the release of the TACC3/MSPD during NEBD (Figure 4.4D), supporting the idea that the MSPD associated with the spindle is released (or in part released) from the aMTOCs surrounding the nuclear envelope.

6.1.1 Strategies to deplete PCM1 in oocytes

6.1.1.1 Conventional strategies to deplete PCM1

One of the initial challenges of working with PCM1 was the difficulty of depleting this long-lived protein in mouse oocytes. Although oocytes are transcriptionally silent (Pan et al., 2005), maternal mRNA and proteins accumulate in the oocyte's large cytoplasm to ensure proper oocyte maturation and embryo development.

We tried a number of different methods, which I will discuss here in more detail, as this played an important part in the optimisation work. These results are only partially included in the results section of this thesis, as they were either attempted before my work on this project was initiated, or they were preliminary test experiments that were not further investigated but do merit brief mention.

RNA interference (RNAi) strategies that involve microinjecting siRNAs into early, follicle-enclosed oocytes combined with prolonged *in vitro* culture (10-11 days) can maximise mRNA depletion efficiency in blocking protein expression (Pfender et al., 2015). However, PCM1 proved to be an example of a long-lived protein that is probably expressed before sufficient RNA degradation could be achieved (Figure 3.5A).

Inhibition of endogenous PCM1 localisation was previously described in mitotic cells, using a C-terminal truncated PCM1 mutant (Dammermann & Merdes, 2002). In this case, the truncated version of PCM1 (1-1468 aa, WT: 1-1904 aa) was shown to aggregate with the endogenous protein in the cytoplasm, suggesting a dominant negative effect. The overexpression of this truncated mutant in mouse oocytes could still localise to the spindle (tested by Dean Clift) and therefore did not allow the endogenous protein to be displaced.

Using another approach, oocyte conditional PCM1 knockout was unsuccessful (tried by Dean Clift). However, with this approach one should also consider that interfering with PCM1 protein expression during early stages of oogenesis may give more severe phenotypes that are not specific to meiosis, as PCM1 is also essential for centrosome organisation and mitotic division (Hori & Toda, 2017; Lopes et al., 2011). Other strategies that were thought of, included depletion of known satellite components such as BBS4, which has been shown to be required for PCM1-satellite assembly (Hori & Toda,

2017; Lopes et al., 2011). BBS4 that also localised to the MSPD was an attractive option, but the antibodies used were unsuccessful.

PCM1 has been shown to require dynein for its localisation (Hori & Toda, 2017; Kubo et al., 1999a; Staples et al., 2012). Assuming that this is a conserved mechanism during meiosis, microinjection of inhibitory dynein or its adaptor dynactin antibody, or the recombinant p150-CC1 (dominant negative) dynactin inhibitor (King et al., 2003; Quintyne et al., 1999), as well as treatment with Ciliobrevin D (a pharmacological dynein inhibitor) could potentially disrupt PCM1 localisation (Firestone et al., 2012; Roossien et al., 2015). However, dynein function is required for a number of spindle functions, including spindle pole organisation, aMTOC fragmentation and localisation and kinetochore-microtubule interactions; therefore, its inhibition would interfere with other, off-target components of spindle assembly even if PCM1 localisation could be perturbed by these strategies (Clift & Schuh, 2015; Jones et al., 2014; McHugh & Welburn, 2017; Quintyne et al., 1999; Reck-Peterson et al., 2018).

Importantly, PCM1 was also identified as a PLK4 substrate (Hori et al., 2016). A conserved PLK4 phosphorylation site (S372) was found to be important for PCM1 dimerization, interaction with other proteins, and conversely essential for cell cycle regulation of pericentriolar satellite formation during the G1 phase (Hori et al., 2016). After overexpression of the PCM1 phosphomutant (S372A) in mouse oocytes, PCM1 could localise normally to the meiotic spindle and form the spindle pole domain with no prominent phenotype apparent (preliminary experiment not shown). PLK4 inhibition was also performed using Centrinone B (selective PLK4 inhibitor) (by Chun So), but again no effect on the assembly of the spindle pole domain or any significant phenotype could be observed.

6.1.1.2 Depletion of PCM1 using Trim-Away

Having attempted to interfere with PCM1 expression, function or localisation by a number of conventional methods, I then attempted a new antibody-based depletion method that was developed in our laboratory (Clift et al., 2017). This method, termed Trim-Away, uses an intracellular pathogen recognition receptor (TRIM21) that recognises the Fc-region of an antibody. TRIM21 is a highly active E3 ubiquitin ligase, which decorates the antibody-bound target protein with ubiquitin molecules. These

ubiquitin (chains) are then recognised by the proteasomal pathway, and the antibody-TRIM21-protein target complex is degraded (Mallery et al., 2010; McEwan et al., 2011).

This method allowed PCM1 to be rapidly depleted at the protein level and suggested that we could now use this approach to acutely deplete PCM1 at different time points during meiosis (Figure 3.5). There are considerations that should be mentioned regarding this approach. The main limitation of this method when working with oocytes is that it requires a high concentration of target-specific antibody in order to deplete the protein of interest. Efficient depletion of the target protein, requires expression of TRIM21 in excess of target protein expression (Clift et al., 2017). While this approach is highly efficient for protein degradation, as seen for acute PCM1 depletion (Figure 3.5H-I), it is difficult to fully adjust antibody and TRIM21 levels for rescue experiments. This is especially challenging when working with oocytes, as several injections are necessary (target specific antibody and TRIM21 mRNA and reporters), and each injection reduces the viability of the oocyte. Another important consideration is to ensure that proteins within a complex can be specifically depleted. In our case, PCM1 is known to interact with a large number of proteins. Pericentrin was an ideal target for testing, as it is known to interact directly with PCM1 (Dammermann & Merdes, 2002; Li et al., 2000), which was suggested to be conserved during meiosis (Figure 3.10 and Figure 3.12). Western blot analysis of the two proteins demonstrated that specific depletion could be achieved (Figure 3.5B, Figure 3.12E).

Overall, this approach is currently the only protein depletion method that is truly post-translational, and it was invaluable for the characterisation of the PCM1 phenotype in oocytes. However, further optimisation of the PCM1 Trim-Away method is needed for recue experiments, in order to confirm the specificity of the PCM1 phenotype and investigate if aMTOC assembly could be rescued once PCM1 levels are restored.

6.1.2 PCM1 depletion phenotype in mouse oocytes

The PCM1 depletion phenotype in mouse oocytes suggested an important function both for spindle assembly and for the overall spindle structure. In the absence of PCM1, the onset of microtubule nucleation was significantly delayed, and spindles appeared significantly smaller, with reduced total microtubule density (Figure 3.6). Live cell

imaging also revealed that the efficiency of chromosome congression in PCM1-depleted oocytes is disrupted. Bivalents appeared unstretched and loosely aligned on the metaphase plate, but no significant meiotic defects were observed (misaligned and lagging chromosomes) and oocytes progressed into anaphase at a comparable rate to controls (Figure 3.6 and Figure 3.8).

6.1.2.1 aMTOCs and the PCM1/MSPD: a close cooperation during meiosis

Based on the observed phenotypes, a number of clues pointed to MTOC-related dysfunction in PCM1-depleted oocytes. Firstly, immunofluorescence and live cell imaging showed a close association between PCM1/MSPD and aMTOCs (Figure 3.2). Secondly, PCM1 is known to have an important function at centrosomes and to interact with Pericentrin, which may suggest a conserved role during meiosis (Dammermann & Merdes, 2002; Hori & Toda, 2017; Li et al., 2000). Assuming a conserved interaction between these two scaffold proteins in mouse oocytes, an effect on Pericentrin levels or organisation would have a direct impact on aMTOCs, as Pericentrin was shown to be an essential component of aMTOCs (Baumann et al., 2017). In line with this, two previous studies have described Pericentrin depletion to result in reduced spindle size/density and delay in microtubule nucleation (Baumann et al., 2017; Ma & Viveiros, 2014), a similar phenotype to that observed in PCM1-depleted oocytes (Figure 3.6). Indeed, staining Pericentrin, γ-tubulin and CEP192 (some of the main components of aMTOCs) in PCM1-depleted oocytes, showed that aMTOCs had disassembled (Figure 3.10A-C). High resolution imaging combined with acute depletion of PCM1 at the MI stage revealed that PCM1 is not only required for aMTOC assembly and/or recruitment, but also for maintaining their structural integrity throughout meiosis (Figure 3.10). The loss of aMTOCs was also shown to coincide with reduced spindle size and lower amounts of spindle microtubules when PCM1 was depleted acutely (Figure 3.10F-H).

6.1.2.2 Pericentrin and PCM1 are interdependent in mouse oocytes

The phenotype described in PCM1-depleted oocytes showed very close similarities to that of Pericentrin depletion (Figure 3.12). This was in line with results of a recent study that removed Pericentrin through a conditional knockout in mice (Baumann et al., 2017). However, the phenotype described in their work was more severe, showing lower anaphase progression rate with increased chromosome attachment errors as well as

severe misalignment and lagging chromosome defects (Baumann et al., 2017). It could be that Pericentrin knockout led to the accumulation of defects throughout oogenesis, which would explain the more severe phenotype.

Pericentrin depletion also suggested that PCM1 and Pericentrin localisation is interdependent in mouse oocytes (Figure 3.12). Although it was shown that Pericentrin levels were reduced at centrosomes in mitotic cells in the absence of PCM1 (Dammermann and Merdes, 2002), complete loss of Pericentrin localisation was not reported. It is possible however, that the depletion methods used in the previous study (PCM1 antibody injection, RNAi and truncated PCM1 overexpression) may have failed to deplete the entire endogenous pool of PCM1, and Pericentrin levels were therefore only mildly affected. Nonetheless, this is the first time that complete interdependence of these proteins has been reported (Figure 3.10 and Figure 3.12). Other evidence supporting the direct interaction between these two proteins comes from *in vitro* assays. PCM1 and Pericentrin were found to coimmunoprecipitate from cytoplasmic extracts, suggesting that they may form a functional complex that enables recruitment of other centrosomal components (Li et al., 2000). Importantly, their association with centrosomes was microtubule dependent (Li et al., 2000). Mechanistically, it is possible that PCM1 and Pericentrin are transported together on microtubules to the meiotic spindle via dynein, as both have previously been shown to interact with cytoplasmic dynein (Hori & Toda, 2017; A Kubo et al., 1999b; Purohit et al., 1999; Young et al., 2000). Another possibility is that direct PCM1-Pericentrin interaction is required at the aMTOC-MSPD interphase to form a stable multicomplex. As both proteins are large coiled-coil scaffold proteins, it would be interesting to carry out high resolution positional mapping of these components, similar to the work done by (Lawo et al., 2012). They used antibodies specific to the N-, central and C-terminal regions of different centrosomal proteins to map their positional arrangements within the centrosome and the surrounding PCM (section 1.5.4.1). It would be interesting to see how these large coiled coil proteins position themselves to form the aMTOC ring domain and the surrounding MSPD, and what other components are essential to maintain their integrity at the spindle poles.

6.1.2.3 K-fibre assembly and microtubule dynamics in the absence of PCM1/MSPD and aMTOCs

Immunofluorescence images of cold treated mouse oocyte spindles surprisingly revealed that PCM1 also localised to the more stable kinetochore fibres (K-fibres) (Figure 3.8E). This localisation, to my knowledge, has not been previously reported for PCM1 in mitotic cells, where satellite foci were mostly shown to disperse within the cytoplasm and only weakly associate with the centrosomes during mitosis (Dammermann & Merdes, 2002). What is also clear from the immunofluorescence images is that in the absence of the more dynamic spindle microtubules (interpolar and astral-like microtubules), the characteristic spindle pole protrusions can no longer be seen, suggesting that the formation of this domain is dependent on spindle microtubules (Figure 3.8E). This was shown directly by the disassembly of PCM1/MSPD in the absence of microtubules (Figure 3.4). These results suggest that K-fibres alone are not sufficient for the formation of the PCM1/MSPD even in the presence of aMTOCs, perhaps due to the loss of transport via dynein along the interpolar microtubules. This might also suggest the presence of two distinct populations of PCM1, an aMTOC-dependent MSPD pool and an aMTOC-independent K-fibre associated pool (similar to TACC3, as discussed later).

One of the key phenotypes of PCM1-depletion showed chromosome congression defects and unstretched bivalents, which could indicate altered K-fibre function and/or attachment (Figure 3.8). In order to further investigate this phenotype, K-fiber properties in fixed oocytes were analysed (Figure 3.8G-I). The results did not show a difference in the average K-fibre density (mean microtubule fluorescent intensity) in PCM1-depleted spindles (Figure 3.8G). However, it cannot be excluded that overall reduction in K-fibre volume (Figure 3.8I), perhaps as an indirect result of the reduced total amount of nucleated microtubule, could have an impact on chromosome alignment. Severe misalignment defects or lagging chromosomes were not significant in PCM1-depleted oocytes, which could indicate K-fibre attachment errors. However, it would be interesting to explore this possibility further by investigating kinetochore attachments in PCM1-depleted oocytes directly. As part of this experiment, one could also label kinetochores in oocytes using CREST staining to test whether the K-fibre tension is

affected in these spindles and compare the average inter-kinetochore distance with control oocytes.

The small spindles and unstretched chromosomes could also indicate reduced microtubule dynamics. In order to test this, photoactivable GFP tagged α-tubulin in MI mouse spindles was tested in PCM1-depleted oocytes, but this showed no significant difference in either the poleward flux rate or the rate of microtubule turnover (Figure 3.14A-E). Surprisingly, direct assessment of growing ends of the microtubules revealed a significantly faster growth rate in oocytes depleted of PCM1 or Pericentrin (Figure 3.14H). This experiment, however, was carried out only once, and the growth rate of only astral-like microtubules was measured manually (section 2.5.5). Although the measured microtubule growth rate (24.54 ± 1.75 μm/min) in the control group (Figure 3.14H) was comparable to that published previously in mouse oocytes (~21 μm/min) (Schuh and Ellenberg, 2007), the growth rate measurements should be repeated using an automated method that can resolve single particles in dense spindle microtubule regions (Jaqaman et al., 2008) to determine if there is a consistent difference in plus-end growth velocity when PCM1 or Pericentrin is depleted.

6.1.2.4 How can a spindle form without aMTOCs in mouse oocytes?

In line with Baumann *et al.* (2017), we found that oocytes relied on the RanGTP microtubule nucleation pathway in the absence of aMTOCs, with delayed spindle assembly, originating predominantly from the chromosome surface (Figure 3.13 and Figure 3.15). It is known that both the RanGTP and the aMTOC nucleation pathways are essential for spindle assembly in mouse oocytes (Schuh and Ellenberg, 2007). However, the contribution of aMTOCs once the bipolar spindle is fully formed is not fully understood. Using acute Trim-Away depletion to disrupt aMTOCs at the late MI stage provided a valuable tool, showing that the loss of aMTOCs within 20-25 minutes following antibody injection coincided with a reduction in spindle size and the total amount of spindle microtubules (Figure 3.10F-H, Figure 3.12J-M). This demonstrates that although aMTOC free spindles can maintain their bipolar spindle morphology, aMTOCs at the spindle poles do contribute to replenish spindle microtubules throughout meiosis.

When one looks at the contribution of aMTOCs to the overall nucleation of spindle microtubules from NEBD (Figure 3.11), it is clear that aMTOCs are the dominant nucleation sites just after NEBD, as shown previously (Schuh and Ellenberg, 2007). However, the role of MTOCs gradually decreases as the bipolar spindle forms, most likely due to the combined contribution of other microtubule nucleation pathways (Figure 3.11, section 1.6), such as the chromosomal and Augmin pathways (section 1.6.3), as well as the activity of microtubule stabilising/polymerising proteins (section 1.5.2.1). The Augmin pathway was shown to supplement multiple microtubule nucleation pathways (centrosomal and chromosomal) in fly embryos that form mitotic spindles (Hayward et al., 2014), contributing to the overall spindle microtubule density (Goshima et al., 2008; Uehara et al., 2009; Wainman et al., 2009). Importantly, the authors also measured an increased contribution from other pathways in the absence of one microtubule nucleation pathway. Their results suggest that there is an inherent flexibility: cells can adapt to modulate the relative contribution of the different microtubule nucleation pathways (Hayward *et al.*, 2014). Mouse oocytes can achieve bipolar spindle assembly in the absence of the main MTOCs, and it is possible that oocytes also have the ability to regulate coordination of the different microtubule generating pathways, by upregulating the chromosomal and Augmin pathways to compensate for the loss of the dominant MTOCs. It would be interesting to further investigate how oocytes are able to detect and switch or modulate the different microtubule pathways.

6.1.3 PCM1/MSPD: Conclusions and perspectives

Overall, results presented here indicate that the described PCM1-depleted phenotype is likely due to disassembly of the aMTOCs in mouse oocytes, or perhaps to the combination of PCM1/MSPD. However, it was not possible to specifically dissect the role of the PCM1/MSPD independently of the aMTOCs in the mouse model. It is clear however, that PCM1 is essential for aMTOC assembly and maintenance during meiosis, as described in the first part of the results section (Results: Part I).

To test whether PCM1 has a conserved role in the formation of the MSPD as the main scaffold protein for the centrosomal satellite proteins, it would be necessary to test which components are actually affected by PCM1 depletion. Selective depletion of other proteins that are known to localise to the MSPD, such as CEP72, LRRC36, BBS4, AKAP9 and Myo10, would also provide information about the hierarchy of the components of the MSPD. This would be an interesting direction to pursue, as functional antibodies for some of the above-mentioned proteins have only recently become available. It would also be interesting to remove putative aMTOC-spindle pole linkers, such as CDK5RAP2 (Chavali et al., 2016), to see if the localisation of PCM1 depends on the proximity of aMTOCs.

Studying other MTOC free systems such as human oocytes was an exciting prospect, to investigate whether the MSPD requires aMTOCs, or has adapted to an aMTOC-free system. If the MSPD does not form in the absence of aMTOCs, it would be intriguing to test if its absence could account (in part) for the observed spindle instability in human oocytes (Holubcová *et al.*, 2015). My goal of understanding the role of PCM1/MSPD in human oocytes was hindered by the lack of commercially available antibody that was effective in human cells. Trim-Away depletion using an affinity purified anti-PCM1 serum (kind gift from the Merdes lab, (Dammermann and Merdes, 2002)) was tried: although a strong PCM1 signal (Figure 4.8 and Figure 6.2) was seen on the meiotic spindle in fixed oocytes, Trim-Away using this antibody showed insufficient depletion of PCM1 (Figure 6.2). Specificity of this antibody in human oocytes needs to be tested to exclude non-specific binding to microtubules.

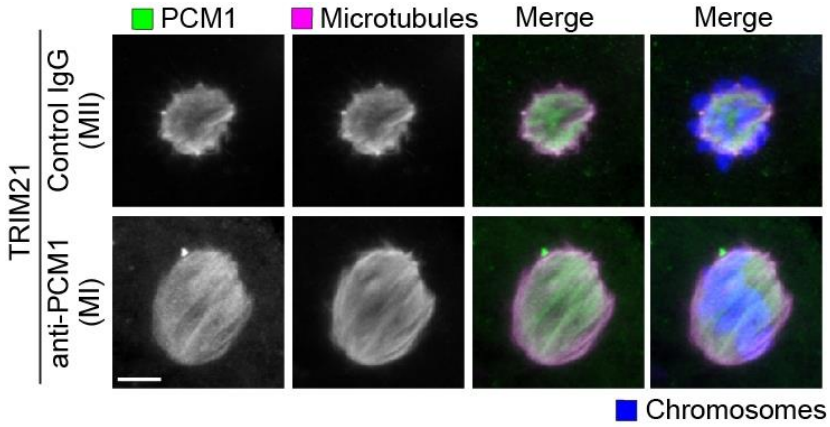

Figure 6.1 Trim-Away of PCM1 in human oocytes.

Immunofluorescence images showing oocytes microinjected with recombinant His-Lipoyl-TRIM21 protein (Clift et al., 2017) and either non-specific control IgG antibody or anti-PCM1 antibody (affinity purified from (Dammermann & Merdes, 2002)). Control oocyte shows an MII spindle that is not parallel (top panel), while PCM1-Trim oocyte shows a parallel MI spindle (button panel). Scale bar shows 5 µm.

In mouse oocytes, in all depletion experiments via the Trim-Away method the commercially available PCM1 antibody (HPA023374, batch number C95754, Sigma-Aldrich) was used. Unfortunately, this PCM1 antibody batch was no longer available and the new antibody batch (F105843) could not fully reproduce the mouse spindle phenotype as described in the first part of the results section (Results: Part I). The reasons are still not fully clear, but it is likely due to the reduced efficiency of PCM1 depletion using the new antibody batch.

Therefore, our screen was expanded to include a wider population of centrosomal proteins in order to find a better candidate that could be used to further characterise the MSPD. Other spindle pole related proteins were also included, as the domain was concentrated predominantly around the spindle poles following bipolar spindle formation (Figure 3.2).

6.2 Extended view of the meiotic spindle pole domain in mouse oocytes

Localisation of centrosomal proteins confirmed by immunofluorescence and/or live-cell imaging showed that all tested proteins were found either at aMTOCs or at the MSPD (Table 4.1, Figure 4.1, Figure 4.2). Importantly, in addition to the pericentriolar satellite proteins, several other centrosomal proteins (clathrin, ch-TOG, KIZ and TACC3) and dynein cargo adaptors (Nde1 and Ndel1) were also found within the MSPD (Figure 4.2).

Quantification of fluorescence recovery after photobleaching (FRAP) of selected PCM components gave us an insight into the dynamics of these proteins at the spindle poles (Figure 4.3). In mouse oocytes, the main aMTOC components (Pericentrin, CEP192 and CDK5RAP2) did not show dynamic recovery, while all tested MSPD proteins recovered at a similar rate (Figure 4.3). These results suggested that Pericentrin, CEP192 and CDK5RAP2, the core PCM components previously proposed to form a functional recruiting scaffold around the centrioles in mitotic cells (Dix & Raff, 2007; Gomez-Ferreria et al., 2007; Lawo et al., 2012; O'Connell et al., 2000; Zhu et al., 2008), may have a conserved role in meiotic aMTOCs.

Depletion of TACC3 using the Trim-Away method revealed that all the tested MSPD components could no longer localise to this domain, suggesting an important role for TACC3 in the assembly of the MSPD. Importantly, TACC3-depletion now showed that loss of Pericentrin/aMTOCs in PCM1-depleted oocytes is probably due to a specific interdependence between Pericentrin and PCM1, and not due to the absence of the MSPD: in TACC3-depleted oocytes, PCM1 could no longer localise to the MSPD (Figure 4.4E); however, aMTOCs still associated with the spindle poles (Figure 4.4E). Although the aMTOCs were not disassembled in TACC3-depleted oocytes, we did observe a strong aMTOC related phenotype. aMTOCs overclustered at spindle poles and did not form their characteristic ring domains, accompanied by a focused spindle pole morphology (Figure 4.4E and Figure 6.3).

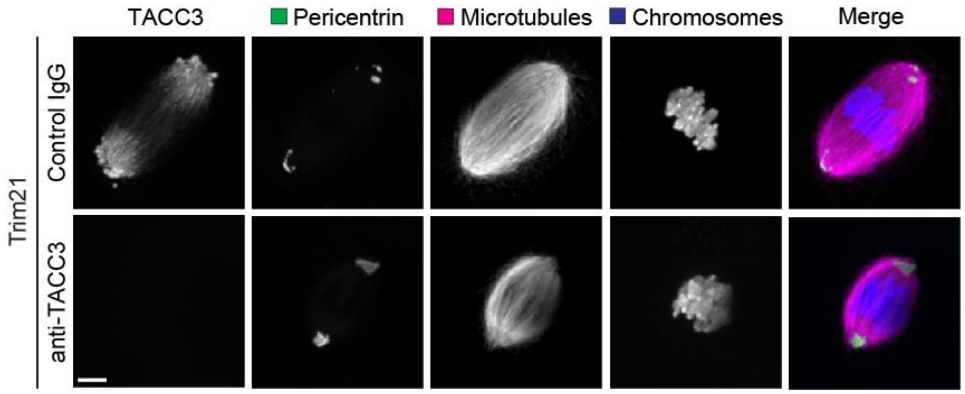

Figure 6.2. Depletion of TACC3 in mouse MI oocytes.

Immunofluorescence images showing oocytes overexpressed TRIM21 mRNA and microinjected with either control IgG or anti-TACC3 antibody. aMTOCs (green), α-tubulin (magenta) and chromosomes (blue) are shown. Scale bar shows 5 μm. (Image taken by Chun So).

6.2.1 MSPD assembly is dependent on aMTOCs in mouse oocytes

High resolution immunofluorescence and live cell imaging of TACC3 (Figure 4.4A-D) confirmed the localisation pattern of PCM1/MSPD and its close association with aMTOCs (Figure 3.2). To see if the MSPD is truly an aMTOC dependent component of the spindle poles, we devised strategies that might reveal different distribution patterns of the aMTOCs, including acute Nocodazole treatment at MI to induce asymmetric aMTOC localisation via RanGTP inhibition and aMTOC bipolar redistribution, and to describe localisation of the MSPD in the complete absence of aMTOCs (Pericentrin-depletion) (Figure 4.6A-E). The asymmetric, monopolar distribution of aMTOCs in RanGTP inhibited oocytes (95% of Ran(T24N) injected oocytes) (Figure 4.5A) provided a robust model to further investigate our hypothesis. While these spindles have monopolar aMTOC arrangements, they could form a small bipolar spindle (Figure 4.5A). It is possible that the Eg5 mediated second phase of aMTOC fragmentation is disrupted in these oocytes (Clift & Schuh, 2015), as it has been previously suggested that Eg5 is regulated by RanGTP (Wilde et al., 2001). The fact that these spindles could still eject the two spindle poles suggests that perhaps only the initial MTOC-fragmentation function of Eg5 is affected by RanGTP inhibition. Nevertheless, live cell imaging showed that TACC3/MSPD mirrored the asymmetric distribution of aMTOCs (Figure 4.5A and C). Two other approaches showed equivalent results, where TACC3/MSPD

trafficked together with aMTOCs during their redistribution following Nocodazole washout (Figure 4.5D) and TACC3/MSPD was lost in the absence of aMTOCs (Figure 4.5E). Together, these results confirm that the MSPD, as described by loss of PCM1/MSPD localisation in Pericentrin-depleted oocytes (Figure 3.11A-C), is dependent on aMTOC localisation at spindle poles.

Interestingly, a second population of TACC3 could still localise to the spindle in the absence of the MSPD, which was faintly visible in both immunofluorescence and live cell images (Figure 4.5F-H). Based on the dissipation curve of photoactivated TACC3-mPA-GFP, we identified two protein populations (slow and fast populations) that supported our observation of an aMTOC-independent TACC3 population (Figure 4.6 and 4.7). TACC3 is known to form a functional complex with ch-TOG (CKAP5) and clathrin (CLTC) and has been implicated in spindle pole integrity as well as K-fibre stabilisation via cross-linking microtubules (Booth et al., 2011; Burgess et al., 2018; W. Fu et al., 2010; Gergely et al., 2000; Hood et al., 2013; C.-H. Lin et al., 2010). We had already shown that TACC3 localises to the K-fibres in the presence of aMTOCs (Figure 4.5H). However, in order to show the localisation pattern of the second, non-MSPD / aMTOC-dependent population, we performed a cold stable assay to visualise K-fibres in Pericentrin-depleted oocytes as well (Figure 6.2). Indeed, TACC3 could still localise to the K-fibres in aMTOC free mouse oocytes, suggesting that the second TACC3 population is distinct from that of the MSPD and can localise to the spindle microtubules via another pathway.

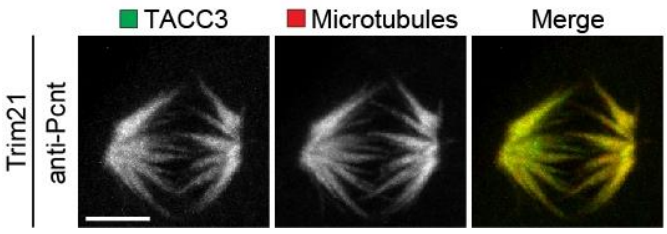

Figure 6.3 TACC3 localisation at K-fibres in the absence of the MSPD / aMTOCs.

Immunofluorescence of anti-TACC3 (green) and anti-α-tubulin (magenta). Oocytes overexpressed TRIM21 mRNA and microinjected with either control IgG or anti-Pericentrin antibody, allowed to mature (7 hours post NEBD) and treated with cold prior to fixing. Scale bar shows 5 µm. Image taken by Chun So.

An important point to mention here is that TACC3 may not be the only MSPD component that can be recruited to the meiotic spindle independently of aMTOCs/MSPD. Following TACC3-depletion, immunofluorescence images showed that at least two or three other proteins (PCM1, Myo10 and Nde(l)) may localise a second population to the spindle microtubules independently of the described aMTOCs/MSPD pool (Figure 4.4). In particular, the unconventional myosin-10 is still prominently localised to the spindle following disassembly of the MSPD population after TACC3-depletion, which might suggest an additional role for this unconventional myosin during meiosis. Although the spindle actin network in PCM1 depleted oocytes that showed the loss of Myo10 signal was examined, no direct link between the MSPD, spindle actin and Myo10 were prominent (Figure 3.9). Specific depletion of Myo10 in mouse oocytes could be another approach to further investigate its role at the meiotic spindle as a microtubule-spindle actin integrator.

6.2.2 Aurora A: a key regulator of the TACC3/MSPD

PLK4, PLK1 and Aurora A, the main regulatory kinases known to be important for centrosome function and spindle assembly, all localise to the aMTOCs in mouse oocytes (Figure 4.2) (Bury et al., 2017; Pahlavan et al., 2000; Yao et al., 2004). This hinted that the aMTOC-dependence of the MSPD might be driven by one of these main regulators. In fact, TACC3 is known to be an Aurora A kinase substrate, and its phosphorylation is essential for interaction with clathrin and spindle localisation (Booth et al., 2011; Cheeseman et al., 2011; Fu et al., 2010; Kinoshita et al., 2005; LeRoy et al., 2007; Lin et al., 2010).

We wanted to further investigate whether Aurora A could have a regulatory function on TACC3, which might explain the aMTOC dependence of the MSPD. Indeed, following Aurora A inhibition (MLN8237 treatment), the MSPD could no longer form (Figure 6.5). Inhibition of the two other kinases (PLK1 and PLK4 with BI2536 and centrinone, respectively) did not alter assembly of the MSPD (tested by Chun So).

Another important point worthy of mention is the association of TACC3 with clathrin and ch-TOG, especially as both localise to the MSPD (Figure 4.2). Phosphorylation of TACC3 via Aurora A has been shown to regulate the clathrin/TACC3 interaction that

forms a composite microtubule binding site, which is required for recruitment of both proteins to the spindle microtubules in mitotic cells (Hood et al., 2013). Ch-TOG interaction alone cannot recruit TACC3 to the mitotic spindle, and it is therefore possible that TACC3 recruitment and assembly of the MSPD is driven by the previously described pathway, via Aurora A phosphorylation and clathrin/TACC3 complex formation that can recruit ch-TOG.

Overall, this confirms that Aurora A is an important upstream regulator that can control the formation of the MSPD, most likely via the well characterised interaction between clathrin and TACC3.

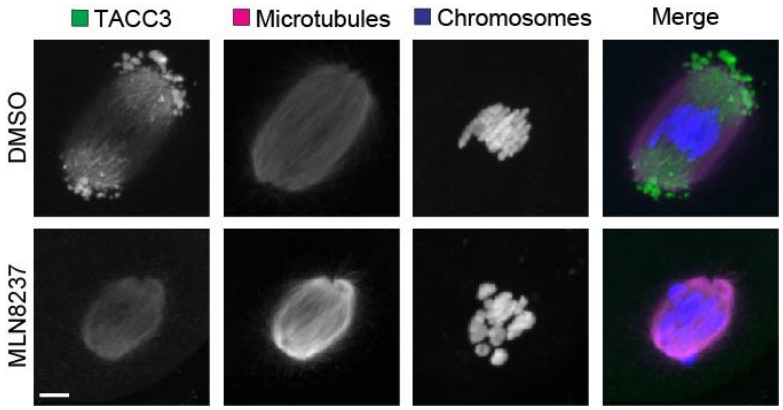

Figure 6.4. Aurora A activity is essential for assembly of the MSPD.

Immunofluorescence of anti-TACC3 (green) anti-α-tubulin (magenta) and chromosomes (blue). Oocytes were treated with either DMSO (control) or Aurora A inhibitor (MLN8237) prior to fixing. Scale bar shows 5 µm. Image taken by Chun So.

6.3 The MSPD pole protrusions are not conserved in the MTOC free human oocytes

Investigation of human oocytes was initiated by testing centrosomal and spindle pole components to first confirm the localisation of the main PCM scaffold proteins. Although Pericentrin has been previously tested (Holubcová *et al.*, 2015), I also investigated γ-tubulin, NEDD1, CEP120 and CDK5RAP2, all of which have supported our current understanding that human oocytes do not contain prominent MTOC foci (Figure 4.8). With this in mind, I wanted to investigate whether the MSPD could assemble in the absence of MTOCs in these oocytes. Apart from PLK1, which has also shown kinetochore localisation, all tested components localised to the meiotic spindle (Figure 4.8). Further live cell imaging of these components would be invaluable as spindle pole enrichment could be seen in some of the immunofluorescence images.

Capturing live the dynamic remodelling of spindles in human oocytes labelled with TACC3 revealed that TACC3 recruitment coincided with the expected time of microtubule nucleation (Holubcová *et al.*, 2015). It also provided insight into how TACC3 is recruited and organised within the small meiotic spindle (Figure 4.9A). During dynamic bipolarisation, TACC3 could be seen to concentrate at multiple spindle poles and then mark the two main poles once spindle bipolarity is achieved (Figure 4.9A). Closer investigation of its localisation with high-resolution immunofluorescence imaging showed that both MI and MII spindles do not show the characteristic micron sized protrusions seen in mouse oocytes (Figure 4.9B, D and E). In addition, TACC3 was also found to co-localise with α-tubulin on K-fibres (Figure 4.9F), suggesting that the aMTOC-independent population of TACC3 identified in mouse oocytes is conserved in human oocytes.

To confirm microtubule dependence of TACC3 localisation, microtubules were depolymerised in MI oocytes (Figure 4.10). Surprisingly, spindle microtubules were resistant to Nocodazole treatment even at high concentrations (10 μM) and following 45 minutes incubation (Figure 4.10A). As an alternative, I tried Colcemid, which efficiently depolymerised all microtubules within minutes and also confirmed microtubule dependence of TACC3 (Figure 4.10B and C). Nocodazole resistance could indicate different post-translational modification of microtubules in human oocytes, e.g.

acetylation of microtubules is known to make them more stable (Wloga et al., 2017), an interesting investigation that could be further explored.

6.3.1 Spindle pole focusing in MTOC free human oocytes

TACC3 was implicated in spindle assembly through its interaction with ch-TOG and clathrin (stabilising minus-ends at centrosomes) and K-fibre stabilisation (formation of intermicrotubule bridges) (Booth et al., 2011; Burgess et al., 2018; Fu et al., 2010; Gergely et al., 2000; Hood et al., 2013; Lin et al., 2010). Although the aMTOC population of TACC3 and the TACC3-mediated MSPD formation is not conserved in human oocytes, it is possible that the previously described association of spindle microtubules via the TACC3-ch-TOG-clathrin interaction may also have an important role in spindle stability in human oocytes. In support of this, clathrin staining showed co-localisation at the meiotic spindle in human oocytes (Figure 4.8).

The most striking phenotype of TACC3 depleted oocytes is the high frequency (60%) of fragmented or multipolar spindles (Figure 4.11). On closer examination, microtubule fibres appear misaligned and frequently radiate outwards from spindle poles (Figure 4.11E and F). This could suggest a conserved role of TACC3 in organising spindle pole microtubules. In addition, K-fibre organisation showed a similar disorganised structure, suggesting that perhaps the cross-linking of K-fibres in these oocytes is also affected (Figure 4.11G-I). TACC3 has recently been implicated in direct interaction with HURP, a RanGTP-dependent microtubule associated protein also know to stabilise K-fibres (Zhang et al., 2018). Considering the misaligned microtubule phenotype, it would be interesting to look at the assembly and stability of K-fibres is TACC3-depleted oocytes. In addition, although microtubule organisation was severely affected by TACC3 depletion, which is potentially also responsible for the severe chromosome misalignment seen in these oocytes (Figure 4.11A), the total amount of nucleated microtubules was not affected (Figure 4.11C-D and H-I). This suggests that TACC3 and perhaps the aMTOC related Aurora A control do not contribute to microtubule nucleation in the absence of MTOCs, unlike in mitotic spindles where TACC3 was implicated in the assembly of γ-TuRC at centrosomes (Ding et al., 2017; Gutie et al., 2015; Singh et al., 2014).

While a high proportion of human oocytes depleted of TACC3 showed spindle pole organisation defects, it does appear that some degree of microtubule minus-end anchoring does still occur, as the split or multipolar spindles all show clear focal points (Figure 4.11A). In the absence of prominent MTOCs, human oocytes likely rely on microtubule associated proteins and motors to focus their spindle poles and organise a bipolar spindle structure. Therefore, further investigation of the role of cytoplasmic dynein and its main spindle pole adaptor NuMA would be an important starting point to further dissect the main spindle pole organising mechanisms in human oocytes.

Overall, the role of an aMTOC/MSPD-independent population of TACC3 in human oocytes indicates an important function for spindle pole organisation. This mechanism is probably not the only one that human oocytes use for the focusing of spindle poles, and the main minus-end organiser dynein is a strong candidate for playing a complementary role at spindle poles. Nonetheless, the absence of the newly described MSPD protrusions in human oocytes could raise an interesting possibility to explain why human oocyte spindles are highly unstable.

7 OUTLOOK

Our understanding of how oocytes assemble their microtubule spindle and maintain a stable bipolar structure is still poorly understood. The difference in spindle assembly mechanisms between mouse and human oocytes is an intriguing subject in particular, as a possible explanation as to why human oocyte spindles are more unstable and prone to meiotic errors.

The work presented here describes a unique meiotic spindle pole domain (MSPD) in mouse oocytes, which is shown to closely associate with the aMTOCs. Further investigation revealed that the characteristic MSPD protrusions are absent in human oocytes. It is tempting to speculate that the absence of the aMTOCs and/or MSPD protrusions could be one of the reasons why human spindles are more unstable. Testing this hypothesis first requires a better understanding of the function of the MSPD in mouse oocytes. One possibility is that the MSPD acts as a reservoir for proteins that are required for aMTOC and spindle pole stabilisation. Disassembly of the MSPD might possibly reduce the local concentration of all components recruited in this domain. Therefore, it would be interesting to test whether the overexpression of specific MSPD proteins could rescue or partially recover the TACC3 depletion phenotype. Another possibility would be to test if there is a direct interaction between the MSPD and the aMTOCs. For this it would be necessary to first identify the core proteins that potentially link both cellular structures and remove them using Trim-Away. Once we understand the structural organisation and function of the MSPD, we might be able to identify the key MSPD components and reconstitute this domain *in vitro* using recombinant proteins.

The data presented shows that upon disassembly of aMTOCs (PCM1 or Pericentrin depletion), mouse oocytes form a smaller, bipolar spindle with a mechanism similar to that previously shown in human oocytes (Holubcová et al., 2015). Thus, it would be interesting to test if this phenotype could be rescued by overexpressing key MSPD proteins that might form a functional subcomplex in this domain, and recruit other

components. The final goal would be to repeat this experiment in human oocytes to see whether we could improve human meiotic spindle stability by the overexpression of key aMTOC and MSPD components that could reconstitute a more robust, 'mouse-like' spindle pole structure.

Importantly, one should also look at other mammalian species, such as , pig, cow or sheep as these oocytes were also found to lack prominent cytoplasmic or spindle pole MTOC foci, similar to human oocytes (Holubcová et al., 2015; Le Guen & Crozet, 1989; Lee et al., 2000; Long et al., 1993). This could reveal whether the MSPD protrusions are indeed a unique component of the acentrosomal mouse spindle or if other mammalian oocytes may have also adapted similar domains to stabilise their meiotic spindles in the absence of MTOCs. This would be an important investigation to show if the absence of MSPD protrusions in human oocytes could distinctively account for the intrinsic spindle instability observed in these cells.

8 REFERENCES

Agrimson, K. S., & Hogarth, C. A. (2016). Germ Cell Commitment to Oogenic Versus Spermatogenic Pathway: The Role of Retinoic Acid. In R. P. Piprek (Ed.), *Molecular Mechanisms of Cell Differentiation in Gonad Development* (pp. 135–166). Springer, Cham.

Akhmanova, A., & Steinmetz, M. O. (2015). Control of microtubule organization and dynamics: two ends in the limelight. *Nature Reviews Molecular Cell Biology*, *16*(12), 711–726.

Alberts, B., Johnson, A., Lewis, J., Raff, M., Roberts, K., & Walter, P. (2002). Components of the Cell-Cycle Control System. In *Molecular Biology of the Cell* (4th editio). New York: Garland Science.

Anderson, R. G., & Brenner, R. M. (1971). The formation of basal bodies (centrioles) in the Rhesus monkey oviduct. *The Journal of Cell Biology*, *50*(1), 10–34.

Askjaer, P., Galy, V., Hannak, E., & Mattaj, I. W. (2002). Ran GTPase cycle and importins alpha and beta are essential for spindle formation and nuclear envelope assembly in living Caenorhabditis elegans embryos. *Molecular Biology of the Cell*, *13*(12), 4355–4370.

Azoury, J., Lee, K. W., Georget, V., Rassinier, P., Leader, B., & Verlhac, M.-H. (2008). Spindle positioning in mouse oocytes relies on a dynamic meshwork of actin filaments. *Current Biology : CB*, *18*(19), 1514–1519.

Azoury, J., Verlhac, M.-H., & Dumont, J. (2009). Actin filaments: key players in the control of asymmetric divisions in mouse oocytes. *Biology of the Cell / under the Auspices of the European Cell Biology Organization*, *101*(2), 69–76.

Bahe, S., Stierhof, Y.-D., Wilkinson, C. J., Leiss, F., & Nigg, E. A. (2005). Rootletin forms centriole-associated filaments and functions in centrosome cohesion. *The Journal of Cell Biology*, *171*(1), 27–33.

Bajar, B. T., Wang, E. S., Lam, A. J., Kim, B. B., Jacobs, C. L., Howe, E. S., … Chu, J. (2016). Improving brightness and photostability of green and red fluorescent proteins for live cell imaging and FRET reporting. *Scientific Reports*, *6*(1), 20889.

Balboula, A. Z., Nguyen, A. L., Gentilello, A. S., Quartuccio, S. M., Drutovic, D., Solc, P., & Schindler, K. (2016). Haspin kinase regulates microtubule-organizing center clustering and stability through Aurora kinase C in mouse oocytes. *Journal of Cell Science*, *129*(19), 3648–3660.

Balczon, R., Bao, L., & Zimmer, W. E. (1994). PCM-1, A 228-kD centrosome autoantigen with a distinct cell cycle distribution. *The Journal of Cell Biology*, *124*(5), 783–793.

Balczon, R., Varden, C. E., & Schroer, T. A. (1999). Role for microtubules in centrosome doubling in chinese hamster ovary cells. *Cell Motility and the Cytoskeleton*, *42*(1), 60–72.

Balczon, R., & West, K. (1991). The identification of mammalian centrosomal antigens using human autoimmune anticentrosome antisera. *Cell Motility and the Cytoskeleton*, *20*(2), 121–135.

Bärenz, F., Mayilo, D., & Gruss, O. J. (2011). Centriolar satellites: Busy orbits around the centrosome. *European Journal of Cell Biology*, *90*, 983–989.

Barr, A. R., & Gergely, F. (2007). Aurora-A: the maker and breaker of spindle poles. *Journal of Cell Science*, *120*(Pt 17), 2987–2996.

Barr, A. R., Kilmartin, J. V, & Gergely, F. (2010). CDK5RAP2 functions in centrosome to spindle pole attachment and DNA damage response. *The Journal of Cell Biology*, *189*(1), 23–39.

Bartolini, F., & Gundersen, G. G. (2006). Generation of noncentrosomal microtubule arrays. *Journal of Cell Science*, *119*(Pt 20), 4155–4163.

Baumann, C., Wang, X., Yang, L., & Viveiros, M. M. (2017). Error-prone meiotic division and subfertility in mice with oocyte-conditional knockdown of pericentrin. *Journal of Cell Science*, *130*(7), 1251–1262.

Bennabi, I., Terret, M.-E., & Verlhac, M.-H. (2016). Meiotic spindle assembly and

chromosome segregation in oocytes. *The Journal of Cell Biology*, *215*(5), 611–619.

Berbari, N. F., Lewis, J. S., Bishop, G. A., Askwith, C. C., & Mykytyn, K. (2008). Bardet-Biedl syndrome proteins are required for the localization of G protein-coupled receptors to primary cilia. *Proceedings of the National Academy of Sciences of the United States of America*, *105*(11), 4242–4246.

Bieling, P., Telley, I. A., & Surrey, T. (2010). A minimal midzone protein module controls formation and length of antiparallel microtubule overlaps. *Cell*, *142*(3), 420–432.

Bindels, D. S., Haarbosch, L., van Weeren, L., Postma, M., Wiese, K. E., Mastop, M., … Gadella, T. W. J. (2017). mScarlet: a bright monomeric red fluorescent protein for cellular imaging. *Nature Methods*, *14*(1), 53–56.

Blagden, S. P., & Glover, D. M. (2003). Polar expeditions--provisioning the centrosome for mitosis. *Nature Cell Biology*, *5*(6), 505–511.

Booth, D. G., Hood, F. E., Prior, I. A., & Royle, S. J. (2011). A TACC3/ch-TOG/clathrin complex stabilises kinetochore fibres by inter-microtubule bridging. *EMBO Journal*.

Bornens, M. (2012). The centrosome in cells and organisms. *Science (New York, N.Y.)*, *335*(6067), 422–426.

Bowles, J., Knight, D., Smith, C., Wilhelm, D., Richman, J., Mamiya, S., … Koopman, P. (2006). Retinoid Signaling Determines Germ Cell Fate in Mice. *Science*, *312*(5773), 596–600.

Breuer, M., Kolano, A., Kwon, M., Li, C.-C., Tsai, T.-F., Pellman, D., … Verlhac, M.-H. (2010). HURP permits MTOC sorting for robust meiotic spindle bipolarity, similar to extra centrosome clustering in cancer cells. *The Journal of Cell Biology*, *191*(7), 1251–1260.

Brunet, S., Maria, A. S., Guillaud, P., Dujardin, D., Kubiak, J. Z., Maro, B., … Monod, I. J. (1999). Kinetochore Fibers Are Not Involved in the Formation of the First Meiotic Spindle in Mouse Oocytes , but Control the Exit from the First Meiotic M Phase, *146*(1), 1–11.

Burgess, S. G., Mukherjee, M., Sabir, S., Joseph, N., Gutiérrez-Caballero, C., Richards,

M. W., … Bayliss, R. (2018). Mitotic spindle association of TACC3 requires Aurora-A-dependent stabilization of a cryptic α-helix. *The EMBO Journal*, *37*(8).

Bury, L., Coelho, P. A., Simeone, A., Ferries, S., Eyers, C. E., Eyers, P. A., … Glover, D. M. (2017). Plk4 and Aurora A cooperate in the initiation of acentriolar spindle assembly in mammalian oocytes. *The Journal of Cell Biology*, *216*(11), 3571–3590.

Calarco, P. G. (2000). Centrosome precursors in the acentriolar mouse oocyte. *Microscopy Research and Technique*, *49*(5), 428–434.

Carabatsos, M. J., Combelles, C. M. H., Messinger, S. M., & Albertini, D. F. (2000). Sorting and reorganization of centrosomes during oocyte maturation in the mouse. *Microscopy Research and Technique*, *49*(5), 435–444.

Carazo-Salas, R. E., Gruss, O. J., Mattaj, I. W., & Karsenti, E. (2001). Ran–GTP coordinates regulation of microtubule nucleation and dynamics during mitotic-spindle assembly. *Nature Cell Biology*, *3*(3), 228–234.

Carazo-Salas, R. E., Guarguaglini, G., Gruss, O. J., Segref, A., Karsenti, E., & Mattaj, I. W. (1999). Generation of GTP-bound Ran by RCC1 is required for chromatin-induced mitotic spindle formation. *Nature*, *400*(6740), 178–181.

Cesario, J., & McKim, K. S. (2011). RanGTP is required for meiotic spindle organization and the initiation of embryonic development in Drosophila. *Journal of Cell Science*, *124*(Pt 22), 3797–3810.

Chalfie, M., Tu, Y., Euskirchen, G., Ward, W. W., & Prasher, D. C. (1994). Green fluorescent protein as a marker for gene expression. *Science (New York, N.Y.)*, *263*(5148), 802–805.

Chambon, J.-P., Touati, S. A., Berneau, S., Cladière, D., Hebras, C., Groeme, R., … Wassmann, K. (2013). The PP2A Inhibitor I2PP2A Is Essential for Sister Chromatid Segregation in Oocyte Meiosis II. *Current Biology*, *23*(6), 485–490.

Chavali, P. L., Chandrasekaran, G., Barr, A. R., Tátrai, P., Taylor, C., Papachristou, E. K., … Gergely, F. (2016). A CEP215–HSET complex links centrosomes with spindle poles and drives centrosome clustering in cancer. *Nature Communications*, *7*, 11005.

Chavali, P. L., Peset, I., & Gergely, F. (2015). Centrosomes and mitotic spindle poles: a recent liaison? *Biochemical Society Transactions*, *43*(1), 13–18.

Cheeseman, L. P., Booth, D. G., Hood, F. E., Prior, I. A., & Royle, S. J. (2011). Aurora A kinase activity is required for localization of TACC3/ch-TOG/clathrin inter-microtubule bridges, (August), 409–412.

Cheeseman, L. P., Harry, E. F., Mcainsh, A. D., Prior, I. A., & Royle, S. J. (2013). Specific removal of TACC3 – ch-TOG – clathrin at metaphase deregulates kinetochore fiber tension.

Choi, Y.-K., Liu, P., Sze, S. K., Dai, C., & Qi, R. Z. (2010). CDK5RAP2 stimulates microtubule nucleation by the gamma-tubulin ring complex. *The Journal of Cell Biology*, *191*(6), 1089–1095.

Clift, D., McEwan, W. A., Labzin, L. I., Konieczny, V., Mogessie, B., James, L. C., & Schuh, M. (2017). A Method for the Acute and Rapid Degradation of Endogenous Proteins. *Cell*.

Clift, D., & Schuh, M. (2013). Restarting life: fertilization and the transition from meiosis to mitosis. *Nature Reviews. Molecular Cell Biology*, *14*(9), 549–562.

Clift, D., & Schuh, M. (2015). A three-step MTOC fragmentation mechanism facilitates bipolar spindle assembly in mouse oocytes. *Nature Communications*, *6*, 1–12.

Colombié, N., Głuszek, A. A., Meireles, A. M., & Ohkura, H. (2013). Meiosis-specific stable binding of augmin to acentrosomal spindle poles promotes biased microtubule assembly in oocytes. *PLoS Genetics*, *9*(6), e1003562.

Cota, R. R., Teixidó-Travesa, N., Ezquerra, A., Eibes, S., Lacasa, C., Roig, J., & Lüders, J. (2017). MZT1 regulates microtubule nucleation by linking γTuRC assembly to adapter-mediated targeting and activation. *Journal of Cell Science*, *130*(2), 406–419.

Courtois, A., Schuh, M., Ellenberg, J., & Hiiragi, T. (2012). The transition from meiotic to mitotic spindle assembly is gradual during early mammalian development. *The Journal of Cell Biology*, *198*(3), 357–370.

Crozet, N. (1990). Behavior of the sperm centriole during sheep oocyte fertilization.

European Journal of Cell Biology, *53*(2), 326–332.

Dammermann, A., & Merdes, A. (2002). Assembly of centrosomal proteins and microtubule organization depends on PCM-1. *The Journal of Cell Biology*, *159*(2), 255–266.

Das, A., Cesario, J., Hinman, A. M., Jang, J. K., & McKim, K. S. (2018). Kinesin 6 Regulation in Drosophila Female Meiosis by the Non-conserved N- and C-Terminal Domains. *G3 (Bethesda, Md.)*, *8*(5), 1555–1569.

Das, A., Shah, S. J., Fan, B., Paik, D., DiSanto, D. J., Hinman, A. M., … McKim, K. S. (2016). Spindle Assembly and Chromosome Segregation Requires Central Spindle Proteins in Drosophila Oocytes. *Genetics*, *202*(1), 61–75.

Ding, Z.-M., Huang, C.-J., Jiao, X.-F., Wu, D., & Huo, L.-J. (2017). The role of TACC3 in mitotic spindle organization. *Cytoskeleton*, *74*(10), 369–378.

Dirksen, E. R. (1991). Centriole and basal body formation during ciliogenesis revisited. *Biology of the Cell*, *72*(1–2), 31–38.

Dix, C. I., & Raff, J. W. (2007). Drosophila Spd-2 recruits PCM to the sperm centriole, but is dispensable for centriole duplication. *Current Biology : CB*, *17*(20), 1759–1764.

Domnitz, S. B., Wagenbach, M., Decarreau, J., & Wordeman, L. (2012). MCAK activity at microtubule tips regulates spindle microtubule length to promote robust kinetochore attachment. *The Journal of Cell Biology*, *197*(2), 231–237.

Dumont, J., Petri, S., Pellegrin, F., Terret, M. E., Bohnsack, M. T., Rassinier, P., … Verlhac, M. H. (2007). A centriole- and RanGTP-independent spindle assembly pathway in meiosis I of vertebrate oocytes. *Journal of Cell Biology*.

Dziugiel, M. (2015). The biology of acentriolar MTOCs in the mouse oocyte - PhD Thesis.

Elder, K., Van den Bergh, M., & Woodward, B. (2015). *Troubleshooting and Problem-Solving in the IVF Laboratory*. Cambridge: Cambridge University Press.

Elisa, Z., Toon, B., De Smedt, S. C., Katrien, R., Kristiaan, N., & Kevin, B. (2018). Technical implementations of light sheet microscopy. *Microscopy Research and*

Technique.

Elting, M. W., Suresh, P., & Dumont, S. (2018). The Spindle: Integrating Architecture and Mechanics across Scales. *Trends in Cell Biology*, *0*(0).

Evsikov, A. V, & Marín de Evsikova, C. (2009). Gene expression during the oocyte-to-embryo transition in mammals. *Molecular Reproduction and Development*, *76*(9), 805–818.

Firestone, A. J., Weinger, J. S., Maldonado, M., Barlan, K., Langston, L. D., O'Donnell, M., … Chen, J. K. (2012). Small-molecule inhibitors of the AAA+ ATPase motor cytoplasmic dynein. *Nature*, *484*(7392), 125–129.

Fleig, U., Salus, S. S., Karig, I., & Sazer, S. (2000). The fission yeast ran GTPase is required for microtubule integrity. *The Journal of Cell Biology*, *151*(5), 1101–1111.

Foraker, A. B., Camus, S. M., Evans, T. M., Majeed, S. R., Chen, C., Taner, S. B., … Brodsky, F. M. (2012). Clathrin promotes centrosome integrity in early mitosis through stabilization of centrosomal ch-TOG, *198*(4).

Fritzsche, M., & Charras, G. (2015). Dissecting protein reaction dynamics in living cells by fluorescence recovery after photobleaching. *Nature Protocols*, *10*(5), 660–680.

Fry, A. M., Sampson, J., Shak, C., & Shackleton, S. (2017). Recent advances in pericentriolar material organization: ordered layers and scaffolding gels. *F1000Research*, *6*(0), 1622.

Fu, J., & Glover, D. M. (2012). Structured illumination of the interface between centriole and peri-centriolar material. *Open Biology*, *2*(8), 120104.

Fu, W., Tao, W., Zheng, P., Fu, J., Bian, M., Jiang, Q., … Zhang, C. (2010). Clathrin recruits phosphorylated TACC3 to spindle poles for bipolar spindle assembly and chromosome alignment. *Journal of Cell Science*, *123*(Pt 21), 3645–3651.

Fujita, H., Yoshino, Y., & Chiba, N. (2016). Regulation of the centrosome cycle. *Molecular & Cellular Oncology*, *3*(2), e1075643.

Gard, D. L., & Kirschner, M. W. (1987). A microtubule-associated protein from Xenopus eggs that specifically promotes assembly at the plus-end. *The Journal of Cell Biology*, *105*(5), 2203–2215.

Ge, X., Frank, C. L., Calderon de Anda, F., & Tsai, L.-H. (2010). Hook3 interacts with PCM1 to regulate pericentriolar material assembly and the timing of neurogenesis. *Neuron*, *65*(2), 191–203.

Gergely, F., Draviam, V. M., & Raff, J. W. (2003). The ch-TOG/XMAP215 protein is essential for spindle pole organization in human somatic cells. *Genes & Development*, *17*(3), 336–341.

Gergely, F., Karlsson, C., Still, I., Cowell, J., Kilmartin, J., Raff, J. W., & Mcintosh, J. R. (2000). The TACC domain identifies a family of centrosomal proteins that can interact with microtubules.

Gerlich, D., Beaudouin, J., Gebhard, M., Ellenberg, J., & Eils, R. (2001). Four-dimensional imaging and quantitative reconstruction to analyse complex spatiotemporal processes in live cells. *Nature Cell Biology*, *3*(9), 852–855.

Gillingham, A. K., & Munro, S. (2000). The PACT domain, a conserved centrosomal targeting motif in the coiled-coil proteins AKAP450 and pericentrin. *EMBO Reports*, *1*(6), 524–529.

Giunta, K. L., Jang, J. K., Manheim, E. A., Subramanian, G., & McKim, K. S. (2002). Subito encodes a kinesin-like protein required for meiotic spindle pole formation in Drosophila melanogaster. *Genetics*, *160*(4), 1489–1501.

Gomez-Ferreria, M. A., Rath, U., Buster, D. W., Chanda, S. K., Caldwell, J. S., Rines, D. R., & Sharp, D. J. (2007). Human Cep192 is required for mitotic centrosome and spindle assembly. *Current Biology : CB*, *17*(22), 1960–1966.

Gómez, R., Valdeolmillos, A., Parra, M. T., Viera, A., Carreiro, C., Roncal, F., … Suja, J. A. (2007). Mammalian SGO2 appears at the inner centromere domain and redistributes depending on tension across centromeres during meiosis II and mitosis. *EMBO Reports*, *8*(2), 173–180.

Goodson, H. V, & Jonasson, E. M. (2018). Microtubules and Microtubule-Associated Proteins. *Cold Spring Harbor Perspectives in Biology*, *10*(6), a022608.

Gosden, R. G., Laing, S. C., Felicio, L. S., Nelson, J. F., & Finch, C. E. (1983). Imminent oocyte exhaustion and reduced follicular recruitment mark the transition to

acyclicity in aging C57BL/6J mice. *Biology of Reproduction*, *28*(2), 255–260.

Goshima, G., & Kimura, A. (2010). New look inside the spindle: microtubule-dependent microtubule generation within the spindle. *Current Opinion in Cell Biology*, *22*(1), 44–49.

Goshima, G., Mayer, M., Zhang, N., Stuurman, N., & Vale, R. D. (2008). Augmin: a protein complex required for centrosome-independent microtubule generation within the spindle. *The Journal of Cell Biology*, *181*(3), 421–429.

Goshima, G., Wollman, R., Goodwin, S. S., Zhang, N., M, J., Vale, R. D., & Stuurman, N. (2007). Genes required for mitotic spindle assembly in Drosophila S2 cells. *Science*, *316*(5823), 417–421.

Gruss, O. J., & Vernos, I. (2004). The mechanism of spindle assembly: functions of Ran and its target TPX2. *The Journal of Cell Biology*, *166*(7), 949–955.

Gutie, C., Burgess, S. G., Bayliss, R., & Royle, S. J. (2015). TACC3 – ch-TOG track the growing tips of microtubules independently of clathrin and Aurora-A phosphorylation, 170–179.

Gutierrez-Caballero, C., Burgess, S. G., Bayliss, R., & Royle, S. J. (2015). TACC3-ch-TOG track the growing tips of microtubules independently of clathrin and Aurora-A phosphorylation. *Biology Open*, *4*(2), 170–179.

Hames, R. S., & Fry, A. M. (2002). Alternative splice variants of the human centrosome kinase Nek2 exhibit distinct patterns of expression in mitosis. *The Biochemical Journal*, *361*(Pt 1), 77–85.

Haren, L., Remy, M. H., Bazin, I., Callebaut, I., Wright, M., & Merdes, A. (2006). NEDD1-dependent recruitment of the γ-tubulin ring complex to the centrosome is necessary for centriole duplication and spindle assembly. *Journal of Cell Biology*, *172*(4), 505–515.

Haren, L., Stearns, T., & Lüders, J. (2009). Plk1-dependent recruitment of gamma-tubulin complexes to mitotic centrosomes involves multiple PCM components. *PloS One*, *4*(6), e5976.

Hayashi, I., & Ikura, M. (2003). Crystal structure of the amino-terminal microtubule-

binding domain of end-binding protein 1 (EB1). *The Journal of Biological Chemistry*, *278*(38), 36430–36434.

Hayward, D., Metz, J., Pellacani, C., & Wakefield, J. (2014). Synergy between Multiple Microtubule-Generating Pathways Confers Robustness to Centrosome-Driven Mitotic Spindle Formation. *Developmental Cell*, *28*(1), 81–93.

He, R., Huang, N., Bao, Y., Zhou, H., Teng, J., & Chen, J. (2013). LRRC45 is a centrosome linker component required for centrosome cohesion. *Cell Reports*, *4*(6), 1100–1107.

Heald, R., & Khodjakov, A. (2015). Thirty years of search and capture: The complex simplicity of mitotic spindle assembly. *The Journal of Cell Biology*, *211*(6), 1103–1111.

Heald, R., Tournebize, R., Blank, T., Sandaltzopoulos, R., Becker, P., Hyman, A., & Karsenti, E. (1996). Self-organization of microtubules into bipolar spindles around artificial chromosomes in Xenopus egg extracts. *Nature*, *382*(6590), 420–425.

Heddleston, J. M., & Chew, T.-L. (2016). Light sheet microscopes: Novel imaging toolbox for visualizing life's processes. *The International Journal of Biochemistry & Cell Biology*, *80*, 119–123.

Helenius, J., Brouhard, G., Kalaidzidis, Y., Diez, S., & Howard, J. (2006). The depolymerizing kinesin MCAK uses lattice diffusion to rapidly target microtubule ends. *Nature*, *441*(7089), 115–119.

Hepler, P. K., McIntosh, J. R., & Cleland, S. (1970). Intermicrotubule bridges in mitotic spindle apparatus. *The Journal of Cell Biology*, *45*(2), 438–444.

Hernandez, S. F., Vahidi, N. A., Park, S., Weitzel, R. P., Tisdale, J., Rueda, B. R., & Wolff, E. F. (2015). Characterization of extracellular DDX4- or Ddx4-positive ovarian cells. *Nature Medicine*, *21*(10), 1114–1116.

Hertig, A. T., & Adams, E. C. (1967). Studies on the human oocyte and its follicle. I. Ultrastructural and histochemical observations on the primordial follicle stage. *The Journal of Cell Biology*, *34*(2), 647–675.

Hinchcliffe, E. H., Miller, F. J., Cham, M., Khodjakov, A., & Sluder, G. (2001).

Requirement of a centrosomal activity for cell cycle progression through G1 into S phase. *Science (New York, N.Y.)*, *291*(5508), 1547–1550.

Hine, K., & Sandquist, J. (2014). Understanding the role of myosin-10 at the mitotic spindle. *FASEB J*, *28*(1_Supplement), 801.3-.

Hoang-Minh, L. B., Deleyrolle, L. P., Nakamura, N. S., Parker, A. K., Martuscello, R. T., Reynolds, B. A., & Sarkisian, M. R. (2016). PCM1 Depletion Inhibits Glioblastoma Cell Ciliogenesis and Increases Cell Death and Sensitivity to Temozolomide. *Translational Oncology*, *9*(5), 392–402.

Holubcová, Z., Blayney, M., Elder, K., & Schuh, M. (2015). Error-prone chromosome-mediated spindle assembly favors chromosome segregation defects in human oocytes. *Science*, *348*(6239), 1143–1147.

Hood, F. E., Williams, S. J., Burgess, S. G., Richards, M. W., Roth, D., Straube, A., … Royle, S. J. (2013). Coordination of adjacent domains mediates TACC3-ch-TOG-clathrin assembly and mitotic spindle binding. *Journal of Cell Biology*, *202*(3), 463–478.

Hori, A., Barnouin, K., Snijders, A. P., & Toda, T. (2016). A non-canonical function of Plk4 in centriolar satellite integrity and ciliogenesis through PCM1 phosphorylation. *EMBO Reports*, *17*, 326–337.

Hori, A., & Toda, T. (2017). Regulation of centriolar satellite integrity and its physiology. *Cellular and Molecular Life Sciences : CMLS*, *74*(2), 213–229.

Howard, J., & Hyman, A. A. (2007). Microtubule polymerases and depolymerases. *Current Opinion in Cell Biology*, *19*(1), 31–35.

Huang, J., Roberts, A. J., Leschziner, A. E., & Reck-Peterson, S. L. (2012). Lis1 Acts as a “Clutch” between the ATPase and Microtubule-Binding Domains of the Dynein Motor. *Cell*, *150*(5), 975–986.

Hunter, N. (2015). Meiotic Recombination: The Essence of Heredity. *Cold Spring Harbor Perspectives in Biology*, *7*(12), a016618.

Hyman, A. A., Salser, S., Drechsel, D. N., Unwin, N., & Mitchison, T. J. (1992). Role of GTP hydrolysis in microtubule dynamics: information from a slowly hydrolyzable

analogue, GMPCPP. *Molecular Biology of the Cell*, *3*(10), 1155–1167.

Icha, J., Weber, M., Waters, J. C., & Norden, C. (2017). Phototoxicity in live fluorescence microscopy, and how to avoid it. *BioEssays*, *39*(8), 1700003.

Jaffe, L. A., & Terasaki, M. (2004). Quantitative microinjection of oocytes, eggs, and embryos. *Methods in Cell Biology*, *74*, 219–242.

Jang, J. K., Rahman, T., & McKim, K. S. (2005). The Kinesinlike Protein Subito Contributes to Central Spindle Assembly and Organization of the Meiotic Spindle in Drosophila Oocytes. *Molecular Biology of the Cell*, *16*, 4684–4694.

Jaqaman, K., Loerke, D., Mettlen, M., Kuwata, H., Grinstein, S., Schmid, S. L., & Danuser, G. (2008). Robust single-particle tracking in live-cell time-lapse sequences. *Nature Methods*, *5*(8), 695–702.

Job, D., Valiron, O., & Oakley, B. (2003). Microtubule nucleation. *Current Opinion in Cell Biology*, *15*(1), 111–117.

Johnson, J., Canning, J., Kaneko, T., Pru, J. K., & Tilly, J. L. (2004). Germline stem cells and follicular renewal in the postnatal mammalian ovary. *Nature*, *428*(6979), 145–150.

Jones, L. A., Villemant, C., Starborg, T., Salter, A., Goddard, G., Ruane, P., … Allan, V. J. (2014). Dynein light intermediate chains maintain spindle bipolarity by functioning in centriole cohesion. *The Journal of Cell Biology*, *207*(4), 499–516.

Kajtez, J., Solomatina, A., Novak, M., Polak, B., Vukušić, K., Rüdiger, J., … Tolić, I. M. (2016). Overlap microtubules link sister k-fibres and balance the forces on bi-oriented kinetochores. *Nature Communications*, *7*, 10298.

Kalab, P., & Heald, R. (2008). The RanGTP gradient - a GPS for the mitotic spindle. *Journal of Cell Science*, *121*(Pt 10), 1577–1586.

Kaláb, P., Pralle, A., Isacoff, E. Y., Heald, R., & Weis, K. (2006). Analysis of a RanGTP-regulated gradient in mitotic somatic cells. *Nature*, *440*(30), 697–701.

Kamasaki, T., O'Toole, E., Kita, S., Osumi, M., Usukura, J., McIntosh, J. R., & Goshima, G. (2013). Augmin-dependent microtubule nucleation at microtubule walls in the spindle. *The Journal of Cell Biology*, *202*(1), 25–33.

Kardon, J. R., & Vale, R. D. (2009). Regulators of the cytoplasmic dynein motor. *Nature Reviews. Molecular Cell Biology*, *10*(12), 854–865.

Kelly, A. E., Sampath, S. C., Maniar, T. A., Woo, E. M., Chait, B. T., & Funabiki, H. (2007). Chromosomal enrichment and activation of the aurora B pathway are coupled to spatially regulate spindle assembly. *Developmental Cell*, *12*(1), 31–43.

Khodjakov, a, Cole, R. W., Oakley, B. R., & Rieder, C. L. (2000). Centrosome-independent mitotic spindle formation in vertebrates. *Current Biology : CB*, *10*, 59–67.

Kim, J. C., Badano, J. L., Sibold, S., Esmail, M. A., Hill, J., Hoskins, B. E., … Beales, P. L. (2004). The Bardet-Biedl protein BBS4 targets cargo to the pericentriolar region and is required for microtubule anchoring and cell cycle progression. *Nature Genetics*, *36*(5), 462–470.

Kim, J., Ishiguro, K., Nambu, A., Akiyoshi, B., Yokobayashi, S., Kagami, A., … Watanabe, Y. (2015). Meikin is a conserved regulator of meiosis-I-specific kinetochore function. *Nature*, *517*(7535), 466–471.

Kim, J., Krishnaswami, S. R., & Gleeson, J. G. (2008). CEP290 interacts with the centriolar satellite component PCM-1 and is required for Rab8 localization to the primary cilium. *Human Molecular Genetics*, *17*(23), 3796–3805.

Kim, K., & Rhee, K. (2011). The pericentriolar satellite protein CEP90 is crucial for integrity of the mitotic spindle pole. *Journal of Cell Science*, *124*(Pt 3), 338–347.

Kim, S., & Rhee, K. (2014). Importance of the CEP215-pericentrin interaction for centrosome maturation during mitosis. *PloS One*, *9*(1), e87016.

Kimura, M., Yoshioka, T., Saio, M., Banno, Y., Nagaoka, H., & Okano, Y. (2013). Mitotic catastrophe and cell death induced by depletion of centrosomal proteins. *Cell Death & Disease*, *4*(4), e603.

King, S. J., Brown, C. L., Maier, K. C., Quintyne, N. J., & Schroer, T. A. (2003). Analysis of the Dynein-Dynactin Interaction In Vitro and In Vivo. *Molecular Biology of the Cell*, *14*(12), 5089–5097.

Kinoshita, K., Habermann, B., & Hyman, A. A. (2002). XMAP215: a key component of

the dynamic microtubule cytoskeleton. *Trends in Cell Biology*, *12*(6), 267–273.

Kinoshita, K., Noetzel, T. L., Pelletier, L., Mechtler, K., Drechsel, D. N., Schwager, A., … Hyman, A. A. (2005). Aurora A phosphorylation of TACC3/maskin is required for centrosome-dependent microtubule assembly in mitosis. *The Journal of Cell Biology*, *170*(7), 1047–1055.

Kirschner, M., & Mitchison, T. (1986). Beyond self-assembly: from microtubules to morphogenesis. *Cell*, *45*(3), 329–342.

Kitajima, T. S., Ohsugi, M., & Ellenberg, J. (2011). Complete Kinetochore Tracking Reveals Error-Prone Homologous Chromosome Biorientation in Mammalian Oocytes. *Cell*, *146*(4), 568–581.

Klebe, C., Bischoff, F. R., Ponstingl, H., & Wittinghofer, A. (1995). Interaction of the nuclear GTP-binding protein Ran with its regulatory proteins RCC1 and RanGAP1. *Biochemistry*, *34*(2), 639–647.

Kodani, A., Tonthat, V., Wu, B., & Sütterlin, C. (2010a). Par6 alpha interacts with the dynactin subunit p150 Glued and is a critical regulator of centrosomal protein recruitment. *Molecular Biology of the Cell*, *21*(19), 3376–3385.

Kodani, A., Tonthat, V., Wu, B., & Sütterlin, C. (2010b). Par6α Interacts with the Dynactin Subunit p150 ^{Glued} and Is a Critical Regulator of Centrosomal Protein Recruitment. *Molecular Biology of the Cell*, *21*(19), 3376–3385.

Koffa, M. D., Casanova, C. M., Santarella, R., Köcher, T., Wilm, M., & Mattaj, I. W. (2006). HURP is part of a Ran-dependent complex involved in spindle formation. *Current Biology : CB*, *16*(8), 743–754.

Kohlmaier, G., Loncarek, J., Meng, X., McEwen, B. F., Mogensen, M. M., Spektor, A., … Gönczy, P. (2009). Overly long centrioles and defective cell division upon excess of the SAS-4-related protein CPAP. *Current Biology : CB*, *19*(12), 1012–1018.

Kolano, A., Brunet, S., Silk, A. D., Cleveland, D. W., & Verlhac, M.-H. (2012). Error-prone mammalian female meiosis from silencing the spindle assembly checkpoint without normal interkinetochore tension. *Proceedings of the National Academy of*

Sciences of the United States of America, *109*(27), E1858-67.

Kollman, J. M., Merdes, A., Mourey, L., & Agard, D. a. (2011). Microtubule nucleation by γ-tubulin complexes. *Nature Reviews. Molecular Cell Biology*, *12*(11), 709–721.

Korenbaum, E., & Rivero, F. (2002). Calponin homology domains at a glance. *Journal of Cell Science*, *115*(Pt 18), 3543–3545.

Koubova, J., Menke, D. B., Zhou, Q., Capel, B., Griswold, M. D., & Page, D. C. (2006). Retinoic acid regulates sex-specific timing of meiotic initiation in mice. *Proceedings of the National Academy of Sciences*, *103*(8), 2474–2479.

Kubo, A. (2003). Non-membranous granular organelle consisting of PCM-1: subcellular distribution and cell-cycle-dependent assembly/disassembly. *Journal of Cell Science*, *116*(5), 919–928.

Kubo, A., Sasaki, H., Yuba-Kubo, A., Tsukita, S., & Shiina, N. (1999a). Centriolar satellites: molecular characterization, ATP-dependent movement toward centrioles and possible involvement in ciliogenesis. *The Journal of Cell Biology*, *147*(5), 969–980.

Kubo, A., Sasaki, H., Yuba-Kubo, A., Tsukita, S., & Shiina, N. (1999b). Centriolar satellites: molecular characterization, ATP-dependent movement toward centrioles and possible involvement in ciliogenesis. *The Journal of Cell Biology*, *147*(5), 969–980.

Kubo, A., & Tsukita, S. (2002). Non-membranous granular organelle consisting of PCM-1: subcellular distribution and cell-cycle- dependent assembly/disassembly. *Journal of Cell Science*, *116*, 919–928.

Kubo, A., & Tsukita, S. (2003). Non-membranous granular organelle consisting of PCM-1: subcellular distribution and cell-cycle-dependent assembly/disassembly. *Journal of Cell Science*, *116*(Pt 5), 919–928.

Lawo, S., Hasegan, M., Gupta, G. D., & Pelletier, L. (2012). Subdiffraction imaging of centrosomes reveals higher-order organizational features of pericentriolar material. *Nature Cell Biology*, *14*(11), 1148–1158.

Lawrence, C. J., Dawe, R. K., Christie, K. R., Cleveland, D. W., Dawson, S. C., Endow,

S. A., … Wordeman, L. (2004). A standardized kinesin nomenclature: Table I. *The Journal of Cell Biology*, *167*(1), 19–22.

Le Guen, P., & Crozet, N. (1989). Microtubule and centrosome distribution during sheep fertilization. *European Journal of Cell Biology*, *48*(2), 239–249.

Lee, J., Kitajima, T. S., Tanno, Y., Yoshida, K., Morita, T., Miyano, T., … Watanabe, Y. (2008). Unified mode of centromeric protection by shugoshin in mammalian oocytes and somatic cells. *Nature Cell Biology*, *10*(1), 42–52.

Lee, J., Miyano, T., & Moor, R. M. (2000). Spindle Formation and Dynamics of γ-Tubulin and Nuclear Mitotic Apparatus Protein Distribution During Meiosis in Pig and Mouse Oocytes1. *Biology of Reproduction*, *62*(5), 1184–1192.

Lee, K., & Rhee, K. (2011). PLK1 phosphorylation of pericentrin initiates centrosome maturation at the onset of mitosis. *The Journal of Cell Biology*, *195*(7), 1093–1101.

Lee, M. J., Gergely, F., Jeffers, K., Peak-Chew, S. Y., & Raff, J. W. (2001). Msps/XMAP215 interacts with the centrosomal protein D-TACC to regulate microtubule behaviour. *Nature Cell Biology*, *3*(7), 643–649.

LeRoy, P. J., Hunter, J. J., Hoar, K. M., Burke, K. E., Shinde, V., Ruan, J., … Ecsedy, J. A. (2007). Localization of human TACC3 to mitotic spindles is mediated by phosphorylation on Ser558 by Aurora A: a novel pharmacodynamic method for measuring Aurora A activity. *Cancer Research*, *67*(11), 5362–5370.

Li, Q., Hansen, D., Killilea, A., Joshi, H., Palazzo, R., & Balczon, R. (2000). Kendrin/pericentrin-B, a centrosome protein with homology to pericentrin that complexes with PCM-1 Qingqin. *Journal of Cell Science*, *114*, 797–809.

Li, R., & Albertini, D. F. (2013). The road to maturation: somatic cell interaction and self-organization of the mammalian oocyte. *Nature Reviews. Molecular Cell Biology*, *14*(3), 141–152.

Lim, J., Lee, H. K., Yu, W., & Ahmed, S. (2014). Light sheet fluorescence microscopy (LSFM): past, present and future. *The Analyst*, *139*(19), 4758–4768.

Liman, E. R., Tytgat, J., & Hess, P. (1992). Subunit stoichiometry of a mammalian K+ channel determined by construction of multimeric cDNAs. *Neuron*, *9*(5), 861–871.

Lin, C.-H., Hu, C.-K., & Shih, H.-M. (2010). Clathrin heavy chain mediates TACC3 targeting to mitotic spindles to ensure spindle stability. *The Journal of Cell Biology*, *189*(7), 1097–1105.

Lin, T.-C., Neuner, A., Flemming, D., Liu, P., Chinen, T., Jäkle, U., … Schiebel, E. (2016). MOZART1 and γ-tubulin complex receptors are both required to turn γ-TuSC into an active microtubule nucleation template. *The Journal of Cell Biology*, *215*(6), 823–840.

Lioutas, A., & Vernos, I. (2013). Aurora A kinase and its substrate TACC3 are required for central spindle assembly. *EMBO Reports*, *14*(9), 829–836.

Liska, F., Gosele, C., Rivkin, E., Tres, L., Cardoso, M. C., Domaing, P., … Hubner, N. (2009). Rat hd mutation reveals an essential role of centrobin in spermatid head shaping and assembly of the head-tail coupling apparatus. *Biology of Reproduction*, *81*(6), 1196–1205.

Long, C. R., Pinto-Correia, C., Duby, R. T., De Leon, F. A. P., Boland, M. P., Roche, J. F., & Robl, J. M. (1993). Chromatin and microtubule morphology during the first cell cycle in bovine zygotes. *Molecular Reproduction and Development*, *36*(1), 23–32.

Longo, F. J., & Anderson, E. (1969). Cytological aspects of fertilization in the lamellibranch, Mytilus edulis. I. Polar body formation and development of the female pronucleus. *The Journal of Experimental Zoology*, *172*(1), 69–95.

Lopes, C. A. M., Prosser, S. L., Romio, L., Hirst, R. A., O'Callaghan, C., Woolf, A. S., & Fry, A. M. (2011). Centriolar satellites are assembly points for proteins implicated in human ciliopathies, including oral-facial-digital syndrome 1. *Journal of Cell Science*, *124*(Pt 4), 600–612.

Losada, A., Hirano, M., & Hirano, T. (1998). Identification of Xenopus SMC protein complexes required for sister chromatid cohesion. *Genes & Development*, *12*(13), 1986–1997.

Łuksza, M., Queguigner, I., Verlhac, M.-H., & Brunet, S. (2013). Rebuilding MTOCs upon centriole loss during mouse oogenesis. *Developmental Biology*, *382*(1), 48–56.

Lukyanov, K. A., Chudakov, D. M., Lukyanov, S., & Verkhusha, V. V. (2005). Photoactivatable fluorescent proteins. *Nature Reviews Molecular Cell Biology*, *6*(11), 885–890.

Lupas, A., Van Dyke, M., & Stock, J. (1991). Predicting coiled coils from protein sequences. *Science (New York, N.Y.)*, *252*(5009), 1162–1164.

Ma, N., Tulu, U. S., Ferenz, N. P., Fagerstrom, C., Wilde, A., & Wadsworth, P. (2010). Poleward transport of TPX2 in the mammalian mitotic spindle requires dynein, Eg5, and microtubule flux. *Molecular Biology of the Cell*, *21*(6), 979–988.

Ma, W., Baumann, C., & Viveiros, M. M. (2010). NEDD1 is crucial for meiotic spindle stability and accurate chromosome segregation in mammalian oocytes. *Developmental Biology*, *339*(2), 439–450.

Ma, W., & Viveiros, M. M. (2014). Depletion of pericentrin in mouse oocytes disrupts microtubule organizing center function and meiotic spindle organization. *Molecular Reproduction and Development*, *81*(11), 1019–1029.

Mahen, R., & Venkitaraman, A. R. (2012). Pattern formation in centrosome assembly. *Current Opinion in Cell Biology*, *24*(1), 14–23.

Mahoney, N. M., Goshima, G., Douglass, A. D., & Vale, R. D. (2006). Making microtubules and mitotic spindles in cells without functional centrosomes. *Current Biology*, *16*(6), 564–569.

Mallery, D. L., McEwan, W. a, Bidgood, S. R., Towers, G. J., Johnson, C. M., & James, L. C. (2010). Antibodies mediate intracellular immunity through tripartite motif-containing 21 (TRIM21). *Proceedings of the National Academy of Sciences of the United States of America*, *107*(46), 19985–19990.

Manandhar, G., Schatten, H., & Sutovsky, P. (2005). Centrosome Reduction During Gametogenesis and Its Significance1. *Biology of Reproduction*, *72*(1), 2–13.

Mandl, A. M., & Zuckerman, S. (1951). The relation of age to numbers of oocytes. *The Journal of Endocrinology*, *7*(2), 190–193.

Mardin, B. R., Agircan, F. G., Lange, C., & Schiebel, E. (2011). Plk1 controls the Nek2A-PP1γ antagonism in centrosome disjunction. *Current Biology : CB*, *21*(13),

1145–1151.

Mardin, B. R., & Schiebel, E. (2012). Breaking the ties that bind: new advances in centrosome biology. *The Journal of Cell Biology*, *197*(1), 11–18.

Maresca, T. J., Groen, A. C., Gatlin, J. C., Ohi, R., Mitchison, T. J., & Salmon, E. D. (2009). Spindle assembly in the absence of a RanGTP gradient requires localized CPC activity. *Current Biology : CB*, *19*(14), 1210–1215.

Margolin, G., Gregoretti, I. V., Cickovski, T. M., Li, C., Shi, W., Alber, M. S., & Goodson, H. V. (2012). The mechanisms of microtubule catastrophe and rescue: implications from analysis of a dimer-scale computational model. *Molecular Biology of the Cell*, *23*(4), 642–656.

Maro, B., Howlett, S. K., & Webb, M. (1985). Non-spindle microtubule organizing centers in metaphase II-arrested mouse oocytes. *The Journal of Cell Biology*, *101*(5 Pt 1), 1665–1672.

Marston, A. L., & Amon, A. (2004). Meiosis: cell-cycle controls shuffle and deal. *Nature Reviews. Molecular Cell Biology*, *5*(12), 983–997.

Maurer, S. P., Cade, N. I., Bohner, G., Gustafsson, N., Boutant, E., & Surrey, T. (2014). EB1 Accelerates Two Conformational Transitions Important for Microtubule Maturation and Dynamics. *Current Biology*, *24*(4), 372–384.

McEwan, W. a, Mallery, D. L., Rhodes, D. a, Trowsdale, J., & James, L. C. (2011). Intracellular antibody-mediated immunity and the role of TRIM21. *BioEssays : News and Reviews in Molecular, Cellular and Developmental Biology*, *33*(11), 803–809.

McHugh, T., & Welburn, J. P. I. (2017). Dynein at kinetochores: Making the connection. *The Journal of Cell Biology*, *216*(4), 855–857.

McKenney, R. J., Huynh, W., Tanenbaum, M. E., Bhabha, G., & Vale, R. D. (2014). Activation of cytoplasmic dynein motility by dynactin-cargo adapter complexes. *Science (New York, N.Y.)*, *345*(6194), 337–341.

Mehlmann, L. M., Jones, T. L. Z., & Jaffe, L. A. (2002). Meiotic arrest in the mouse follicle maintained by a Gs protein in the oocyte. *Science (New York, N.Y.)*,

297(5585), 1343–1345.

Mehlmann, L. M., Saeki, Y., Tanaka, S., Brennan, T. J., Evsikov, A. V, Pendola, F. L., … Jaffe, L. A. (2004). The Gs-Linked Receptor GPR3 Maintains Meiotic Arrest in Mammalian Oocytes. *Science*, *306*(5703), 1947–1950.

Mennella, V., Keszthelyi, B., McDonald, K. L., Chhun, B., Kan, F., Rogers, G. C., … Agard, D. A. (2012). Subdiffraction-resolution fluorescence microscopy reveals a domain of the centrosome critical for pericentriolar material organization. *Nature Cell Biology*, *14*(11), 1159–1168.

Merdes, A., Heald, R., Samejima, K., Earnshaw, W. C., & Cleveland, D. W. (2000). Formation of spindle poles by dynein/dynactin-dependent transport of NuMA. *The Journal of Cell Biology*, *149*(4), 851–862.

Merdes, A., Ramyar, K., Vechio, J. D., & Cleveland, D. W. (1996). A complex of NuMA and cytoplasmic dynein is essential for mitotic spindle assembly. *Cell*, *87*(3), 447–458.

Michaelis, C., Ciosk, R., & Nasmyth, K. (1997). Cohesins: Chromosomal Proteins that Prevent Premature Separation of Sister Chromatids. *Cell*, *91*(1), 35–45.

Mikeladze-Dvali, T., von Tobel, L., Strnad, P., Knott, G., Leonhardt, H., Schermelleh, L., & Gönczy, P. (2012). Analysis of centriole elimination during C. elegans oogenesis. *Development (Cambridge, England)*, *139*(9), 1670–1679.

Mogessie, B., Scheffler, K., & Schuh, M. (2018). Assembly and Positioning of the Oocyte Meiotic Spindle. *Annual Review of Cell and Developmental Biology*, *34*(1), annurev-cellbio-100616-060553.

Mogessie, B., & Schuh, M. (2017). Actin protects mammalian eggs against chromosome segregation errors. *Science (New York, N.Y.)*, *357*(6353), eaal1647.

Mollinari, C., Kleman, J. P., Jiang, W., Schoehn, G., Hunter, T., & Margolis, R. L. (2002). PRC1 is a microtubule binding and bundling protein essential to maintain the mitotic spindle midzone. *Journal of Cell Biology*.

Müller, S., & Almouzni, G. (2017). Chromatin dynamics during the cell cycle at centromeres. *Nature Reviews Genetics*, *18*(3), 192–208.

Musacchio, A., & Hardwick, K. G. (2002). The spindle checkpoint: structural insights into dynamic signalling. *Nature Reviews. Molecular Cell Biology*, *3*(10), 731–741.

Nagaoka, S. I., Hassold, T. J., & Hunt, P. A. (2012). Human aneuploidy: mechanisms and new insights into an age-old problem. *Nature Reviews. Genetics*, *13*(7), 493–504.

NatureEducation. (2013). Unit 5: How Do Cells Know When to Divide? In *Essentials of Cell Biology*. Nature Education.

Neef, R., Preisinger, C., Sutcliffe, J., Kopajtich, R., Nigg, E. A., Mayer, T. U., & Barr, F. A. (2003). Phosphorylation of mitotic kinesin-like protein 2 by polo-like kinase 1 is required for cytokinesis. *Journal of Cell Biology*, *162*(5), 863–875.

Neuwald, A. F., Aravind, L., Spouge, J. L., & Koonin, E. V. (1999). AAA+: A class of chaperone-like ATPases associated with the assembly, operation, and disassembly of protein complexes. *Genome Research*, *9*(1), 27–43.

Newton, C. N., Wagenbach, M., Ovechkina, Y., Wordeman, L., & Wilson, L. (2004). MCAK, a Kin I kinesin, increases the catastrophe frequency of steady-state HeLa cell microtubules in an ATP-dependent manner in vitro. *FEBS Letters*, *572*(1–3), 80–84.

Nixon, F. M., Gutiérrez-Caballero, C., Hood, F. E., Booth, D. G., Prior, I. A., & Royle, S. J. (2015). The mesh is a network of microtubule connectors that stabilizes individual kinetochore fibers of the mitotic spindle. *ELife*, *4*.

Nogales, E. (2015). An electron microscopy journey in the study of microtubule structure and dynamics. *Protein Science*, *24*(12), 1912–1919.

Norris, R. P., Ratzan, W. J., Freudzon, M., Mehlmann, L. M., Krall, J., Movsesian, M. A., … Jaffe, L. A. (2009). Cyclic GMP from the surrounding somatic cells regulates cyclic AMP and meiosis in the mouse oocyte. *Development (Cambridge, England)*, *136*(11), 1869–1878.

O'Connell, K. F., Maxwell, K. N., & White, J. G. (2000). The spd-2 gene is required for polarization of the anteroposterior axis and formation of the sperm asters in the Caenorhabditis elegans zygote. *Developmental Biology*, *222*(1), 55–70.

Ohtsubo, M., Okazaki, H., & Nishimoto, T. (1989). The RCC1 protein, a regulator for the onset of chromosome condensation locates in the nucleus and binds to DNA. *The Journal of Cell Biology*, *109*(4 Pt 1), 1389–1397.

Oshimori, N., Li, X., Ohsugi, M., & Yamamoto, T. (2009). Cep72 regulates the localization of key centrosomal proteins and proper bipolar spindle formation. *The EMBO Journal*, *28*(14), 2066–2076.

Pacchierotti, F., Adler, I.-D., Eichenlaub-Ritter, U., & Mailhes, J. B. (2007). Gender effects on the incidence of aneuploidy in mammalian germ cells. *Environmental Research*, *104*(1), 46–69.

Pahlavan, G., Polanski, Z., Kalab, P., Golsteyn, R., Nigg, E. A., & Maro, B. (2000). Characterization of Polo-like Kinase 1 during Meiotic Maturation of the Mouse Oocyte. *Developmental Biology*, *220*(2), 392–400.

Pan, H., O'brien, M. J., Wigglesworth, K., Eppig, J. J., & Schultz, R. M. (2005). Transcript profiling during mouse oocyte development and the effect of gonadotropin priming and development in vitro. *Developmental Biology*, *286*(2), 493–506.

Patterson, G. H., & Lippincott-Schwartz, J. (2002). A photoactivatable GFP for selective photolabeling of proteins and cells. *Science (New York, N.Y.)*, *297*(5588), 1873–1877.

Pereira, A. L., Pereira, A. J., Maia, A. R. R., Drabek, K., Sayas, C. L., Hergert, P. J., … Maiato, H. (2006). Mammalian CLASP1 and CLASP2 cooperate to ensure mitotic fidelity by regulating spindle and kinetochore function. *Molecular Biology of the Cell*, *17*(10), 4526–4542.

Peset, I., Seiler, J., Sardon, T., Bejarano, L. A., Rybina, S., & Vernos, I. (2005). Function and regulation of Maskin, a TACC family protein, in microtubule growth during mitosis. *The Journal of Cell Biology*, *170*(7), 1057–1066.

Peterman, E. J. G., & Scholey, J. M. (2009). Mitotic Microtubule Crosslinkers: Insights from Mechanistic Studies. *Current Biology*, *19*(23), R1089–R1094.

Petry, S., & Vale, R. D. (2015). Microtubule nucleation at the centrosome and beyond.

Nature Cell Biology, *17*(9), 1089–1093.

Pfeiffer, M. J., Siatkowski, M., Paudel, Y., Balbach, S. T., Baeumer, N., Crosetto, N., … Boiani, M. (2011). Proteomic Analysis of Mouse Oocytes Reveals 28 Candidate Factors of the " Reprogrammome " *J. Proteome Res*, *10*, 2140–2153.

Pfender, S., Kuznetsov, V., Pasternak, M., Tischer, T., Santhanam, B., & Schuh, M. (2015). Live imaging RNAi screen reveals genes essential for meiosis in mammalian oocytes. *Nature*, *524*(7564), 239–242.

Pfender, S., Kuznetsov, V., Pleiser, S., Kerkhoff, E., & Schuh, M. (2011). Spire-type actin nucleators cooperate with Formin-2 to drive asymmetric oocyte division. *Current Biology : CB*, *21*(11), 955–960.

Pihan, G. A. (2013). Centrosome dysfunction contributes to chromosome instability, chromoanagenesis, and genome reprograming in cancer. *Frontiers in Oncology*, *3*, 277.

Pimenta-Marques, A., Bento, I., Lopes, C. A. M., Duarte, P., Jana, S. C., & Bettencourt-Dias, M. (2016). A mechanism for the elimination of the female gamete centrosome in Drosophila melanogaster. *Science*, *353*(6294), aaf4866-aaf4866.

Politi, A. Z., Cai, Y., Walther, N., Hossain, M. J., Koch, B., Wachsmuth, M., & Ellenberg, J. (2018). Quantitative mapping of fluorescently tagged cellular proteins using FCS-calibrated four-dimensional imaging. *Nature Protocols*, *13*(6), 1445–1464.

Power, R. M., & Huisken, J. (2017). A guide to light-sheet fluorescence microscopy for multiscale imaging. *Nature Methods*, *14*(4), 360–373.

Prosser, S. L., & Pelletier, L. (2017). Mitotic spindle assembly in animal cells: a fine balancing act. *Nature Reviews Molecular Cell Biology*, *18*(3), 187–201.

Purich, D. L., & Kristofferson, D. (1984). Microtubule assembly: a review of progress, principles, and perspectives. *Advances in Protein Chemistry*, *36*, 133–212.

Purohit, A., Tynan, S. H., Vallee, R., & Doxsey, S. J. (1999). Direct interaction of pericentrin with cytoplasmic dynein light intermediate chain contributes to mitotic spindle organization. *The Journal of Cell Biology*, *147*(3), 481–492.

Quintyne, N. J., Gill, S. R., Eckley, D. M., Crego, C. L., Compton, D. A., & Schroer, T. A. (1999). Dynactin is required for microtubule anchoring at centrosomes. *The Journal of Cell Biology*, *147*(2), 321–334.

Quintyne, N. J., & Schroer, T. A. (2002). Distinct cell cycle-dependent roles for dynactin and dynein at centrosomes. *The Journal of Cell Biology*, *159*(2), 245–254.

Raaijmakers, J. A., Tanenbaum, M. E., & Medema, R. H. (2013). Systematic dissection of dynein regulators in mitosis. *The Journal of Cell Biology*, *201*(2), 201–215.

Rabut, G., & Ellenberg, J. (2004). Automatic real-time three-dimensional cell tracking by fluorescence microscopy. *Journal of Microscopy*, *216*(Pt 2), 131–137.

Radford, S. J., Nguyen, A. L., Schindler, K., & McKim, K. S. (2017). The chromosomal basis of meiotic acentrosomal spindle assembly and function in oocytes. *Chromosoma*, *126*(3), 351–364.

Raynaud-Messina, B., & Merdes, A. (2007). γ-tubulin complexes and microtubule organization. *Current Opinion in Cell Biology*, *19*(1), 24–30.

Reck-Peterson, S. L., Redwine, W. B., Vale, R. D., & Carter, A. P. (2018). The cytoplasmic dynein transport machinery and its many cargoes. *Nature Reviews Molecular Cell Biology*, *19*(6), 382–398.

Ritter, A., Kreis, N.-N., Louwen, F., Wordeman, L., & Yuan, J. (2016). Molecular insight into the regulation and function of MCAK. *Critical Reviews in Biochemistry and Molecular Biology*, *51*(4), 228–245.

Rogers, G. C., Rogers, S. L., Schwimmer, T. A., Ems-McClung, S. C., Walczak, C. E., Vale, R. D., … Sharp, D. J. (2004). Two mitotic kinesins cooperate to drive sister chromatid separation during anaphase. *Nature*, *427*(6972), 364–370.

Romé, P., & Ohkura, H. (2018). A novel microtubule nucleation pathway for meiotic spindle assembly in oocytes. *The Journal of Cell Biology*, *217*(10), 3431–3445.

Roossien, D. H., Miller, K. E., & Gallo, G. (2015). Ciliobrevins as tools for studying dynein motor function. *Frontiers in Cellular Neuroscience*, *9*, 252.

Royle, S. J. (2013). Protein adaptation: Mitotic functions for membrane trafficking proteins. *Nature Reviews Molecular Cell Biology*, *14*(9), 592–599.

Royle, S. J., Bright, N. A., & Lagnado, L. (2005). Clathrin is required for the function of the mitotic spindle. *Nature*, *434*(7037), 1152–1157.

Ruthmann, A. (1959). The fine structure of the meiotic spindle of the crayfish. *The Journal of Biophysical and Biochemical Cytology*, *5*(1), 177–180.

Sampath, S. C., Ohi, R., Leismann, O., Salic, A., Pozniakovski, A., & Funabiki, H. (2004). The chromosomal passenger complex is required for chromatin-induced microtubule stabilization and spindle assembly. *Cell*, *118*(2), 187–202.

Sanchez, A. D., & Feldman, J. L. (2017). Microtubule-organizing centers: from the centrosome to non-centrosomal sites. *Current Opinion in Cell Biology*, *44*, 93–101.

Sánchez, F., & Smitz, J. (2012). Molecular control of oogenesis. *Biochimica et Biophysica Acta (BBA) - Molecular Basis of Disease*, *1822*(12), 1896–1912.

Sanders, J. R., & Jones, K. T. (2018). Regulation of the meiotic divisions of mammalian oocytes and eggs. *Biochemical Society Transactions*, *46*(4), 797–806.

Sathananthan, A. H., Ratnam, S. S., Ng, S. C., Tarín, J. J., Gianaroli, L., & Trounson, A. (1996). The sperm centriole: its inheritance, replication and perpetuation in early human embryos. *Human Reproduction (Oxford, England)*, *11*(2), 345–356.

Schlager, M. A., Hoang, H. T., Urnavicius, L., Bullock, S. L., & Carter, A. P. (2014). In vitro reconstitution of a highly processive recombinant human dynein complex. *The EMBO Journal*, *33*(17), 1855–1868.

Schuh, M., & Ellenberg, J. (2007). Self-organization of MTOCs replaces centrosome function during acentrosomal spindle assembly in live mouse oocytes. *Cell*, *130*(3), 484–498.

Schuh, M., & Ellenberg, J. (2008). A new model for asymmetric spindle positioning in mouse oocytes. *Current Biology : CB*, *18*(24), 1986–1992.

Shaner, N. C., Campbell, R. E., Steinbach, P. A., Giepmans, B. N. G., Palmer, A. E., & Tsien, R. Y. (2004). Improved monomeric red, orange and yellow fluorescent proteins derived from Discosoma sp. red fluorescent protein. *Nature Biotechnology*, *22*(12), 1567–1572.

Silljé, H. H. W., Nagel, S., Körner, R., & Nigg, E. A. (2006). HURP is a Ran-importin

beta-regulated protein that stabilizes kinetochore microtubules in the vicinity of chromosomes. *Current Biology : CB*, *16*(8), 731–742.

Singh, P., Thomas, G. E., Gireesh, K. K., & Manna, T. K. (2014). TACC3 protein regulates microtubule nucleation by affecting γ-tubulin ring complexes. *The Journal of Biological Chemistry*, *289*(46), 31719–31735.

Sir, J.-H., Pütz, M., Daly, O., Morrison, C. G., Dunning, M., Kilmartin, J. V, & Gergely, F. (2013). Loss of centrioles causes chromosomal instability in vertebrate somatic cells. *The Journal of Cell Biology*, *203*(5), 747–756.

Sluder, G., Miller, F. J., Lewis, K., Davison, E. D., & Rieder, C. L. (1989). Centrosome inheritance in starfish zygotes: selective loss of the maternal centrosome after fertilization. *Developmental Biology*, *131*(2), 567–579.

Sonnen, K. F., Schermelleh, L., Leonhardt, H., & Nigg, E. A. (2012). 3D-structured illumination microscopy provides novel insight into architecture of human centrosomes. *Biology Open*, *1*(10), 965–976.

Sorokin, S. P. (1968). Centriole formation and ciliogenesis. *Aspen Emphysema Conference*, *11*, 213–216.

Staples, C. J., Myers, K. N., Beveridge, R. D. D., Patil, a. a., Lee, a. J. X., Swanton, C., … Collis, S. J. (2012). The centriolar satellite protein Cep131 is important for genome stability. *Journal of Cell Science*, 4770–4779.

Steinman, R. M. (1968). An electron microscopic study of ciliogenesis in developing epidermis and trachea in the embryo of Xenopus laevis. *The American Journal of Anatomy*, *122*(1), 19–55.

Stowe, T. R., Wilkinson, C. J., Iqbal, A., & Stearns, T. (2012). The centriolar satellite proteins Cep72 and Cep290 interact and are required for recruitment of BBS proteins to the cilium.

Stowe, T. R., Wilkinson, C. J., Iqbal, A., & Stearns, T. (2012). The centriolar satellite proteins Cep72 and Cep290 interact and are required for recruitment of BBS proteins to the cilium. *Molecular Biology of the Cell*, *23*(17), 3322–3335.

Strnad, P., Gunther, S., Reichmann, J., Krzic, U., Balazs, B., de Medeiros, G., …

Ellenberg, J. (2016). Inverted light-sheet microscope for imaging mouse pre-implantation development. *Nature Methods*, *13*(2), 139–142.

Su, A. I., Wiltshire, T., Batalov, S., Lapp, H., Ching, K. A., Block, D., … Vogt, P. K. (2004). A gene atlas of the mouse and human protein-encoding transcriptomes. *Proceedings of the National Academy of Sciences*, *101*(16), 6062–6067.

Subramanian, R., Wilson-Kubalek, E. M., Arthur, C. P., Bick, M. J., Campbell, E. A., Darst, S. A., … Kapoor, T. M. (2010). Insights into Antiparallel Microtubule Crosslinking by PRC1, a Conserved Nonmotor Microtubule Binding Protein. *Cell*, *142*(3), 433–443.

Sutovsky, P., Navara, C. S., & Schatten, G. (1996). Fate of the sperm mitochondria, and the incorporation, conversion, and disassembly of the sperm tail structures during bovine fertilization. *Biology of Reproduction*, *55*(6), 1195–1205.

Sweeney, H. L., & Holzbaur, E. L. F. (2018). Motor Proteins. *Cold Spring Harbor Perspectives in Biology*, *10*(5), a021931.

Szollosi, D., Calarco, P., Donahue, R. P., Puget, A., Wright, M., Yanagida, M., & Maro, B. (1972). Absence of centrioles in the first and second meiotic spindles of mouse oocytes. *Journal of Cell Science*, *11*(2), 521–541.

Talapatra, S. K., Harker, B., & Welburn, J. P. I. (2015). The C-terminal region of the motor protein MCAK controls its structure and activity through a conformational switch. *ELife*, *2015*(4), 1–55.

Templado, C., Vidal, F., & Estop, A. (2011). Aneuploidy in Human Spermatozoa. *Cytogenetic and Genome Research*, *133*(2–4), 91–99.

Toli, I. M., Pavin, N., & Iva Toli tolic, C. M. (2016). Bridging the gap between sister kinetochores. *Cell Cycle*, *15*.

Tollenaere, M. A. X., Mailand, N., & Bekker-Jensen, S. (2015). Centriolar satellites: Key mediators of centrosome functions. *Cellular and Molecular Life Sciences*, *72*(1), 11–23.

Tournebize, R., Popov, A., Kinoshita, K., Ashford, A. J., Rybina, S., Pozniakovsky, A., … Hyman, A. A. (2000). Control of microtubule dynamics by the antagonistic

activities of XMAP215 and XKCM1 in Xenopus egg extracts. *Nature Cell Biology*, *2*(1), 13–19.

Trivedi, P., & Stukenberg, P. T. (2016). A Centromere-Signaling Network Underlies the Coordination among Mitotic Events. *Trends in Biochemical Sciences*, *41*(2), 160–174.

Uehara, R., & Goshima, G. (2010). Functional central spindle assembly requires de novo microtubule generation in the interchromosomal region during anaphase. *The Journal of Cell Biology*, *191*(2), 259–267.

Uehara, R., Nozawa, R., Tomioka, A., Petry, S., Vale, R. D., Obuse, C., & Goshima, G. (2009). The augmin complex plays a critical role in spindle microtubule generation for mitotic progression and cytokinesis in human cells. *Proceedings of the National Academy of Sciences of the United States of America*, *106*(17), 6998–7003.

Vaccari, S., Horner, K., Mehlmann, L. M., & Conti, M. (2008). Generation of mouse oocytes defective in cAMP synthesis and degradation: endogenous cyclic AMP is essential for meiotic arrest. *Developmental Biology*, *316*(1), 124–134.

Valente, E. M., Silhavy, J. L., Brancati, F., Barrano, G., Krishnaswami, S. R., Castori, M., … Gleeson, J. G. (2006). Mutations in CEP290, which encodes a centrosomal protein, cause pleiotropic forms of Joubert syndrome. *Nature Genetics*, *38*(6), 623–625.

Van Blerkom, J. (1991). Microtubule mediation of cytoplasmic and nuclear maturation during the early stages of resumed meiosis in cultured mouse oocytes. *Proceedings of the National Academy of Sciences of the United States of America*, *88*(11), 5031–5035.

van Breugel, M., Hirono, M., Andreeva, A., Yanagisawa, H., Yamaguchi, S., Nakazawa, Y., … Zuber, B. (2011). Structures of SAS-6 suggest its organization in centrioles. *Science (New York, N.Y.)*, *331*(6021), 1196–1199.

Verhey, K. J., & Hammond, J. W. (2009). Traffic control: regulation of kinesin motors. *Nature Reviews Molecular Cell Biology*, *10*(11), 765–777.

Virant-Klun, I., Knez, K., Tomazevic, T., & Skutella, T. (2013). Gene expression

profiling of human oocytes developed and matured in vivo or in vitro. *BioMed Research International*, *2013*, 879489.

Wade, R. H. (2009). On and Around Microtubules: An Overview. *Molecular Biotechnology*, *43*(2), 177–191.

Wainman, A., Buster, D. W., Duncan, T., Metz, J., Ma, A., Sharp, D., & Wakefield, J. G. (2009). A new Augmin subunit, Msd1, demonstrates the importance of mitotic spindle-templated microtubule nucleation in the absence of functioning centrosomes. *Genes & Development*, *23*(16), 1876–1881.

Waitzman, J. S., & Rice, S. E. (2014). Mechanism and regulation of kinesin-5, an essential motor for the mitotic spindle. *Biology of the Cell*, *106*(1), 1–12.

Walczak, C. E., Gayek, S., & Ohi, R. (2013). Microtubule-depolymerizing kinesins. *Annual Review of Cell and Developmental Biology*, *29*(1), 417–441.

Walczak, C. E., Mitchison, T. J., & Desai, A. (1996). XKCM1: a Xenopus kinesin-related protein that regulates microtubule dynamics during mitotic spindle assembly. *Cell*, *84*(1), 37–47.

Walker, R. A., O'Brien, E. T., Pryer, N. K., Soboeiro, M. F., Voter, W. A., Erickson, H. P., & Salmon, E. D. (1988). Dynamic instability of individual microtubules analyzed by video light microscopy: rate constants and transition frequencies. *The Journal of Cell Biology*, *107*(4), 1437–1448.

Wang, S., Kou, Z., Jing, Z., Zhang, Y., Guo, X., Dong, M., … Gao, S. (2010). Proteome of mouse oocytes at different developmental stages. *Proceedings of the National Academy of Sciences*.

Wang, Z., Wu, T., Shi, L., Zhang, L., Zheng, W., Qu, J. Y., … Qi, R. Z. (2010). Conserved motif of CDK5RAP2 mediates its localization to centrosomes and the Golgi complex. *The Journal of Biological Chemistry*, *285*(29), 22658–22665.

Watanabe, Y., & Nurse, P. (1999). Cohesin Rec8 is required for reductional chromosome segregation at meiosis. *Nature*, *400*(6743), 461–464.

Waterman-Storer, C. M., Karki, S., & Holzbaur, E. L. (1995). The p150Glued component of the dynactin complex binds to both microtubules and the actin-related

protein centractin (Arp-1). *Proceedings of the National Academy of Sciences of the United States of America*, *92*(5), 1634–1638.

Weber, K. L., Sokac, A. M., Berg, J. S., Cheney, R. E., & Bement, W. M. (2004). A microtubule-binding myosin required for nuclear anchoring and spindle assembly. *Nature*, *431*(7006), 325–329.

Webster, A., & Schuh, M. (2016). Mechanisms of Aneuploidy in Human Eggs. *Trends in Cell Biology*, *xx*(1), 1–14.

Welburn, J. P. I., & Cheeseman, I. M. (2008). Toward a molecular structure of the eukaryotic kinetochore. *Developmental Cell*, *15*(5), 645–655.

White, Y. A. R., Woods, D. C., Takai, Y., Ishihara, O., Seki, H., & Tilly, J. L. (2012). Oocyte formation by mitotically active germ cells purified from ovaries of reproductive-age women. *Nature Medicine*, *18*(3), 413–421.

Whitehead, L. W., McArthur, K., Geoghegan, N. D., & Rogers, K. L. (2017). The reinvention of twentieth century microscopy for three-dimensional imaging. *Immunology and Cell Biology*, *95*(6), 520–524.

Widlund, P. O., Stear, J. H., Pozniakovsky, A., Zanic, M., Reber, S., Brouhard, G. J., … Howard, J. (2011). XMAP215 polymerase activity is built by combining multiple tubulin-binding TOG domains and a basic lattice-binding region. *Proceedings of the National Academy of Sciences of the United States of America*, *108*(7), 2741–2746.

Wiese, C., Zheng, Y., Detraves, C., Julian, M., Moisand, A., Gueth-Hallonet, C., … Mazarguil, H. (2006). Microtubule nucleation: gamma-tubulin and beyond. *Journal of Cell Science*, *119*(Pt 20), 4143–4153.

Wilde, A., Lizarraga, S. B., Zhang, L., Wiese, C., Gliksman, N. R., Walczak, C. E., & Zheng, Y. (2001). Ran stimulates spindle assembly by altering microtubule dynamics and the balance of motor activities. *Nature Cell Biology*, *3*(3), 221–227.

Wilkins, A. S., & Holliday, R. (2009). The evolution of meiosis from mitosis. *Genetics*, *181*(1), 3–12.

Wloga, D., Joachimiak, E., Fabczak, H., Wloga, D., Joachimiak, E., & Fabczak, H. (2017). Tubulin Post-Translational Modifications and Microtubule Dynamics.

International Journal of Molecular Sciences, *18*(10), 2207.

Woodruff, J. B., Ferreira Gomes, B., Widlund, P. O., Mahamid, J., Honigmann, A., & Hyman, A. A. (2017). The Centrosome Is a Selective Condensate that Nucleates Microtubules by Concentrating Tubulin. *Cell*, *169*(6), 1066–1077.e10.

Woolner, S., O'Brien, L. L., Wiese, C., & Bement, W. M. (2008). Myosin-10 and actin filaments are essential for mitotic spindle function. *The Journal of Cell Biology*, *182*(1), 77–88.

Wordeman, L., & Mitchison, T. J. (1995). Identification and partial characterization of mitotic centromere-associated kinesin, a kinesin-related protein that associates with centromeres during mitosis. *The Journal of Cell Biology*, *128*(1–2), 95–104.

Wu, C., Xu, B., Li, X., Ma, W., Zhang, P., Chen, X., & Wu, J. (2017). Tracing and Characterizing the Development of Transplanted Female Germline Stem Cells In Vivo. *Molecular Therapy*, *25*(6), 1408–1419.

Wueseke, O., Zwicker, D., Schwager, A., Wong, Y. L., Oegema, K., Jülicher, F., … Woodruff, J. B. (2016). Polo-like kinase phosphorylation determines Caenorhabditis elegans centrosome size and density by biasing SPD-5 toward an assembly-competent conformation. *Biology Open*, *5*(10), 1431–1440.

Yan, L., Yang, M., Guo, H., Yang, L., Wu, J., Li, R., … Tang, F. (2013). Single-cell RNA-Seq profiling of human preimplantation embryos and embryonic stem cells. *Nature Publishing Group*, *20*(9).

Yao, L.-J., Zhong, Z.-S., Zhang, L.-S., Chen, D.-Y., Schatten, H., & Sun, Q.-Y. (2004). Aurora-A Is a Critical Regulator of Microtubule Assembly and Nuclear Activity in Mouse Oocytes, Fertilized Eggs, and Early Embryos1. *Biology of Reproduction*, *70*(5), 1392–1399.

Young, A., Dictenberg, J. B., Purohit, A., Tuft, R., & Doxsey, S. J. (2000). Cytoplasmic dynein-mediated assembly of pericentrin and gamma tubulin onto centrosomes. *Molecular Biology of the Cell*, *11*(6), 2047–2056.

Zamboni, L., & Stefanini, M. (1971). The fine structure of the neck of mammalian spermatozoa. *The Anatomical Record*, *169*(2), 155–172.

Zeng, F., Baldwin, D. A., & Schultz, R. M. (2004). Transcript profiling during preimplantation mouse development. *Developmental Biology*, *272*, 483–496.

Zhang, H., Panula, S., Petropoulos, S., Edsgärd, D., Busayavalasa, K., Liu, L., … Liu, K. (2015). Adult human and mouse ovaries lack DDX4-expressing functional oogonial stem cells. *Nature Medicine*, *21*(10), 1116–1118.

Zhang, P., Zucchelli, M., Bruce, S., Hambiliki, F., Stavreus-Evers, A., Levkov, L., … Hovatta, O. (2009). Transcriptome Profiling of Human Pre-Implantation Development. *PLoS ONE*, *4*(11).

Zhang, Q.-H., Yuen, W. S., Adhikari, D., Flegg, J. A., FitzHarris, G., Conti, M., … Carroll, J. (2017). Cyclin A2 modulates kinetochore-microtubule attachment in meiosis II. *The Journal of Cell Biology*, *216*(10), 3133–3143.

Zhang, Y., Tan, L., Yang, Q., Li, C., & Liou, Y.-C. (2018). The microtubule-associated protein HURP recruits the centrosomal protein TACC3 to regulate K-fiber formation and support chromosome congression. *Journal of Biological Chemistry*.

Zheng, Y., Wong, M. L., Alberts, B., & Mitchison, T. (1995). Nucleation of microtubule assembly by a gamma-tubulin-containing ring complex. *Nature*, *378*(6557), 578–583.

Zhu, F., Lawo, S., Bird, A., Pinchev, D., Ralph, A., Richter, C., … Pelletier, L. (2008). The mammalian SPD-2 ortholog Cep192 regulates centrosome biogenesis. *Current Biology : CB*, *18*(2), 136–141.